12-1-1988

Harmonic Characteristics and Voltage Support for Inverters With a Weak AC Supply

Ahmed Bensenouci
Purdue University

C. M. Ong
Purdue University

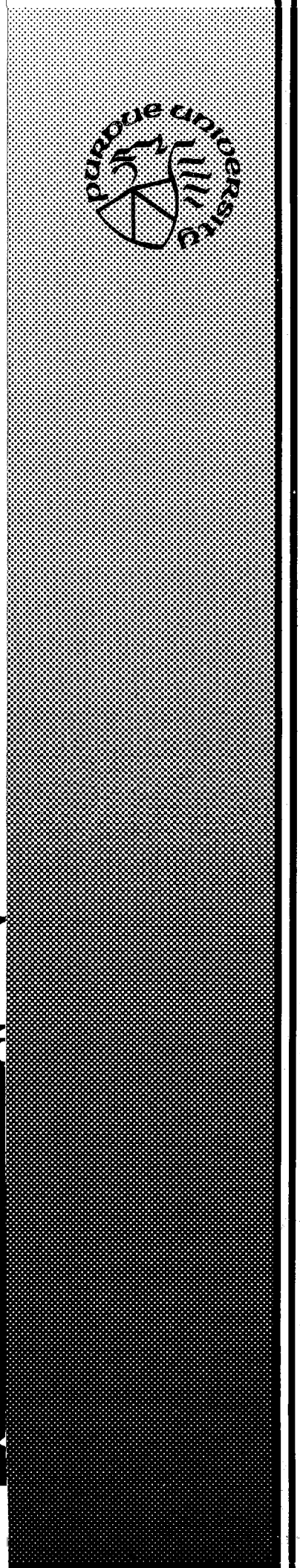

Harmonic Characteristics and Voltage Support for Inverters With a Weak AC Supply

Ahmed Bensenouci
C. M. Ong

TR-EE 88-56
December 1988

School of Electrical Engineering
Purdue University
West Lafayette, Indiana 47907

HARMONIC CHARACTERISTICS AND VOLTAGE SUPPORT FOR INVERTERS WITH A WEAK AC SUPPLY

Ahmed Bensenouci and C. M. Ong

School of Electrical Engineering
Purdue University
West Lafayette, Indiana 47907

TR-EE 88-56

December 1988

TABLE OF CONTENTS

Page

Page

APPENDICES

LIST OF TABLES

Appendix
Table

LIST OF FIGURES

Figure Page

Figure Page

Appendix
Figure

NOMENCLATURE

Subscripts

a	-	phase a
b	-	phase b
c	-	phase c
r	-	rectifier side
ref	-	reference
th	-	Thevenin

Symbols

I_d	-	DC current
I_s	-	inverter AC network current
I_c	-	equivalent capacitor (including the filters) current
I_L	-	TCR current
I_{c1}	-	TSC1 current
I_{c2}	-	TSC2 current
I_{dc}	-	DC component in the transformer secondary current
I_{11}	-	eleventh harmonic filter current
I_{13}	-	thirteenth harmonic filter current
I_{hp1}	-	high-pass 1 harmonic filter current
I_{flt}	-	filtered AC converter current
i_1	-	valve 1 current
i_Δ	-	TCR Δ-branch current
I_D	-	direct-axis current component of I_s
I_Q	-	quadrature-axis current component of I_s
i	-	AC converter current
i_m	-	converter transformer magnetizing current
P_d	-	inverter DC power
Q_d	-	reactive power absorbed by the inverter

P_s - real power injected into the AC bus
Q_s - reactive power injected into the AC bus
V - voltage magnitude of the inverter terminal AC bus
V_d - inverter DC voltage
v_{c11} - voltage across the capacitor of the 11th harmonic filter
V_{Lo} - output control voltage of the TCR controller
v_{c1} - voltage across TSC1
E_{c1} - commutating voltage of valve 1
v_1 - valve 1 forward voltage
V_{bc} - voltage between phases b and c
V_{IC} - initial value of EP ramping function
V_{END} - final value of EP ramping function
h - harmonic order
Z_{th} - Thevenin equivalent impedance of the inverter AC network
Z_f - equivalent filter and capacitor impedance
Z_{eq} - equivalent impedance of the parallel combination of Z_{th} and Z_f
X_c - equivalent capacitance (including filters)
X_{slp} - TCR controller slope (V-control)
Xm1 - linear magnetizing reactance
Xm2 - nonlinear magnetizing reactance
X_t - converter transformer short-circuit reactance
L_d - smoothing reactor inductance
K_p - proportional gain value of the PI controller
K_i - integral gain value of the PI controller
T - time constant
ω - AC system angular frequency
θ - angle between the positive and negative sequence fundamental AC voltages
ϕ - angle between I_s and V
α - ignition (firing) angle
μ - commutation (overlap) angle
β - advance angle ($\pi-\alpha$)
γ - extinction angle($\beta-\mu$)

ABSTRACT

In recent years, the world-wide use of high voltage direct current (HVDC) power transmission has increased sharply. Most of the recent projects involve transmitting large amounts of power from remote generations to load centers, where the short-circuit capacity at the receiving bus is often only a few times that of the rated DC power transfer -- indicative of a weak AC support that is more susceptible to various operational problems, such as harmonic amplification, poor voltage regulation and adverse effects on the firing control.

This report is on a two-part investigation. The first part deals with the harmonics characteristics of an inverter with weak AC support under balanced and unbalanced network conditions using the two most common firing schemes; the individual pulse control and the equidistant pulse control. The second part examines the operational behavior of the inverter with weak AC support when supplementary VAR support in the form of static VAR compensator is used. Aside from dynamic and transient behaviors, the study also looked into possible interaction between the inverter and the thyristor-controlled reactor at the harmonic level.

CHAPTER 1

INTRODUCTION

In recent years, the world-wide use of HVDC transmission has grown not only in terms of capacity installed, but also in terms of variety of applications (e.g. back-to-back and asynchronous ties). Many of these cases have weak AC support, in that the rated capacity of the DC system is a significant fraction of the short-circuit capacity at the inverter AC bus. The strength of the AC bus is often measured by the short-circuit ratio (SCR), which is defined as the ratio of the short-circuit capacity at the AC bus feeding the converter to the rated HVDC power. In the context of HVDC system operation, an SCR less than 3 is usually considered to be weak [1,2]. This is typical of many of the recent HVDC schemes; for example, Nelson River bipole-2 has a minimum SCR of 2.5 whereas Square Butte has a minimum SCR of 3.2 [3].

Attenuated somewhat by the shunt filters on the local bus, a portion of the harmonic currents is injected by the converter into the AC network; these currents, in turn, produce harmonic voltages at the converter bus which become significant when the AC network impedance is large. They cause irregularities in the spacing of the firing pulses, and if these irregularities happen to reinforce the troublesome harmonics, harmonic instability may occur. The individual pulse firing schemes, which depend on the peak value and shape of the AC network voltage, are particularly susceptible to the presence of these harmonic voltages. The effect of these harmonics could produce a DC offset in the current on the secondary side of the converter transformer. A small DC offset can drive the converter transformer core well into saturation, further distorting the AC voltage. Because of some of the above mentioned problems, equidistant pulse firing schemes are usually preferred [4,5,6]. An equidistant pulse scheme, in steady-state, has equally spaced firing pulses that are synchronized to the zero crossings of the AC voltage through a phase-locked loop control. Consequently, the firings are less dependent on the AC voltage magnitude and shape.

Another characteristic of weak AC support is poor voltage regulation. Excessive overvoltages can be destructive to equipment, especially voltage sensitive semiconductor components, whereas excessive undervoltages can cause commutation failures. A fast-acting device to control the terminal voltage within acceptable limits is a necessity for very weak AC conditions.

1.1 Motivation

Weak AC support is synonymous with high source impedance, coupled with the harmonic current injections and reactive power requirement (as much as 60% of the real power transfer) of the inverter, presents some challenging operational problems. The harmonic currents flowing into the large source impedance result in higher harmonic voltage levels at the inverter bus, which can interfere with the firing control causing serious harmonic resonance and instability problems. A large amount of reactive power flowing through the large source impedance also results in poor voltage regulation at the inverter bus and likely overvoltage conditions when the inverter is suddenly blocked.

The simple solution of shunt capacitive compensation has a tendency to increase the equivalent Thevenin AC impedance seen from the AC bus feeding the converter, resulting in a decrease in the short-circuit capacity at that bus. Some of the problems associated with weak AC support that have been observed [7] include:

- complication of the interaction between DC and AC systems by the reactive power requirement [8-12];
- possibility of voltage/power instability [8,9];
- possibility of resonance at low order harmonic, due to high AC system impedance and local shunt capacitors [13-17];
- increased overvoltage following a load rejection (blocking the converter) [18-19];
- increased susceptibility to commutation failure because of wider AC voltage fluctuations, which, if repeated, will force the shutdown of the converter (the loss of transfer capacity could in certain cases present a stability problem to the AC system [20]);
- transformer saturation by overvoltage and by magnetic flux producing high magnetizing current, which contains sizable low order harmonics [21];
- fast recovery from faults or commutation failures, usually more difficult to achieve with a higher and less damped AC impedance [9];

- irregular spacing of the firing pulse train due to voltage distortion, causing more harmonic generation at the AC bus (in-phase amplification might lead to unstable operation of the converter [22]).

The use of a synchronous condenser would increase the short-circuit capacity and provide balanced AC voltage support at the bus. However due to its higher cost, higher maintenance, and slower response time (in the order of seconds), it is seldom the choice [23].

A more promising solution is to use a static VAR compensator (SVC), which could provide fast and continuous voltage control [24]. The use of an SVC could eliminate extensive arrangement of breaker-switched capacitor banks, or the need to increase the extinction angle of the inverter because of larger voltage fluctuations. Since an SVC generates harmonic currents, careful consideration has to be given to additional filtering and sizing of the SVC components [23,24]. Because of their close proximity, possible control interaction between the SVC and the HVDC converter has to be investigated.

1.2 Research objectives

The objectives of this research are: first, to study the steady-state harmonic of an inverter with weak AC support, including the effects of transformer saturation and static VAR compensator; second, to study the dynamic and transient behaviors of the inverter with a static VAR compensator on the inverter AC bus.

1.3 Outline of the report

In Chapter 2, the analog simulation of a complete AC-DC network is presented. This includes the simulation of two types of firing schemes, transformer saturation, AC and DC networks, thyristor-controlled reactor (TCR) with terminal voltage, power factor or direct-axis current control, and thyristor-switched capacitors (TSC). Some simulation results of steady-state operations under balanced and unbalanced conditions are presented.

In Chapter 3 we examine the harmonics generated by the converter operating in steady-state under balanced and unbalanced AC voltage conditions. The relationship between the uncharacteristic harmonics generated by the converter and those of the AC source voltage is established. Differences in the responses between an individual phase and an equidistant pulse firing

schemes are discussed. This part of the study also deals with the harmonics generated by the converter transformer saturation and the thyristor-controlled reactor (TCR).

In Chapter 4, the effect of low effective short-circuit ratio (ESCR) on the power transfer limit and on the steady-state voltage instability is discussed. The voltage instability factor is introduced and applied to predict problematic operating conditions.

Chapter 5 deals with the transient response of the AC/DC system. It includes separate investigations of the dynamic (small disturbance) and transient (large disturbance) responses of the system with and without the TCR. Overvoltages due to load rejection (blocking of the inverter) and the effect of lowering the ESCR on the transient overvoltages are studied.

Chapter 6 presents the conclusions of this report and some suggestions for future research.

CHAPTER 2

MODELING OF THE AC/DC SYSTEMS

2.1 Introduction

Digital and analog simulations are widely used to study the dynamic behavior of AC/DC interconnected systems. When harmonics can be neglected, average-value model of the converter is used, as in transient stability programs [25]. When harmonics are of interest, the average-value model is inadequate; in that case, detailed modeling of the converter switching and firing control is needed [26-28].

In many studies involving harmonic generation or load rejection overvoltages, saturation effects are very crucial. The modeling of the converter transformer without representing its saturation would give pessimistic estimates of the overvoltages (higher overvoltages). If the saturation is not well represented, it will reveal unrealistic saturation effects (overvoltages which are too low and die quickly) [29,30]. The common models may be classified into two types: mathematical [29,31-33] representations and piece-wise linear approximations [34-39]. The latter are more attractive because of their relatively simple representation whose use is justified in large power transformers where the saturation characteristic presents a large magnetizing reactance in the linear part and a very small magnetizing reactance in the nonlinear part. It has been shown that two-, five- and seven-segment piece-wise linear representations of the saturation and field measurements give nearly identical results for large power transformers, with a small difference in some of the higher frequency components [36,39]. Due to increased core losses with frequency, it was found [40,41] that a piece-wise representation overestimates the core losses at higher frequencies (beyond ninth), although results are quite accurate at lower harmonics.

The model of the AC system impedance should be good for at least the lower harmonics [30]. The impedance angle, which has considerable effect on the damping, should be carefully chosen [30,42,43].

The DC network can be represented by one or more T-circuits; the number depends on the DC line distance and on the accuracy desired. Three T-sections for the DC transmission line model have been used in this study [44].

The system shown in Fig. 2.1 has been simulated in full detail. It represents a typical bipolar AC/DC/AC system. The standard components, like the converter circuit, the AC and DC networks, were simulated on the special power system simulator [45]; newer components, like the SVC and equidistant pulse control for the HVDC converter, were simulated on the EAI-680.

In the following sections we will describe the simulation of the following major components: the converter bridge and its controls, the AC and DC networks, the converter transformer saturation, and the static VAR compensators and their controls.

2.2 Simulation of the converter bridge

The basic converter bridge used is the so-called Graetz bridge or 6-pulse converter bridge. It consists of six valves (a valve is composed of one or more thyristors in series). This is a line-commutated or naturally commutated converter bridge. Two such bridges when connected in parallel on the AC side and in series on the DC side form a 12-pulse converter bridge. The 30° phase-shift AC supply to the 12-pulse bridge could be obtained from two separate transformers; one connected wye-wye and the other wye-delta or delta-wye. Figure 2.2 shows a 12-pulse converter bridge circuit with its converter transformer.

The basic control of the bridge consists of the converter control pulse (CCP) and the converter regulator (CR). The function of the CCP module is to provide the firing pulses to all valves at the proper time. The CR performs the function of regulating the direct current I_d, the DC power P_d, the ignition angle α, or the extinction angle γ. At its input, the measured variable is compared to its reference value, the error is amplified, and the output drives the CCP.

There are two types of firing schemes widely used in HVDC converters: the individual pulse control [46,47] and the equidistant pulse control [5,6,47,48]. The main difference between these two types is that the individual pulse control utilizes the AC voltage wave signals and comparators to directly synchronize each converter valve firing with the AC system, while the equidistant pulse

control uses a phase locked oscillator to indirectly synchronize each converter valve firing with the AC system.

During steady-state operation, the pulses from an individual pulse control may not be equally spaced, especially so when the AC system voltages are asymmetric or distorted; while the equidistant pulse control in steady-state generates equally spaced firing pulses, it is sensitive to the zero crossings of the AC system voltages and not to their shapes. As a result of these differences, the harmonic characteristics, even under steady-state condition, and the dynamic performance of an inverter with one type of firing control will not be the same as those with the other type of firing control.

In this report, the individual pulse control is represented by the inverse cosine control [46,47], and the equidistant pulse control by the pulse phase control [48].

Typically the DC link is operated with the rectifier controlling the DC current I_d and the inverter controlling the DC voltage V_d directly or through the extinction angle γ.

Figure 2.3 shows the V_d/I_d control characteristics corresponding to the three most common modes:

- the constant current (CC),
- the constant ignition angle (CIA) control, and
- the constant extinction angle (CEA) control.

Point T represents the operation where the rectifier is controlling the DC current I_d and the inverter is controlling the minimum extinction angle γ_{min}; this is the usual operating point. Point U represents the operation where the rectifier is controlling the minimum ignition angle α_{min} and the inverter is controlling the DC current I_d. WT is the voltage margin, introduced to avoid frequent mode-shifts that will perturb the DC line current by the current margin ΔI, causing similar undesirable perturbation in the DC power transfer.

2.3 Individual pulse (IP)

In this type of firing scheme, the firing instant of each valve is determined individually by comparing its own AC control voltage (the line-to-line voltage across the valve, scaled down and shifted by 90° backward) with a DC regulator signal, V_c (Fig. 2.4). The DC regulator signal, V_c, is from the primary regulator which could be operating under constant current (CC) control, constant ignition angle (CIA) control, or constant extinction angle (CEA) control.

Figure 2.5 shows the steady-state voltage waveforms with the current and the firing pulse of valve 1.

The analog simulation diagram of the constant ignition angle (CIA) control is shown in Fig. 2.6 (a). The CIA is represented by the following equation:

$$V_c = E \cos \alpha_{min} \tag{2.1}$$

where

E corresponds to the peak AC line-to-neutral voltage,

α_{min} is the minimum ignition angle.

The constant extinction angle (CEA) control is a predictive type, that is it uses the measured values of E and I_d to continuously predict the ignition angle α which will produce the desired extinction angle (γ) according to the steady state converter equation:

$$V_c = - E \cos \gamma_{min} + \frac{2X_t}{\sqrt{3}} I_d \tag{2.2}$$

where

γ_{min} is the minimum extinction angle, and

X_t is the transformer leakage reactance or commutating reactance.

The simulation diagram of the CEA is shown in Fig. 2.6 (b).

The raw value of the peak line-to-neutral AC control voltage, E, is obtained by rectifying the transformed line-to-line voltages from the primary-side of the converter transformer. Spikes on the raw value of E can have adverse effects on the firing; they are eliminated by a 2-pole Butterworth filter shown in Fig. 2.7.

The transition from one mode of operation to another is made possible through high-win circuit shown in Fig. 2.4.

Each valve in the converter is modeled separately as an ideal switch in series with a reactance (X_t), where X_t could be the total reactance of the $\frac{dI}{dt}$ reactor and converter transformer or just that of the $\frac{dI}{dt}$ reactor. For example, the current through valve 1 is determined from

$$i_1(t) = \frac{\omega}{X_t} \int v_1 \, dt, \quad i_1(t) \geq 0 \tag{2.3}$$

where

ω is the nominal AC system frequency (377 rad/sec), and

v_1 is the voltage across valve 1 and X_t.

The simulation of a thyristor is shown in Fig. 2.8.

In the linear converter transformer case, the transformer is represented by its leakage reactance X_t.

2.4 Equidistant pulse (EP)

In an equidistant pulse (EP) [48] scheme, a voltage controlled oscillator (VCO) generates the pulses at a rate proportional to the control voltage V_c. The nominal rate for a 12-pulse converter is 12 times the AC system frequency ω.

The VCO drives a 12-stage ring counter and a pulse generator. The block diagram and the corresponding analog simulation of the pulse-phase controls [49] are shown in Fig. 2.9.

The integrator (ramp generator) starts integrating from an initial value

$$V_{IC} = -V_c + \frac{\Delta V}{2} \tag{2.4}$$

to a final value, given by

$$V_{END} = -V_c - \frac{\Delta V}{2} \tag{2.5}$$

where the range ΔV has to be consistent with the slope of the ramp function and the nominal oscillator frequency. For example, with ΔV selected to be 1 volt and the slope 10 volts in a full period of the system frequency, the nominal frequency of the oscillator is 12ω. On reaching V_{END}, the integrator is reset to V_{IC}.

A comparator detects the crossing of the ramp voltage V_r with the control signal V_c. When V_r reaches $-V_c - \frac{\Delta V}{2}$, a firing pulse is generated to turn on the corresponding valve, and also reset the ramp function generator (Fig. 2.10).

During the steady-state, with control voltage V_c at some nominal value, the frequency of the VCO is 12ω ($\omega = 2\pi 60$ radians/second), and α is constant. If I_d drops slightly, the regulator will cause V_c to decrease. This in turn causes the VCO to speed up so that the control pulses occur earlier than before and α is decreased. This decrease in α causes an increase in V_d and a corresponding increase in I_d. After the transients settle, the oscillator frequency returns to 12ω.

When synchronized, V_c is proportional to the firing angle, α. But V_c alone is not enough to synchronize the firings with the AC system voltages; hence the use of the α-loop is required. The α-loop uses a proportional plus integral (PI)

controller [49,50] of relatively slow response to correct any drift of the VCO with respect to the AC system frequency. The measured α is filtered and compared with the output of the primary controller V_c which represents the α_{ref}. Changes in the AC system frequency are taken care of by the voltage V_{22}, which is proportional to the frequency. Both V_{21} and V_{22} are added to form V_2, which represents the slope of the ramp function.

2.5 Transformer saturation

Some of the studies were performed with a linear transformer representation to isolate the effect of transformer saturation. In the linear representation of the transformer, only the leakage reactance is represented. In the nonlinear transformer, both the saturable magnetizing inductance and the unsaturable leakage inductances are represented. A two-slope piece-wise linear approximation of the magnetizing characteristic has been adopted because it has been previously shown to be sufficiently accurate for this type of transient study. The block diagram showing the simulation is given in Fig. 2.13. Typical of large power transformers, the slope of the linear portion is very steep while the slope of the saturated portion is almost flat. The magnetizing reactance in the unsaturated region is selected to be very high ($X_m = 10.5K\Omega$), and in the saturated region low ($X_m = 10.5\Omega$). Both values are on 2000 MVA and 230 KV base. The knee-point has been selected to be at rated terminal voltage.

2.6 AC network representation

The AC networks on both sides of the DC link are represented by their Thevenin equivalents. The rectifier is fed from a relatively strong AC system with an SCR of 10 and operates under the inverse cosine control firing scheme.

In this study, the inverter simulation operates with either an inverse-cosine or a pulse-phase firing scheme; nominal AC support has an ESCR of 3.97 and a damping angle of 75.33° (base case).

In this study, the strength of the AC support to the inverter is varied above and below the nominal value, with the corresponding Thevenin impedance Z_{th} computed from

$$Z_{th} = \frac{3V^2}{ESCR\ P_d} \tag{2.6}$$

The damping angle is kept constant at 75.33° for all ESCR values used.

From Eq. (2.6), we see that as the ESCR decreases, Z_{th} increases. The increase in Z_{th} would result in large reactive voltage drop across Z_{th}, resulting in poor voltage regulation, where

$$\text{voltage regulation} = \left(\frac{E_{th} - V}{V}\right) 100\%. \tag{2.7}$$

Large fluctuation of the voltage following a variation in the DC current could cause commutation failures which, if repeated could lead to a complete collapse of the AC and DC system unless the bridge is disconnected.

2.7 DC network representation

In this case, the DC network is just a long transmission line; it is represented by three T-sections to give a better approximation of the actual line behavior (Fig. 2.14). A smoothing reactor and a set of DC filters are connected to each end of the DC line. The smoothing reactor helps to reduce the ripples on the DC current, limit the rate of rise of the DC current during faults, and prevent discontinuous conduction [46]. The set of DC filters consists of a filter tuned to the sixth harmonic, a high-pass filter tuned to the twelfth and another tuned to the nineteenth harmonic.

2.8 Static VAR compensation

In this study, two main types of static VAR compensators were examined:

- the thyristor-controlled reactor (TCR), and
- the thyristor-switched capacitors (TSC).

These two types are quite different in their operation and simulation [51-55].

2.8.1 Thyristor-controlled reactor (TCR)

A TCR is a reactor in which the current is switched on at a specific time and off when it reaches zero.

A delta configuration is used to obtain third harmonic cancellation. Figure 2.15 (a) shows a single-phase TCR. The thyristors are back-to-back and are controlled independently while they share the same main control and the same shaping function (Fig. 2.15 (b)). Since the controls of the TCR depend highly on the zero-crossings of the supply voltage, a four Butterworth filter of the type

$\frac{4}{(1+\frac{s}{\omega})^4}$ is used in the control loop to filter out the higher harmonics riding on the supply voltage.

The main blocks in the TCR simulation are (Fig. 2.16):

- the main control,
- the shaping function, and
- the firing scheme.

The main control is basically a proportional-plus-integral (PI) type of controller where a measured variable (V, $\sin\phi$, or I_D) is compared to its reference value. The error drives the PI, whose gains are given in Table A5. When full conduction or zero current is attained, the PI is saturated. To avoid drifting of the integrator used in the PI, the output is fed back. The output of the PI, I_r, is allowed to vary between 0 and 5 Volts, corresponding to $\alpha = 0^\circ$ and $\alpha = 90^\circ$, respectively.

A shaping function, SF, is used to provide a linear relationship between the required TCR current and the firing angle α. This is basically a relationship which represents the relation between the fundamental TCR current and the firing angle α, given by

$$I_r = 1 - \frac{2\alpha}{\pi} - \frac{\sin 2\alpha}{\pi} \tag{2.8}$$

for α ranging from 0 to 90° (with respect to the corresponding peak of the phase voltage). With $I_r = 0$ per unit (pu), $\alpha = 90$, whereas for $I_r = 1.0$ per unit, $\alpha = 0$ (Fig. 2.15 (d)). Solving this transcendental equation for α on the analog computer requires the use of sine/cosine and multiplier units. Some of these introduce inaccuracy around the singular value of $\alpha = 90^\circ$. This is avoided in the simulation by not forcing the TCR current to zero at turn off, corresponding to $\alpha = 90^\circ$, but instead allow for some small but negligible value of current to flow.

The firing instant is determined by a pedestal-ramp scheme, where the pedestal value corresponds to the output of the regulator and the ramp has a constant slope. The ramp is initiated at the zero-crossing of the corresponding Δ-phase voltage. When the ramp reaches the ceiling of 10 volts, a firing pulse is generated to fire the specific valve and to reset the ramp function generator. A new ramp is generated one period later. The slope of the ramp function is kept constant. It is selected such that when the initial value is zero (corresponds to

α=90°), the ramp hits the ceiling in half a period [53]. This way, α is kept within the limits described.

The following sections describe the following common control functions used in the TCR:

- the terminal voltage control
- the power factor control, and
- the direct-axis current control.

2.8.1.1 Terminal voltage control

In this control mode, the reactive current drawn by the TCR is adjusted continuously to regulate the terminal voltage V close to some reference value V_{ref}. The measurement of the terminal voltage is achieved through rectification and filtering. For stable operating condition, a small slope allowing for few percent regulation of the terminal voltage is used.

The magnitude of all the capacitor currents (including the filters), I_c, and that of the TCR current, I_L, are both measured in a similar manner as the terminal voltage V. The voltage error, $V_{ref} - V$, is compensated by the difference in current, $X_{slp}(I_L - I_c)$, to give a small steady-state slope of 5%. Figure 2.17 shows the V-I characteristic of a TCR alone. Figure 2.18 shows the steady-state characteristic of a TCR in parallel with a fixed capacitor. Below point A, the TCR is blocked (no TCR). At point B, a complete cancellation of the capacitor VAR output is achieved. At point C, the TCR is fully on. Beyond point C, the reactor operates as a plain reactor (with a constant reactance assuming a linear reactor).

2.8.1.2 Power factor control

Here the control objective of the TCR is to regulate the power factor as seen by the AC source at the terminal bus. The power factor is computed from the real and reactive power, P_s and Q_s, respectively. P_s and Q_s are computed by first transforming the phase quantities, V and I_s, to stationary reference frame components [56].

As the power factor, $\cos\phi$, is usually close to unity, the $\frac{d\cos\phi}{d\phi}$ variation about the nominal operating condition is small and results in a poorly defined operating point. Around the nominal operating condition, $\sin\phi$ is a closer approximation to the power factor angle ϕ, it changes sign along with ϕ and has

a more linear relationship with ϕ; hence we chose to regulate $\sin\phi$ instead. It is computed from the following equation

$$\sin\phi = \frac{Q_s}{\sqrt{P_s^2 + Q_s^2}} \tag{2.9}$$

The simulation block diagram for computing $\sin\phi$ is shown in Fig. 2.19.

2.8.1.3 Direct-axis current control

The current I_s could be resolved into DQ components, where I_Q is the quadrature-axis current and I_D is the direct-axis current, respectively. I_Q is in phase with V and I_D is 90° lagging or leading V. Track-and-store (TS) amplifiers were used to measure I_D. As the current I_s crosses zero and goes positive, TS1 tracks I_s while TS2 stores the old value of TS1 [45]. Then when the voltage V crosses zero and goes positive, TS1 changes to the store mode, storing the I_s value while TS2 continues to track the output of TS1. The average of the track-and-store output from all 3 phases is used as the controlled variable.

2.8.2 Thyristor-switched capacitor (TSC)

A single-phase switched-capacitor (TSC) is shown in Fig. 2.21. It basically consists of a capacitor C1, two back-to-back thyristors and a small reactor L. The reactor is used to limit the surge current during switching under abnormal conditions. In some cases, it is used to avoid resonance with the system impedance at some specific harmonic [23,55].

If the applied voltage is

$$v = V\sin\omega t, \tag{2.10}$$

then the steady-state current can be written as

$$i = V\,\frac{n^2}{n^2 - 1}\,\omega C\,\cos\omega t \tag{2.11}$$

where

$$n = \frac{1}{\sqrt{LC1}}. \tag{2.12}$$

The thyristor switches off at zero current, whereupon the capacitor is left charged to its peak voltage. In practice, it is allowed to discharge slowly. The

voltage across the thyristors varies between zero and the peak-to-peak value of the applied voltage. To minimize the transient disturbance, usually the capacitor is switched on at a time when the voltage across the switch (thyristors) is zero.

2.8.3 TCR-TSC operation

A basic TCR-TSC combination is shown in Fig. 2.22. The particular combination shown, and also simulated, consists of a TCR and two TSC connected to the same bus (through transformers in general). The function of the TCR-TSC is to provide rapid and continuous inductive or capacitive compensation over a wide range.

The operation of a TCR-TSC is as follow. The switching of the TSC depends on the TCR current; when the TCR current reaches zero, an order is sent to the TSC to switch-off, and when the TCR current is close to its rated value, an order signal is sent to switch in another TSC. The current in the TSC should always be in excess in order to keep the TCR in its operating range. To avoid chattering (switching-in and -off), hysteresis is used (Fig. 2.23); the switching-in time and the switching-off time are clearly defined, and no overlap can occur.

The combination is used to reduce the TCR size and to reduce losses due to the use of a large TCR in the absence of a TSC. Power losses in a TCR are mainly due to the resistance of the reactor, the switching process, and the losses in the thyristor controller, and they increase with the TCR current. Losses associated with the TSC are of constant magnitude and are due to the surge reactor resistance (Fig. 2.24) [23].

In this simulation, the TCR was simulated in the EAI-680, and the TSC was simulated in the power system simulator.

When an order to switch in a TSC arrives, the switching process waits until the computed voltage across the thyristor is zero; only then does the switching-in occur. To avoid too large an initial voltage across the thyristor, a reduced value of the voltage across the TSC capacitor is compared with the supply voltage. During the switching-off process, the capacitor is switched-off only when its current croses zero, and this occurs independently for each phase.

In this case, two TSC were simulated, each with capacity corresponding to 20% of the total capacitance on that bus.

2.9 Bypass valve representation

When a commutation failure persists or a valve fault occurs, it may be necessary to disconnect the inverter. This is achieved by blocking the inverter, effected simply by inhibiting the firing pulses to the inverter valves. The DC current is then diverted to a bypass valve, BV [46,57,58], before the inverter is disconnected from the AC and the DC networks.

When an inverter is to be blocked, a signal is sent to turn off the main valves and to turn on the BV. During inverter operation, with the DC voltage across the bypass valve forward biased, the unblocking of the BV is made possible simply by applying a firing pulse to its gate. When the BV turns on, the DC voltage becomes zero, and a commutation process between the BV valve and the main converter valves starts [46]. The bypass valve creates a short-circuit on the DC side and hence prevents the DC current from entering the converter. Each converter has a bypass valve across its DC terminals.

Figure 2.25 (a) shows that the bypass across the DC inverter terminals is represented by a switch. When this switch is open, the inverter operates normally; when it is closed and the inverter is blocked, the BV is operating. Figure 2.25 (b) shows the analog simulation of the bypass valve used in this study. The BV is simulated like the thyristor valves of the inverter with a very small series inductance L_{d1} of 11 μH. To incorporate the bypass valve simulation into the DC side simulation, the smoothing reactor is split into two components L_{d1} and L_{d3}, where $L_{d3} = 1.18$ mH and $L_d = L_{d1} + L_{d3} = 1.191$ mH.

2.10 Steady-state results

As shown in Fig. 2.5, at the nominal operating point T the rectifier is controlling the DC current I_d, and the inverter is controlling the extinction angle γ. The simulation results for balanced AC voltages at both the rectifier and the inverter ends. Those with the the inverter operating under the inverse cosine-control firing scheme are given in Fig. 2.26, and those with the inverter operating under the pulse-phase control firing scheme are given in Fig. 2.27. With either firing scheme, the operating point was stable. Due to non-ideal AC voltage waveforms, and incomplete filtering, harmonic distortions on the AC bus voltages can be seen.

The inverter operating under either firing scheme was stable down to an ESCR of 1.5. At the lower ESCR, the fluctuations of the terminal voltage were large and accompanied by similar variations in the DC current I_d. Below an

ESCR of 1.5, and with the basic controls, the inverter could not operate stably with either firing scheme; the controls would have to be modified for stable operation.

To validate the simulation, the measured values of V_d, I_d, μ, ... from the simulation were cross-checked against those computed from a steady-state load flow, where the average-model [46] was used for the converter. Moreover, the characteristic harmonics were also measured and compared with the theoretical ones. The conclusion is that they both agree; hence, the modeling and simulation were validated.

Steady-state operation waveforms of the TCR are shown in Fig. 2.30. Figures 2.30 (a), (b), (c), (d), and (e) correspond to firing angles of 0°, 18°, 36°, 54° and 78°, with an ideal AC voltage supply applied to the TCR. They show how the shape of the TCR current is changing with the firing angle. The magnitudes of the characteristic harmonic currents were measured and compared with the theoretical ones given in [23]. The results also agree.

2.11 Conclusion

The detailed simulation of a sample AC/DC system was successfully realized on the power system simulator and the EAI-680 analog computer. Two common firing schemes for the inverter were implemented. The simulation was validated by steady-state load flow calculations based on the average-value model of the converters. Some steady-state waveforms of the system from the simulation were presented.

This chapter also dealt with the techniques used to simulate the nonlinear magnetization characteristics of the converter transformer, the thyristor-controlled reactor, the thyristor- switched capacitors, and the bypass valves.

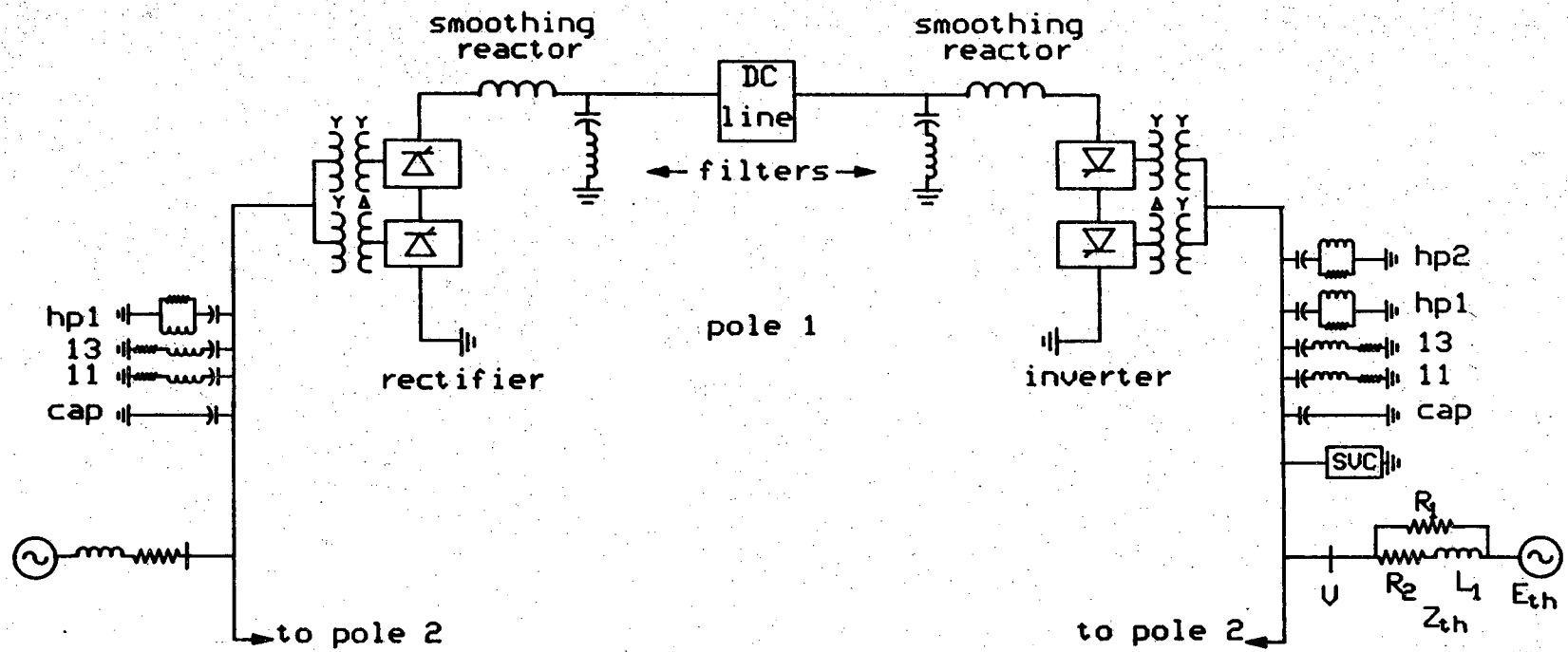

Figure 2.1 Simplified AC/DC system

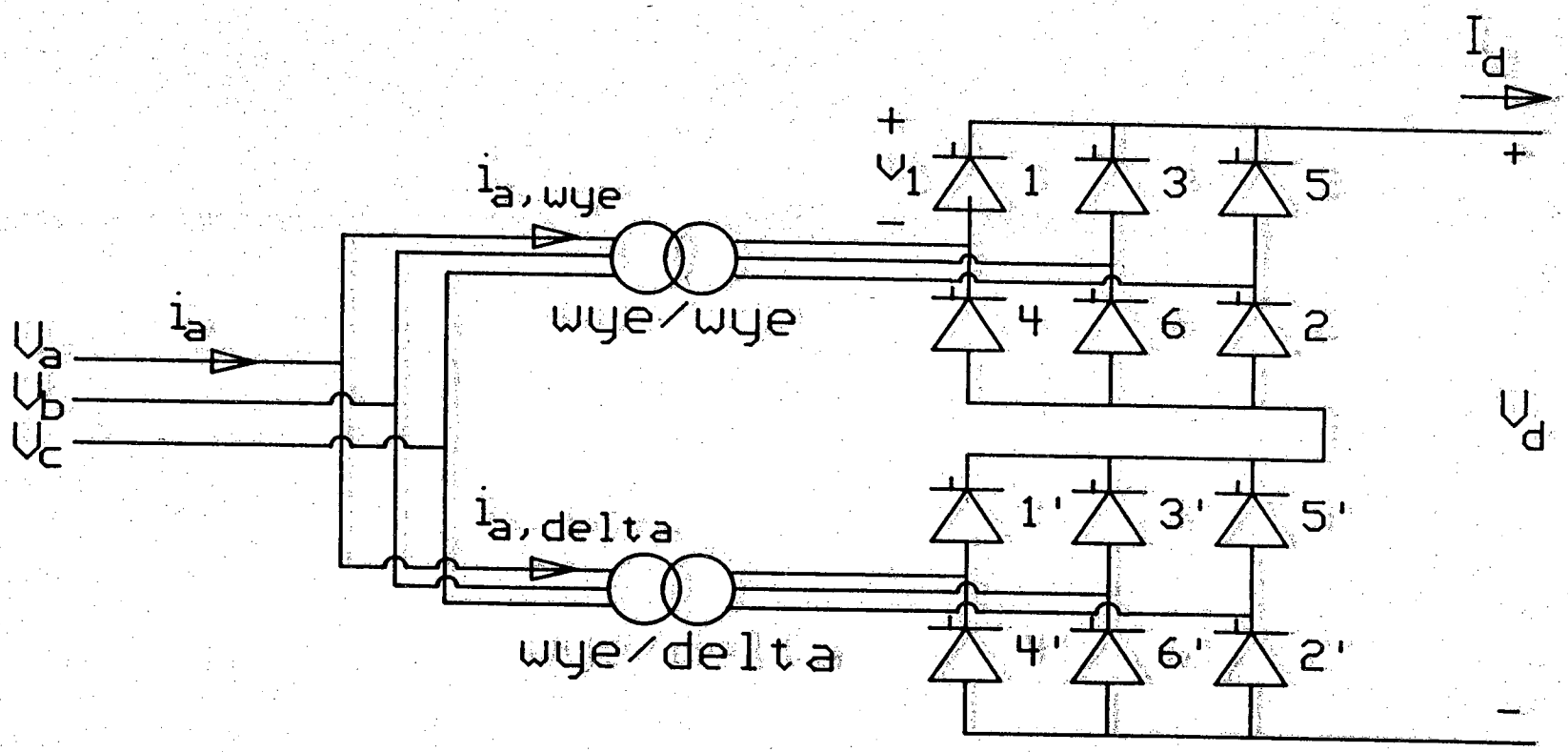

Figure 2.2 Twelve-pulse converter bridge

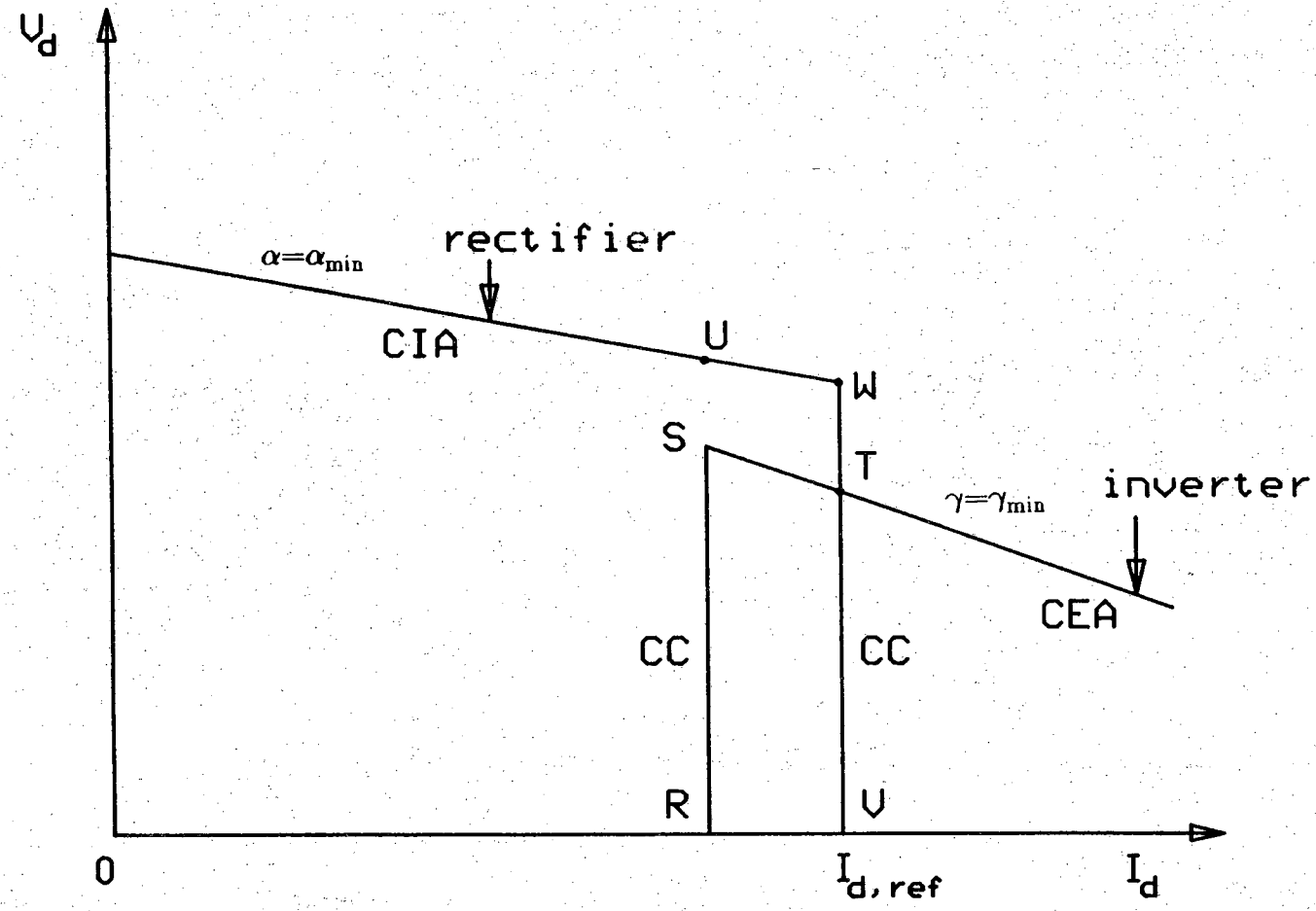

Figure 2.3 Control characteristics of a DC link

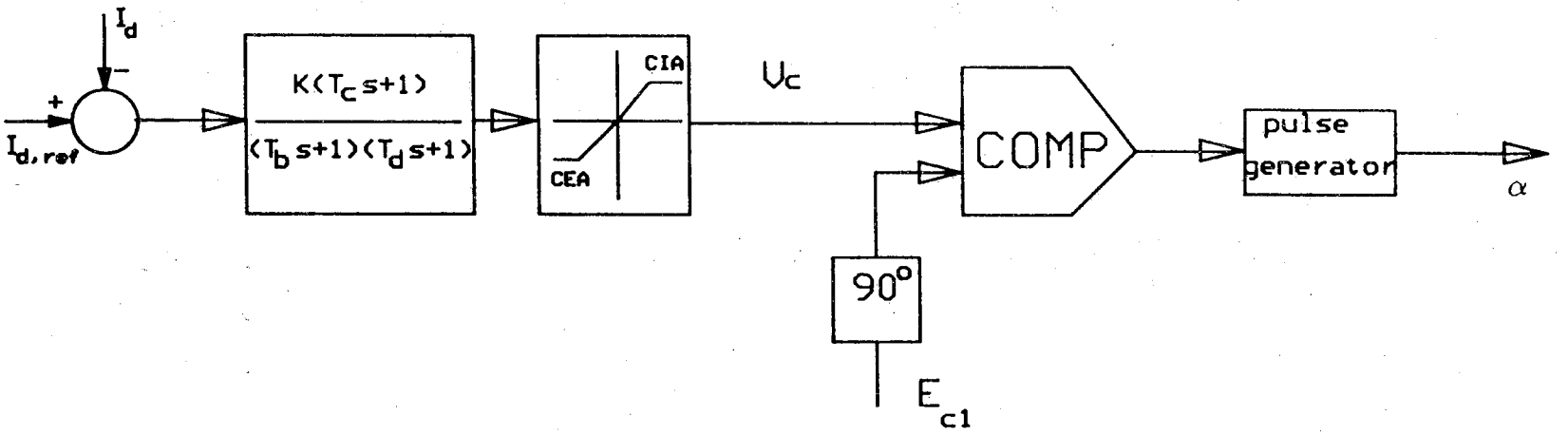

Figure 2.4 Control pulse generator

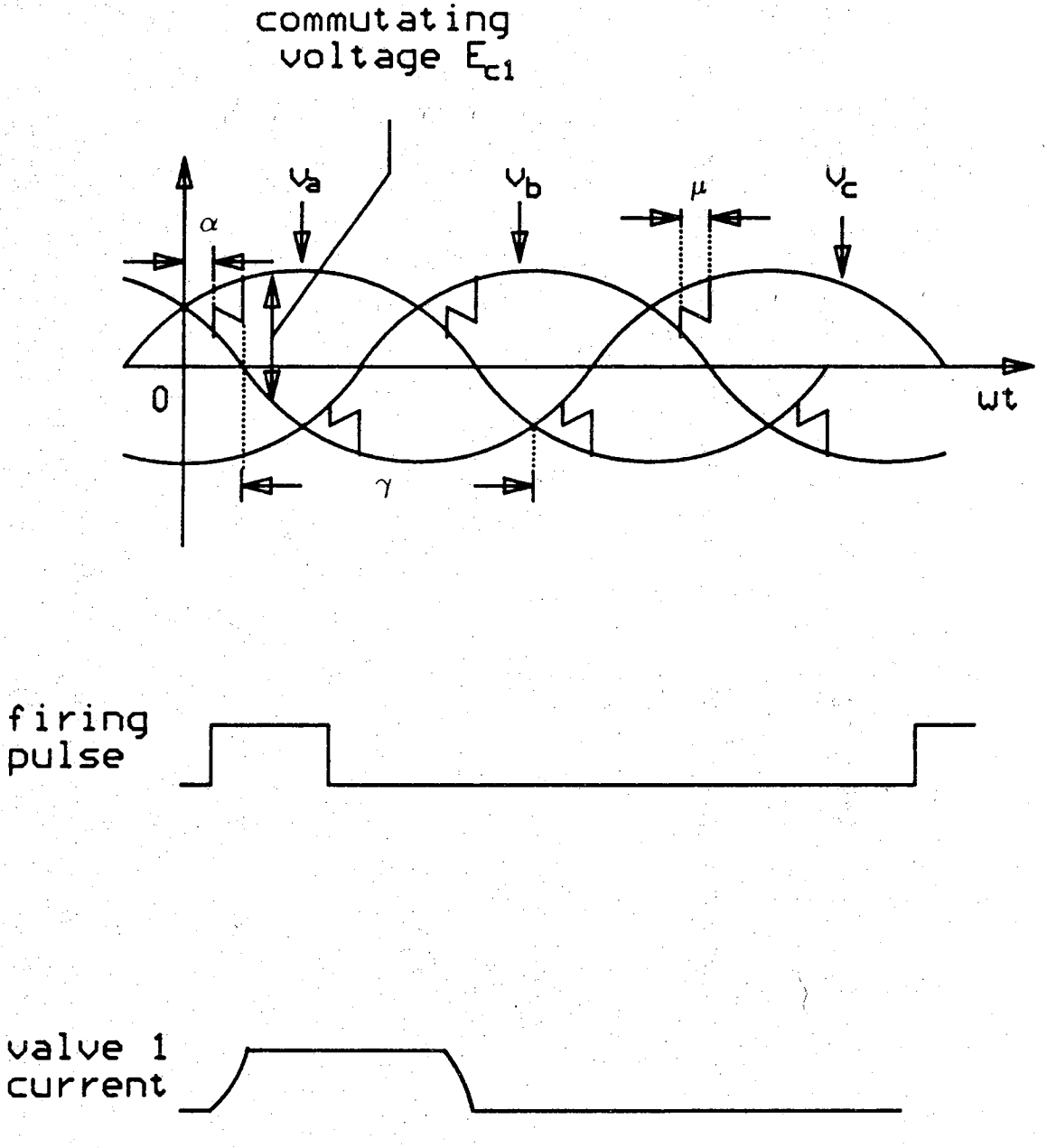

Figure 2.5 Six-pulse waveforms

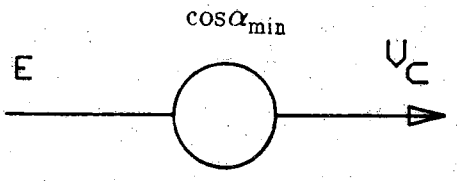

(a) Constant ignition angle (CIA) control

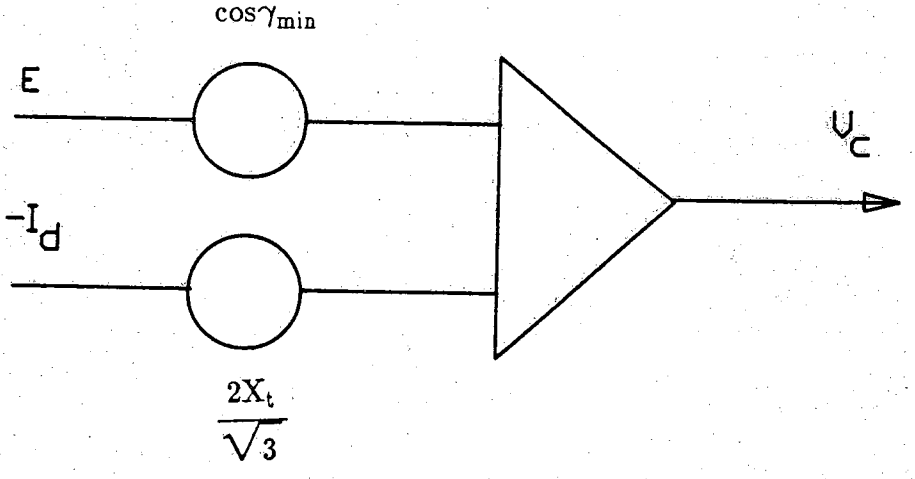

(b) Constant extinction angle (CEA) control

Figure 2.6 Ignition and extinction angle control circuits

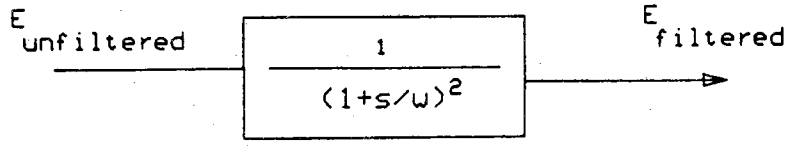

(a) Block diagram

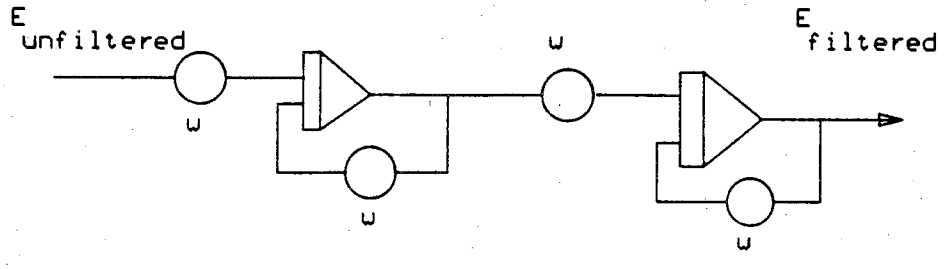

(b) Analog simulation

Figure 2.7 Control filters

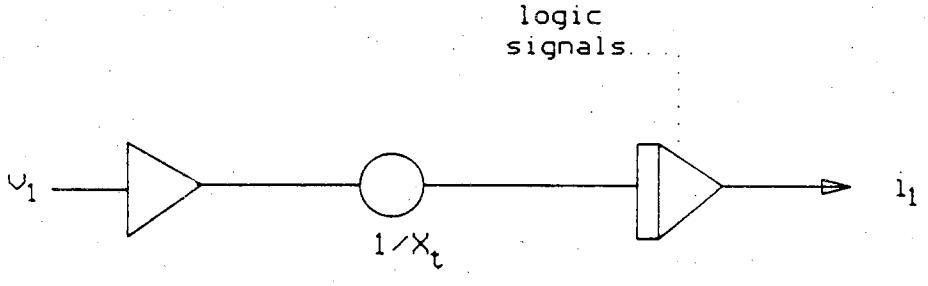

Figure 2.8 Analog simulation of a thyristor

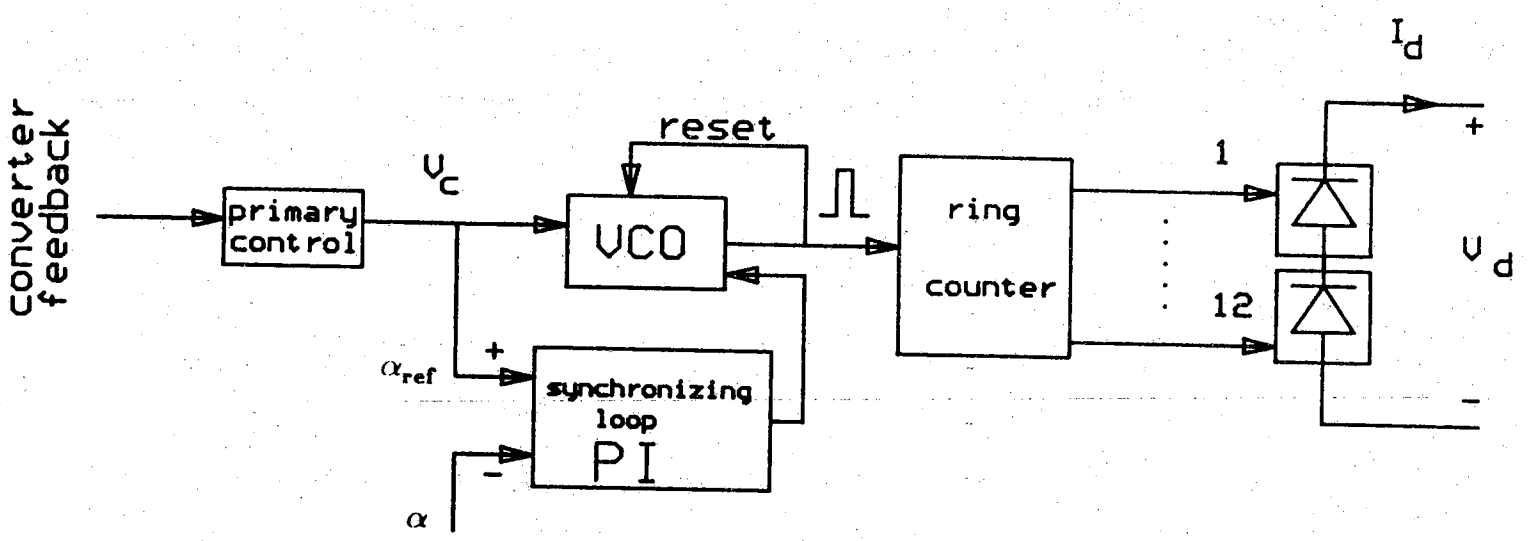

(a) Block diagram

Figure 2.9 Pulse phase control

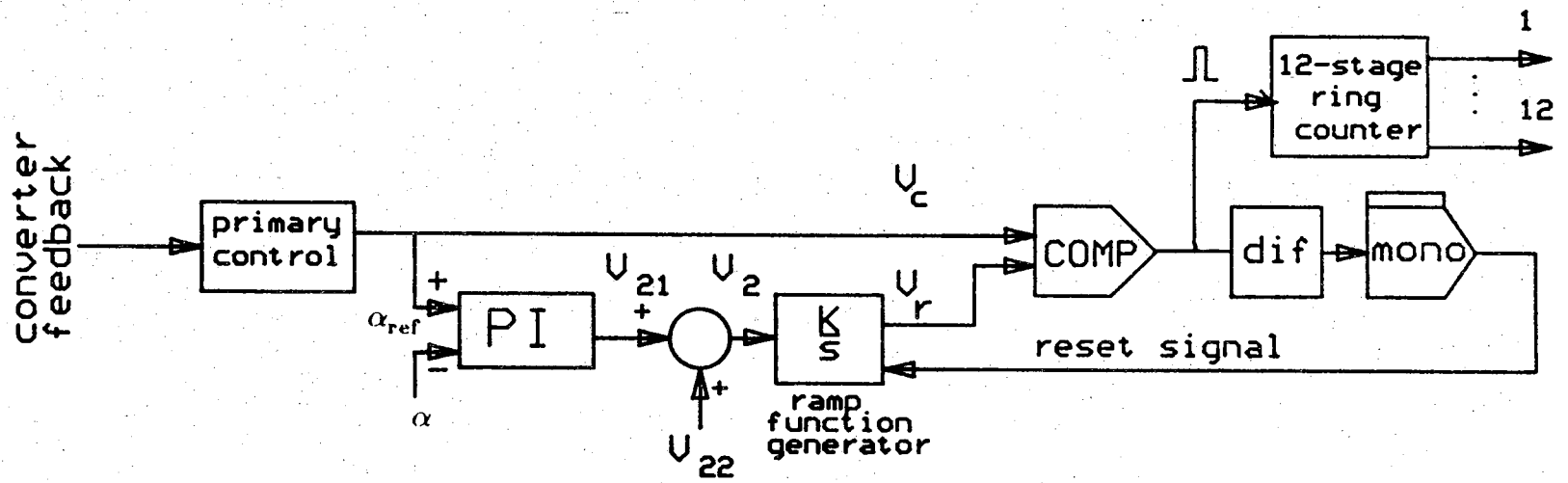

(b) Analog simulation

Figure 2.9 continued

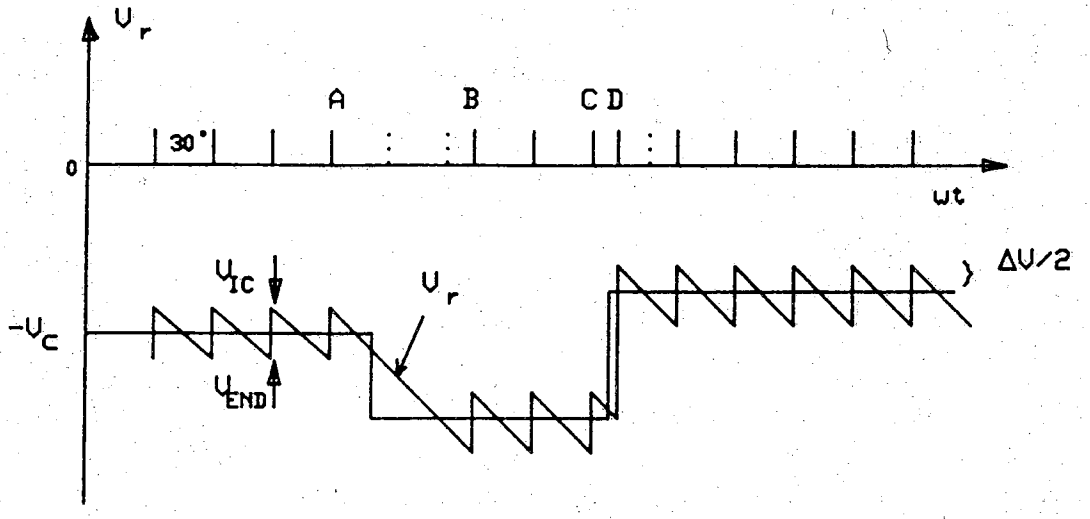

Figure 2.10 Operation of a pulse phase control

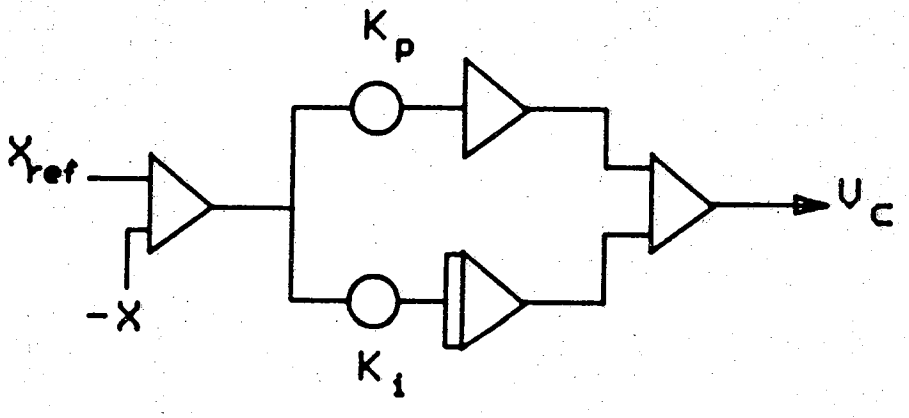

Figure 2.11 Analog simulation of a proportional plus integral compensator

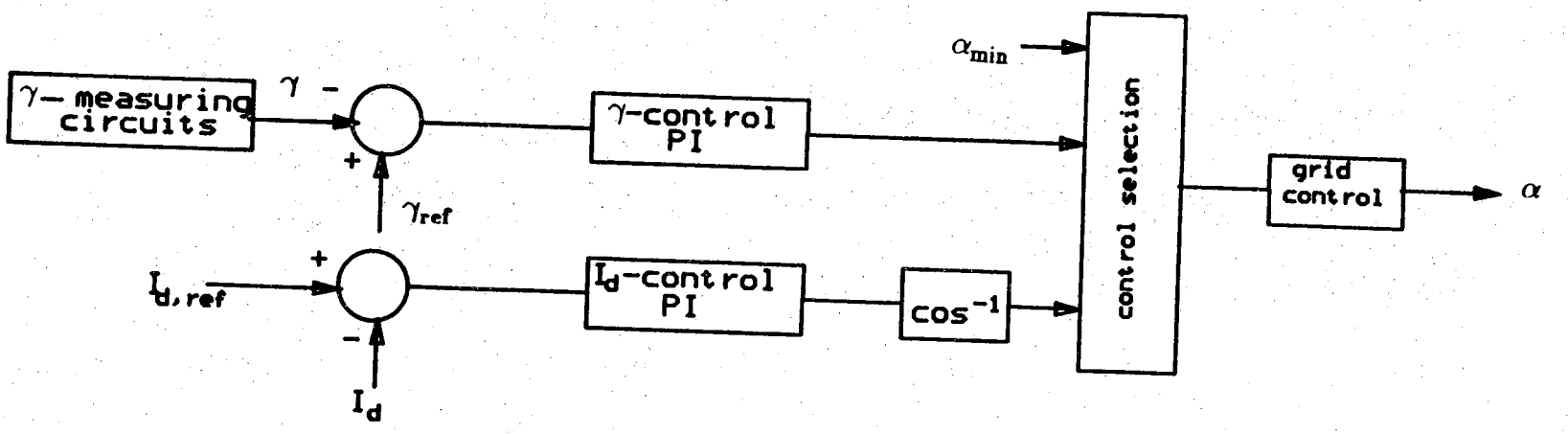

Figure 2.12 Block diagram of the primary controls

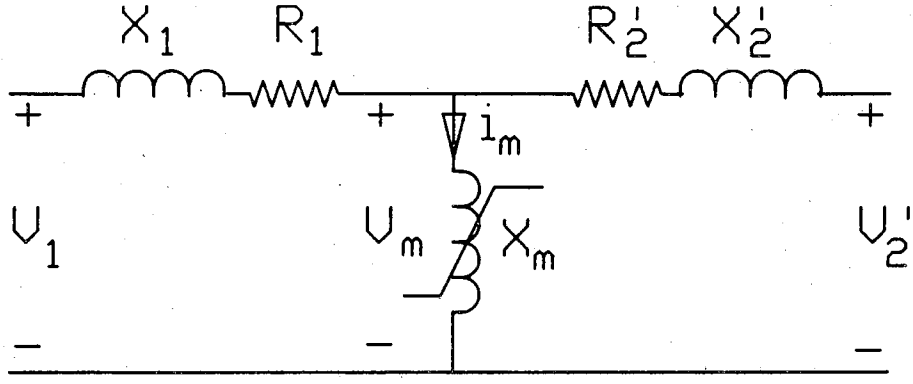

(a) equivalent circuit

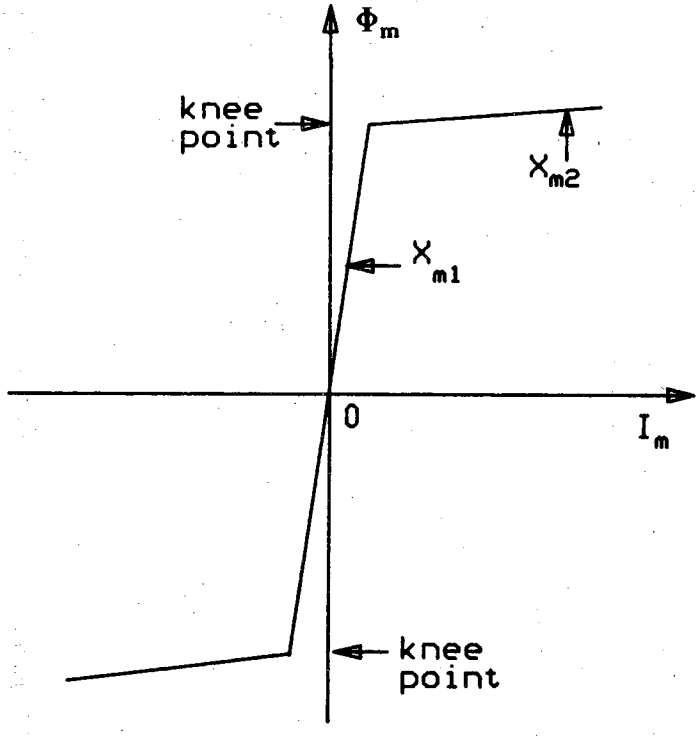

(b) saturation characteristic

Figure 2.13 Transformer saturation

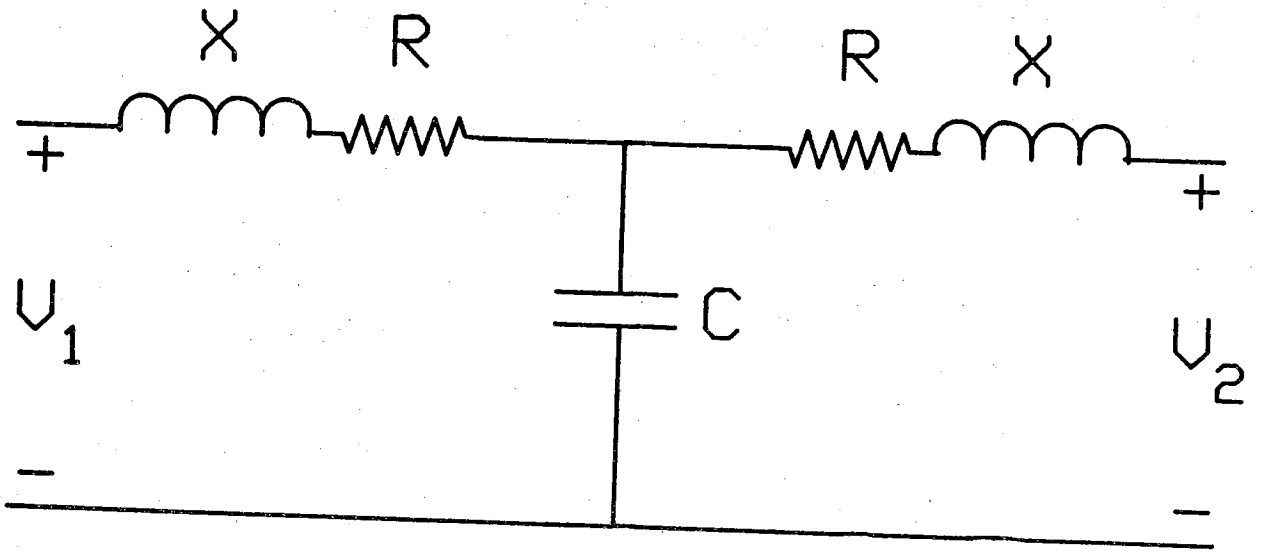

Figure 2.14 One T-section representation of the DC line

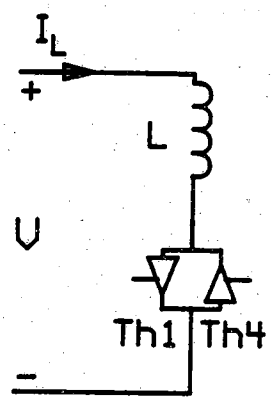

(a) Basic circuit

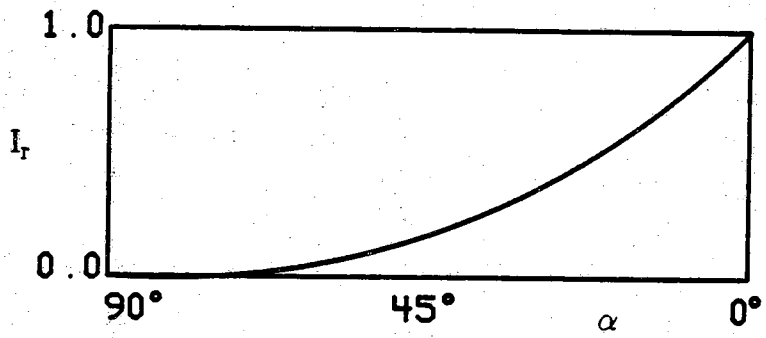

(b) Current and firing angle relationship

Figure 2.15 Thyristor-controlled reactor (TCR)

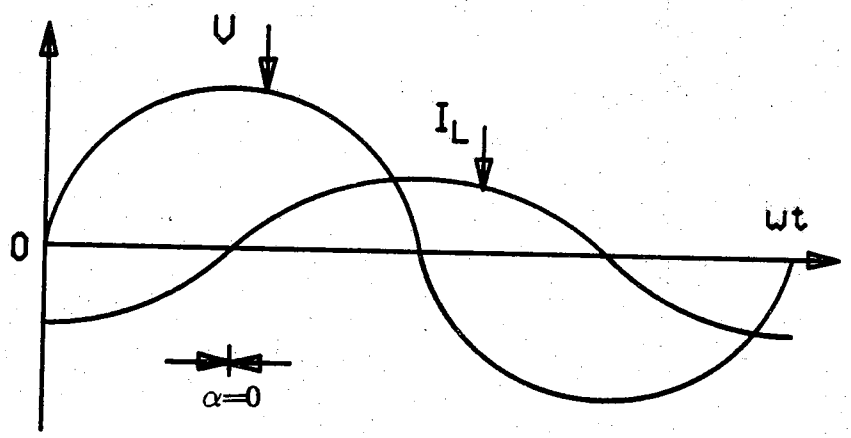

(c) Voltage and current waveforms for a TCR operating with $\alpha = 0$

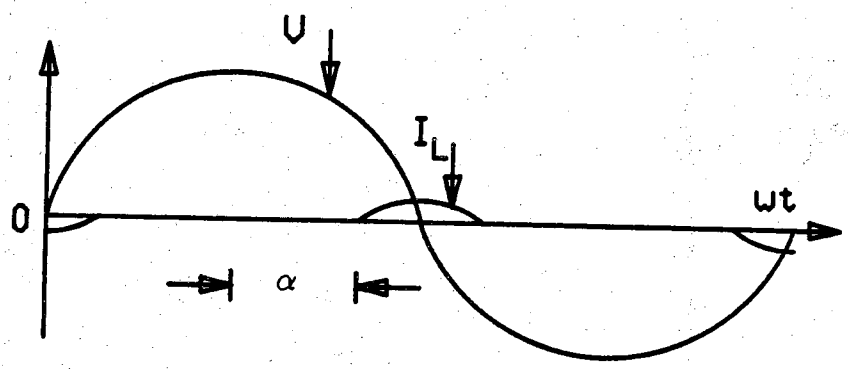

(d) Voltage and current waveforms for a TCR operating with $\alpha > 0$

Figure 2.15 continued

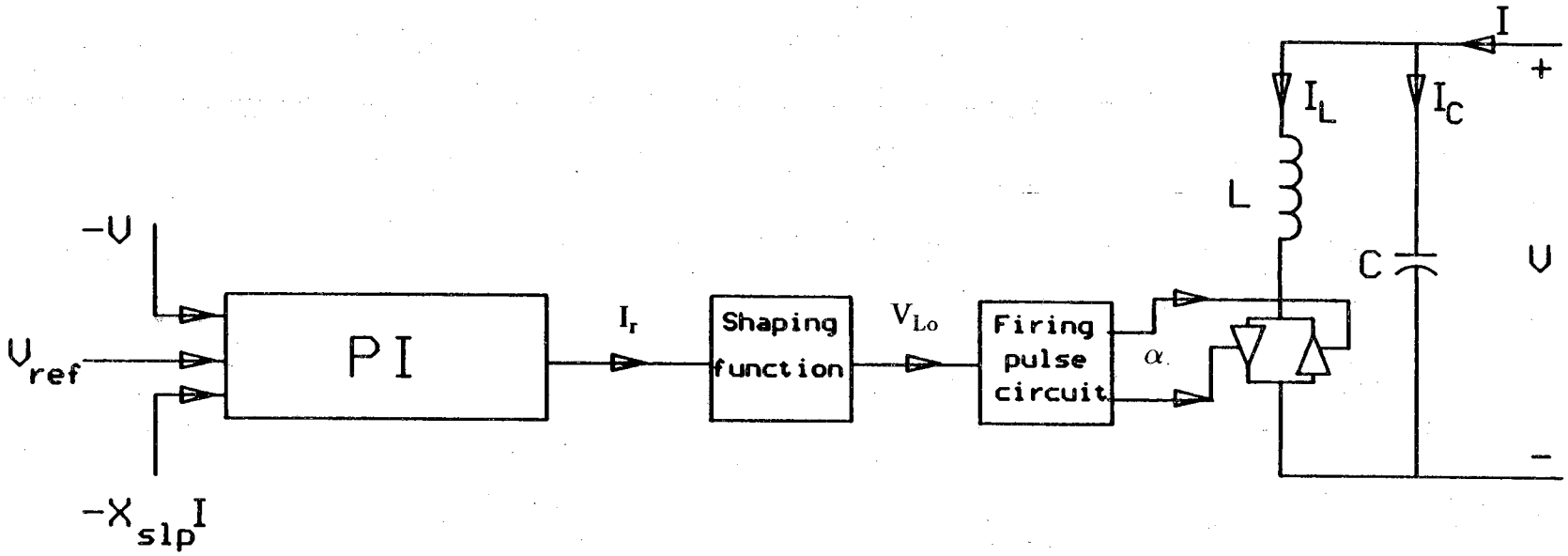

Figure 2.16 Thyristor-controlled reactor (TCR) control

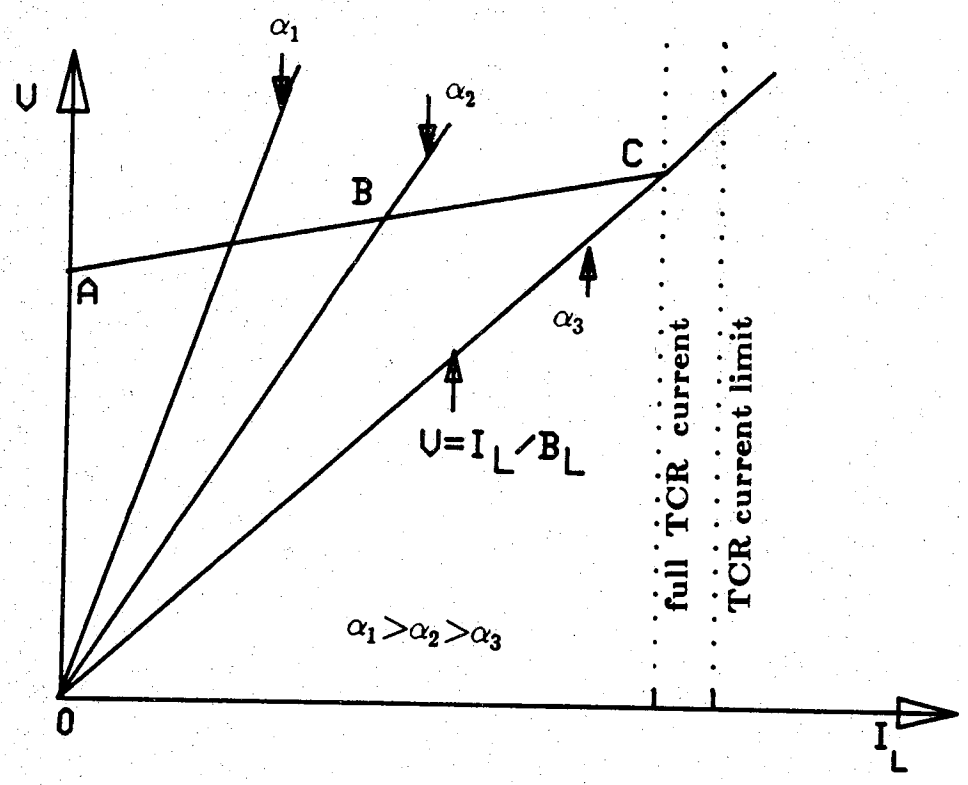

Figure 2.17 Voltage-current characteristic of a TCR

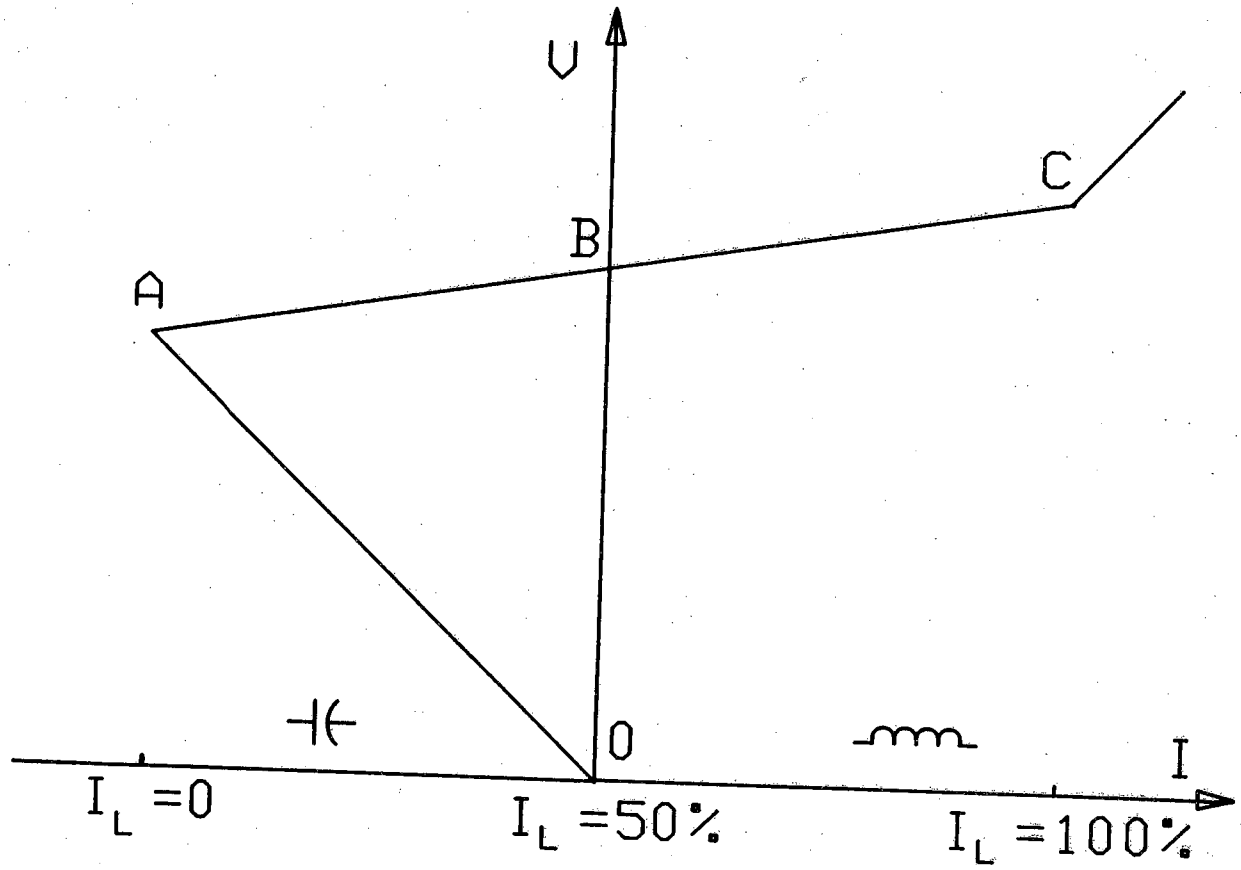

Figure 2.18 Voltage-current characteristic of a TCR and a fixed capacitor

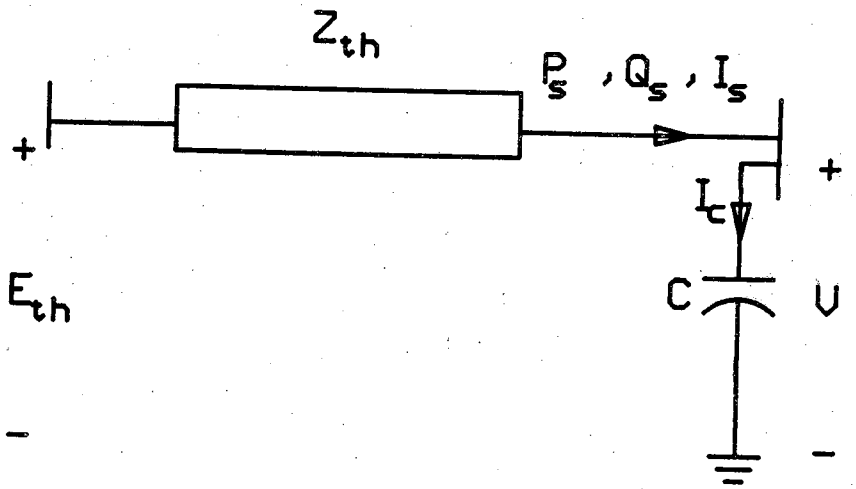

(a) Circuit

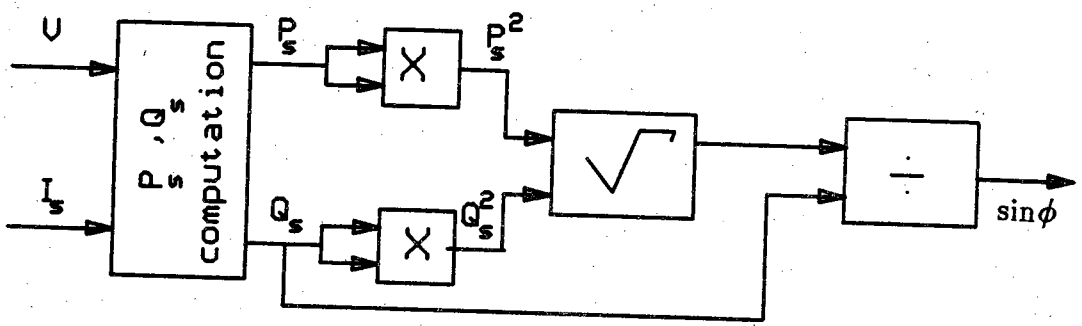

(b) Simulation of $\sin\phi$

Figure 2.19 Power factor simulation

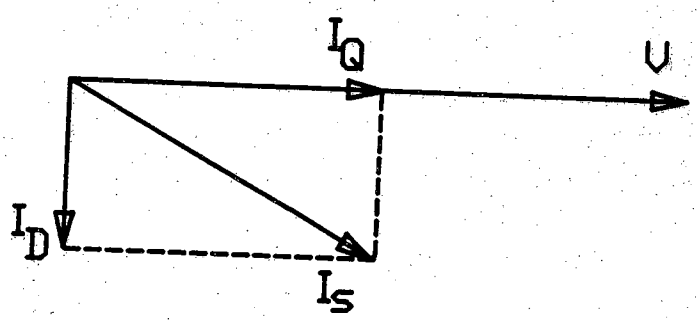

(a) Phasor diagram

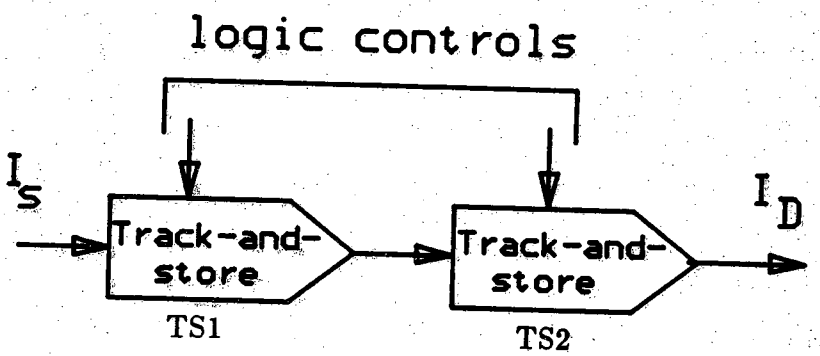

(b) I_D measurement (per phase)

Figure 2.20 Direct-axis current I_D control

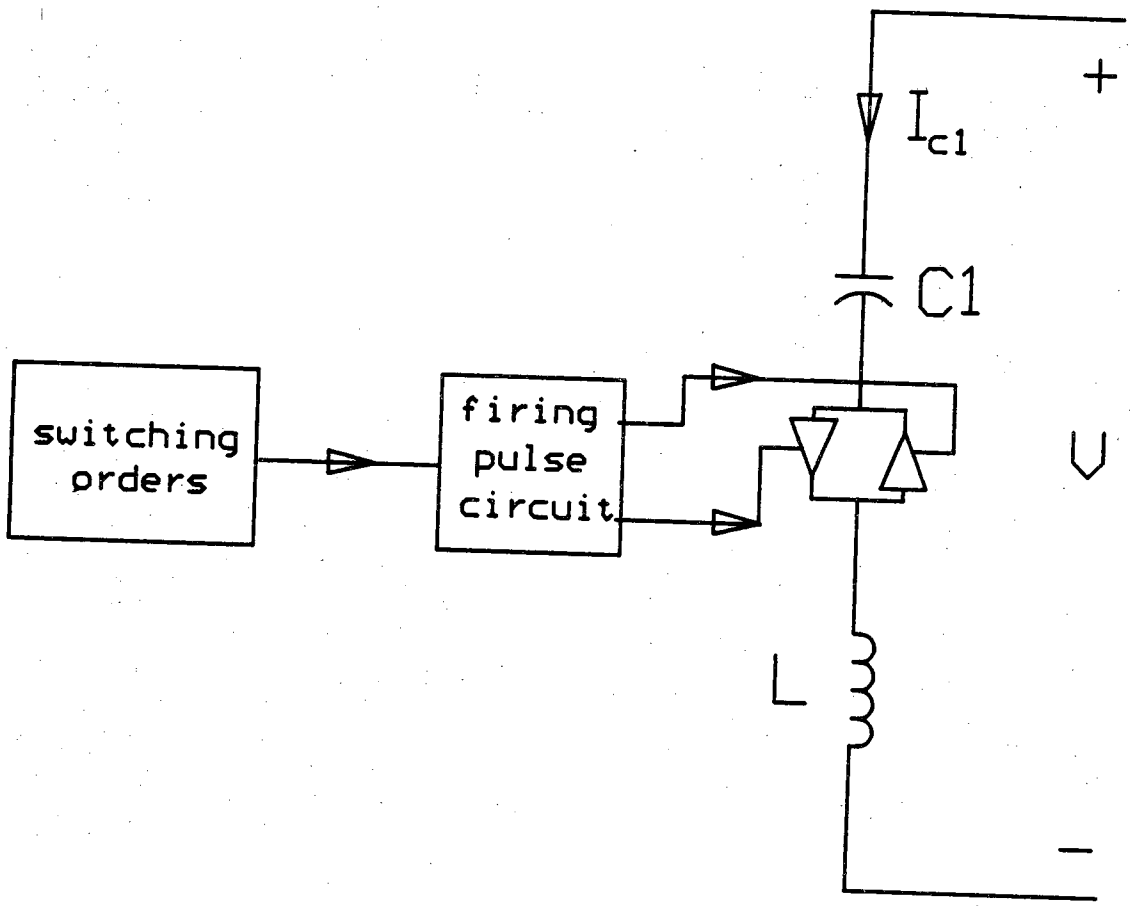

Figure 2.21 Basic circuit of a thyristor-switched capacitor (TSC)

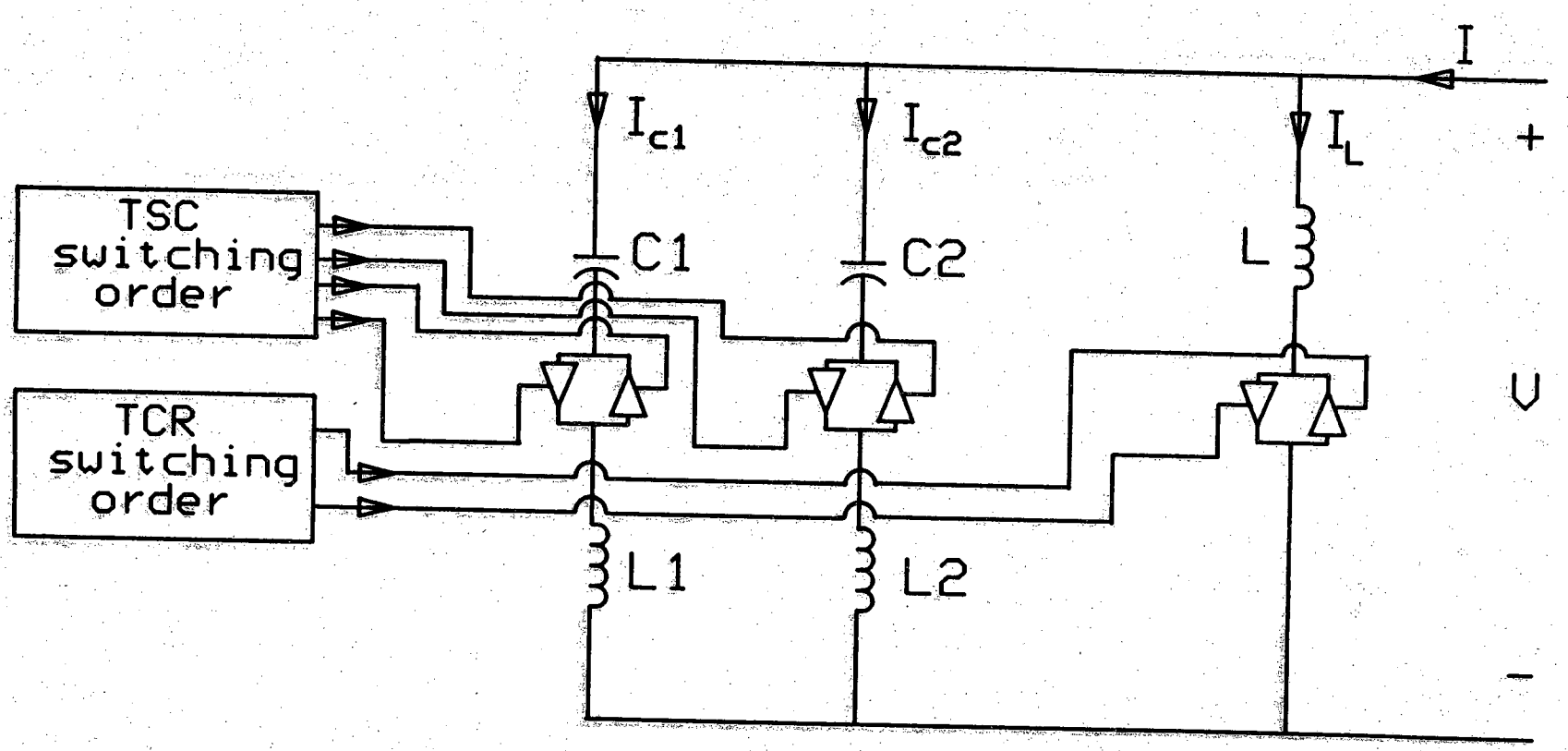

Figure 2.22 Control circuit for TSC-TCR

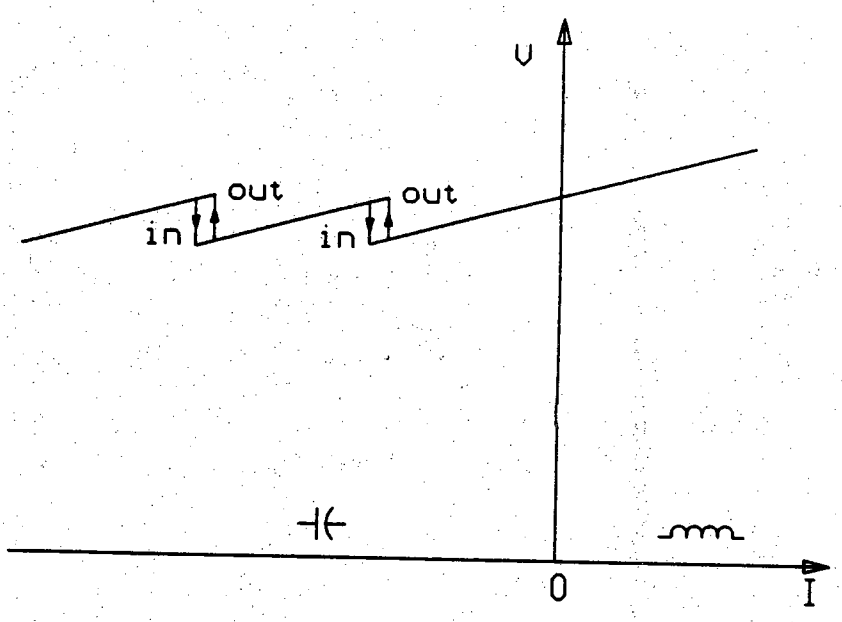

Figure 2.23 Voltage-current characteristic of a TSC-TCR

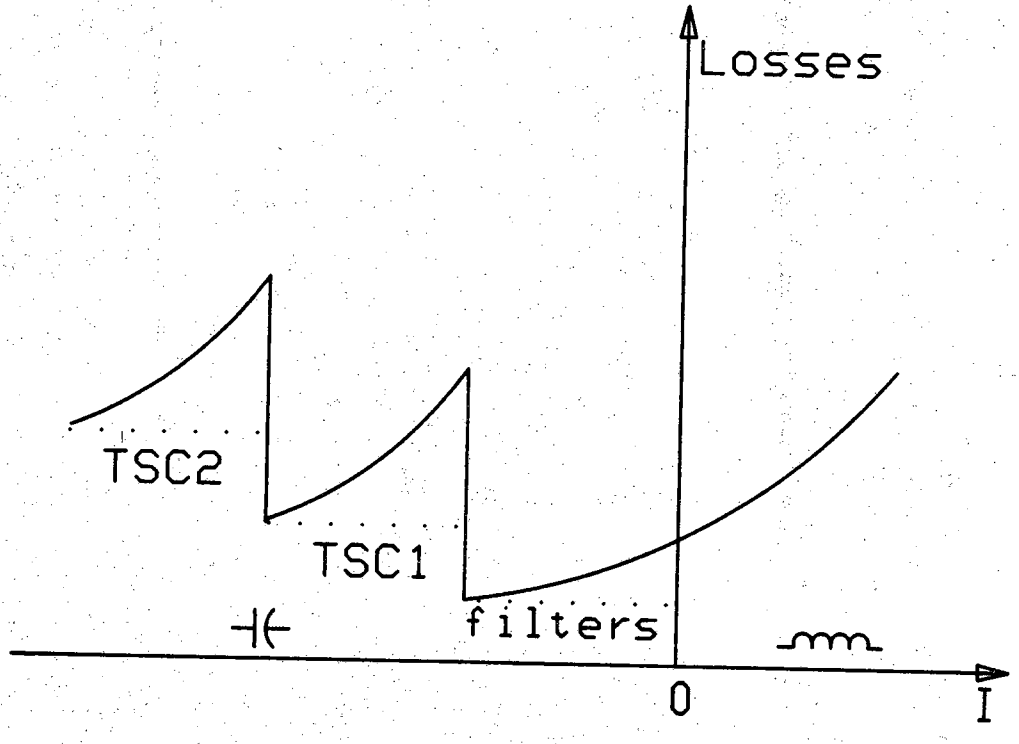

Figure 2.24 Losses associated with a TSC-TCR circuit

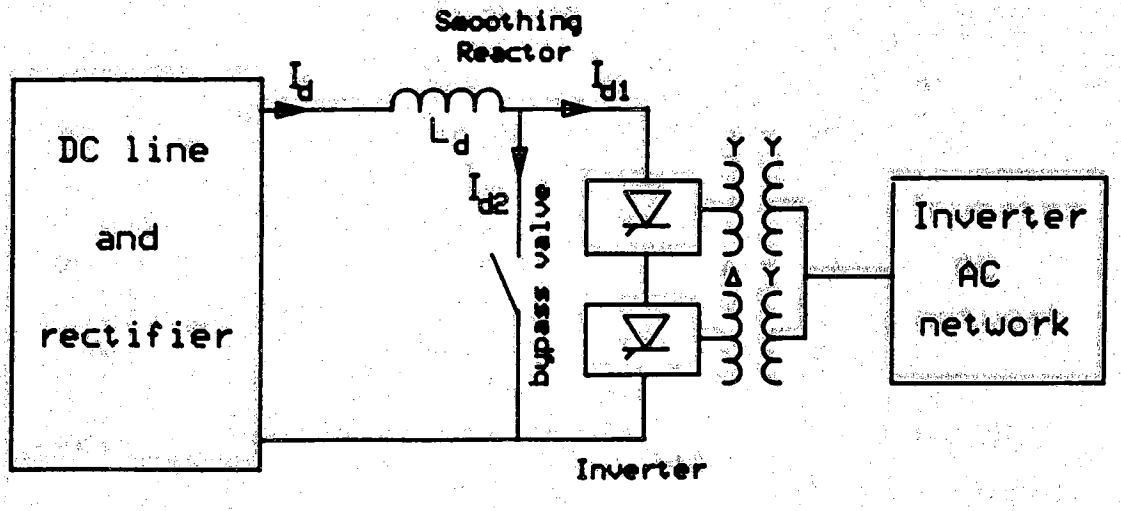

(a) Circuit diagram

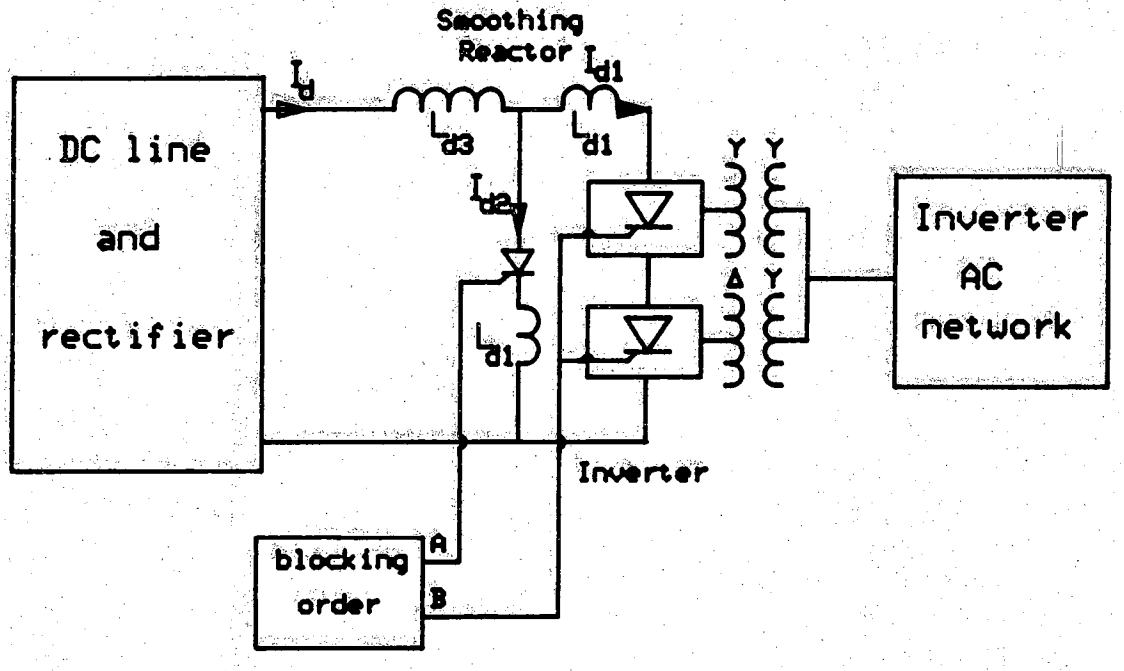

(b) Simulation diagram

Figure 2.25 Bypass valve for blocking the inverter

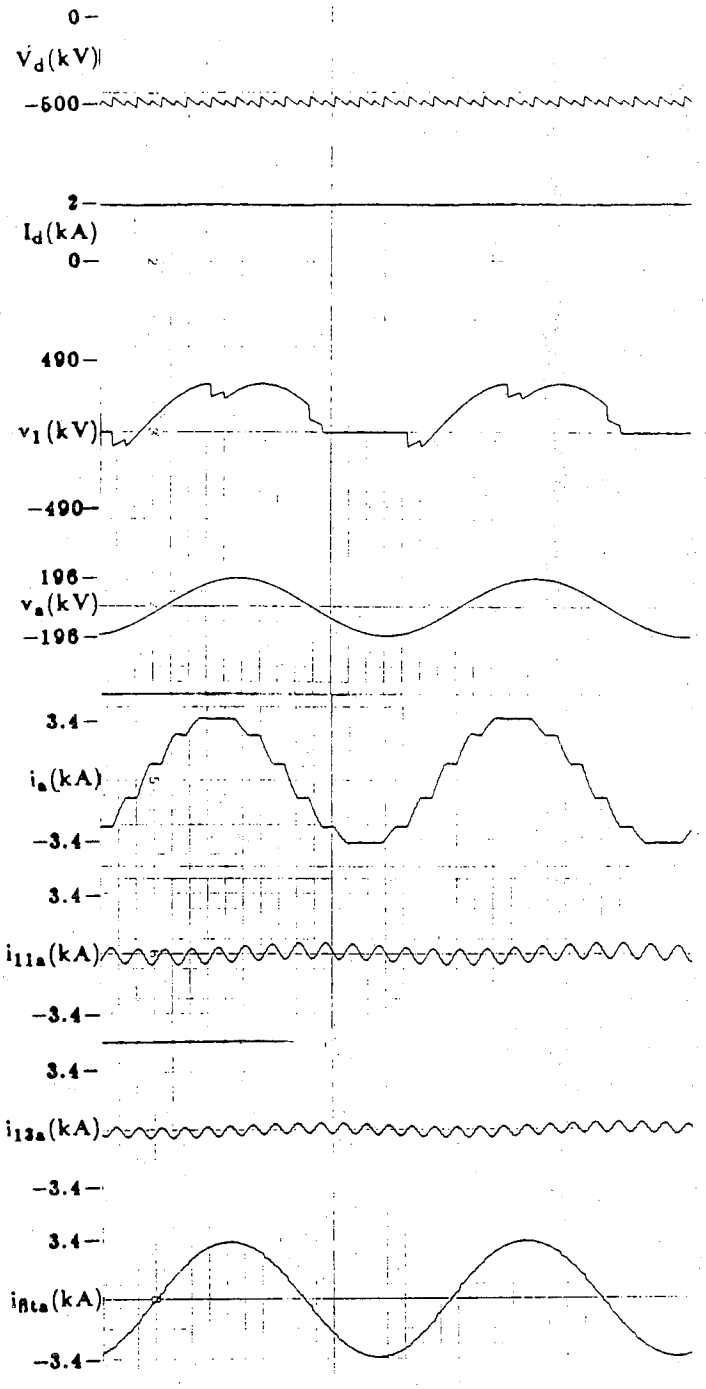

(a)

Figure 2.26 Steady-state waveforms with individual pulse firing at nominal operating point T

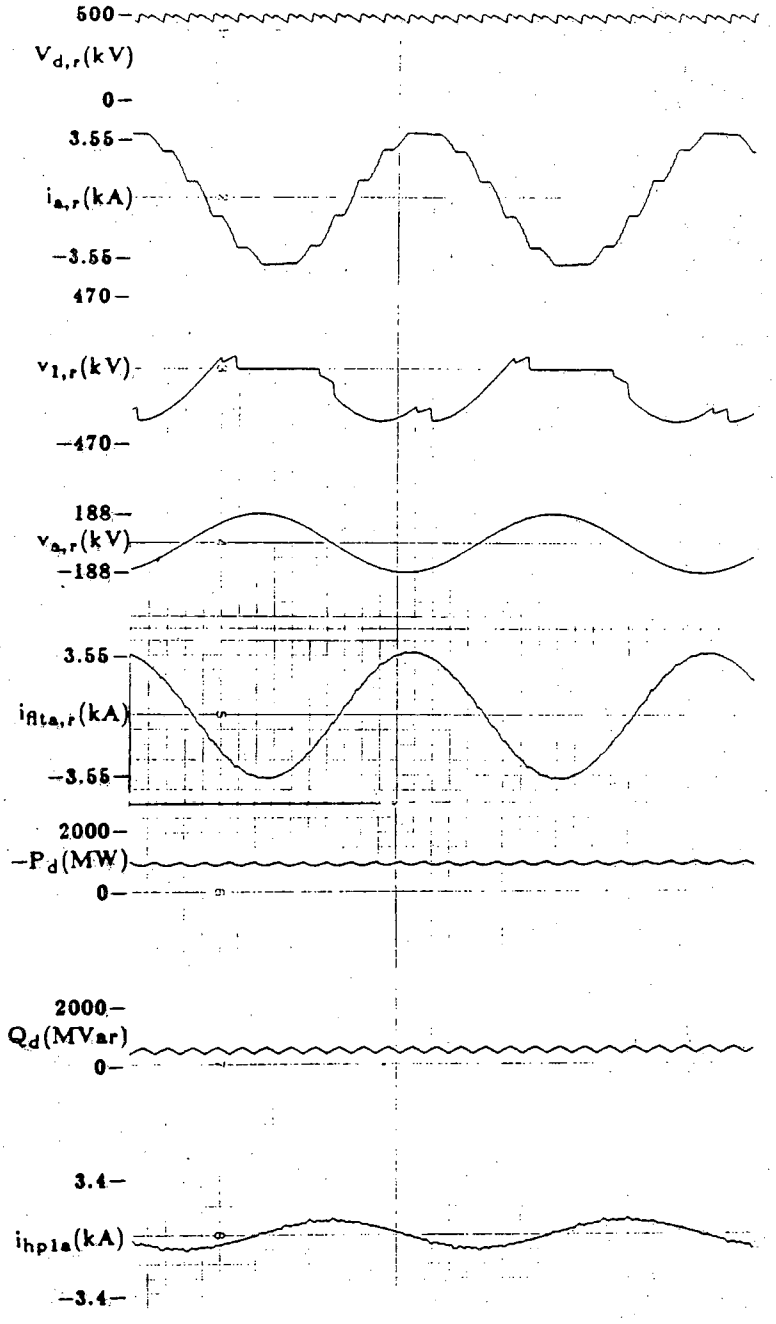

(b)

Figure 2.26 continued

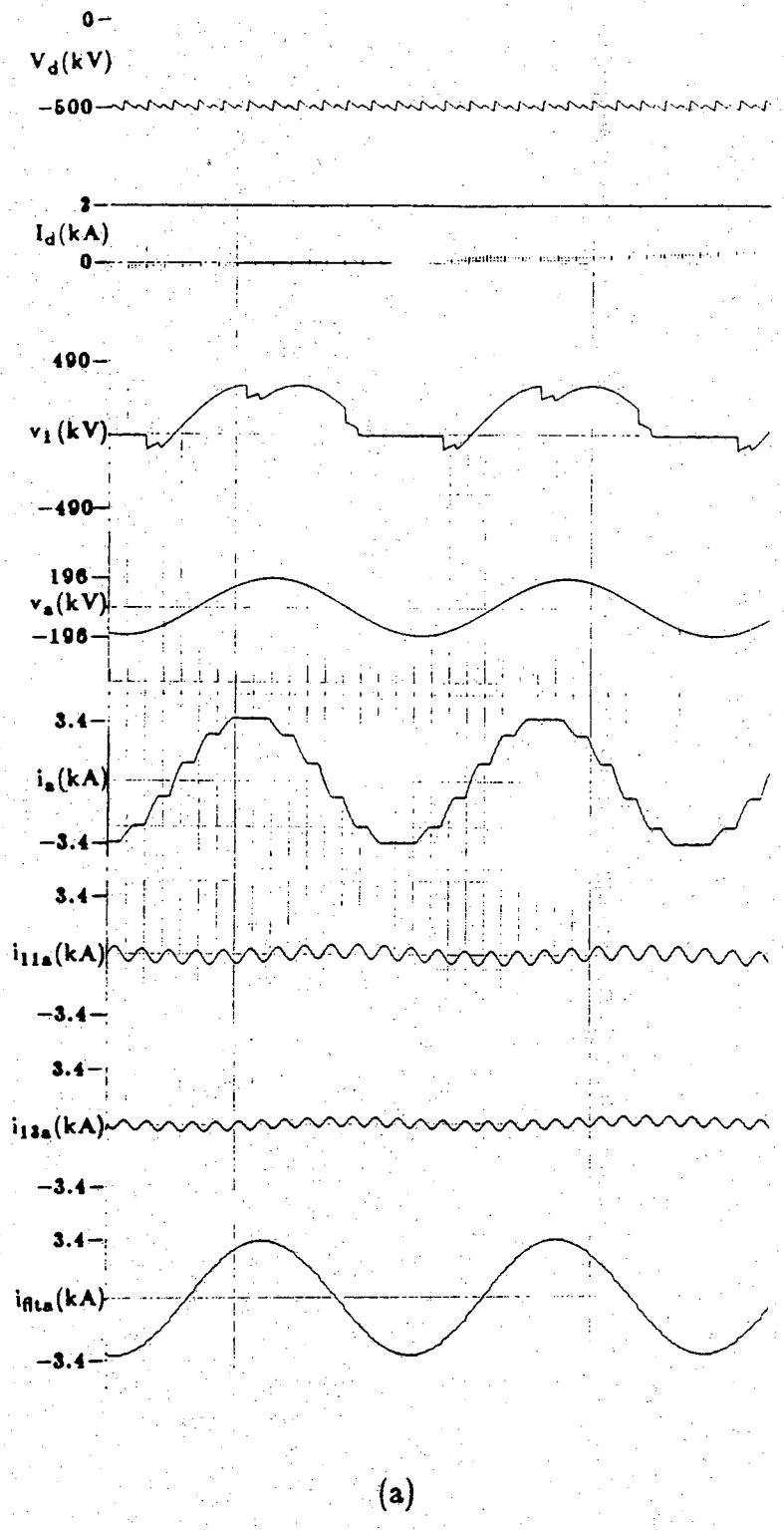

(a)

Figure 2.27 Steady-state waveforms with equidistant pulse firing at nominal operating point T

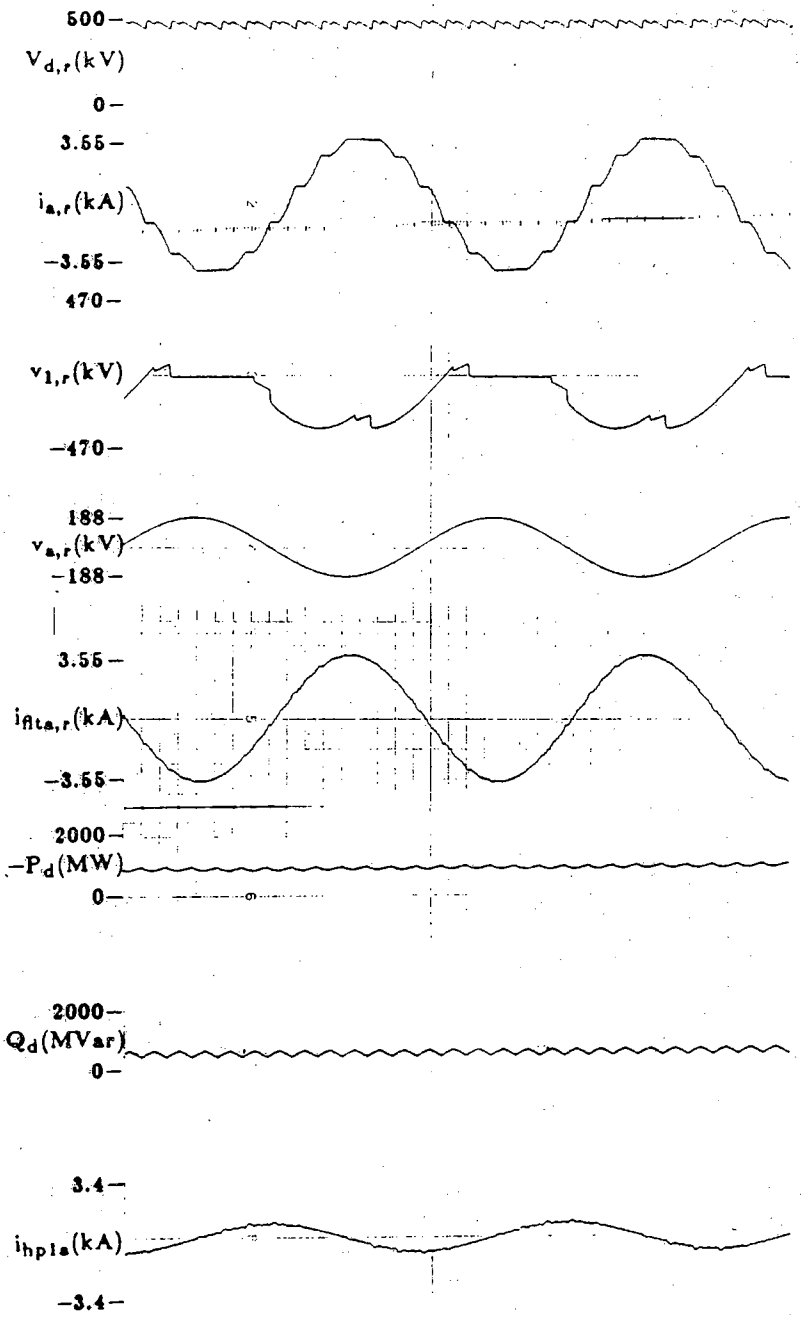

(b)

Figure 2.27 continued

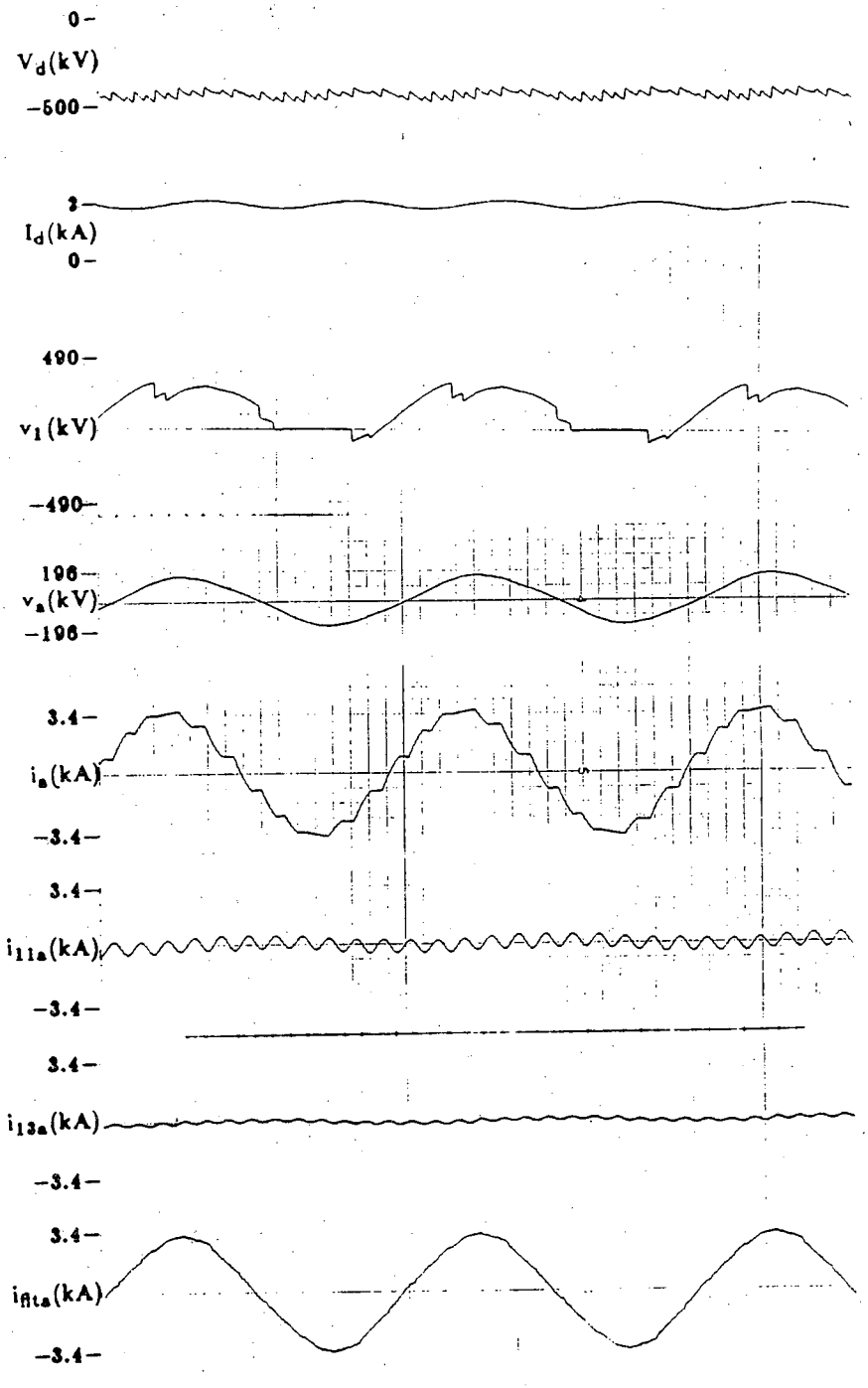

(a)

Figure 2.28 Steady-state operation with a 20% drop in phase A of Thevenin's source voltage (individual pulse)

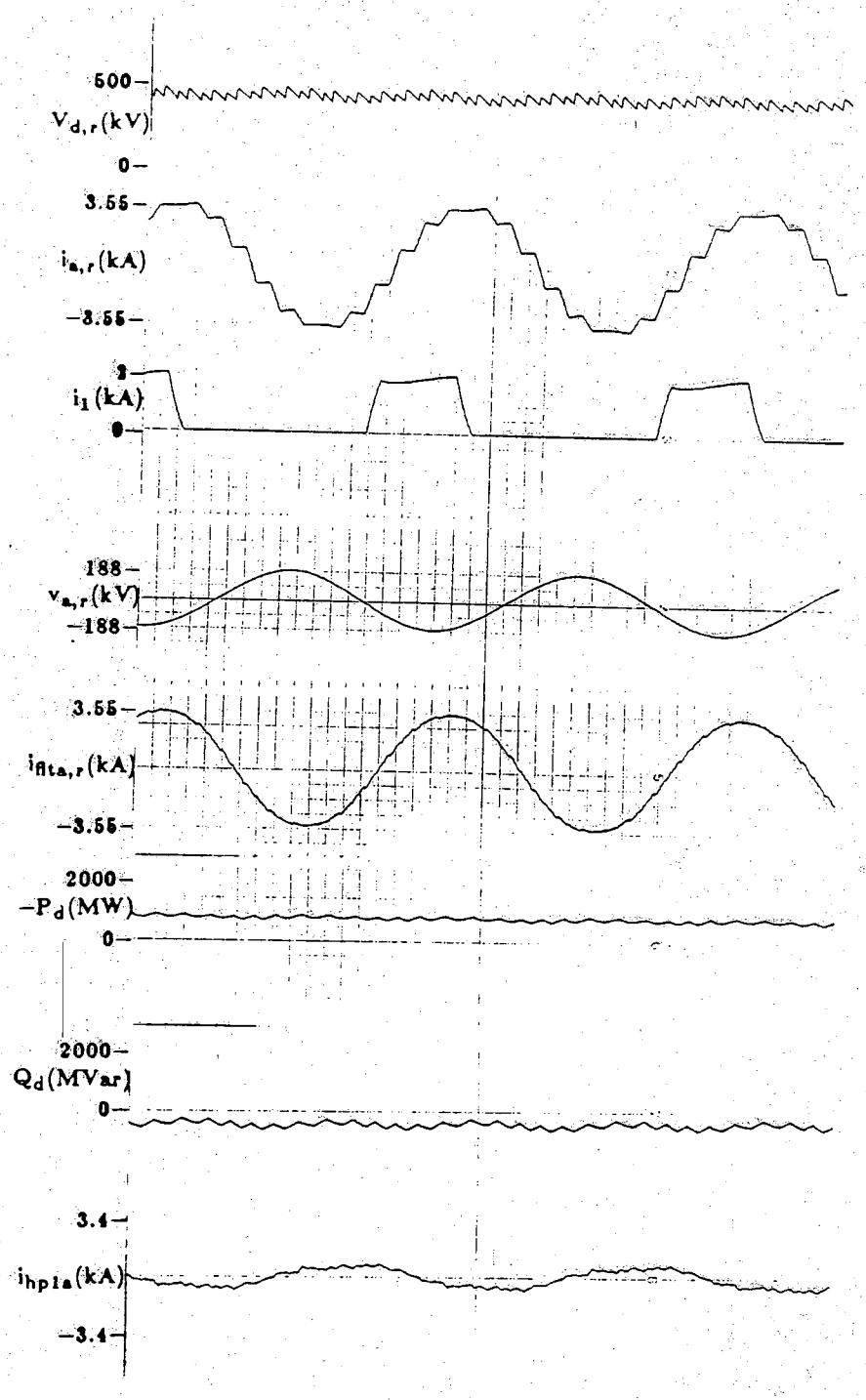

(b)

Figure 2.28 continued

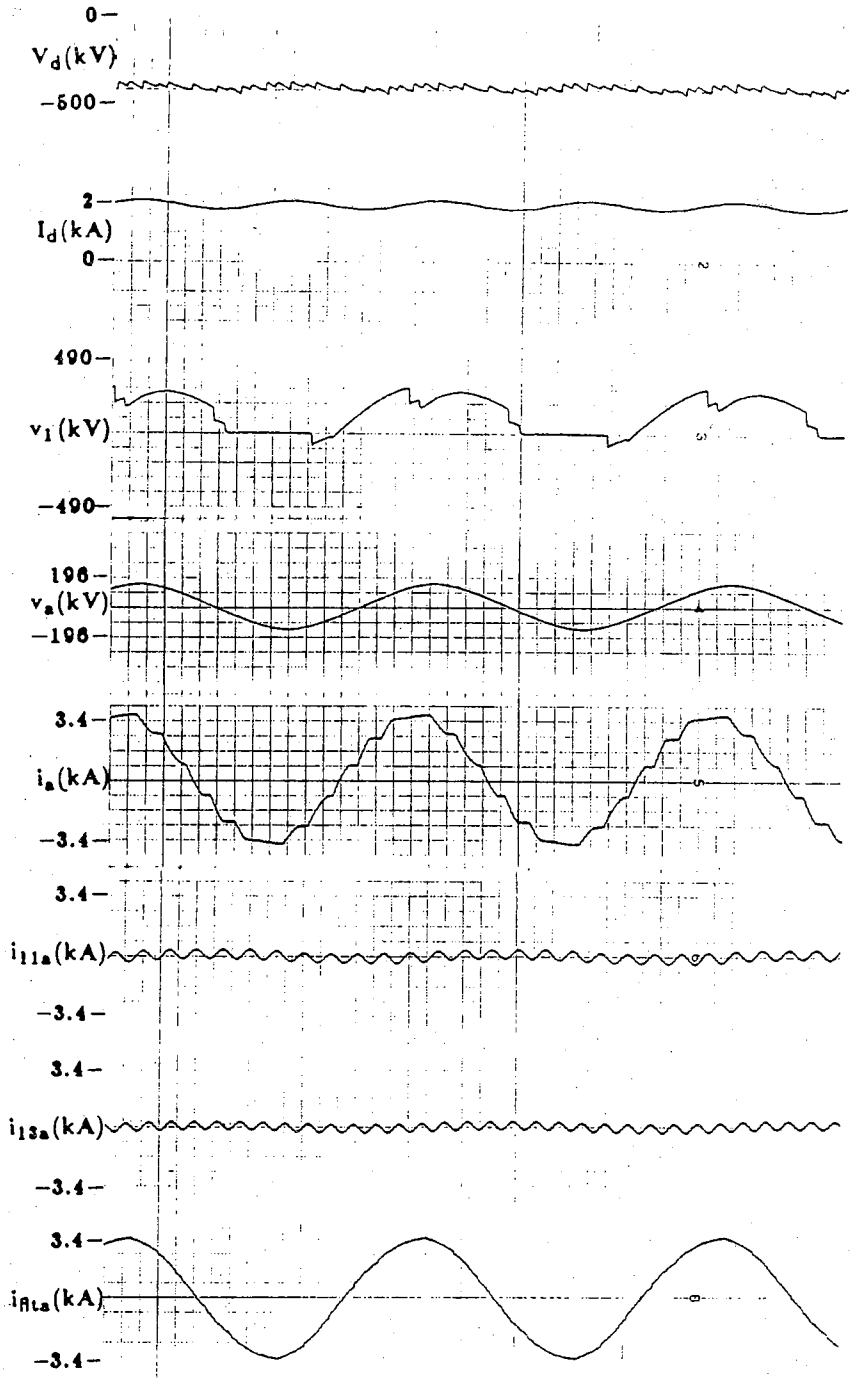

(a)

Figure 2.29 Steady-state operation with a 20% drop in phase A of Thevenin's source voltage (equidistant pulse)

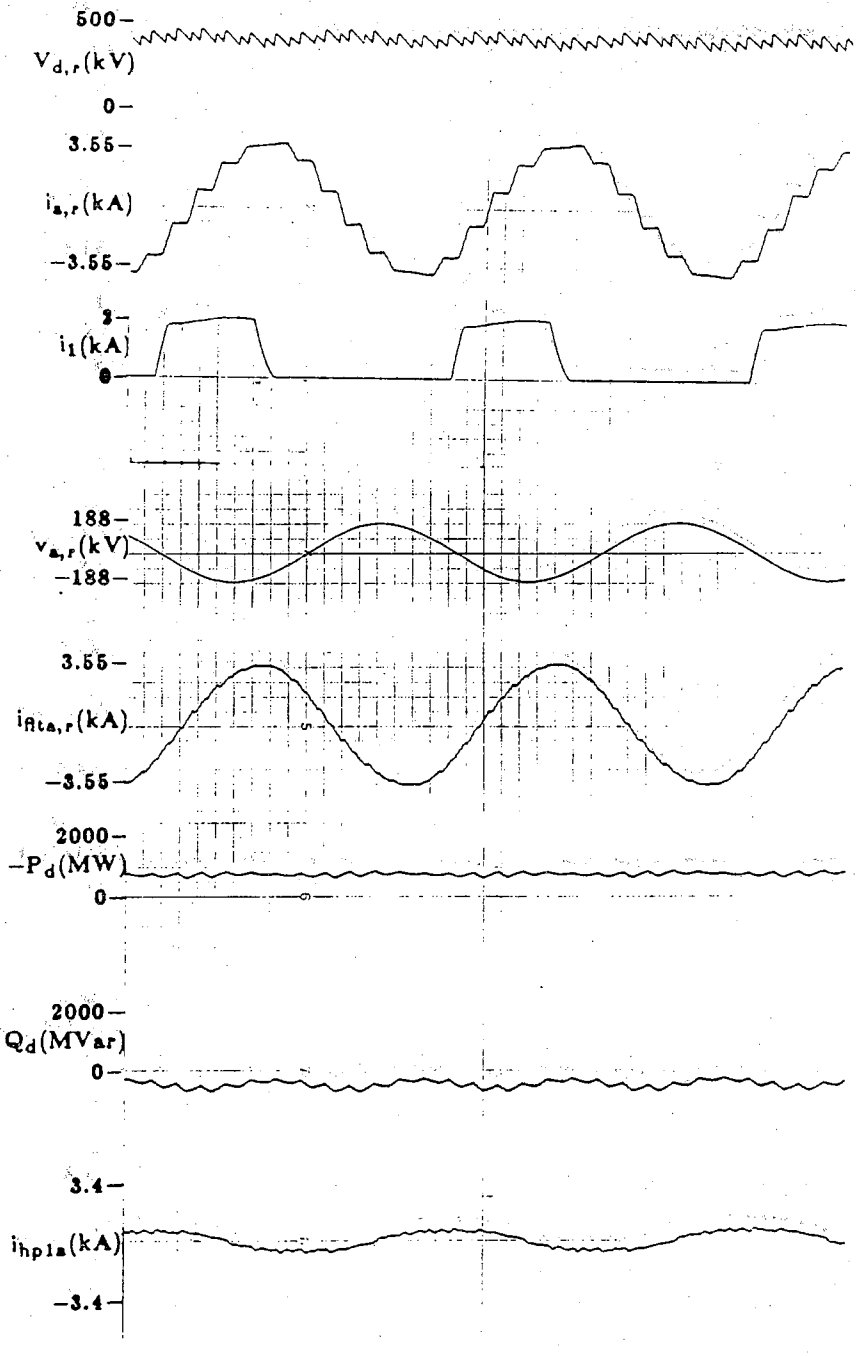

(b)

Figure 2.29 continued

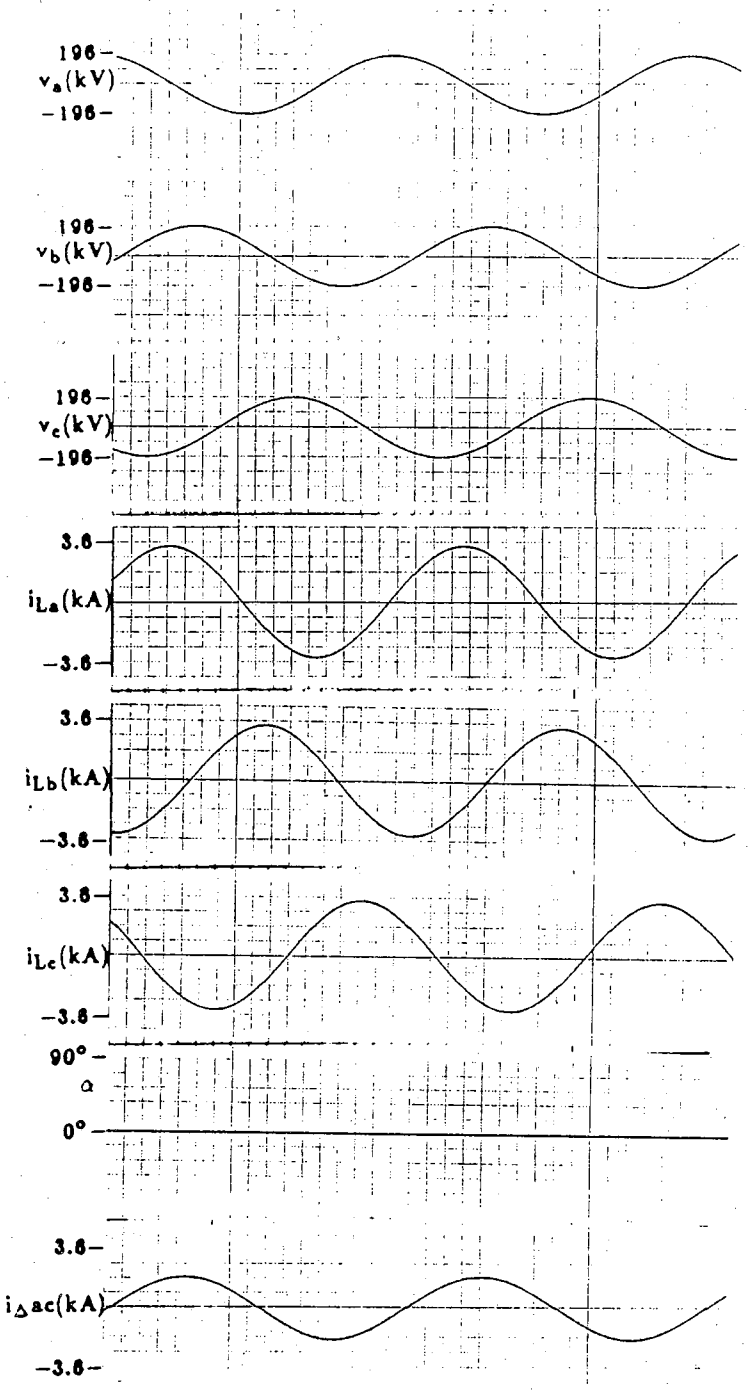

(a) $\alpha = 0°$

Figure 2.30 TCR operation with ideal voltage source

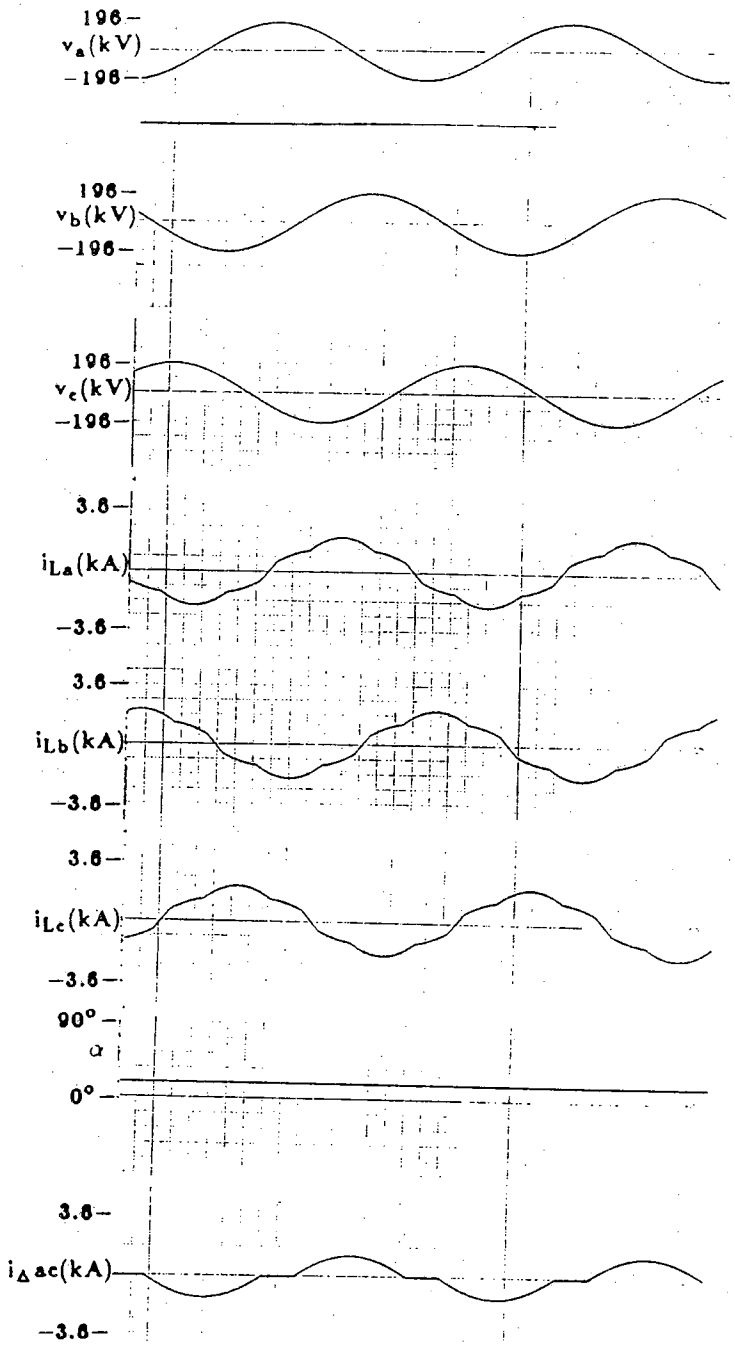

(b) $\alpha = 18°$

Figure 2.30 continued

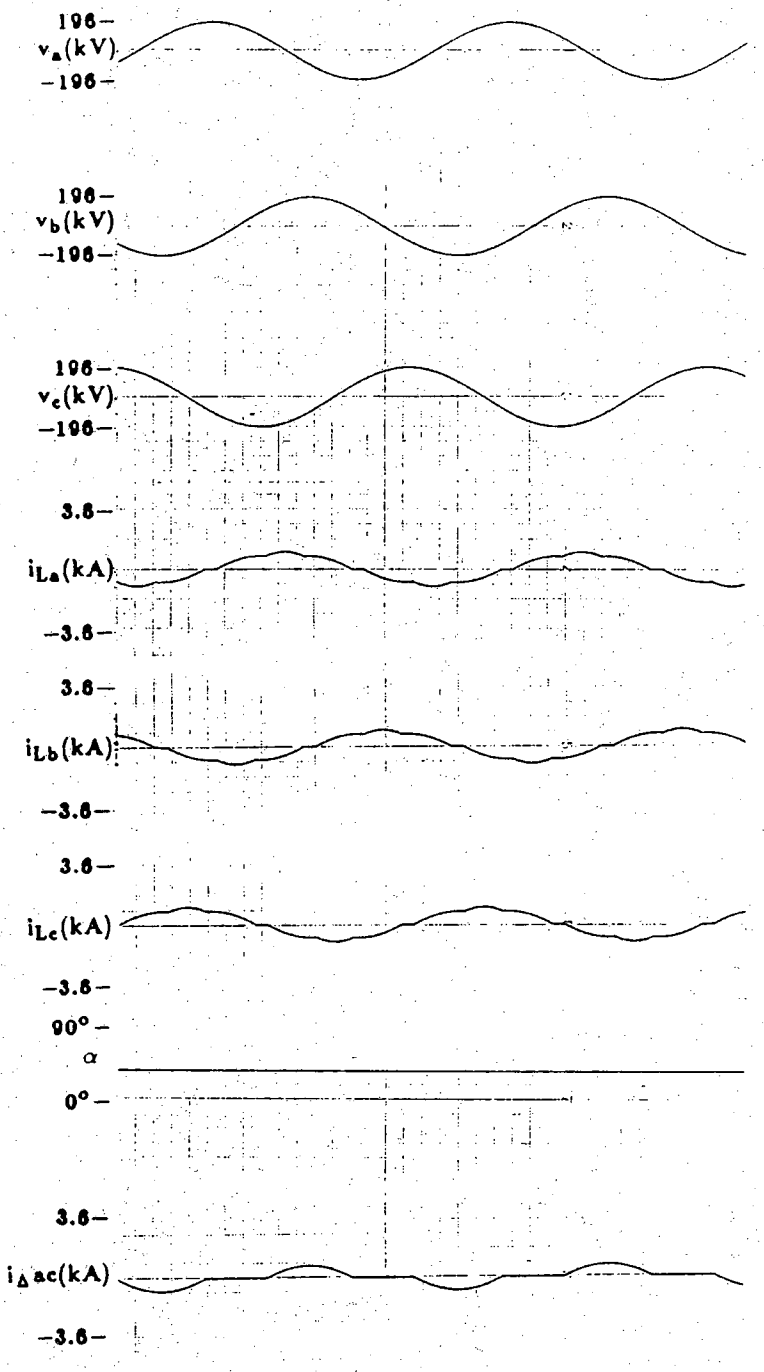

(c) $\alpha = 36°$

Figure 2.30 continued

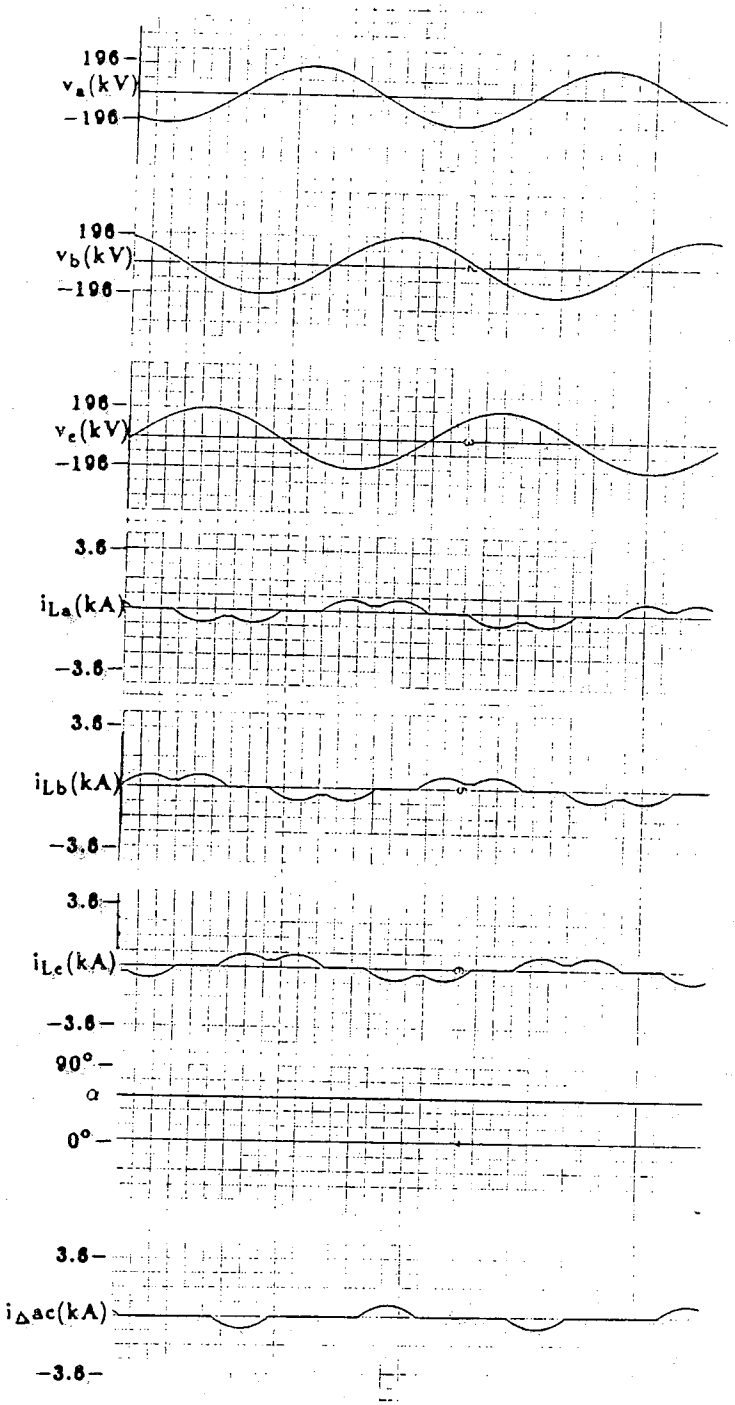

(d) $\alpha = 54°$

Figure 2.30 continued

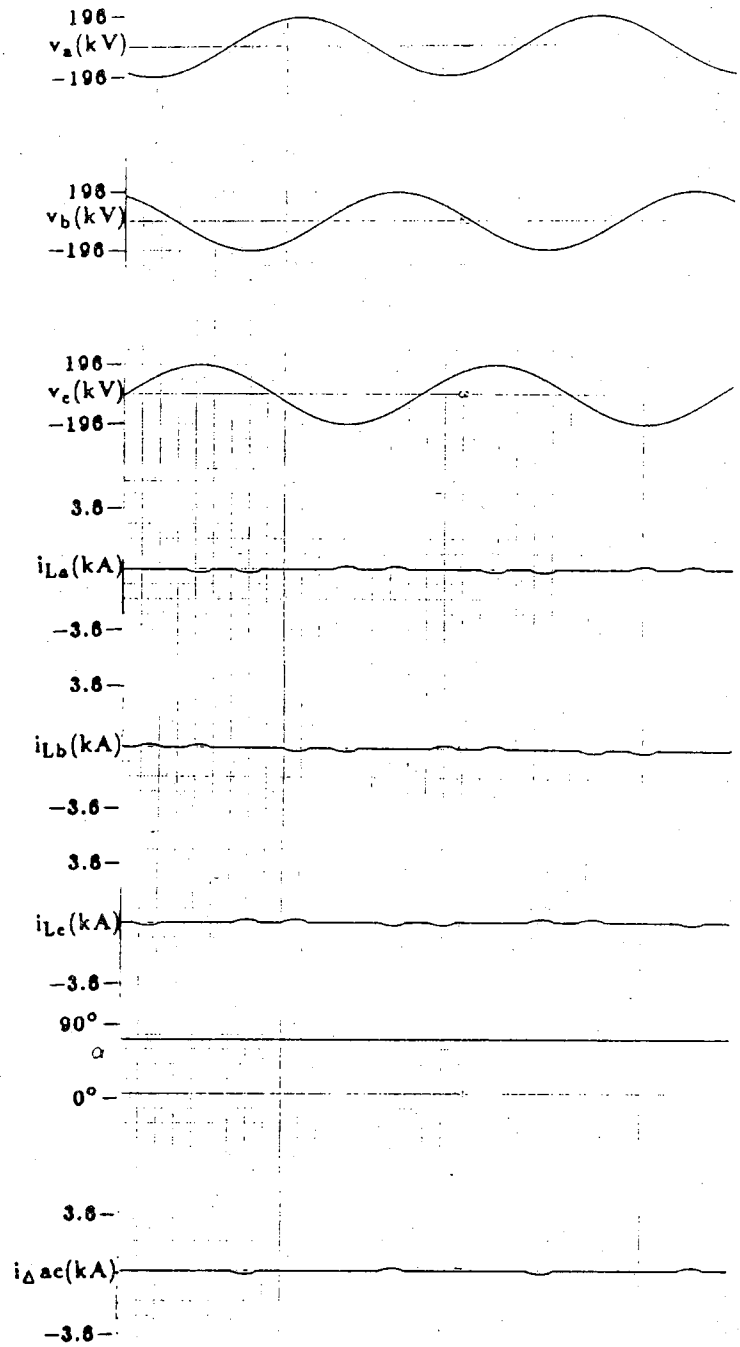

(e) $\alpha = 78°$

Figure 2.30 continued

CHAPTER 3

STEADY-STATE HARMONIC GENERATION

3.1 Introduction

The problem of harmonics is not a new issue. Its importance was recognized in the 1920s when distorted current and voltage waveforms were observed in transmission lines. At that time, the major concerns were their effects on synchronous machines, induction machines, telephone interference and power capacitors [7].

For more than 50 years, harmonics have been reported to cause operational problems. Some of them can be summarized as follow:

- capacitor bank failure from dielectric heating,
- interference with ripple control and power line carrier systems causing misoperation of systems which accomplish remote switching and load control metering,
- excessive losses in and heating of induction and synchronous machines,
- overvoltage and excessive currents on the system from resonance to harmonic voltages or currents on the network,
- dielectric breakdown of insulated cables resulting from harmonic overvoltages on the system,
- inductive interference with telecommunication system,
- errors in induction KWh meters,
- signal interference and relay malfunction, particularly in solid-state and microprocessor controller systems,
- interference with large motor controllers and power plant excitation systems (this can cause motor problems as well as non-uniform output),
- mechanical oscillations of induction and synchronous machines, and
- unstable operation of firing circuits on zero crossings detection or

latching.

Harmonics are generated by static power conversion processes. In the case of an HVDC converter bridge, current harmonics are generated. In normal operation a p-pulse bridge converter generates characteristic AC current harmonics of order (pq±1), q being an integer, and some relatively small abnormal (uncharacteristic) harmonics [46]. When these harmonic currents are injected into a weak AC system with large source impedance, they cause high harmonic voltage drops which will appear on the AC voltages supplying the HVDC converter. The distortion caused by these harmonic voltages may cause instability.

Moreover, at the lower effective short-circuit ratio (ESCR) the AC network impedance increases; as a result, the AC system resonates at a lower harmonic order (h) given by

$$h = \sqrt{\frac{X_c}{X_{th}}} \tag{3.1}$$

where

X_c is the capacitance of the shunt compensation including the AC filters, and

X_{th} is the Thevenin equivalent AC source reactance.

From Eq. 3.1 we can see that with a small value of X_c, or with a high value of X_{th}, the harmonic order at which parallel resonance might occur is low.

For weak AC systems, resonance usually occurs at a harmonic order between three and four. If h is close to three, any unbalance that causes the generation of third harmonic currents could excite a troublesome parallel resonance.

It has been shown [59-63] that unbalance in the AC voltage supply results in nonsymmetrical firing references. Any deviation of the valve current from $\frac{2\pi}{3}$ radians in width results in the generation of the triplen harmonic components on the AC side and second harmonic components on the DC side, in addition to the usual characteristic harmonics.

The saturation of the converter transformer plays an important role in harmonic generation, in that all odd harmonic components are generated. The largest is the third, followed by the fifth, then the seventh, and so on. The third harmonic components will not bother the converter bridge operation as long as

they are of zero sequence type, since the converter responds to the line-to-line instead of the phase voltages. Moreover, interaction between the nonlinear elements present (saturation, TCR and converter) is possible.

The presence of a DC component on the valve side of the converter transformer tends to saturate the converter transformer cores, generating extra magnetizing currents [64].

To determine accurately the harmonics propagated by an AC/DC link, we would require information on the frequency response of the AC and DC networks, and the nonlinear characteristic of the transformer, all of which are not usually easy to get unless field measurements [65,66] are taken.

On the other hand, to get an understanding of what characteristic harmonics are generated by the converter, it is quite sufficient to study the ideal case where constant DC current, balanced and symmetrical AC supply voltages, and negligible commutation process are assumed.

The expressions giving the characteristic harmonics generated by a converter operating under an ideal AC voltage supply will be reviewed first, then the addition of harmonics produced by unbalanced voltage and network parameters, by transformer saturation, and by the TCR, and finally the combined effect of operating with all these in a weak AC system which tends to accentuate the interaction.

3.2 Characteristic harmonics generated by HVDC converters

First, the characteristic harmonics generated by a 6-pulse bridge are described. Results for a 12-pulse configuration will be derived later.

The circuit representing an ideal 12-pulse converter bridge, formed by two 6-pulse bridges, is shown in Fig. 2.2. The valve current, i_1, assuming constant I_d, is a train of positive rectangular pulses of width $\frac{2\pi}{3}$ and height I_d. The Fourier series of i_1 is

$$i_1(\theta)=\frac{2I_d}{\pi}\left[\frac{\pi}{6}+\frac{\sqrt{3}}{2}\cos\theta+\frac{\sqrt{3}}{4}\cos(2\theta)+\cdots\right] \qquad (3.2)$$

where $\theta=\omega t$. The valve current i_4 (current through valve 4) is a train of negative pulses dislaced by π radians with respect to i_1. The Fourier series of i_4 can be found from that of $i_1(\theta)$ by replacing θ with $\pi\pm\theta$ and I_d with $-Id$.

The phase A current in the wye-wye transformer, $i_{a,wye}$, is given by

$$i_{a,wye}=i_1+i_4 \tag{3.3}$$

and has a Fourier series,

$$i_{a,wye}(\theta)=\frac{2\sqrt{3}I_d}{\pi}[\cos(\theta)-\frac{1}{5}\cos(5\theta)+\frac{1}{7}\cos(7\theta)-\frac{1}{11}\cos(11\theta)+...]. \tag{3.4}$$

In Eq. 3.4, only harmonics of $6q\pm1$ ($q=1,2,...$) are present in the line current, and they are generally referred to as the characteristic harmonic currents of the 6-pulse converter bridge.

In a 12-pulse arrangement, the AC supplies to the two 6-pulse converters are displaced 30° apart. The two 6-pulse converters are connected in parallel from the AC side and in series from the DC side (Fig. 2.2). A wye/delta transformer connection is widely used to create the 30°phase shift.

The resultant primary line current for phase A of the 12-pulse converter is given by [4,46]

$$i_a = i_{a,wye}+i_{a,delta} \tag{3.5}$$

$$i_a(\theta)=\frac{4\sqrt{3}I_d}{\pi}[\cos\theta-\frac{1}{11}\cos(11\theta)+\frac{1}{13}\cos(13\theta)-\frac{1}{23}\cos(23\theta)+...] \tag{3.6}$$

Equation 3.6 shows that the resultant AC current has characteristic harmonics of orders $12q\pm1$ ($q=1,2,...$), and because of the 30° fundamental phase shift, those of $(6q\pm1)$, q odd, are canceled out.

So far ignored is the commutation angle, μ, that is equivalent to assuming instant commutation, which is not the case in the practice. The effect of including μ, assuming that the symmetry is preserved, is to round off the current waveforms. This reduces the distortion of the valve currents, thereby reducing the magnitude of the generated harmonics [46].

The triplen harmonics are absent because of the balanced 3-phase condition, and the even harmonics are absent because of the half-wave symmetry condition. The fifth and seventh, in general $(6q\pm1)$ for q odd, harmonic currents circulate between the two transformer banks but do not enter

the AC network. The fundamental, eleventh, thirteenth and the (12q±1), q integer have doubled in value. The magnitude of the characteristic harmonic is inversely proportional to its harmonic order h.

On the DC side, the converter behaves like a harmonic voltage source. For a 6-pulse converter, the DC voltage, V_d, ideally contains only characteristic harmonics of order 6q (q=1,2,...). Similarly, for a 12-pulse converter, V_d ideally contains characteristic harmonics of order 12q, q integer [46].

3.3 Harmonic characteristics of the IP and EP firing schemes

It is of interest to investigate whether there is any difference in harmonic characteristics of an inverter operating under the two firing schemes: individual phase versus equidistant. This investigation has been conducted on an analog simulation of a sample 12-pulse HVDC link with parameters given in Appendix A. The individual phase (IP) firing scheme implemented was the standard inverse cosine firing scheme (with a predictive CEA), and the equidistant pulse (EP) firing scheme implemented was the so-called pulse phase control firing scheme (with a feedback CEA) described in [48]. The harmonic contents of the AC and DC variables were measured using a DATA 6000 wave analyzer. To begin with, a linear model of the converter transformer was used, the purpose of which was to isolate the effects of transformer saturation, allowing us to concentrate just on the harmonics produced by the converter.

3.3.1 Harmonics with ideal AC voltage support

The purpose of this phase of the investigation is to establish the basic relation on harmonic orders between AC and DC variables under balanced AC conditions with the inverter operated under each of the two firing schemes. For this purpose, the inverter is connected directly to a set of balanced AC voltages of the form,

$$\begin{aligned} v_a &= V_1\cos(\omega t) + V_n\cos(n\omega t) \\ v_b &= V_1\cos(\omega t - \frac{2\pi}{3}) + V_n\cos(n\omega t \pm \frac{2n\pi}{3}) \\ v_c &= V_1\cos(\omega t - \frac{4\pi}{3}) + V_n\cos(n\omega t \pm \frac{4n\pi}{3}). \end{aligned} \tag{3.7}$$

The plus and minus signs in the arguments of the cosine terms for the nth

harmonic components in v_b and v_c pertain to the two cases when the sequence of the harmonic components is opposite and when it is the same as that of the fundamental, respectively. When confined to balanced sets, the triplen harmonics (i.e, n = 3,6,9...) are essentially zero sequence components; they have no effect on the 3-phase bridge operation because they cancel out in the line-to-line voltages. Unbalanced triplen harmonic components are, of course, a different matter. At the nominal operating condition simulated, the HVDC link transferred rated power with the DC current controlled by the rectifier and the DC voltage controlled by the inverter.

Separate sets of measurements were taken for the inverter operating with each of the two firing schemes, using the same control set points. The harmonic spectra of the DC voltage V_d, the DC current I_d, and the AC current I_a for the cases of n = 2 and 4 are given in Tables 3.1 and 3.2, respectively. Only the lower order harmonics are shown; normally these are the ones of most concern in practice. The presence of balanced harmonic voltage components in the AC phase voltages introduces extra harmonics, besides the characteristic ones, in the DC voltage and current, and in the AC currents. In addition to the usual characteristic harmonics of order 12q, the DC variables V_d and I_d contain additional harmonics of order either $12q \pm (n-1)$, when the sequence of the nth harmonic component voltages in the AC voltages is the same as that of the fundamental, or $12q \pm (n+1)$ when the sequence of the nth harmonic component is opposite to that of the fundamental. Similarly, besides the characteristic $(12q \pm 1)$ harmonics, the additional harmonics in the AC currents are of order either $(12q \pm 1) \pm (n-1)$, when the sequence of the nth harmonic components in the AC voltages is the same as that of the fundamental, or $(12q \pm 1) \pm (n+1)$ when the sequence of the nth harmonic is opposite to that of the fundamental. These results also indicate that the same order of harmonics in the AC and DC variables is obtained from an inverter operating with either the IP or the EP firing scheme. Some differences in the magnitudes of these harmonics can be seen, but these differences are not consistently in favor of the IP or the EP firing scheme.

3.3.2 Harmonics with relatively weak AC support

In this phase of the investigation, the AC-side of the inverter has the usual eleventh, thirteenth, and high-pass tuned filters, together with a shunt capacitor on the primary side of the converter transformer. The AC network was represented by an AC Thevenin's equivalent RL impedance of angle 75°. It is recognized that the simple AC Thevenin's equivalent can only be an

approximation of the AC network impedance characteristic over a rather limited frequency range at a specific condition, as the actual AC network impedance characteristic would not only have multiple poles and zeroes, but would also vary considerably with loading conditions. The strength of the AC support can be varied by adjusting the Thevenin source impedance Z_{th}. In this case, with the basic control, the inverter was able to operate stably with either one of the two firing schemes for AC support condition down to an ESCR of 1.5; below this value instability sets in. In the interest of keeping the basic control common for the following studies, an SCR of 4.45 and an ESCR of 3.97 were selected. Figure 3.1 shows the magnitude and phase plots of just the Z_{th} and of the equivalent input impedance Z_{eq} formed by the parallel combination of Z_{th} and the shunt elements (shunt filters and capacitor) as seen from the inverter AC bus.

The objective of this phase of the investigation is to examine what effect a large source impedance (lower resonance frequency) or fundamental frequency unbalance in the AC voltages or both has on an inverter operating under each of the two firing schemes. The unbalanced AC voltage condition is of interest because it causes uncharacteristic harmonics, especially those of low orders for which there are no filters provided. In the simulation, an unbalanced AC condition can easily be created in several ways, such as using unequal parameters in the phases of the AC line, the converter transformers, or the shunt elements; or using an unbalanced set of Thevenin's equivalent source voltages. The latter approach, being easier to visualize, is preferred. For simplicity the degree of unbalance is quantified in terms of the percentages of the negative and zero sequence symmetrical components.

As indicated earlier, the presence of zero sequence type voltage components in the phase voltages has no effect on the bridge operation. But the presence of negative sequence type components does affect the bridge operation. Simulations were performed with balanced Thevenin's AC voltages (base case) and with 2.5%, 5%, and 10% of fundamental frequency negative sequence components introduced onto the base case voltages. Because of the distorted AC voltages, the minimum extinction angle has to be raised from the nominal value of 18° to 25° for stable operation. To facilitate comparison, all the measurements taken in this section were for a γ_{min} of 25°. As the shape of the AC voltage waveforms depends not only on the magnitude of the added negative sequence component but also on the relative phase between it and the positive sequence component θ, the simulation for each level of unbalance at 45° intervals was also repeated .

A sample of the measured results for the 5% and the 10% unbalance are presented: Table 3.3 contains the harmonic spectra of the phase primary current injected into the local AC bus by the inverter for the case when the Thevenin's source voltages had 5% fundamental frequency negative sequence components, and Table 3.4 contains the harmonic spectra of the same phase current at 10% unbalance. The case of 2.5% unbalance had similar characteristics of proportionally lower magnitudes. It should be noted that the simulated system had finite impedances in both AC and DC networks.

Using the relation between harmonic orders established in the previous section, we can predict that the presence of fundamental frequency negative sequence components in the AC voltages will introduce extra harmonics of order $12q \pm (1 + 1)$ in the DC variables and $(12q \pm 1) \pm (1 + 1)$ in the AC variables. The presence of the third, ninth (from 11 - 2), and fifteenth (from 13 + 2) in the AC current is evident from Table 3.4.

Two observations can be made from the results given in Table 3.4. First, the magnitudes of these extra harmonics are approximately proportional to the degree of unbalance and they vary cyclically with the relative phase between the negative and positive sequence components. Second, for this kind of voltage distortion both firing schemes seem to generate about the same harmonics, at least for the sample system studied, but the magnitudes of these harmonics are consistently lower with EP than with IP. It is apparent from these results that the IP is more sensitive than the EP to distortions in the AC voltages. This difference in behavior is more noticeable at a higher level of unbalance, as shown here by the plots of the 3rd and 9th harmonic components of the 10% case in Fig. 3.2.

The developed simulation can be used for studying all sorts of unbalance. For example, in Table 3.5, the results for the case of a single phase unbalance of 20% drop in only the a-phase voltage of the Thevenin's equivalent source are presented. This is equivalent to having both negative and zero sequence components of 6.67%. Again, the orders of the harmonics present in the AC and DC variables can be predicted using the relation established earlier. The zero sequence components of the phase voltages have no effect on the bridge. Although the magnitudes of most of the extra order harmonics are lower with EP than with IP, in this case the 6.67% negative sequence components do not distort the AC voltage sufficiently to justify a clear conclusion.

3.4 Effects of transformer saturation

The power transformer is widely used in the power system. Like other power components, it has its own characteristic behavior during transient (inrush currents, faults, ...) and steady-state (saturation, hysteresis, ...) conditions. Usually the transformer is simulated only by its leakage reactances (assuming that most of the leakage occurs in air, a linear medium) in series with its winding resistances. For dynamic and steady-state harmonic studies, it is obvious that the above linear representation could yield misleading results and might not describe the actual transformer behavior. Modern power transformers are made of grain-oriented silicon iron structure, which is known to have a very thin hysteresis loop [34,38]. In this study, hysteresis will be ignored; the nonlinear normal magnetization curve produces only odd harmonic currents in the exciting current, of which the third is the principal one, and the magnitude decreases with the harmonic order. In the case of a magnetic unbalance (no longer half-wave symmetric), the magnetizing current can be very large and contains all harmonics, that is, odd and even harmonics, including a DC component. In practice this asymmetry is frequently caused by the presence of a DC component in the transformer secondary current.

3.4.1 Effect of transformer saturation on the HVDC operation

Under unbalanced AC source voltages, the triplen harmonics generated by the saturated transformer are unbalanced; they add to or substract from those generated by the converter, depending on their relative phase angles.

To better understand how transformer saturation affects the harmonic characteristics of the inverter connected to a relatively weak AC system, the following simulations were performed:

- steady-state operations at the nominal operating point with and without transformer saturation,
- injection of a DC component in the valve-side AC current, and
- the effects of unbalance in the AC voltages, including the effect of variation in the phase angle of the fundamental negative sequence AC voltage, and a drop of 20% of phase A.

From measurements taken of the steady-state operation with and without transformer saturation, there was an observable change in the magnitudes of some harmonics in V_d and I_a. The current I_a had a small DC component due to unequal firing angles. The magnitudes of the characteristic harmonics remained

the most dominant in all cases. An increase in the even harmonics in V_d and odd ones in I_a is clearly seen in Table 3.6.

In the second experiment we injected a DC component of 0, 2.5, 5, 7.5, and 10% of the rated fundamental transformer secondary current into all transformer valve-side currents. Figure 3.3 shows measured values of V_d, I_a, V_a and I_{ma} (phase A only) plotted against the magnitude of the DC component injected. The uncharacteristic even harmonics present in I_a and V_a increase almost linearly with respect to the increase in magnitude of the DC component injected. The odd harmonics are significantly less sensitive to the variation of the DC component, at least up to 10%. Similar observations hold for the magnetizing current where the second harmonic is the most dominant. On the DC side, the opposite is happening. The odd harmonics in V_d and I_d are linearly increasing, while the even ones seem to be only slightly sensitive to the presence of a DC component. One way to explain this phenomena is to use the results obtained in section 3.3.1. According to the relation established, the presence of a second harmonic voltage (negative sequence by its nature in three phase balanced AC system) produces harmonics of order $12q \pm(2+1)$ or $12q \pm 3$ hence the third, ninth, fifteenth, and all odd triplen are generated and are the most significant ones on the DC side. Similarly, the presence of the fourth harmonic order in V_a (positive sequence) produces harmonics of orders $12q \pm (4-1)$. A similar reasoning applies to the eighth harmonic order in V_a; triplen harmonics on the DC side and vice versa. The triplens on the AC side are of zero sequence; therefore, they do not affect the bridge operation since the latter respond to the line-to-line instead of the line-to-neutral voltages.

The third experiment was performed with a nonlinear transformer representation; an unbalance voltage condition was created by introducing 5% and 10% of negative sequence fundamental AC voltage to the nominal Thevenin's voltage source on the inverter side. In each case, the phase angle of the negative sequence component relative to the positive sequence phase angle was varied from 0 to 360°. Figure 3.4 shows only the lower important harmonics on some of the AC and DC variables plotted against the phase angle, θ, between the negative and positive sequence of Thevenin's source voltage. The second harmonics present in V_d and I_d seem to be insensitive to θ. On the AC side, the third and the ninth harmonics are the most dominant, in that order. The harmonics in the magnetizing current, I_{ma}, are of lower magnitudes in the case of the 10% unbalance than in the 5% unbalance. This is because the 10% unbalance condition results in lower AC voltages at the local bus; therefore, the transformer is not driven as highly into saturation as in the case of the 5% unbalance. No saturation is present when θ is around 180° as shown.

In the last experiment a drop of 20% in the phase A of the Thevenin's source voltage was simulated. Results presented in Table 3.7 include those for linear and nonlinear transformer representations and also for the EP and IP firing schemes for the purpose of comparison. The second harmonic is again the most dominant on the DC side and the third on the AC side. The EP again gives better harmonic performance than the IP.

3.5 Harmonics due to the TCR

3.5.1 Combined harmonic characteristics of HVDC and TCR

The TCR is a nonlinear element; it, too, generates current harmonics into the AC system. The magnitude of each current harmonic component is a function of the firing angle α. Full current is flowing in the TCR at $\alpha = 0$, and no harmonics are generated. No current flows in the TCR at $\alpha = 90°$; consequently, no harmonics. When α changes between these two values, the fundamental is changed in a monotonic way with α, but the harmonic component variation can be nonmonotonically, with extrema occuring at different values of α. It can be shown that the maximum magnitudes of the third, fifth, seventh, eleventh, and thirteenth are 13.78, 5.05, 2.59, 1.57, 1.05, and 0.75% of the fundamental full current, respectively [23]. The third harmonic is the most dominant. Fortunately, by just wiring the TCR in a delta-connection fashion, the third harmonic (zero sequence) is kept within the delta circuit and will not propagate into the AC system.

With an ideal voltage source, the fundamental component of the TCR current is given by

$$I_r = \frac{V}{X_l}\left(1 - \frac{2\alpha}{\pi} - \frac{\sin(2\alpha)}{\pi}\right). \tag{3.8}$$

The harmonic current components, as a function of the firing angle, are given by the following closed form relationship:

$$I_h = \frac{4V}{\pi X_l}\left(\frac{\sin\alpha\cos(h\alpha) - h\cos\alpha\sin(h\alpha)}{h(h^2 - 1)}\right) \tag{3.9}$$

These equations could be derived from the ones given in [23]. Plots of Eq. 3.8 and 3.9 are shown in Fig. 3.5.

From Fig. 3.5, we can see that there are more than one extremum, and they occur at different values of α for different harmonic orders. To compute the values at which an extremum occurs, compute the first derivative of the expression in Eq. 3.9 and equate it to zero to get the following simple expression,

$$\alpha_{ext} = (2k+1)\frac{90^{\circ}}{h}. \tag{3.10}$$

The maximum value of the harmonic current of order h is given by,

$$I_{h,ext} = \frac{4V}{\pi X_l}\left(\frac{(-1)^{k+1}\cos\alpha_{ext}}{h(h^2-1)}\right) \tag{3.11}$$

where $k=1,2,3, \ldots$, and $0<\alpha<90^{\circ}$.

Knowing at what α a certain harmonic order is the highest could simplify the filter design by either avoiding the operation of the TCR at that point or designing a tuned filter at that harmonic. The above formula was verified using the simulation.

The type of firing scheme adopted for the TCR plays a major role in minimizing abnormal harmonic generation [67]. A slight delay or advance of the firing angle from its required value could cause unsymmetry in the valve current; in consequence, odd and even harmonics appear in the line currents. Usually a TCR is connected to the bus voltage through a step-down transformer, which, when saturated, would produce its own uncharacteristic harmonics, further distorting the bus voltages and adversely affecting the operation of the firing circuit.

Both fundamental and harmonic components depend on the size of the reactor. A large X_L means a lower rating or size and hence correspondingly lower harmonic magnitudes. A small X_L means a larger rating or size and therefore higher harmonic magnitudes.

Unequal conduction periods can cause even harmonics to appear, including a DC component. To have equal conduction periods for both valves in the same branch, the firing angle has to be limited to 90°. With half-wave symmetry, only odd harmonics are generated. Under balanced condition; all triplen are absent externally (due to the delta connection, as opposed to the case of a 6-pulse converter, where the triplen are canceled because of the $\frac{2\pi}{3}$ period),

circulating inside the delta.

Usually there is a need for harmonic filters for the fifth and seventh if the size of the TCR is significant. A TCR with 12-pulse configuration (in a way similar to a 12-pulse converter bridge) is beneficial in the sense that it eliminates the fifth and seventh without the use of any filter, but at the expense of two extra transformer banks. Even then the fifth and seventh harmonic filters are sometimes neeeded, especially when operation with one or more 6-pulse converter bridges is required.

In filter design, care should be taken to consider all nonlinear elements which generate significant harmonics. The spectrum of the TCR current depends on the firing angle, the firing control, the pulse number, and the control circuit. As with the bridge converter, non-characteristic harmonics are generated under several types of unbalances;

- unbalance in the bus voltages,
- unbalance in the TCR impedance,
- asymmetry in the firing angle in all phases, and
- asymmetry in the firing angle in each branch.

Under unbalanced AC voltages, the triplen harmonics are not of the zero sequence type, and hence they can pass through the transformer. Furthermore, they are not blocked by the delta connection. Even though small (as compared to the characteristic harmonics) for a relatively small unbalance, they should not be neglected because of the possibility of resonance. In the case of a DC component generation, even though small, could drive any transformer deep into saturation. The measuring devices should also be insensitive to distortion in the system voltage to avoid harmonic amplification. Zero crossing detection has to be as clean as possible from any distortion to avoid affecting the firing scheme of the TCR or the HVDC converter. Otherwise, asymmetry in α results and abnormal harmonics are generated. Several tests have been performed and will be described in the following paragraphs.

First, to validate the simulation of the TCR, a pure sinusoidal voltage was applied to the TCR. The firing angle α was then selected to correspond at a specific harmonic extrema, and the harmonics generated by each branch measured. For example, the firing angles of 30° (which corresponds to the extremum of the third harmonic current in the Δ-circuit), 18° and $54,^{\circ}$ (which correspond to the first and second extremum of the fifth harmonic current, respectively), and 13° and 38° (which correspond to the first and second extremum of the seventh harmonic currents, respectively) were confirmed. The TCR is connected in Δ circuit, hence, no triplen are present. The characteristic

harmonic of this 6-pulse TCR are 5, 7, 11, 13, ..., 6q±1 with q integer. Table 3.8 (a) shows the computed harmonic currents from Eq. 3.10 for each of the above values of α. Table 3.8 (b) shows the measured harmonic currents obtained from the simulation. All the harmonic orders are relative to their respective fundamental component. A comparison between the two tables shows that they are very close.

Next, with TCR simulation connected to the same sample AC system on the inverter side, the response of the TCR to different degrees of unbalance was investigated. A 2.5, 5, and 10% of fundamental negative sequence (E_2) with no phase shift with respect to the positive sequence (θ=0) was added to the Thevenin's source voltage; the AC source impedance corresponded to that for an ESCR of 3.97. Table 3.9 shows the harmonics generated by the TCR phase A current for the conditions of 0, 2.5, 5 and 10% of E_2 with $\theta = 0$ at the same α values, for comparison purposes. The harmonic currents are relative to their fundamental component. As expected from section 3.3.1 [68], the most dominant harmonics generated are of the order (6q±1)±2, i.e., 3, 5, 7, 9, ... Moreover, the third and ninth harmonics are increasing, and the fifth harmonic is decreasing, while the seventh harmonic is increasing with the degree of unbalance.

In another experiment, the effect of varying θ, while E_2 is kept constant, was investigated; 10% of negative sequence in the voltage source with $\theta = 0°$, 120° and 240° have been used. Table 3.10 shows the results of such an experiment for an α close to 24°, which is close to the first extremum of the fifth harmonic. The harmonics are referred to their respective fundamental component. The cyclic nature is quite apparent. The magnitudes of the harmonics are the largest at 0° relative to 120° and 240°. The characteristic and uncharacteristic harmonics are all affected by a change in θ.

In this part, the full DC system along with terminal filters and capacitors was used. The interaction between the TCR and HVDC was studied by forcing the TCR to keep the terminal voltage at rated value, corresponding to the knee point of Fig. 2.13 and Table A4. One way to obtain the TCR operating at $90° > \alpha > 0$ was to set the DC reference current to a lower than rated value. Using this process and reducing the DC current to 0.5 per unit of rated value at the rectifier permits a new operating point where the terminal voltage is higher than rated. The TCR operates in this case to bring the voltage back to a value close to rated (due to the TCR slope).

Since no fifth and seventh harmonic filters were used, these harmonics propagated into the AC local network, producing corresponding harmonic voltage drops which were reflected on the AC bus voltages which, in turn,

affected the DC-side harmonics of the link. Applying the expression given in section 3.3.1, we can see that the fifth and seventh harmonics on the AC voltages create the sixth, eighteenth, ... etc. harmonics on the DC side.

Table 3.11 presents some of the results showing the effects of both the TCR and the saturation of the converter transformer on the inverter harmonic characteristics at half rated DC power. Table 3.11 (a) shows the case with balanced AC source voltages, and Table 3.11 (b), (c) and (d) are for 2.5% of E_2 and θ equals 0°, 120°, and 240°, respectively. The case where balanced AC voltages are present is being included for comparison purposes. On the DC side, the second and tenth are increased due to the presence of E_2. The sixth harmonic is due to the presence of the fifth and seventh harmonics on the AC bus voltages. Again the cyclic pattern is present.

It is interesting to examine why and how the triplen harmonics pass through the Δ-connected converter transformer. As explained before, the triplens are present in the valve currents but, due to the $\frac{2\pi}{3}$ pulse length, the triplens cancel out. For the TCR, the Δ-connection prevents them from entering the AC system. For this discussion the case of E_2 =2.5% and $\theta = 0°$ presented in Table 3.12 will be used, but the results hold for any reasonable unbalance.

First, take note that the third harmonic components of the converter secondary currents and TCR currents are not cophasal; they are more like unbalanced 3-phase sets. This explains their propagation beyond the converter transformer. On the other hand, the third and ninth harmonics of the magnetizing currents are of the conventional zero sequence type.

To study the effect of both negative and zero sequence unbalance in the AC voltages, a 15% drop in V_a was applied. DC power was at half rated, and the ESCR was 3.97. The harmonic spectra of V_d, I_d, V_a, I_a and V_{bc} are presented in Table 3.13. The dominant harmonic components present in V_d are the second, fourth, sixth and tenth. On the AC side, the triplens are most dominant. Again, the zero sequence voltages do not seem to have much effect on the operation of the bridge, but the negative sequence voltages do.

The effects of varying the transformer saturation slope (TSS) and the TCR reference voltage (RV) magnitude on the harmonic generation are presented in Table 3.14. The DC current was again half rated, and the ESCR was 3.97. To force a saturated condition, the knee point was decreased to 0.86 pu. Reducing the TSS generates higher harmonic magnitudes and vice versa. This could be explained by the fact that when the slope is reduced, higher magnetizing currents are required at the desired AC voltage, and thus higher harmonic currents. For this system and operating conditions, raising the reference voltage

results in higher harmonic currents being generated, primarily from the higher magnetizing current, but also because the TCR current is reduced at higher AC voltage. This indicates that most saturation effect is dominant. Some unbalance is also present.

Table 3.15 presents the results from another operating condition where the DC current was at rated value and using the TCR operated to hold the terminal voltage at or close to rated value. This particular condition was obtained by raising the rectifier infinite bus voltage a few percent beyond rated value.

3.6 Conclusion

In this chapter, the basic relations governing the extra harmonic orders in the AC and DC variables in the presence of harmonic voltages or fundamental frequency voltage unbalance were set forth. Also presented were results to show that the inverse cosine (a form of IP) firing scheme is more sensitive to the AC voltage distortion, particularly when the distortion is large, than the pulse position control (a form of EP) firing scheme.

Results of transformer response to a DC component in the secondary side current were presented and indicated that the effect of a DC component tends to generate even harmonics on the AC side and odd harmonics on the DC side, which satisfied the above established relationship (section 3.3.1).

It was found also that the effect of the TCR and saturation on the converter could worsen as the operating point is changed, and that filters for the fifth and seventh harmonics are necessary, especially for large rated TCRs. Moreover, when unbalance is present, the triplen harmonics generated on the AC side are not entirely of the conventional zero sequence. These unbalanced triplens produce even harmonics on the DC side, the order of which can be predicted using the relationship set forth.

Operation at higher than rated terminal voltage can be troublesome to the proper operation of the converter in that the converter transformer is driven highly into saturation, which can produce sizeable amounts of uncharacteristic harmonics.

Besides the above general conclusions, this chapter presented a vast array of results on various operating conditions, results which could be useful in specific instances.

Table 3.1 Harmonic orders with second harmonic components

Sequence	V_d only fundamental		V_d opposite to fundamental		V_d same as fundamental		I_d only fundamental		I_d opposite to fundamental		I_d same as fundamental		I_a only fundamental		I_a opposite to fundamental		I_a same as fundamental	
h	IP	EP	IP	EP	IP	EP	IP	EP	IP	EP	IP	EP	IP	EP	IP	EP	IP	EP
0	100	100	100	100	100	100	100	100	100	100	100	100	-	-	-	-	-	-
1	-	-	-	-	3.804	5.935	-	-	-	-	3.379	5.355	100	100	100	100	100	100
2	0.115	0.128	0.115	0.133	0.071	0.287	0.470	0.508	0.367	0.426	0.439	0.394	-	-	-	-	3.542	2.505
3	-	-	8.659	6.883	-	-	-	-	2.010	1.612	-	-	0.185	0.317	0.200	0.365	0.175	0.105
4	-	-	-	-	-	-	-	-	-	-	-	-	-	-	2.979	1.094	-	-
8	-	-	-	-	-	-	-	-	-	-	-	-	-	-	1.223	0.846	-	-
9	-	-	0.386	0.691	-	-	-	-	0.068	0.122	-	-	-	-	-	-	-	-
10	-	-	-	-	-	-	-	-	-	-	-	-	-	-	1.017	0.533	0.838	1.048
11	-	-	-	-	0.544	0.207	-	-	-	-	-	-	5.804	5.719	5.513	5.548	5.483	5.610
12	2.169	2.184	2.068	2.284	2.332	2.304	0.258	0.257	0.252	0.273	0.233	0.251	-	-	-	-	1.268	1.282
13	-	-	-	-	0.071	0.524	-	-	-	-	-	-	4.043	4.007	3.788	3.923	3.753	3.807
14	-	-	-	-	-	-	-	-	-	-	-	-	-	-	1.115	0.453	1.148	0.352
15	-	-	0.717	0.465	-	-	-	-	-	-	-	-	-	-	-	-	-	-
16	-	-	-	-	-	-	-	-	-	-	-	-	-	-	0.888	0.435	-	-
20	-	-	-	-	-	-	-	-	-	-	-	-	-	-	0.161	0.214	-	-
21	-	-	1.277	0.485	-	-	-	-	-	-	-	-	-	-	-	-	-	-
22	-	-	-	-	-	-	-	-	-	-	-	-	-	-	0.196	0.171	0.216	0.086
23	-	-	-	-	0.896	0.960	-	-	-	-	-	-	0.419	0.438	0.350	0.514	0.415	0.557
24	3.231	2.898	2.504	2.638	2.554	2.618	0.190	0.158	0.130	0.151	0.128	0.129	-	-	-	-	0.235	0.189

Table 3.2 Harmonic orders with fourth harmonic components

	V_d				I_d				I_a			
Sequ-	same as fundamental		opposite to fundamental		same as fundamental		opposite to fundamental		same as fundamental		opposite to fundamental	
-ence	.....	.....	.....	.....	.....	.....	.....	.....	.....	.....	.....	.....
h	IP	EP	IP	EP	IP	EP	IP	EP	IP	EP	IP	EP
0	100	100	100	100	100	100	100	100	-	-	-	-
1	-	-	-	-	-	-	-	-	100	100	100	100
2	0.105	0.099	0.092	0.129	0.365	0.407	0.340	0.500	-	-	-	-
3	6.632	6.559	-	-	2.180	2.203	-	-	0.233	0.347	0.231	0.492
4	-	-	-	-	-	-	-	-	1.048	2.314	-	-
5	-	-	5.555	5.679	-	-	1.593	1.586	-	-	-	-
6	-	-	-	-	-	-	-	-	-	-	0.694	0.879
7	-	-	0.715	0.565	-	-	0.151	0.090	-	-	-	-
8	-	-	-	-	-	-	-	-	0.261	0.674	0.186	0.696
9	0.665	0.582	-	-	-	-	-	-	-	-	-	-
10	-	-	-	-	-	-	-	-	0.170	0.699	-	-
11	-	-	-	-	-	-	-	-	5.755	5.578	5.707	5.534
12	2.149	2.340	2.212	2.311	0.250	0.254	0.243	0.226	-	-	-	-
13	-	-	-	-	-	-	-	-	4.016	3.931	3.967	3.730
14	-	-	-	-	-	-	-	-	0.542	0.718	-	-
15	0.729	0.697	-	-	-	-	-	-	-	-	-	-
16	-	-	-	-	-	-	-	-	0.442	0.561	0.444	0.580
17	-	-	0.479	0.345	-	-	-	-	-	-	-	-

Table 3.3 Harmonics of the A-phase converter current with 5% negative sequence

	0°		45°		90°		135°		180°		225°		270°		315°	
h	IP	EP	IP	EP	IP	EP	IP	EP	IP	EP	IP	EP	IP	EP	IP	EP
1	100	100	100	100	100	100	100	100	100	100	100	100	100	100	100	100
2	0.144	0.398	0.177	0.243	0.225	0.390	0.203	0.368	0.219	0.281	0.173	0.291	0.137	0.340	-	0.363
3	2.222	2.138	2.703	1.866	2.486	1.430	2.112	0.931	1.883	0.808	1.973	1.204	2.284	1.774	2.561	2.181
5	-	-	-	0.212	0.115	0.257	-	0.160	0.197	-	0.118	0.180	0.200	0.230	-	0.167
7	0.648	0.164	0.684	0.129	0.603	-	0.508	0.110	0.529	-	0.532	-	0.487	0.106	0.557	0.141
8	0.154	0.103	0.233	0.117	0.327	0.111	0.337	-	0.302	-	0.194	-	0.133	-	0.113	-
9	2.620	1.237	3.118	1.248	3.332	1.142	3.163	1.008	2.972	0.973	2.611	0.975	2.361	1.070	2.336	1.172
10	0.328	-	0.577	-	0.825	-	0.916	-	0.800	-	0.525	-	0.250	-	0.130	-
11	4.367	7.528	6.158	7.476	7.758	6.879	8.202	6.223	7.209	5.660	5.200	5.793	3.221	6.415	2.791	7.147
12	0.690	0.171	0.753	-	0.743	-	0.717	-	0.749	-	0.740	-	0.683	-	0.615	-
13	5.446	4.710	4.613	4.284	3.039	4.096	1.447	4.351	2.749	4.666	4.485	5.007	5.419	5.151	5.714	5.089
14	0.593	-	0.453	-	0.274	-	-	-	0.216	-	0.432	-	0.600	-	0.617	-
15	2.555	0.517	2.349	0.512	1.803	0.520	1.549	0.544	1.744	0.559	2.118	0.567	2.544	0.574	2.795	0.548
16	0.280	-	0.216	-	0.131	-	-	-	0.124	-	0.197	-	0.256	-	0.311	-

Table 3.4 Harmonics of the A-phase converter current with 10% negative sequence

	0°		45°		90°		135°		180°		225°		270°		315°	
h	IP	EP	IP	EP	IP	EP	IP	EP	IP	EP	IP	EP	IP	EP	IP	EP
1	100	100	100	100	100	100	100	100	100	100	100	100	100	100	100	100
2	-	0.257	0.132	0.225	0.185	0.225	0.304	0.207	0.275	-	0.223	-	0.154	0.129	0.194	0.179
3	4.593	3.860	5.090	3.326	5.396	2.585	5.193	2.040	3.606	2.081	4.174	2.514	4.192	3.265	4.270	3.790
4	0.150	0.129	-	0.142	0.137	0.105	-	-	-	-	-	-	0.119	-	0.106	-
5	0.487	0.444	0.440	0.811	0.453	0.625	0.583	0.583	0.837	0.453	0.221	0.456	0.804	0.570	0.290	0.494
6	0.130	-	0.155	-	0.225	-	0.286	-	0.164	-	0.107	-	-	-	-	-
7	1.802	0.619	2.157	0.667	2.596	0.483	2.539	0.641	2.074	0.453	1.982	0.218	1.511	0.396	1.336	0.431
8	0.189	0.105	0.448	0.205	0.695	0.122	0.768	-	0.526	0.112	0.321	-	0.147	-	-	-
9	3.221	2.545	4.975	2.639	6.380	2.570	6.562	2.222	5.660	1.770	4.161	1.638	2.735	1.722	2.236	2.056
10	0.308	-	0.598	0.114	0.925	-	1.036	-	0.684	0.143	0.424	-	0.173	-	0.113	-
11	2.972	7.958	4.523	7.787	5.973	6.551	6.289	5.097	5.196	4.530	2.685	4.859	0.615	6.052	1.605	7.297
12	0.432	-	0.558	-	0.458	0.103	0.149	-	0.342	-	0.413	-	0.303	0.160	0.172	-
13	4.000	4.771	4.273	4.036	4.070	3.241	3.053	3.375	2.377	4.157	3.012	4.691	3.272	5.090	3.571	5.183
14	0.562	-	0.481	-	0.461	-	0.389	-	0.275	-	0.360	-	0.420	-	0.442	-
15	3.796	0.669	3.343	0.669	1.843	0.915	0.838	0.987	2.029	1.086	2.972	1.116	3.663	0.970	3.906	0.836
16	0.474	-	0.356	-	0.116	-	-	-	0.153	-	0.251	-	0.386	-	0.424	-

Table 3.5 Harmonics with 20% drop in phase A of Thevenin's source voltage

	I P				E P			
h	V_d	I_d	V_a	I_a	V_d	I_d	V_a	I_a
0	100	100	-	-	100	100	-	-
1	-	-	100	100	-	-	100	100
2	5.193	7.185	0.609	0.433	4.130	5.934	0.376	0.373
3	0.277	-	6.268	2.700	0.448	-	2.007	0.806
4	0.354	0.124	-	-	0.408	0.153	-	-
5	-	-	-	-	-	-	0.220	0.203
7	-	-	0.361	0.765	-	-	-	0.330
8	0.262	-	0.129	0.395	0.270	-	-	-
9	-	-	0.809	3.358	-	-	0.356	1.277
10	0.732	-	0.100	0.574	1.245	0.153	-	0.153
11	0.131	-	0.237	5.769	-	-	0.163	4.128
12	1.916	0.200	0.129	0.698	2.682	0.285	-	0.163
13	0.215	-	-	1.188	-	-	0.163	3.186
14	1.335	0.131	-	0.361	0.641	-	-	-
15	0.124	-	0.262	1.417	0.146	-	0.157	0.792
16	0.200	-	-	0.268	0.408	-	-	-

Table 3.6 Steady-state balanced AC voltages with a nonlinear converter transformer

	IP				EP			
h	NO SATURATION		WITH SATURATION		NO SATURATION		WITH SATURATION	
	V_d	Ia	V_d	Ia	V_d	Ia	V_d	Ia
0	100.000	0.130	100.000	0.060	100.000	0.029	100.000	0.056
1	0.064	100.000	0.058	100.000	0.078	100.000	0.014	100.000
2	0.071	0.079	0.124	0.081	0.071	0.427	0.092	0.406
3	0.021	0.184	0.007	0.280	0.440	0.503	0.388	0.527
4	0.057	0.018	0.233	0.007	0.041	0.011	0.092	0.015
5	0.064	0.072	0.058	0.453	0.027	0.327	0.035	0.270
6	0.028	0.018	0.385	0.018	0.021	0.015	0.309	0.011
7	0.034	0.074	0.035	0.393	0.014	0.090	0.021	0.167
8	0.014	0.022	0.058	0.028	0.014	0.061	0.021	0.068
9	0.028	0.163	0.	0.177	0.064	0.191	0.048	0.209
10	0.092	0.097	0.079	0.060	0.141	0.105	0.115	0.102
11	0.007	5.977	0.007	6.003	0.021	5.998	0.021	5.957
12	1.847	0.060	2.244	0.032	1.825	0.034	2.172	0.011
13	0.007	4.175	0.022	4.232	0.048	4.315	0.021	4.313
14	0.057	0.039	0.042	0.039	0.041	0.061	0.048	0.090
15	0.041	0.090	0.022	0.086	0.048	0.044	0.042	0.051
16	0.021	0.022	0.042	0.002	0.021	0.044	0.014	0.056
17	0.041	0.022	0.014	0.152	0.021	0.023	0.014	0.075
18	0.021	0.011	0.107	0.007	0.091	0.008	0.099	0.011
19	0.041	0.007	0.028	0.104	0.021	0.049	0.028	0.041
20	0.014	0.018	0.042	0.018	0.007	0.024	0.007	0.034

Table 3.7 Harmonics with 20% drop in phase A of Thevenin's source voltage with a nonlinear converter transformer

	IP				EP			
h	NO SATURATION		WITH SATURATION		NO SATURATION		WITH SATURATION	
	V_d	I_a	V_d	I_a	V_d	I_a	V_d	I_a
0	100.000	0.145	100.000	0.158	100.000	0.178	100.000	0.162
1	0.000	100.000	0.110	100.000	0.367	100.000	0.397	100.000
2	6.131	0.029	7.116	0.023	4.985	0.120	4.638	0.147
3	0.062	3.162	0.087	1.291	0.238	1.075	0.234	1.142
4	0.451	0.011	4.000	0.015	0.487	0.189	0.623	0.183
5	0.045	0.375	0.064	0.797	0.046	0.185	0.096	0.264
6	0.154	0.049	0.245	0.049	0.095	0.142	0.348	0.144
7	0.023	1.062	0.024	1.268	0.064	0.369	0.130	0.531
8	0.381	0.096	0.966	0.099	0.272	0.023	0.509	0.023
9	0.007	3.805	0.024	3.645	0.128	1.503	0.112	1.365
10	0.831	0.091	0.478	0.096	1.393	0.246	1.119	0.237
11	0.007	5.174	0.016	5.591	0.038	4.229	0.047	4.232
12	1.640	0.061	1.470	0.072	2.549	0.081	2.847	0.099
13	0.037	1.311	0.024	1.607	0.054	3.423	0.138	3.418
14	1.439	0.015	1.564	0.035	0.751	0.134	0.924	0.151
15	0.007	1.369	0.016	1.622	0.072	0.881	0.080	0.830
16	0.319	0.023	0.054	0.011	0.503	0.028	0.478	0.046
17	0.023	1.031	0.038	0.695	0.095	0.351	0.104	0.303
18	0.326	0.037	0.414	0.023	0.310	0.060	0.356	0.048
19	0.023	0.554	0.038	0.353	0.087	0.079	0.096	0.122
20	1.080	0.034	1.094	0.011	0.374	0.067	0.371	0.080

Table 3.8 Harmonics of the A-phase TCR current with ideal-voltage source

(a) Computed values

h	α=30°	α=18°	α=54°	α=13°	α=38°
1	39.100	61.290	9.727	71.602	26.892
5	2.757	5.046	3.118	4.584	0.083
7	0.984	2.110	0.190	2.586	2.069
11	0.501	0.283	0.459	0.640	0.678
13	0.303	0.573	0.183	0.154	0.455

(b) Measured values

1	39.100	61.156	9.940	71.476	26.238
5	2.538	5.302	3.329	5.157	0.587
7	1.294	1.847	0.278	2.582	2.139
11	0.337	0.610	0.553	0.325	0.830
13	0.444	0.711	0.127	0.143	0.298

Table 3.9 Harmonics of the A-phase TCR current with 2.5, 5 and 10% negative sequence

(a) Balanced AC voltages

h	α=30°	α=18°	α=54°	α=13°	α=38°
3	0.405	0.171	0.998	0.112	0.746
5	6.492	8.670	33.490	7.215	2.239
7	3.309	3.020	2.796	3.612	8.153
9	0.168	0.016	0.320	0.037	0.014

(b) 2.5% of negative sequence

h	α=30°	α=18°	α=54°	α=13°	α=38°
3	1.840	1.049	3.371	0.785	2.258
5	6.095	8.135	32.077	6.855	2.097
7	3.553	3.137	3.248	3.797	8.648
9	0.471	0.050	1.126	0.257	0.152

(c) 5% of negative sequence

3	4.151	2.331	7.748	1.654	5.295
5	5.631	7.515	29.514	6.426	2.053
7	3.678	3.270	3.428	4.023	8.978
9	1.132	0.087	2.932	0.555	0.312

(d) 10% of negative sequence

3	8.333	4.657	15.837	3.327	10.948
5	4.659	6.249	24.542	5.378	1.668
7	3.808	3.352	3.268	4.141	9.234
9	2.258	0.165	5.244	1.024	0.526

Table 3.10 Harmonics of the A-phase TCR current with 10% of negative sequence

h	θ=0°	θ=120°	θ=240°
3	5.157	3.902	4.113
5	6.675	0.435	0.246
7	0.248	0.172	0.275
9	1.433	1.008	1.035

Table 3.11 Harmonics with 2.5% of negative sequence (nonlinear transformer and TCR included)

(a) Balanced AC voltages

h	V_d	I_d	V_a	I_a	V_{bc}
2	0.235	2.716	0.680	0.444	0.524
3	0.632	0.433	2.799	4.086	1.242
4	0.822	0.883	0.437	0.523	0.464
5	0.356	0.192	0.265	1.187	0.449
6	0.794	0.255	0.052	0.058	0.048
7	0.153	0.096	0.628	1.117	0.826
8	0.114	0.026	0.041	0.212	0.024
9	0.108	0.026	0.048	0.112	0.094
10	0.870	0.053	0.029	0.195	0.007

(b) 2.5% of negative sequence with θ=0°

2	1.164	4.670	0.953	0.502	0.352
3	0.716	0.559	5.251	4.582	0.569
4	1.186	1.091	0.473	0.559	0.372
5	0.354	0.222	0.344	2.091	0.564
6	0.367	0.210	0.020	0.094	0.064
7	0.086	0.035	0.745	1.429	0.796
8	0.382	0.085	0.035	0.192	0.044
9	0.073	0.035	0.219	2.287	0.406
10	1.400	0.182	0.035	0.343	0.011

(c) 2.5% of negative sequence with θ=120°

2	2.313	9.505	0.798	0.301	0.506
3	0.670	0.497	3.292	5.673	3.980
4	1.676	1.615	0.424	0.235	0.332
5	0.388	0.244	0.518	0.771	0.673
6	0.843	0.273	0.029	0.031	0.095
7	0.060	0.026	0.518	0.788	0.864
8	0.180	0.068	0.048	0.341	0.024
9	0.099	0.006	0.286	3.374	0.294
10	1.380	0.165	0.038	0.301	0.011

(d) 2.5% of negative sequence with θ=240°

2	1.940	9.229	0.617	0.413	0.399
3	0.718	0.337	1.237	1.500	1.673
4	0.812	0.665	0.412	0.185	0.385
5	0.395	0.199	0.587	0.700	0.358
6	1.053	0.390	0.081	0.116	0.067
7	0.127	0.026	0.558	0.917	0.791
8	0.032	0.068	0.019	0.153	0.060
9	0.140	0.035	0.315	2.744	0.201
10	1.014	0.165	0.025	0.134	0.067

Table 3.12 Harmonic magnitudes and phases of the converter, magnetizing, and TCR currents with 2.5% of negative sequence

(a) Converter transformer primary currents

	I_a		I_b		I_c	
h	mag	phase	mag	phase	mag	phase
1	100.000	-54.371	100.000	178.340	100.000	60.199
3	6.777	26.883	2.929	23.280	6.438	50.009
5	3.970	70.515	3.176	175.190	2.681	-46.895
7	2.657	92.439	2.201	-30.075	2.637	-142.110
9	2.060	-91.351	2.721	27.559	4.120	150.040

(b) Converter transformer secondary currents

1	100.000	-57.128	100.000	174.440	100.000	56.524
3	2.581	-15.111	1.685	-116.140	2.111	55.134
5	0.441	-30.602	0.251	45.631	0.469	140.590
7	0.432	30.684	0.227	19.055	0.834	-144.320
9	3.164	-65.648	2.638	1.873	3.526	156.870

(c) Magnetizing currents

1	100.000	-165.130	100.000	74.130	100.000	-46.702
3	71.695	-134.050	68.482	-136.950	69.284	-139.590
5	54.447	-104.660	54.022	10.690	51.739	126.490
7	34.181	-76.832	34.809	157.130	31.482	31.492
9	16.458	-55.695	16.590	-63.550	13.502	-71.048

(d) TCR currents

1	100.000	8.613	100.000	-114.780	100.000	126.380
3	4.453	22.110	0.893	-162.760	3.526	-163.980
5	19.692	-135.760	21.904	-34.804	23.508	91.702
7	5.199	63.704	4.669	-75.646	4.721	168.400
9	1.232	68.032	0.520	-156.170	1.268	-134.610

Table 3.13 Harmonics with 15% drop in phase A of Thevenin's source voltage (nonlinear transformer and TCR included)

h	V_d	I_d	V_a	I_a	V_{bc}
2	2.452	9.257	0.050	0.255	0.135
3	0.140	0.238	3.728	4.381	3.905
4	1.840	1.740	0.200	0.315	0.061
5	0.087	0.079	1.565	1.514	0.845
6	1.125	0.523	0.095	0.165	0.033
7	0.017	0.018	0.594	1.931	0.594
8	0.600	0.193	0.039	0.276	0.022
9	0.008	0.044	0.394	5.078	0.201
10	1.577	0.181	0.050	0.251	0.040

Table 3.14 Effects of the transformer saturation characteristic slope and the TCR operating point on harmonic ganeration

(a) X_{m2}=0.5 pu and V_{ref}=0.81 pu

h	V_d	I_d	V_a	I_a	V_{bc}
2	0.919	1.598	0.795	0.417	0.481
3	0.494	0.108	1.115	0.976	2.425
4	0.690	0.178	0.167	0.313	0.204
5	0.109	0.016	0.102	0.099	0.074
6	0.527	0.070	0.046	0.028	0.028
7	0.057	0.008	0.538	0.111	0.383
8	0.049	0.016	0.024	0.078	0.045
9	0.068	0.008	0.074	0.346	0.101
10	0.169	0.038	0.003	0.147	0.018

(b) X_{m2}=0.33 pu and V_{ref}=0.81 pu

2	1.054	1.395	0.607	0.203	0.235
3	0.436	0.149	1.146	1.103	2.612
4	0.673	0.242	0.097	0.134	0.099
5	0.073	0.008	0.459	0.502	0.415
6	0.680	0.126	0.015	0.127	0.048
7	0.088	0.008	0.644	0.759	0.603
8	0.138	0.008	0.029	0.130	0.057
9	0.073	0.008	0.085	0.011	0.105
10	0.130	0.008	0.023	0.145	0.009

(c) X_{m2}=0.5 pu and V_{ref}=0.89 pu

2	0.727	1.522	0.528	0.100	0.319
3	0.456	0.086	1.969	1.697	2.008
4	0.635	0.283	0.079	0.206	0.123
5	0.124	0.008	0.760	0.676	0.743
6	1.131	0.172	0.018	0.060	0.057
7	0.052	0.008	0.379	0.922	0.329
8	0.099	0.023	0.022	0.093	0.049
9	0.052	0.016	0.054	0.127	0.071
10	0.154	0.008	0.014	0.079	0.013

(d) X_{m2}=0.33 pu and V_{ref}=0.89 pu

2	0.876	1.462	0.605	0.328	0.221
3	0.545	0.134	4.239	3.832	2.307
4	0.773	0.268	0.142	0.204	0.076
5	0.078	0.	0.526	2.233	0.874
6	1.078	0.157	0.065	0.211	0.049
7	0.030	0.008	0.652	2.325	0.689
8	0.155	0.024	0.033	0.161	0.054
9	0.148	0.016	0.168	0.966	0.087
10	0.188	0.024	0.033	0.147	0.027

Table 3.15 Harmonics due to saturation effect and TCR operation for rated DC current

(a) Linear transformer and no TCR

h	V_d	I_d	V_a	I_a	V_{bc}
2	0.327	1.323	0.143	0.097	0.034
3	0.063	0.025	0.827	0.408	1.125
4	0.034	0.040	0.036	0.078	0.069
5	0.034	0.008	0.025	0.041	0.019
6	0.021	0.008	0.021	0.015	0.011
7	0.021	0.008	0.032	0.029	0.034
8	0.021	0.008	0.025	0.029	0.044
9	0.034	0.008	0.078	0.306	0.064
10	0.369	0.040	0.032	0.036	0.011

(b) Nonlinear transformer and TCR included

2	0.405	1.092	0.151	0.201	0.078
3	0.622	0.172	0.510	0.864	1.328
4	0.448	0.122	0.354	0.252	0.244
5	0.208	0.090	1.592	0.520	1.278
6	1.643	0.305	0.061	0.002	0.068
7	0.112	0.016	0.021	0.277	0.085
8	0.040	0.	0.036	0.029	0.029
9	0.040	0.008	0.078	0.352	0.083
10	0.313	0.008	0.025	0.023	0.024

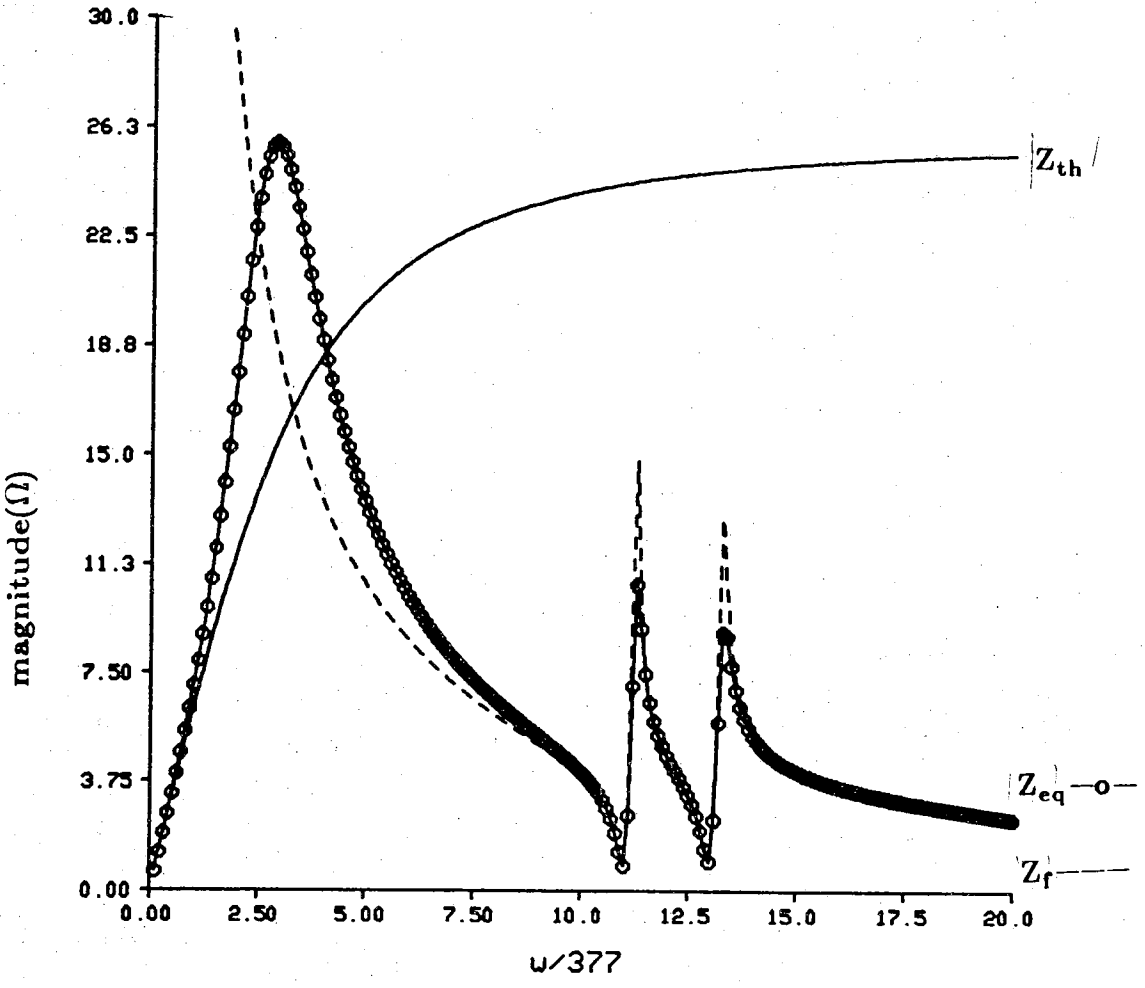

(a) Magnitude

Figure 3.1 AC impedance as seen from the converter bus

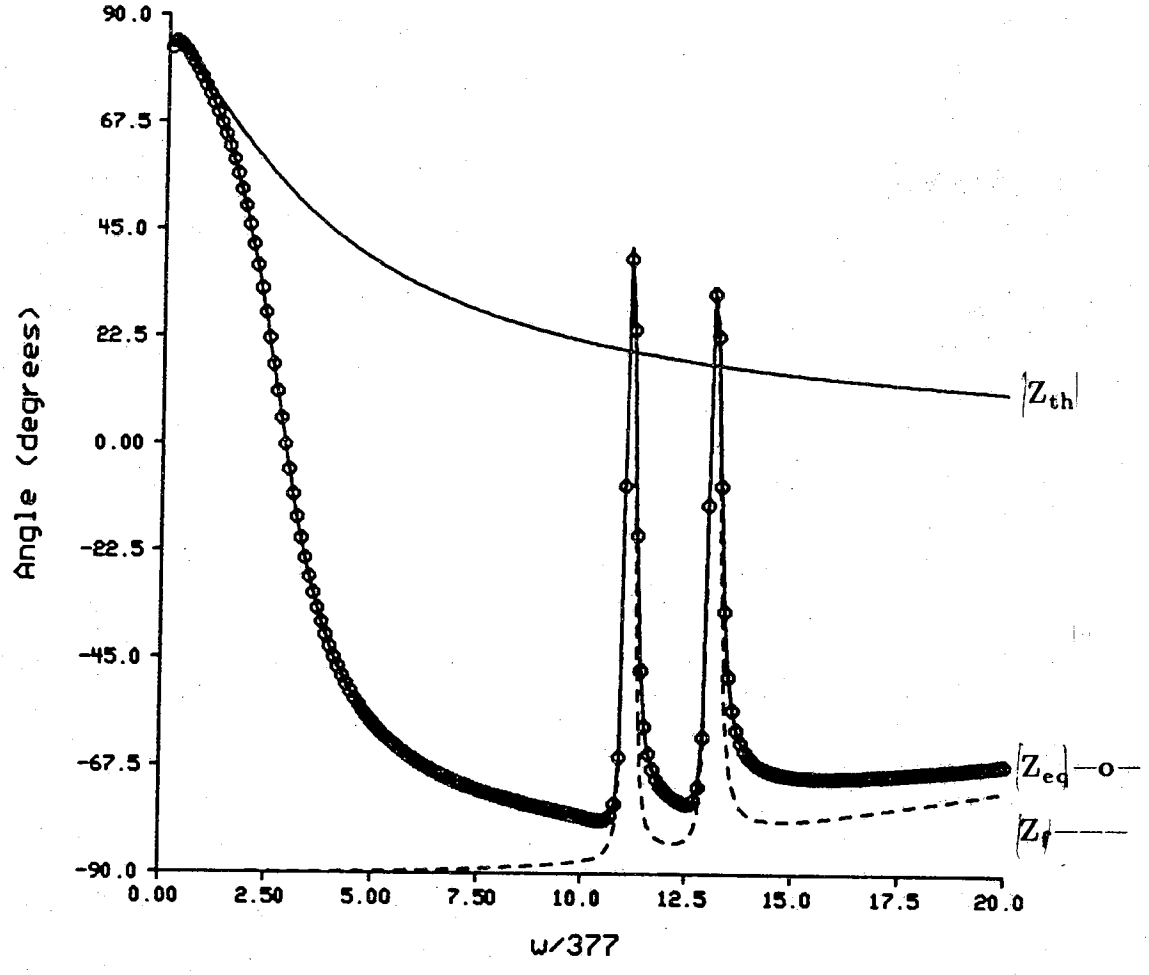

(b) Phase angle

Figure 3.1 continued

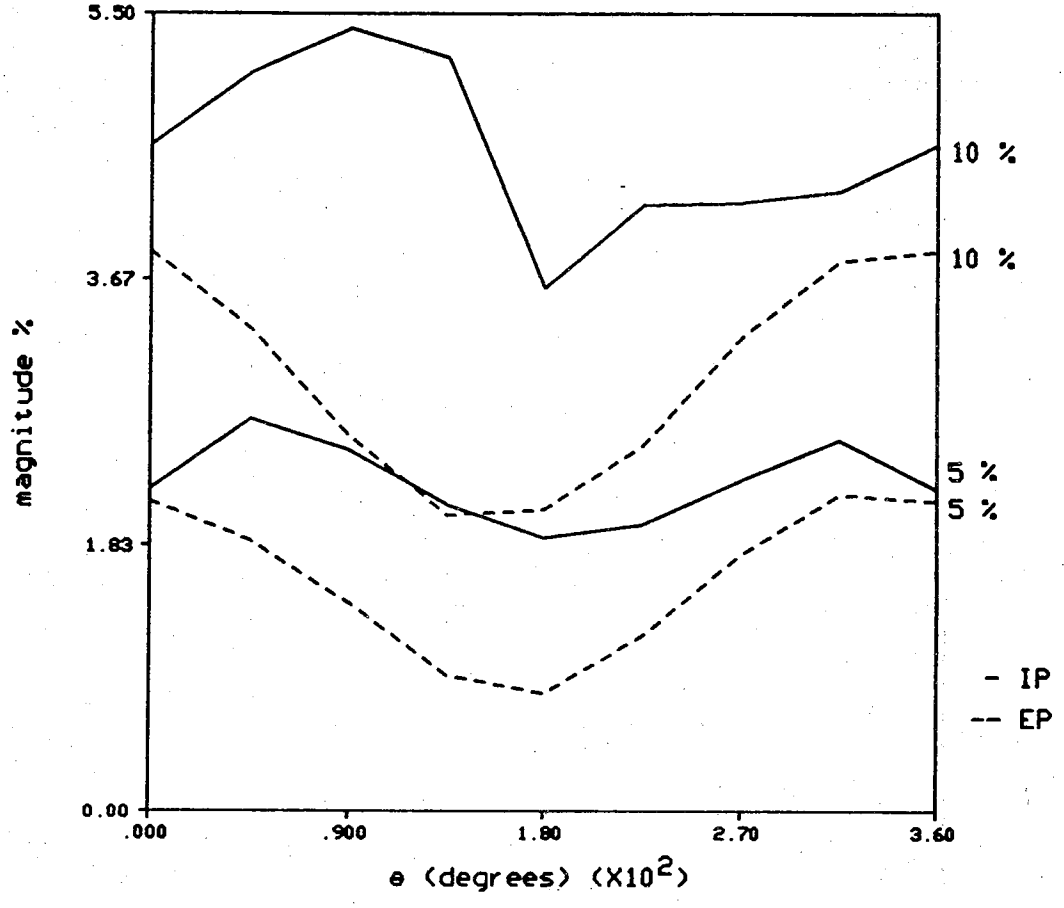

(a) Third harmonic

Figure 3.2 Harmonic characteristic with negative-sequence unbalance

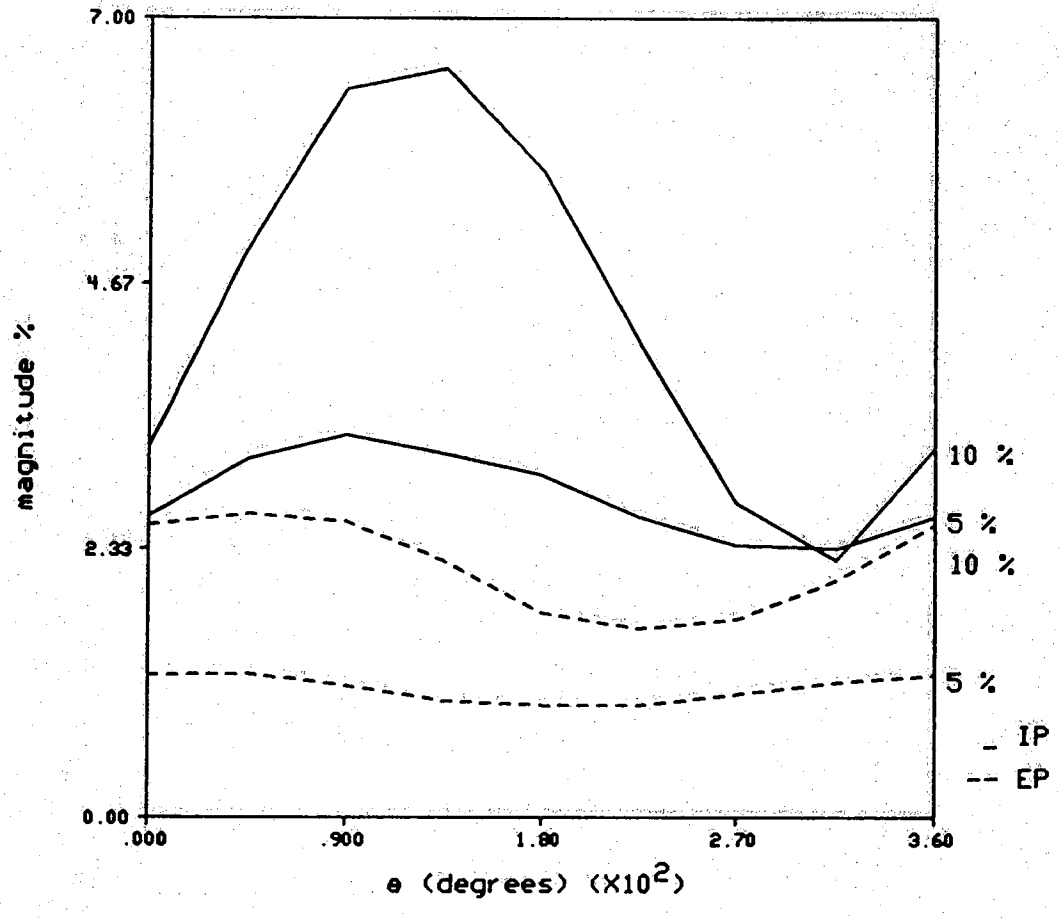

(b) Ninth harmonic

Figure 3.2 continued

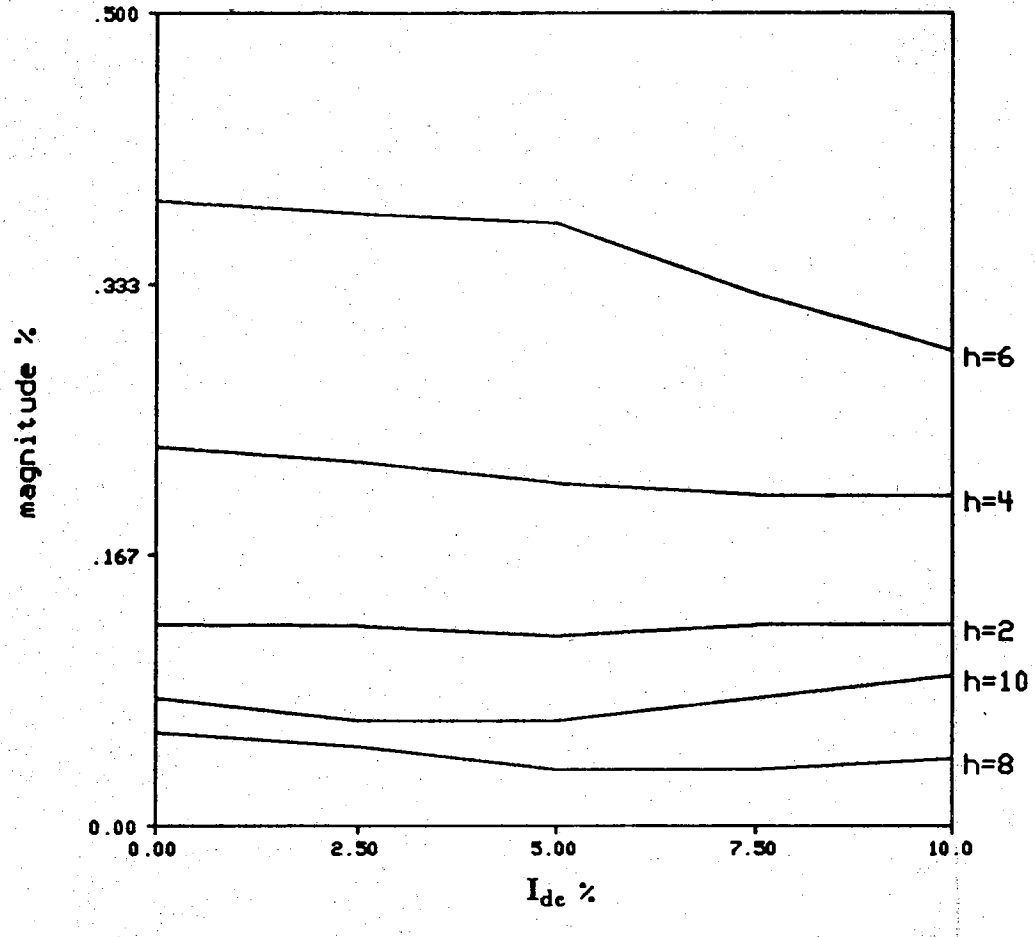

(a) Even harmonics in the DC voltage

Figure 3.3 Uncharacteristic harmonics due to the presence of a DC component in the secondary side of the converter transformer

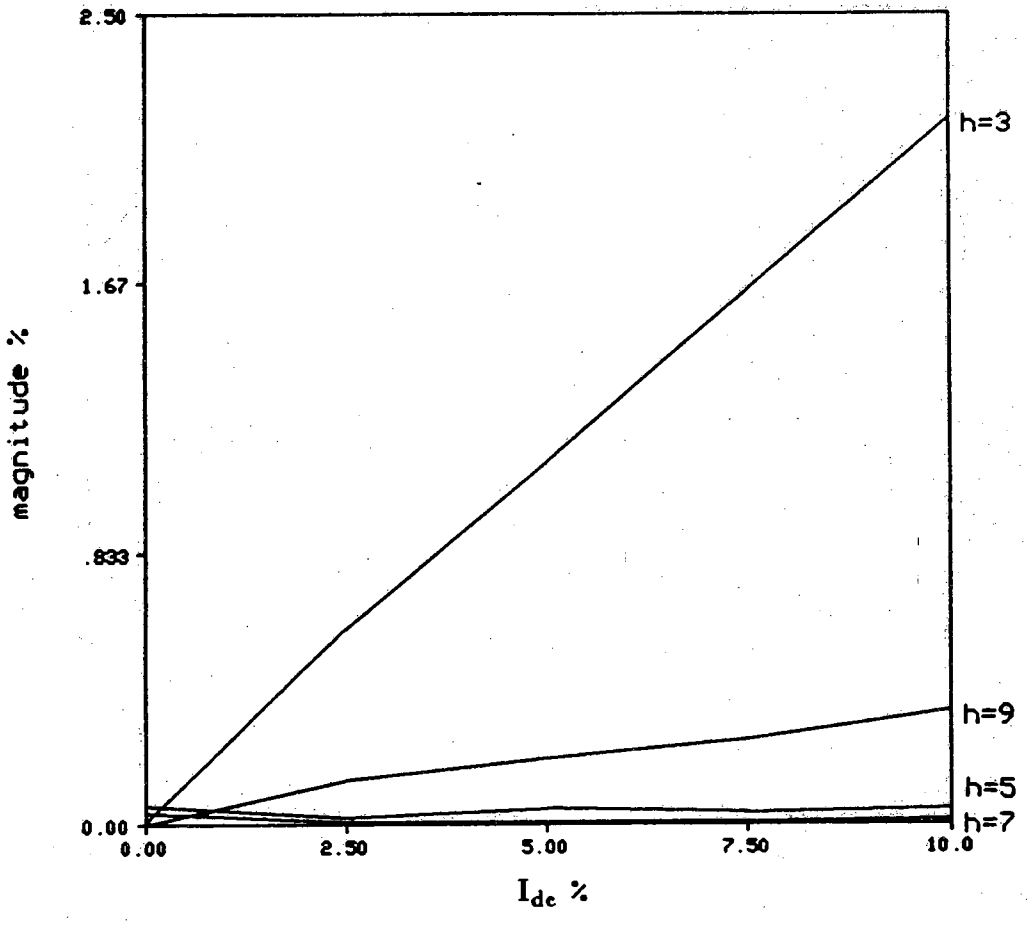

(b) Odd harmonics in the DC voltage

Figure 3.3 continued

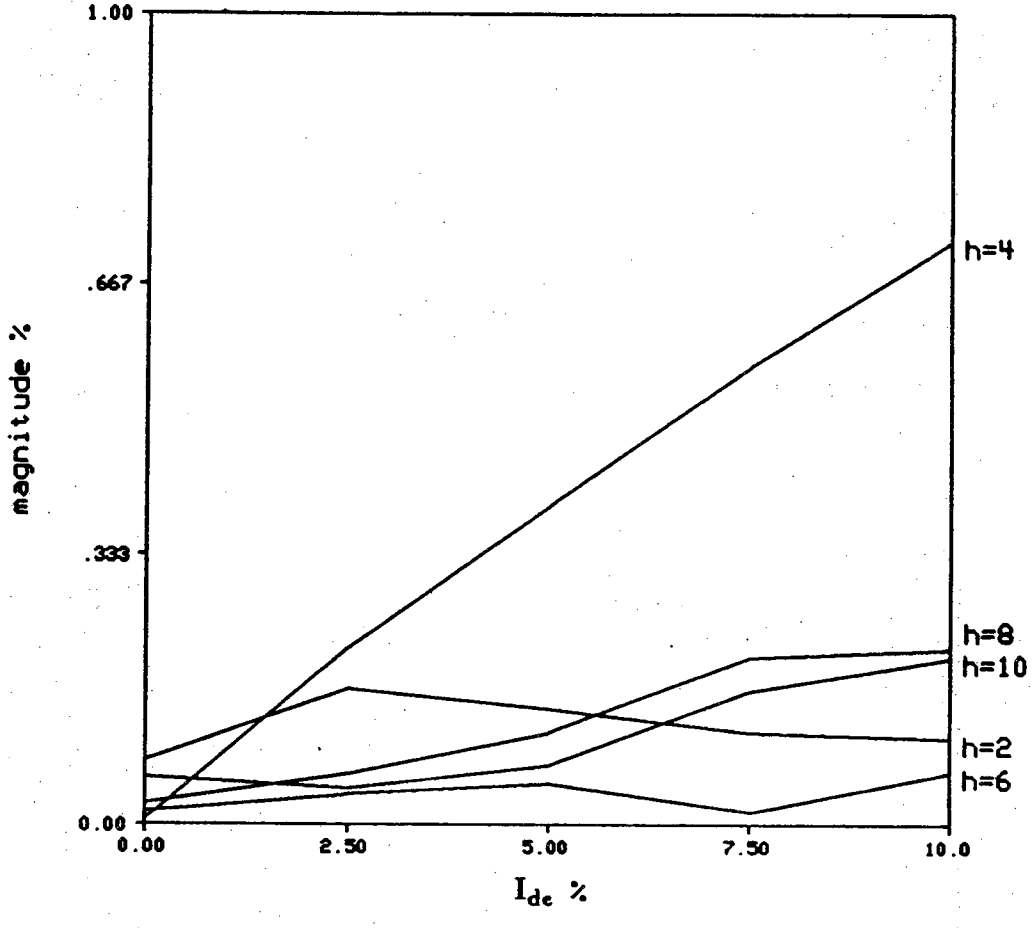

(c) Even harmonics in the converter AC current

Figure 3.3 continued

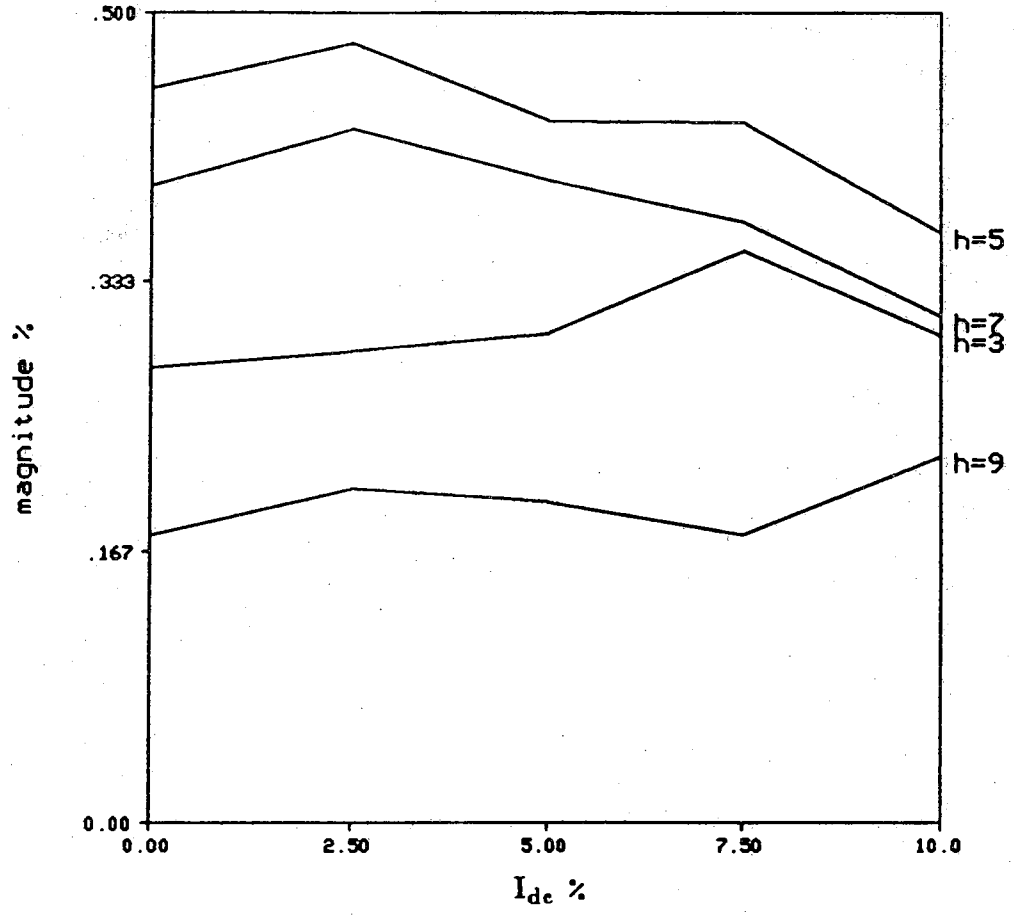

(d) Odd harmonics in the converter AC current

Figure 3.3 continued

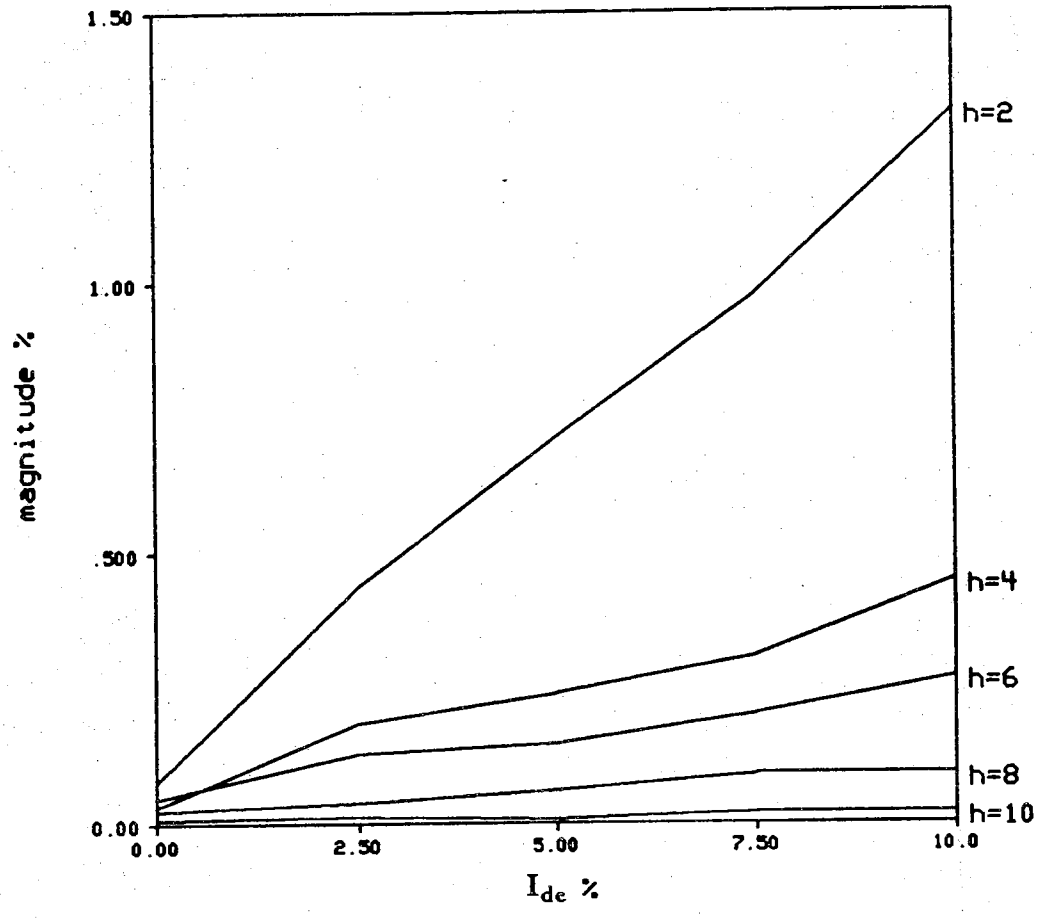

(e) Even harmonics in the terminal AC voltage

Figure 3.3 continued

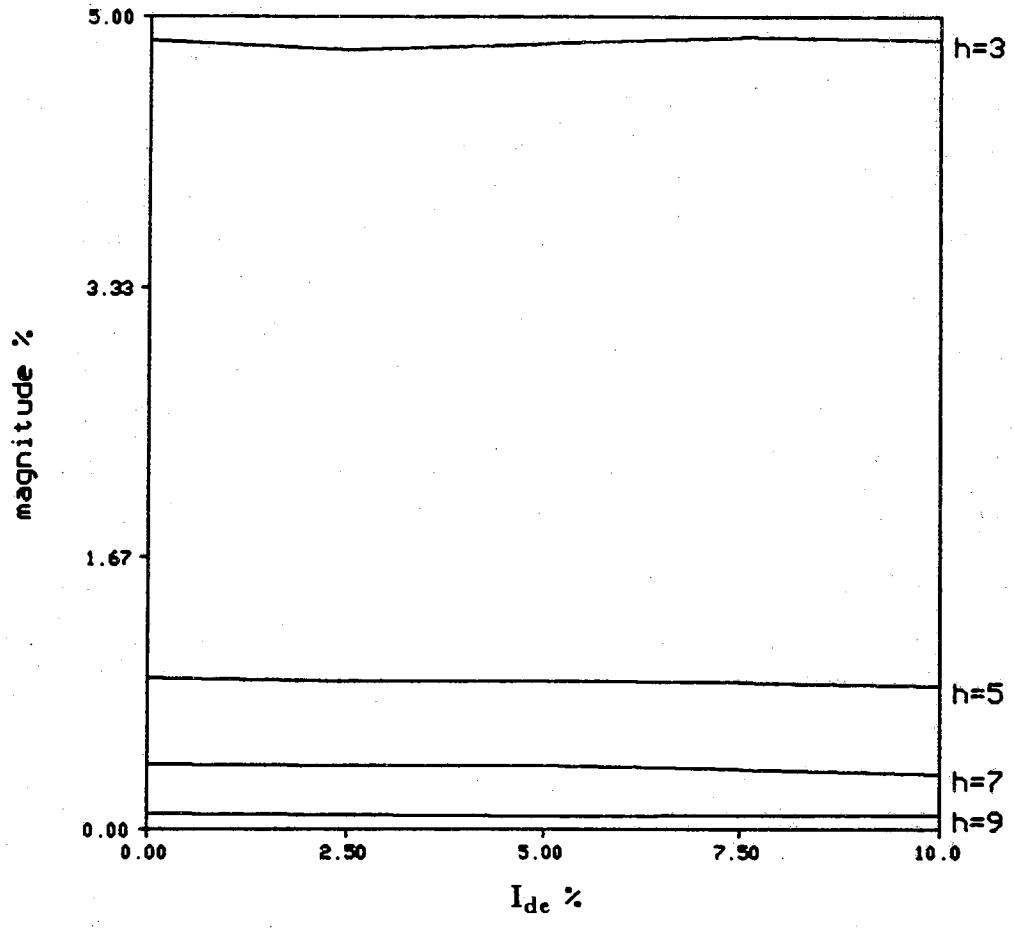

(f) Odd harmonics in the terminal AC voltage

Figure 3.3 continued

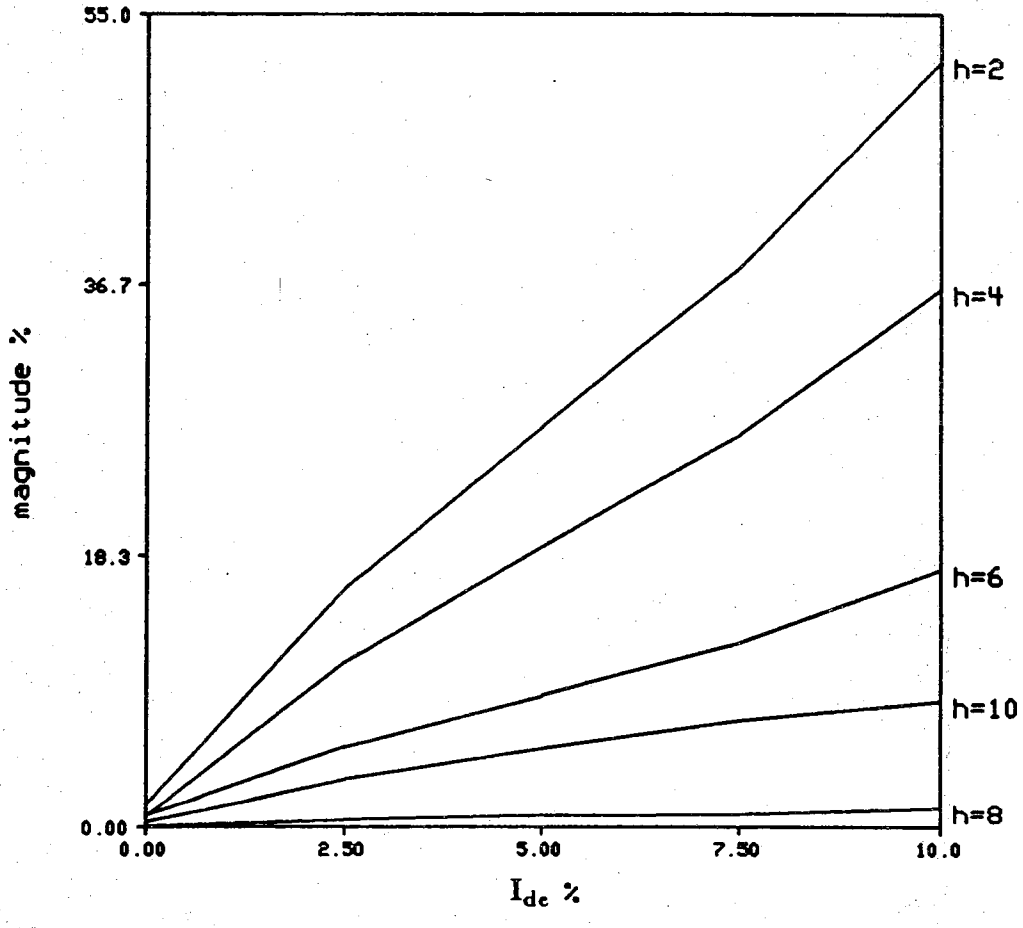

(g) Even harmonics in the transformer magnetizing current

Figure 3.3 continued

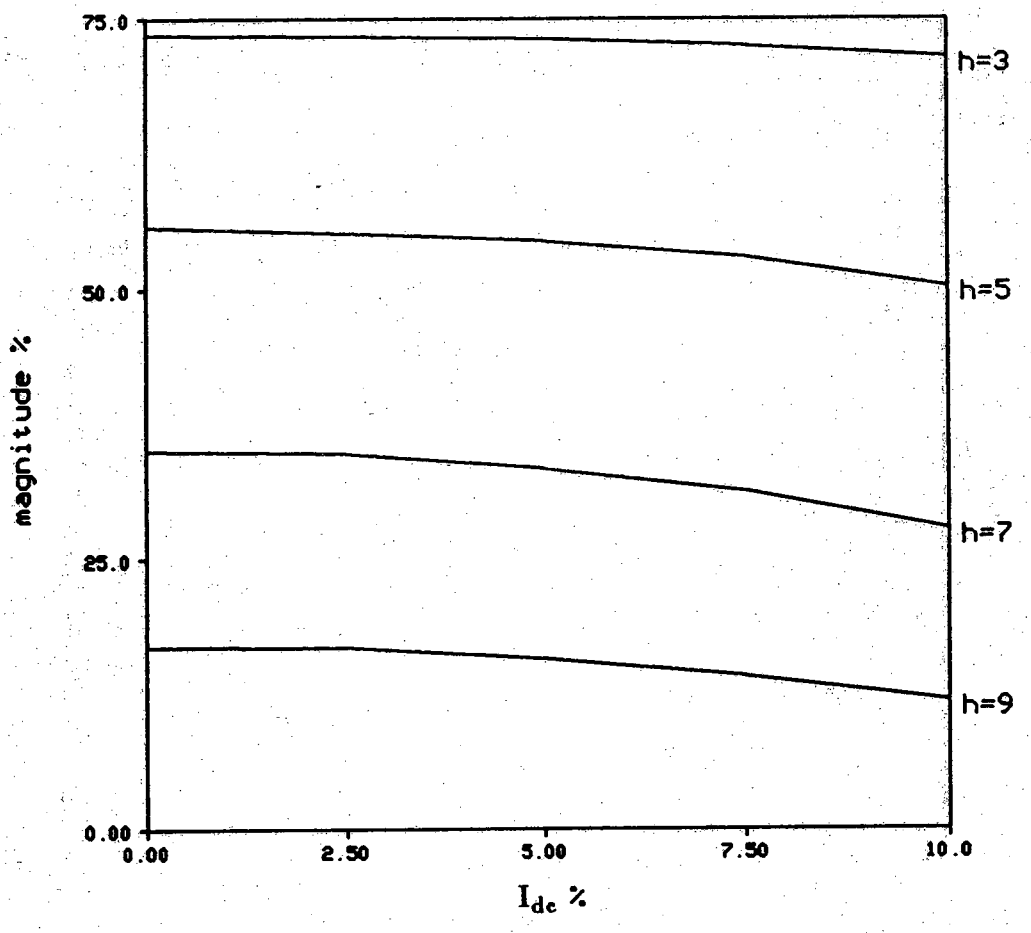

(h) Odd harmonics in the transformer magnetizing current

Figure 3.3 continued

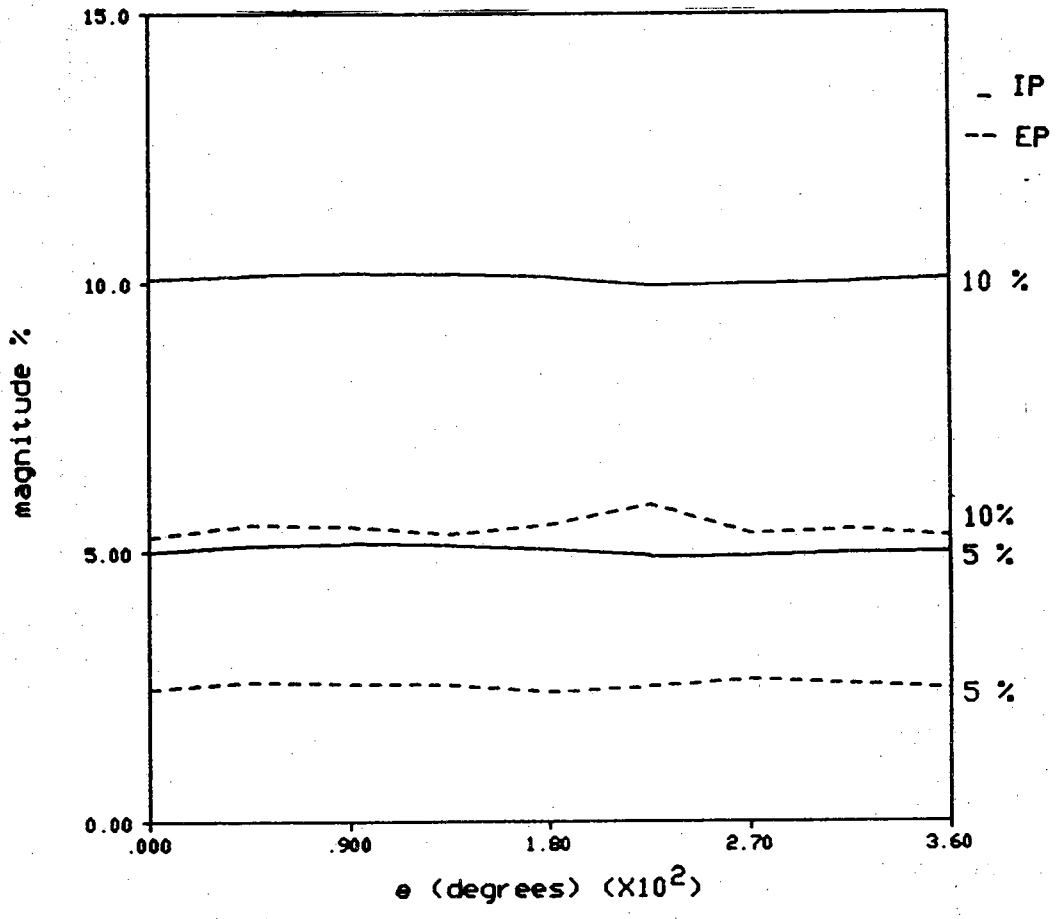

(a) Second harmonic in the DC voltage

Figure 3.4 Uncharacteristic harmonics due to negative-sequence and transformer saturation

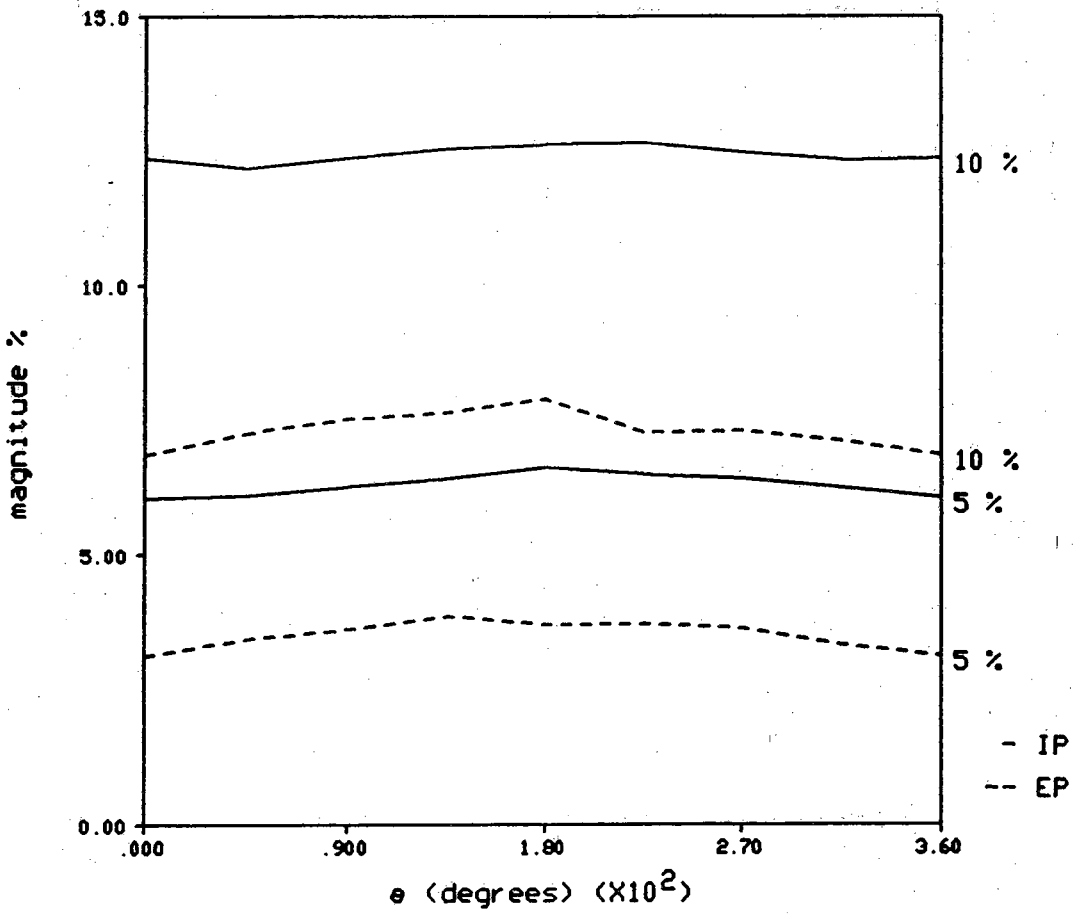

(b) Second harmonic in the DC current

Figure 3.4 continued

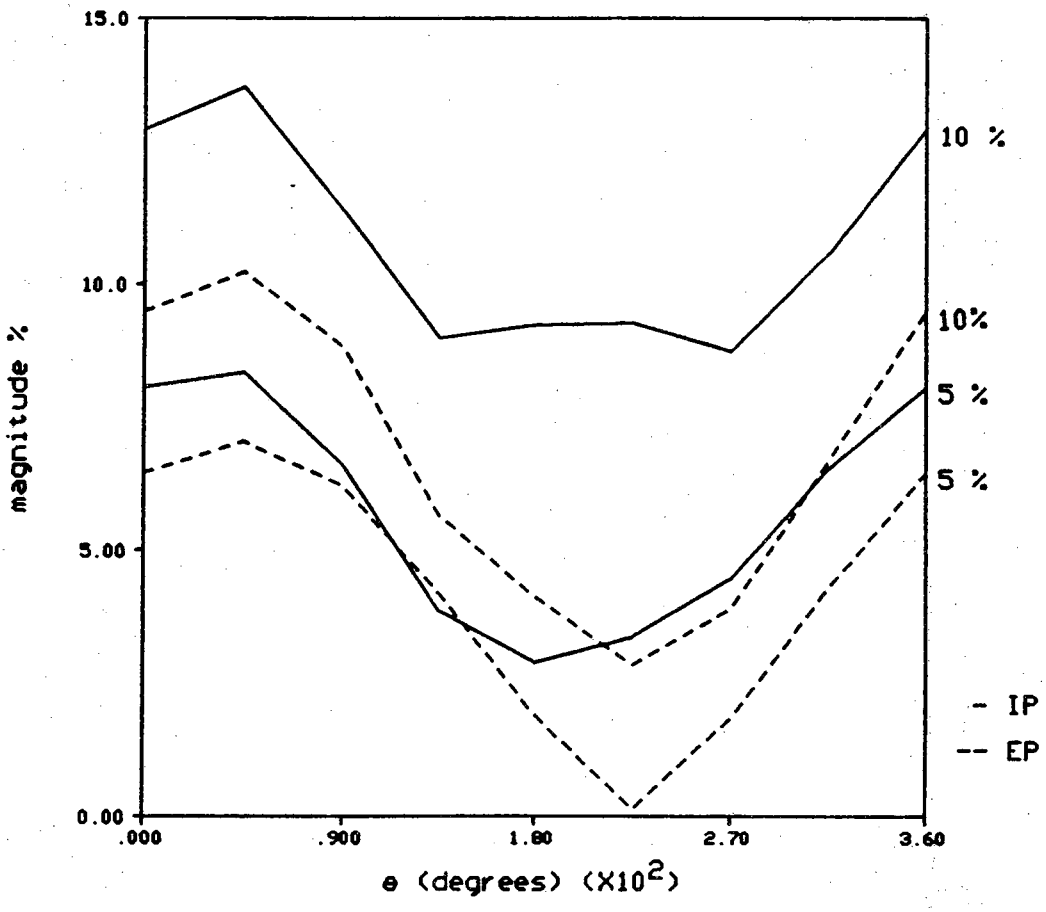

(c) Third harmonic in the converter AC current

Figure 3.4 continued

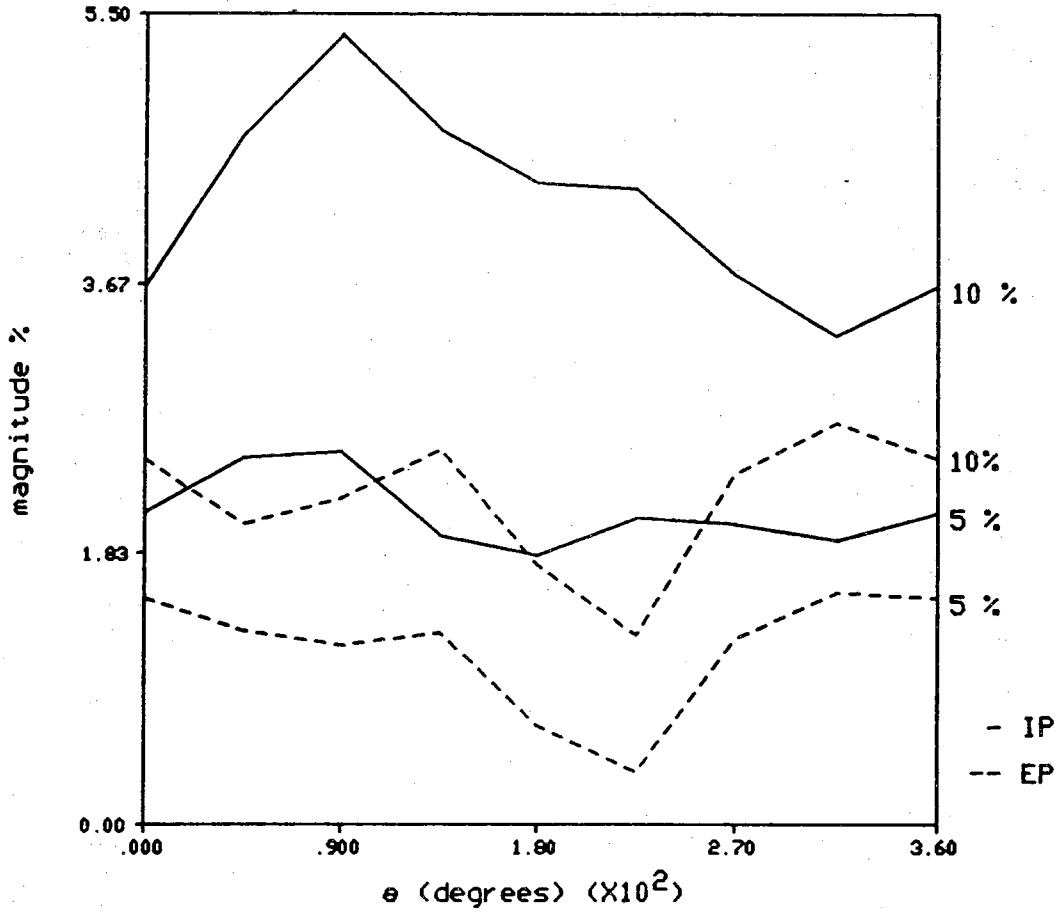

(d) Third harmonic in the terminal AC voltage

Figure 3.4 continued

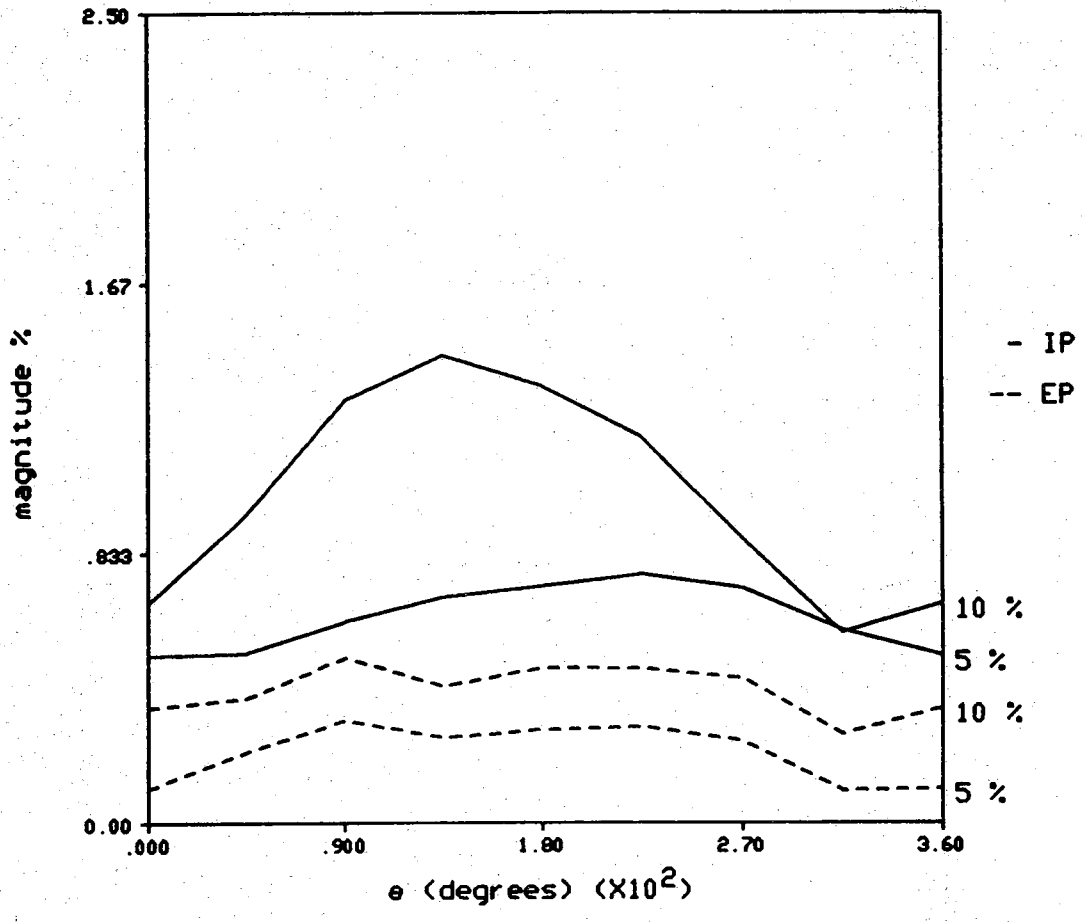

(e) Ninth harmonic in the terminal AC voltage

Figure 3.4 continued

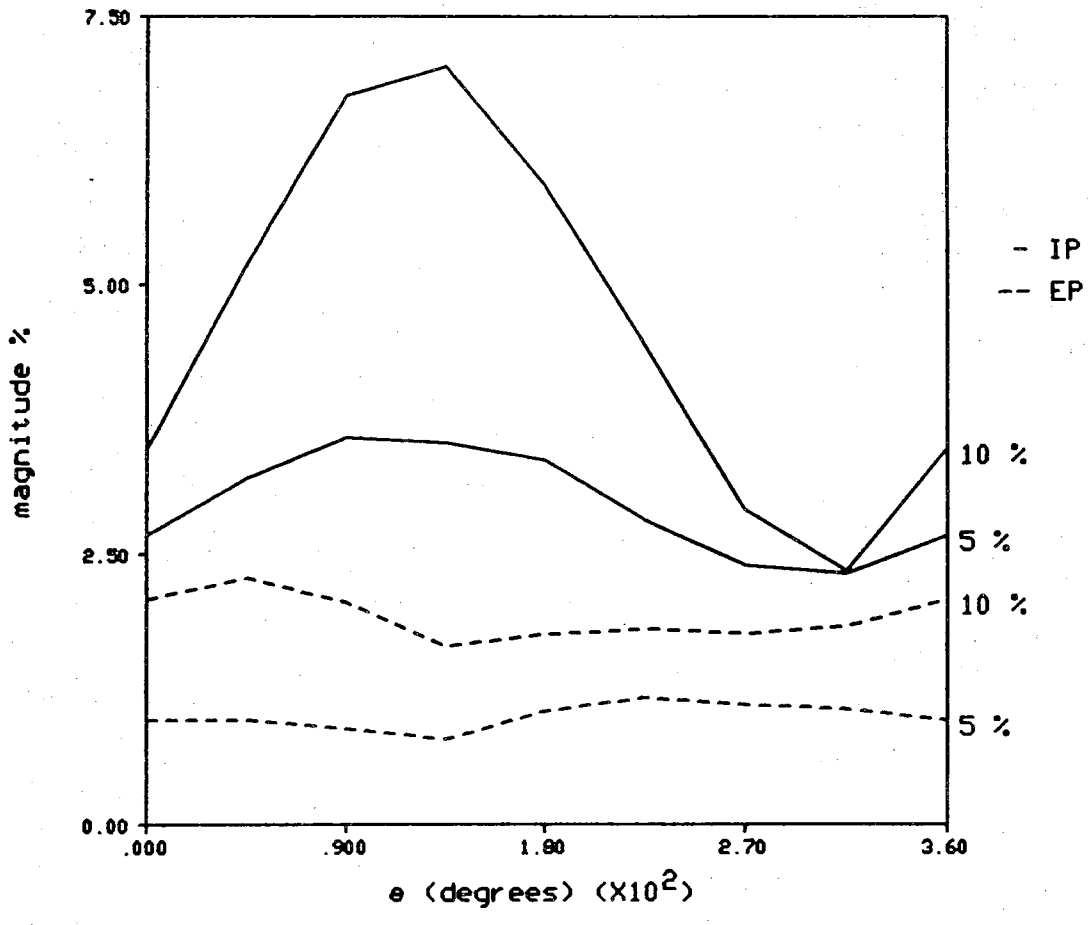

(f) Ninth harmonic in the converter AC current

Figure 3.4 continued

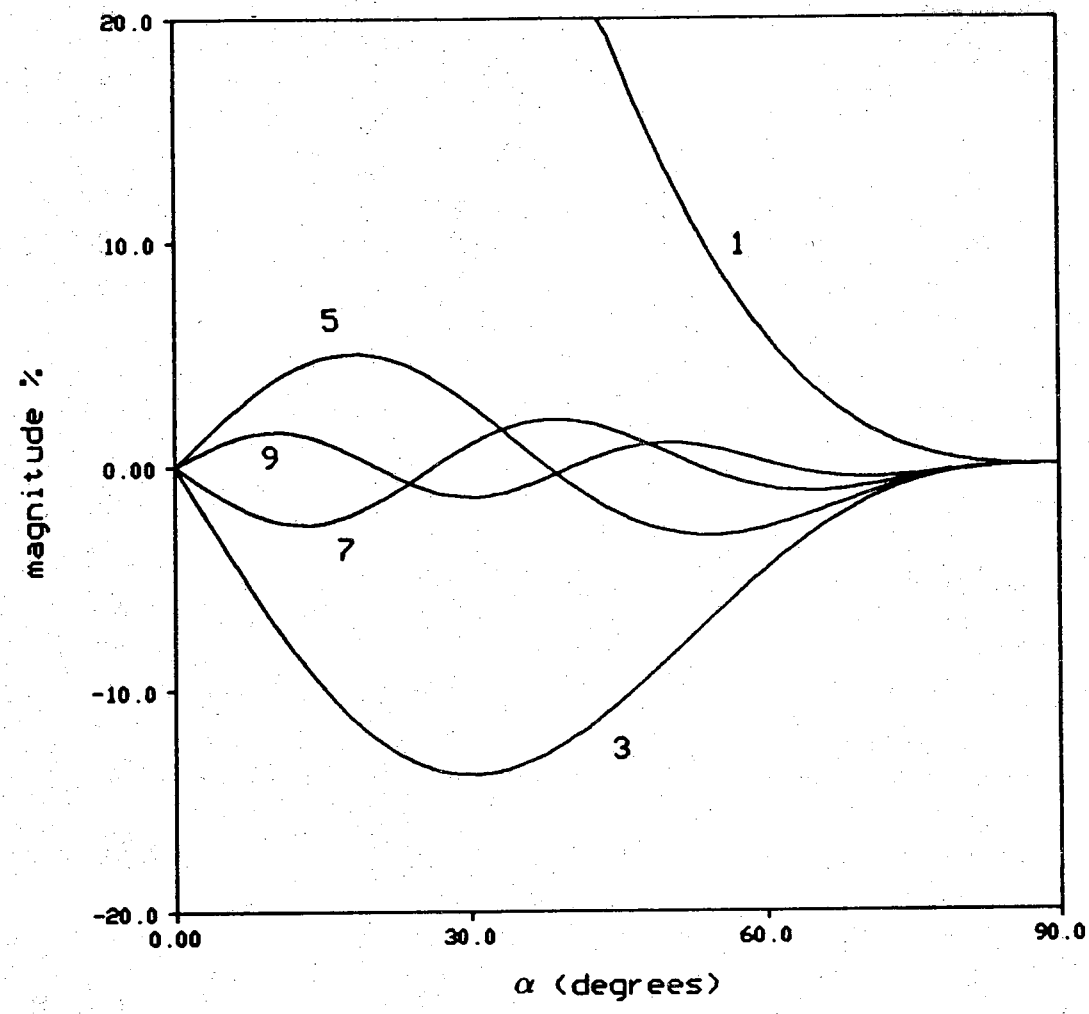

Figure 3.5 Characteristic harmonics of a TCR

CHAPTER 4

VOLTAGE STABILITY

4.1 Introduction

In recent years, with more reactive components connected to the power system, voltage instability has become a major problem. For an AC/DC system, a sudden reduction (drop) in the terminal voltage, especially on the inverter side, could lead to one or more commutation failures, eventually forcing a shutdown of the converter bridge. On the other hand, overvoltages, no matter how short, could damage voltage-sensitive devices and shorten the life of components, and, in a lesser sense, drive the transformers into saturation, causing excessive harmonic generation.

In an AC system, a transfer of power is always limited to a value called the power transfer limit. A plot of V versus P for different values of the power factor is usually implemented by engineers in the transmission line design [9]. An HVDC converter presents a variable power factor source or sink to the AC bus; with such a load, the maximum power transfer limit is more restricted as compared to the constant power factor load. When the AC network is weak, Z_{th} is high; the power transfer limit is further reduced.

The effective short-circuit ratio (ESCR) has been used as a gauge of the level of difficulty in operating an HVDC converter bridge. Unfortunately the use of the ESCR alone does not describe fully the dynamics of the system. Somewhere between the use of a simple parameter (ESCR) and the complicated, detailed and time-consuming simulation, a new method which uses the so-called voltage stability factor, VSF, has emerged [9,69]. This method is based on a sensitive measure of the total reactive power at a terminal bus to changes in its voltage.

The effect of lowering the ESCR on the voltage and power stability is described in the next section. The voltage stability factor is then introduced and applied to the sample system. The focus will be on the response of the inverter and its AC network. The results presented are obtained from a digital

on the equations given in Appendix B.

4.2 Effect of the ESCR on stability

Quite a few of today's HVDC schemes have the ratio of the short-circuit power S_{sc} available at the local AC bus to the rated DC power P_d approaching two. Others, though normally connected to a strong AC system, could be in a similar situation when contingencies (disconnection of one or more transmission lines) occur.

A weak AC system is characterized by its high equivalent source impedance Z_{th} at the local AC bus. High values of Z_{th} cause large steady-state voltage drops across Z_{th}, producing poor voltage regulation and amplifying harmonic interactions.

The simple ESCR measure will not fully describe the system behavior during transient periods, since it is just an admittance on a specific base (P_d and V), although the phase angle of that admittance provides some information on the effective damping presented by the AC system. Figure 4.1 shows the plots of the real and imaginary parts of the parallel combination of Z_{th} and the effective shunt capacitance X_c at the bus. Both parts approach the origin of the s-plane, indicating that the system becomes less stable as the ESCR is lowered.

4.3 Sensitivity of DC power to AC voltage magnitude

In this section, we will examine the sensitivity of the DC power to local bus AC voltage magnitude for the full AC/DC system. As before, the link is operated with the inverter controlling the extinction angle at γ_{min} and the rectifier controlling DC current I_d.

Figure 4.2 shows the variation of the terminal voltage with respect to the DC power (P_d). The intersection point of the curves corresponds to the nominal operating point. Note that with higher ESCR, the voltage variation is larger and the maximum power limit is lower. The maximum power limit is reached when $\frac{dP_d}{dV} = 0$; this is also referred to as the steady-state stability limit. Beyond this limit, a voltage collapse occurs. Adding capacitors would only boost the voltage profile producing an effect similar to lowering the ESCR. This addition of capacitors thus results in a lower ESCR. This can be troublesome to the operation of the system. In contrast to a constant power factor load, the HVDC presents a varying power factor, forcing the power limit to become much

smaller.

Figure 4.3 shows how the ESCR affects the maximum DC power transfer and the terminal voltage magnitude for different values of the DC current (I_d) loadings. For negative $\frac{dP_d}{dI_d}$, an increase in the I_d creates a higher drop in V. Note that for ESCR=1.0, the nominal operating point is the negative slope, indicating that for this system such an operating point will not be stable.

Figure 4.4 shows how the regulation is adversely affected by the decrease in the ESCR. A flat slope indicates good voltage regulation, but a steep slope is undesirable because of the possibility of large fluctuations in the terminal voltage. Figure 4.5 shows how the terminal voltage V behaved with the DC loadings when a TCR was used to regulate the terminal voltage at the local bus. Voltage regulation was maintained by the TCR over a wide range; as expected, it was only effective for overvoltage condition and not undervoltage operation. Figure 4.6 shows the relation between P_d and I_d for the corresponding condition. Note that P_d has a linear relation with I_d when the TCR is active. The variation of V with I_d is given in Fig. 4.7; when contrasted with the V versus P_d plots in Fig. 4.5, we see that, for ESCR=1, P_d folds back when I_d continues to increase beyond the cross-over or nominal operating point. Beyond the nominal operating point, the TCR is, in this case, designed to turn off or operate at minimum current.

As mentioned earlier, capacitor banks can be added to improve the voltage support at the local bus. Figure 4.8 shows the effect of adding more capacitance at the local bus with $X_c = 1$ corresponding to an ESCR=1; with more capacitance the instability point is shifted to the right, that is, to higher DC loadings.

4.4 Voltage stability factor

Another way to look at the stability phenomena is to use the voltage stability factor, VSF, given in [69] as

$$\text{VSF} = \frac{\Delta V}{V \Delta Q} \tag{4.1}$$

with P_d held constant. The details of computing this factor are given in Appendix B.

A small positive value of VSF means that the system is stable and operation is obtained with low AC voltage fluctuations. A large positive value means a stable operation with large fluctuations in the terminal voltage. On the

other hand, a negative value means voltage instability at that operating point.

The VSF for the sample AC/DC system without the TCR is plotted for different values of the ESCR in Fig. 4.9. For ESCR=2, the VSF is positive and much higher than it is for the corresponding ESCR=3.97, which means that the system, though stable in both cases will have larger voltage fluctuations with an ESCR=2 than with an ESCR=3.97. The case of ESCR=1 is as predicted before, unstable and with a break point; the brand with negative VSF is unstable. With the TCR, the corresponding results in Fig. 4.10 shows an improvement in that the instability point has been shifted to the right (i.e., at larger values of I_d). The effect of varying the TCR reactor size is demonstrated in Fig. 4.11, where the break-point moves farther away to the right of the nominal I_d for smaller X_{slp}. In the extreme case of an infinite size TCR where the slope is zero, the terminal voltage is held constant for all DC loadings below the nominal operating point (i.e., in the operating range of the TCR), and no instability is indicated.

4.5 Conclusion

The problem of voltage or power stability of an AC/DC system is of great concern and importance when the AC support at the inverter end is weak. The system can become unstable when the ESCR is lower than some minimum value [8,9,43]. this investigation shows that steady-state voltage and power instabilities can be reasonably predicted by the appropriate sensitivity factors described in this chapter. Using the detailed analog simulation of the sample AC/DC system, the predicted instability from these sensitivity factors was confirmed.

This study has shown that the TCR can play an effective role in stabilizing the AC voltage. Although adding shunt capacitors would also enhance the voltage support and the stability, it has the effect of lowering the ESCR further, thus contributing to power voltage regulation.

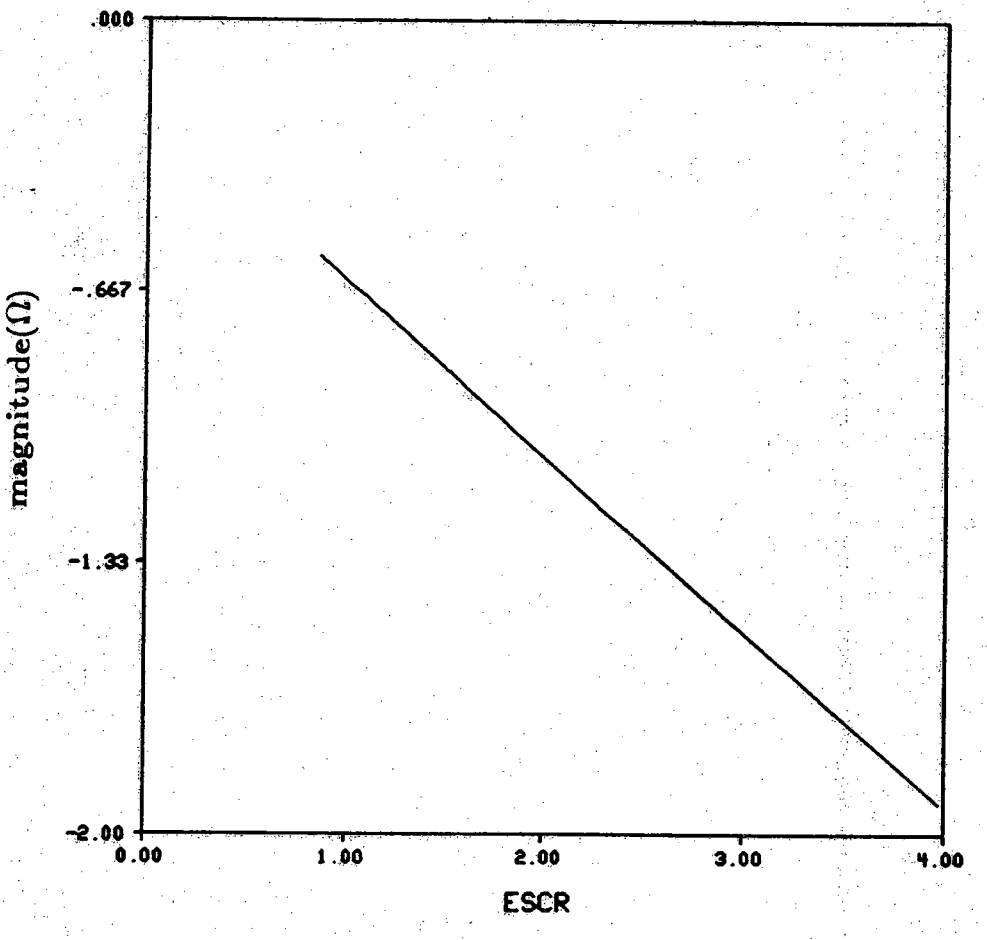

(a) Real part

Figure 4.1 Equivalent impedance seen from the converter bus

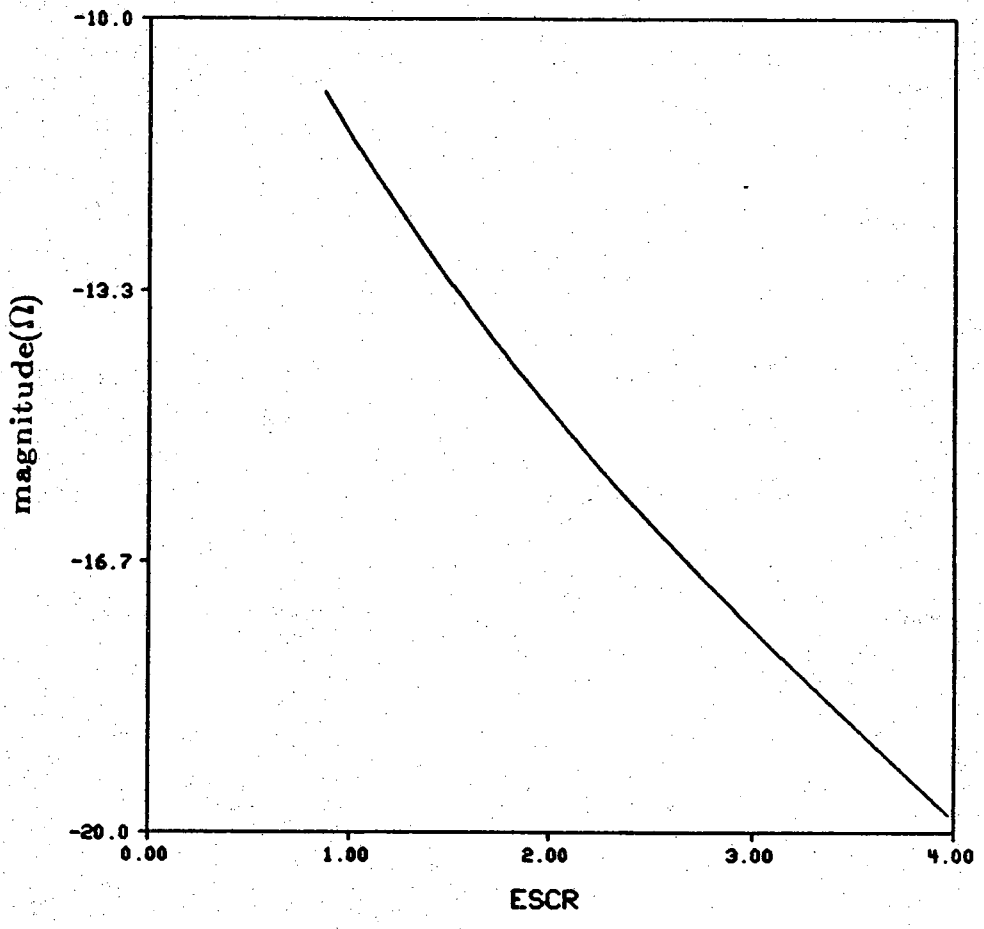

(b) Imaginary part

Figure 4.1. continued

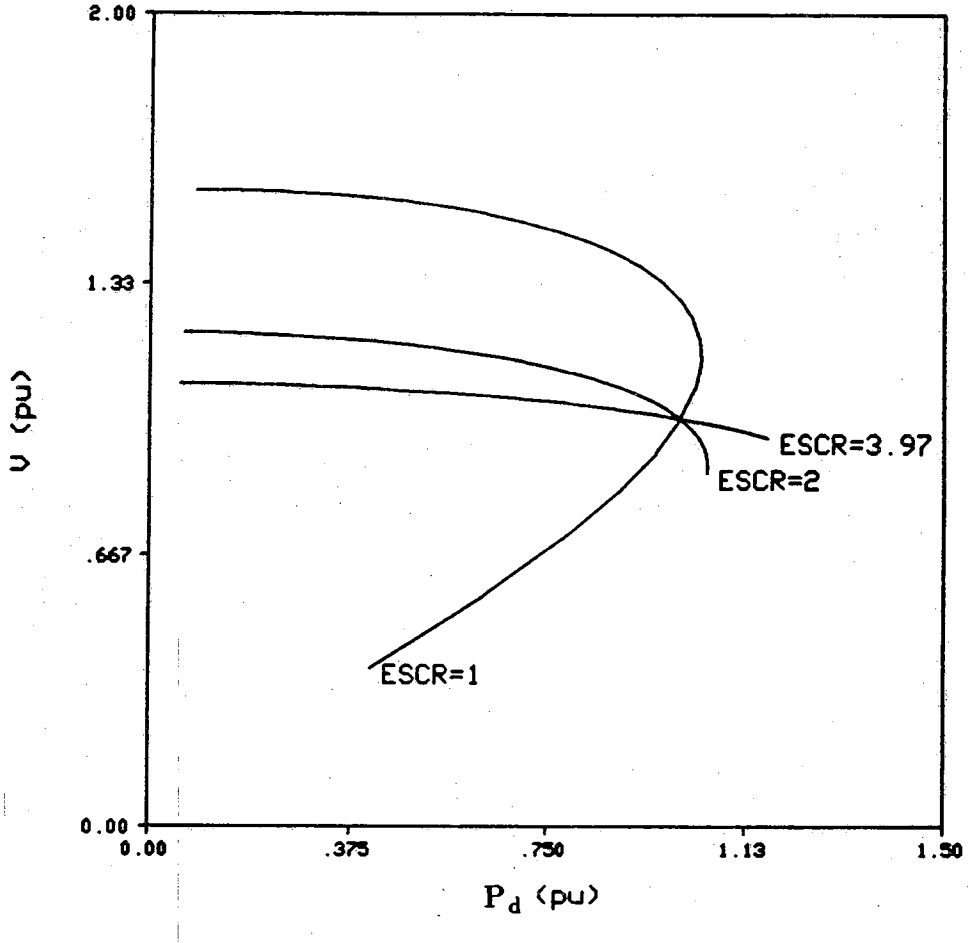

Figure 4.2 Terminal bus voltage versus DC power (without TCR)

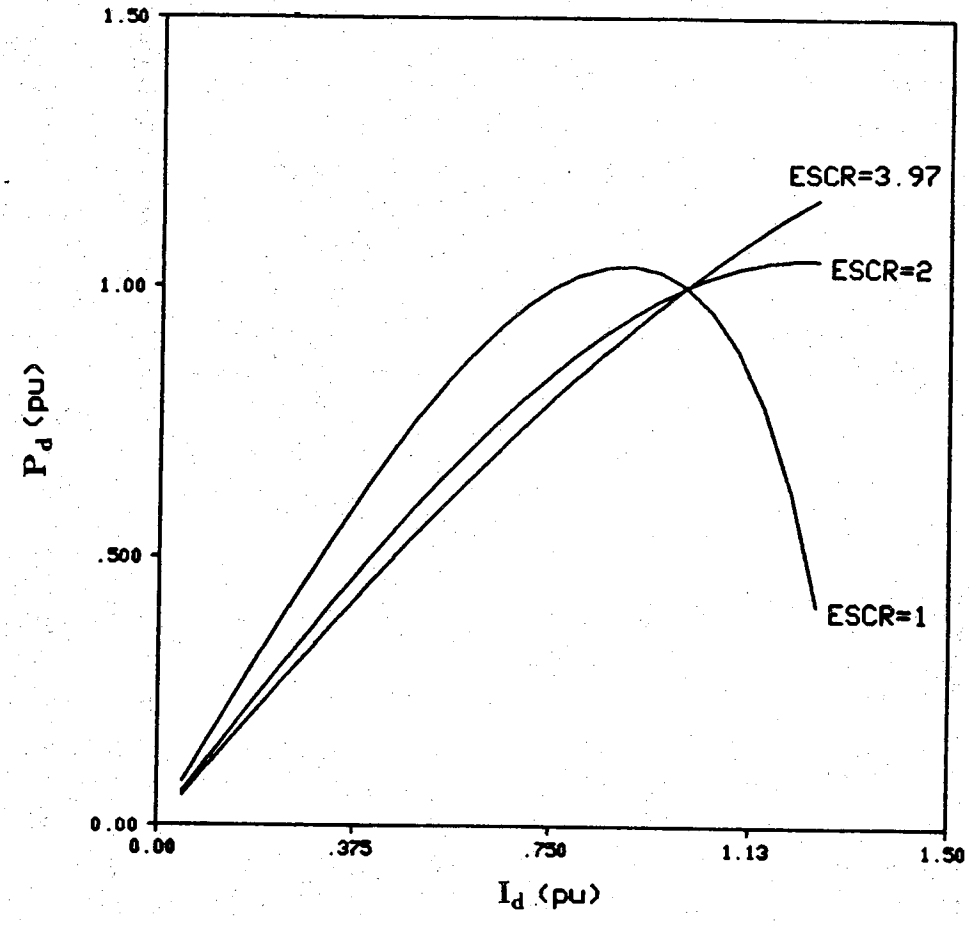

Figure 4.3 DC power versus DC current (without TCR)

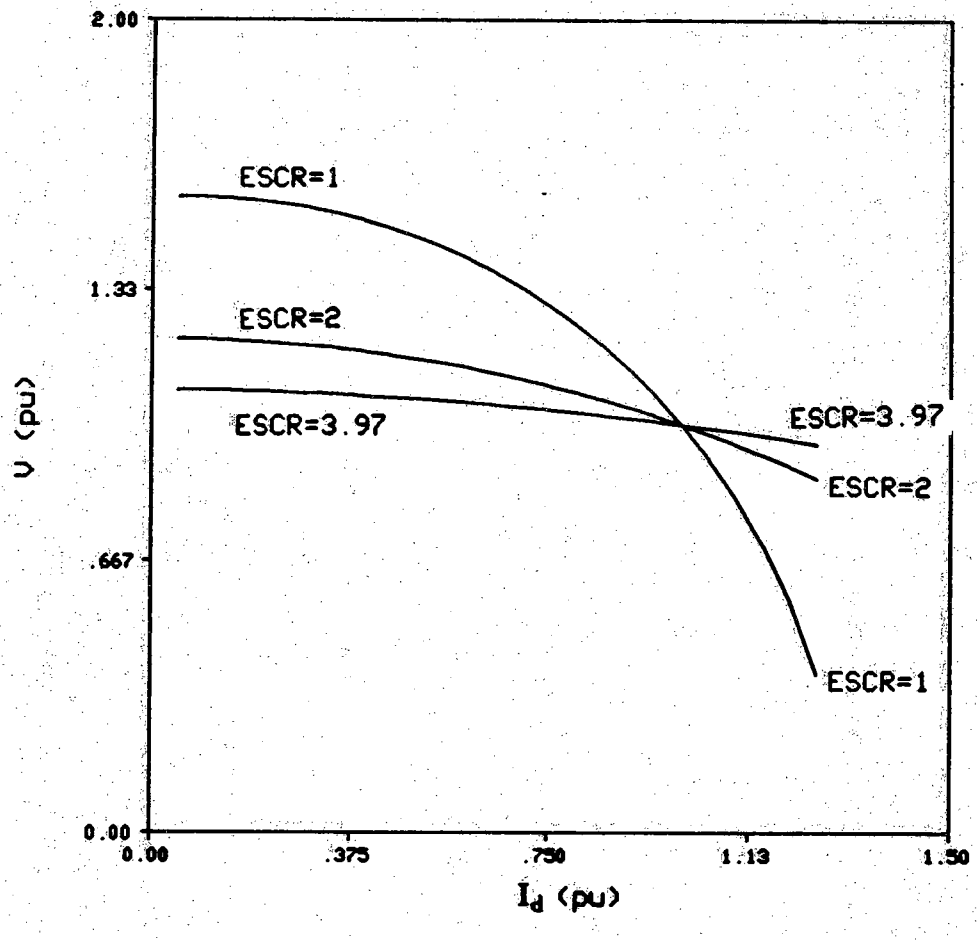

Figure 4.4 Terminal bus voltage versus DC current (without TCR)

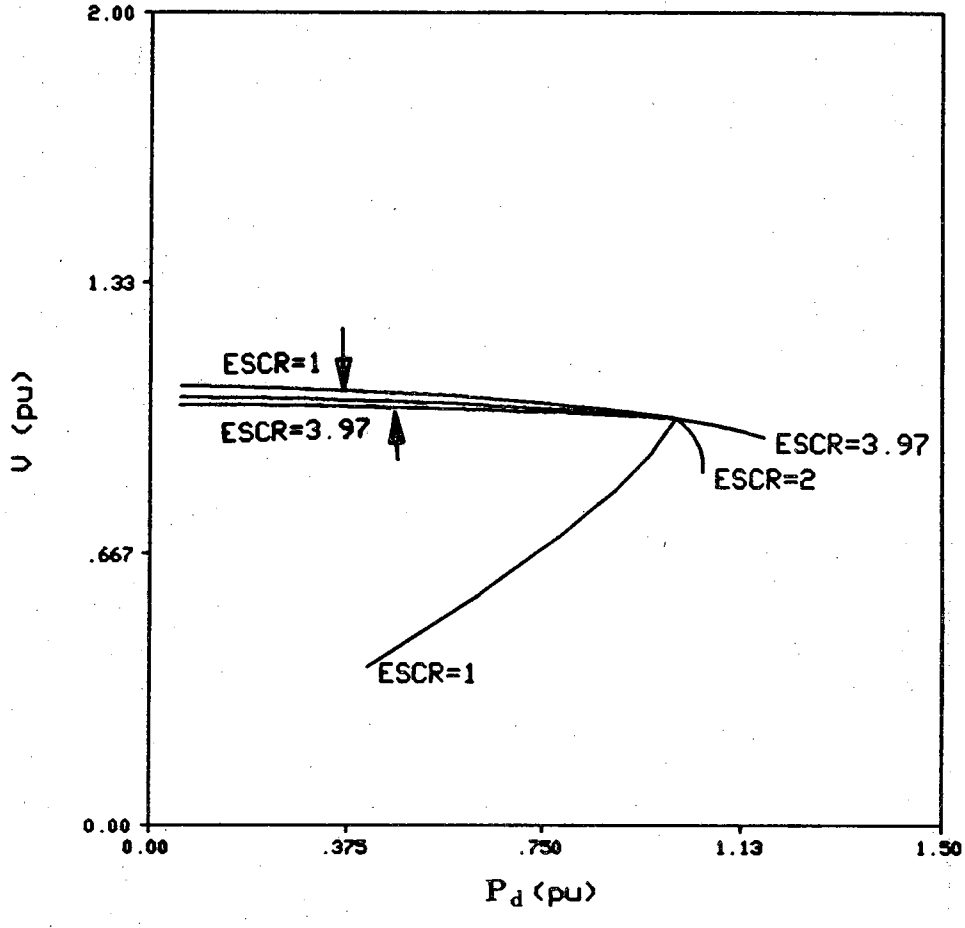

Figure 4.5 Terminal bus voltage versus DC power (with TCR)

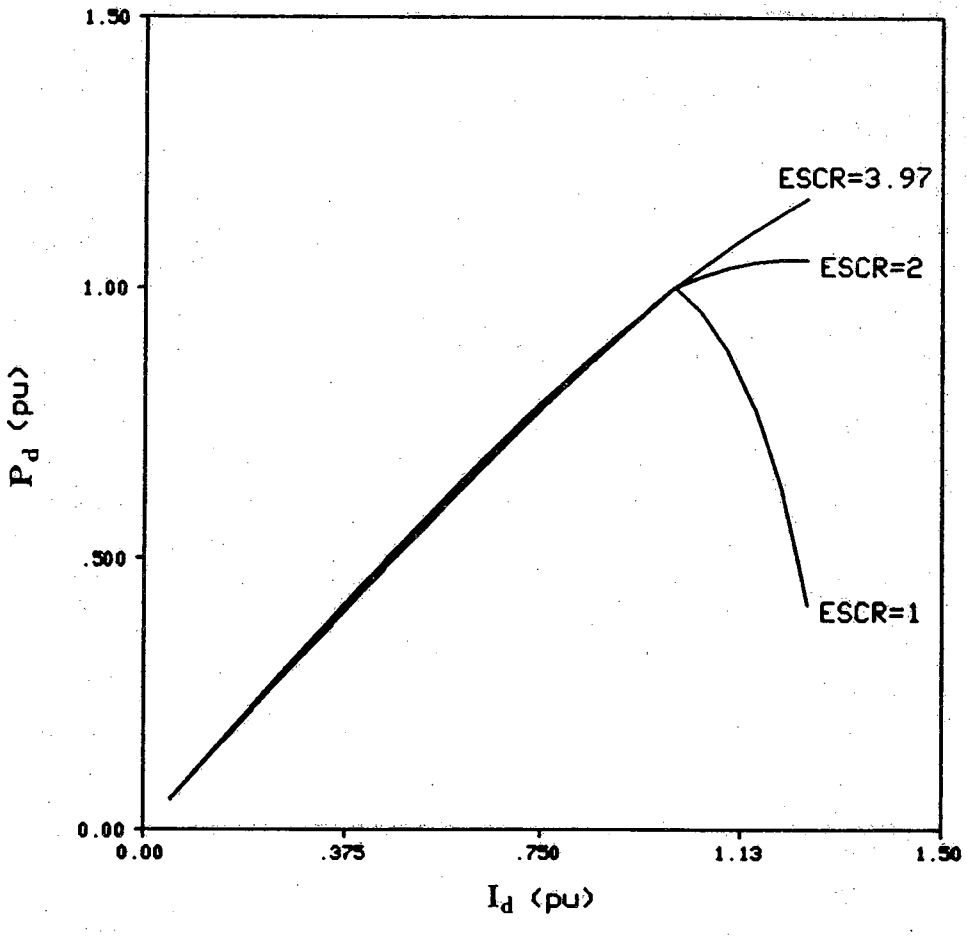

Figure 4.6 DC power versus DC current (with TCR)

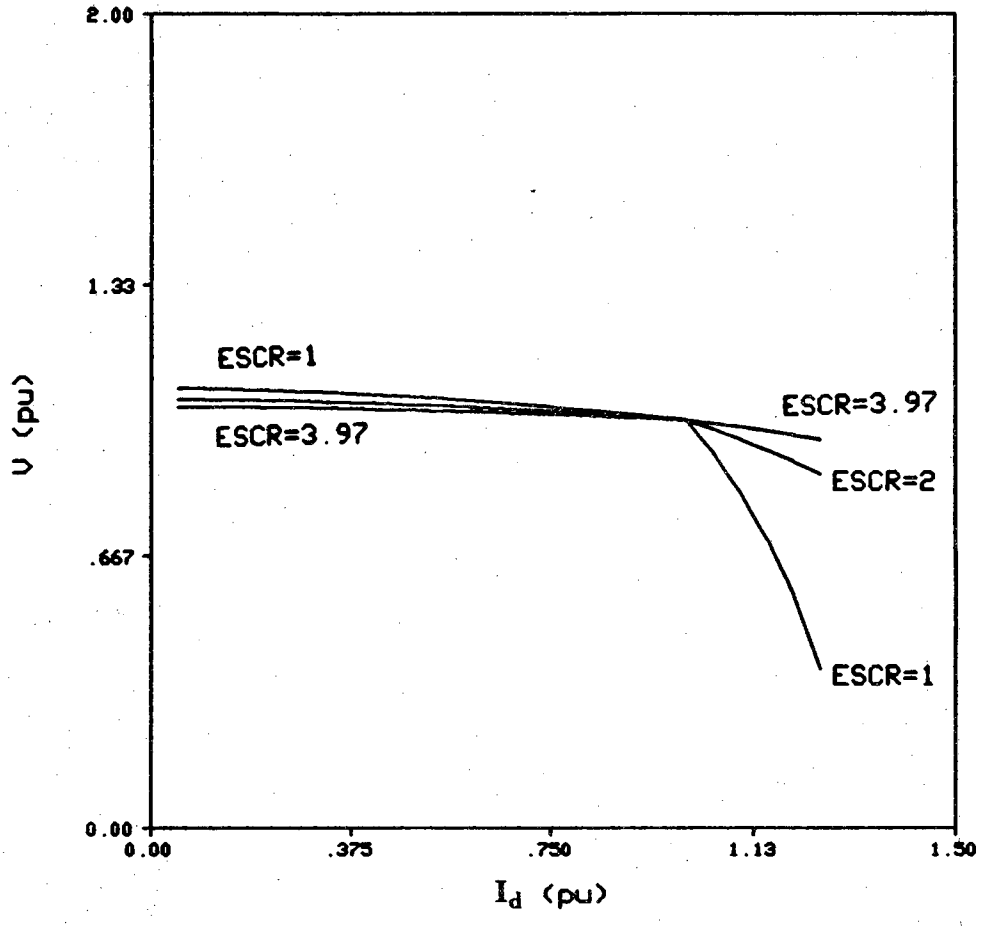

Figure 4.7 Terminal bus voltage versus DC current (with TCR)

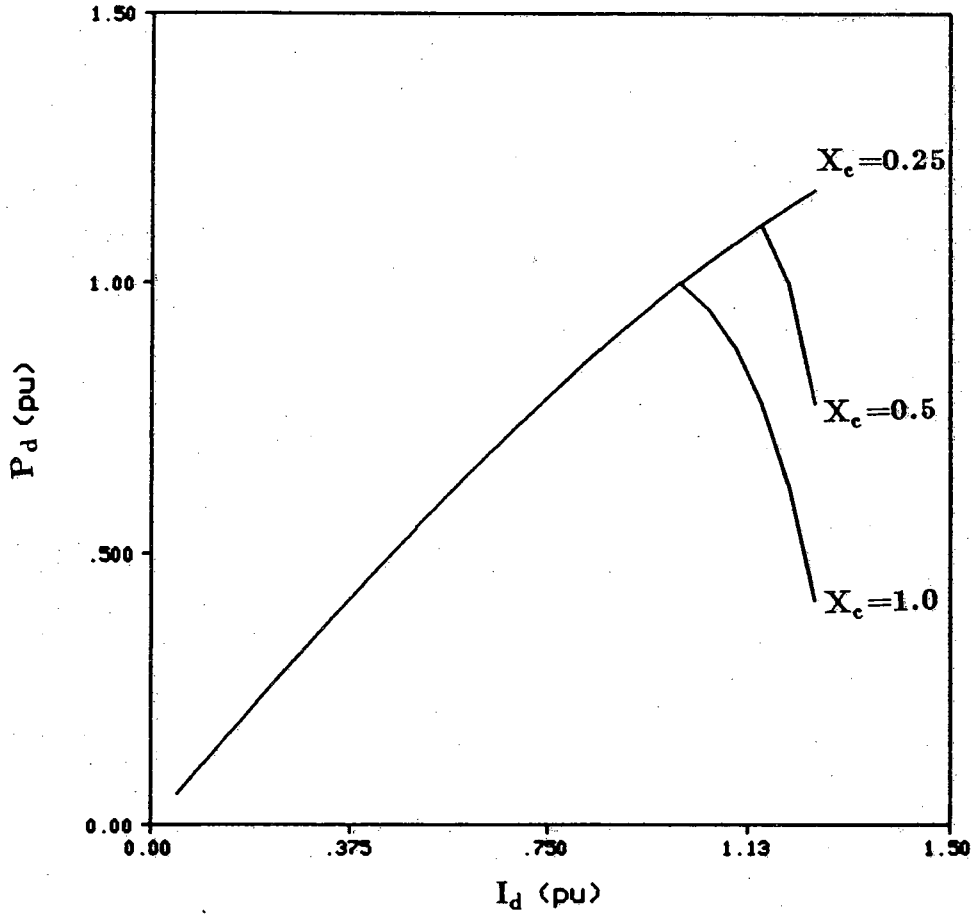

Figure 4.8 DC power versus DC current (with TCR and ESCR=1)

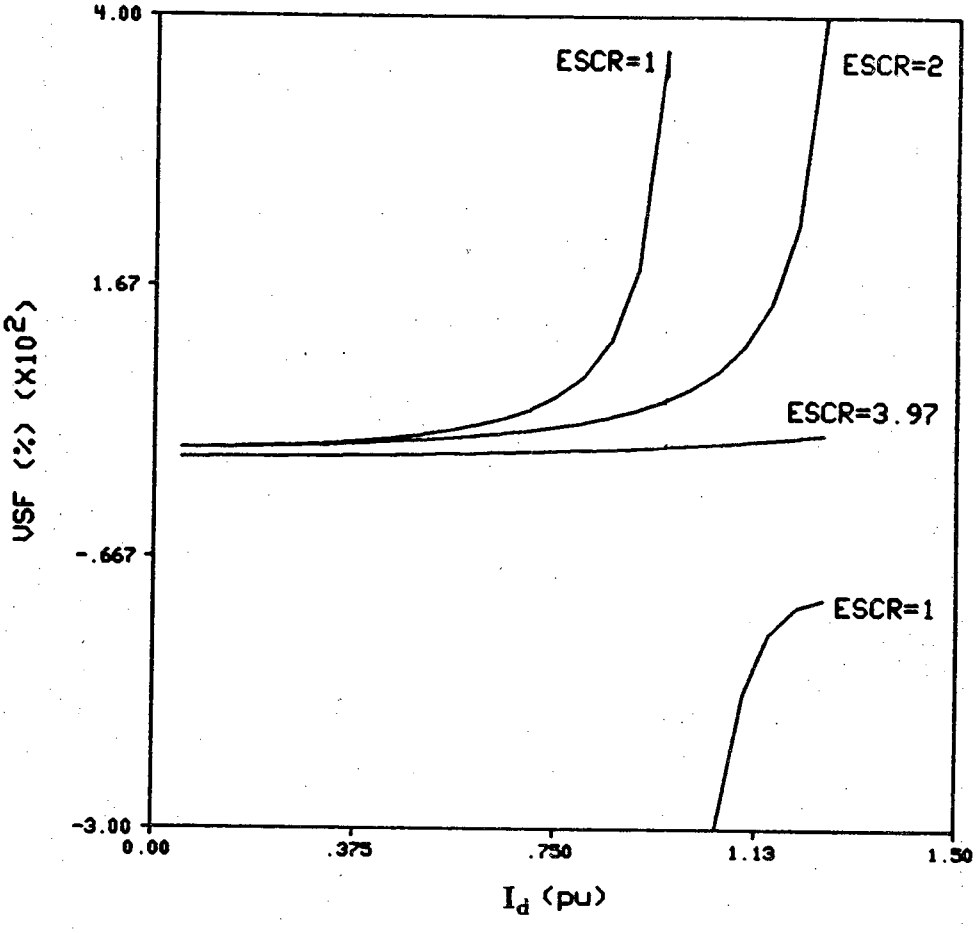

Figure 4.9 Voltage stability factor versus DC current (without TCR)

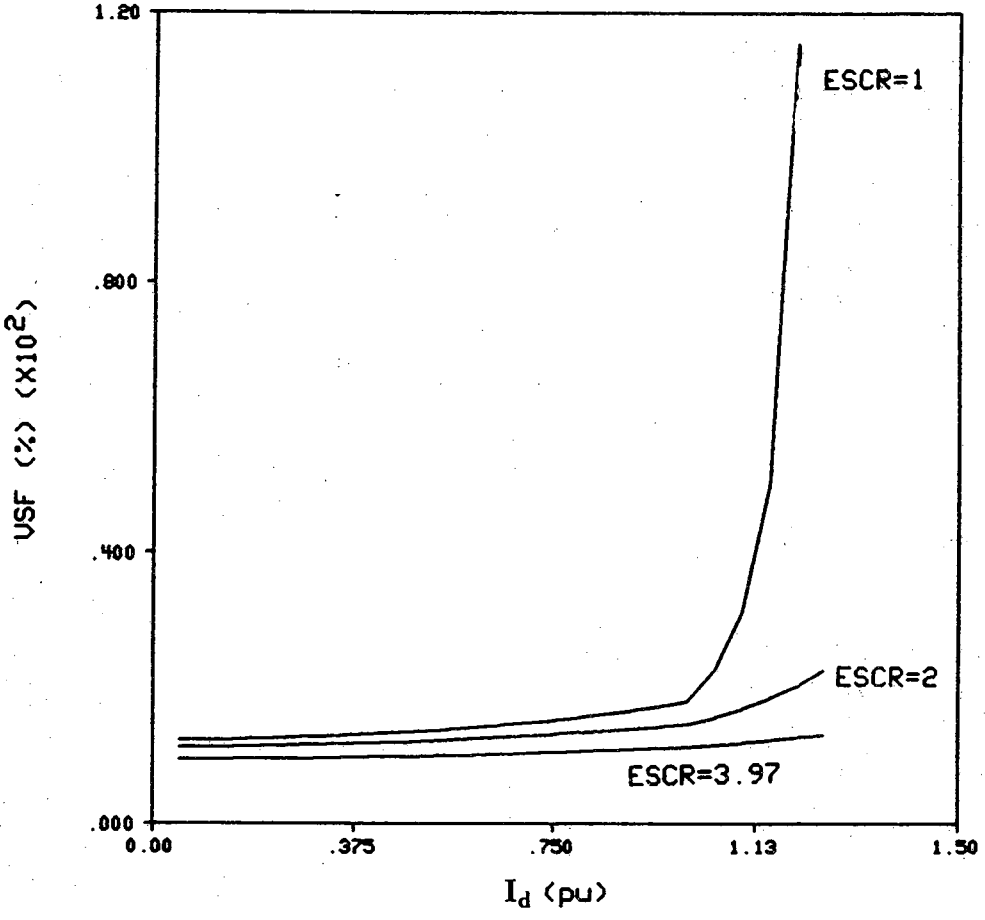

Figure 4.10 Voltage stability factor versus DC current (with TCR)

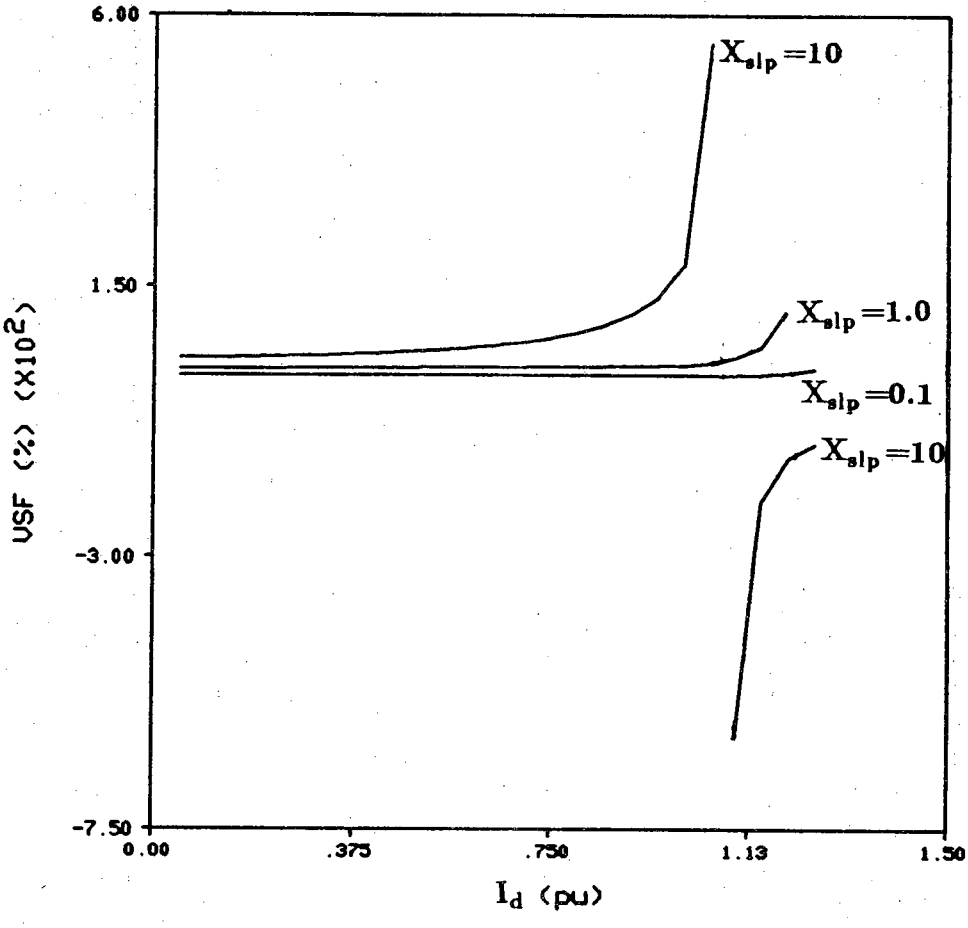

Figure 4.11 Voltage stability factor versus DC current

(with TCR and ESCR=1)

CHAPTER 5

DYNAMIC AND TRANSIENT STUDIES

5.1 Introduction

In this chapter, we will the impact of a TSC-TCR compensator on the dynamics of an inverter with weak AC support In particular, we will consider a TCR equipped with a terminal voltage control, a power factor control, or a direct-axis current control to see which of these control is most suitable. A final section will examine the response of the system to a full load rejection of the entire inverter (blocking). All the tests were applied with the converter transferring full power to the AC network of effective short-circuit ratios 3.97, 3, 2, and 1.5.

5.2 Dynamic response

A system is dynamically stable when it recovers from minor disturbances. Usually, any disturbance large or small could lead to undervoltages or overvoltages. Undervoltages could degradate the performances of the load, while overvoltages could damage the equipment and drive any close transformer deeply into saturation, generating excessive harmonics. Therefore, effective control of the terminal voltage directly or indirectly has to be performed. TCR in conjunction with TSC can be effective in controlling transient overvoltages (TOV). Fast TOVs are difficult to control.

A small voltage margin of a few percent is usually provided in the current margin method operating the link, as such a small, sudden drop in the local AC bus voltage could result in an undesirable mode shift. A fast acting TCR could help minimize such mode shifts. The TCR also alleviates the voltage regulation problems in steady-state operation; this is particularly useful at low power transfer conditions with a weak AC system when overcompensation from the shunt filters and capacitors, if not switched out, can cause a steady-state overvoltage condition at the inverter AC bus. Reactive compensation could also be obtained by operating the inverter at higher than normal extinction angle

during light load conditions, but this would increase commutation losses in the valves.

Three basic tests were used to evaluate the dynamic response of the sample AC/DC system (with an ESCR=1.5 on the inverter AC side) with TCR control; these are:

- a step change in the reference of the controlled variable,
- a drop then a ramping of the rectifier reference DC current, and
- switching in and out of a 200 MVAR (20% of the total capacitance) capacitor bank.

5.2.1 Terminal voltage control

Since the operation of the converter depends highly on the terminal AC voltage, a direct control of it would seem to be the best. This is checked by performing the three tests listed above. A nonlinear representation of the converter transformer is used in these tests unless stated otherwise.

In the first experiment, we applied a step-down of 5.5% of the reference voltage then a step-up, restoring the reference to the same magnitude. The TCR is sized to have a capability of absorbing two times the reactive power generated by the filters alone (50% of the total reactive power). The slope was selected to give 5% regulation (in the operating range of the TCR).

Figure 5.1 shows the system response to a step down from rated voltage then a step-up. The records show good response (i.e., no significant overvoltage or oscillations).

In Figs. 5.2 and 5.3, we applied a 50% drop to $I_{d,ref}$ of the rectifier followed by ramping $I_{d,ref}$ back to rated DC value. The ramp period was selected to correspond to 12 cycles (200 msec) and 24 cycles (400 msec), respectively. Note that for the faster ramp rate in Fig. 5.3, a small overshoot in I_d occurred, but for the lower ramp rate in Fig. 5.2, there was no overshoot in I_d and also no undervoltages. We also investigated using faster ramp rates; at about 6 cycles, commutation failures occurred as a result of high undervoltage condition. Approximately 13% overvoltage is detected in the third cycle following the sudden drop of I_{dref}. The delay in control response can be attributed to the time constants of the filter in the terminal voltage measurement and the PI compensator of the TCR control.

In Fig. 5.4, a 200 MVAR capacitor bank (20% of the effective [actual plus filters] shunt capacitance) was switched in then out. A maximum of 9% overvoltage is detected. No significant overvoltage is shown during the switching

off. The overvoltage, in this case, is moderated by the transformer saturation characteristic; this is indirectly reflected by the increase in magnetizing current following the disturbance.

5.2.2 Power factor control

The response to a step down and up of the $\sin\phi_{ref}$ (from ϕ_{ref}=10° to ϕ_{ref}=0° and vice versa) is shown in Fig. 5.5, ϕ being the angle between the terminal AC voltage V and the network current flowing into Z_{th}. Doubling the step change in $\sin\phi_{ref}$, resulted in instability. The response from dropping the DC reference current by 50% of the rated value then ramping it back over 24 cycles is shown in Fig. 5.6. The system, though stable, was oscillatory, even when the gains of the PI controller were reduced to a minimum. Figure 5.7 shows the response of the system when the ramp rate was increased to 9 cycles; instability occurred. Figure 5.8 shows the response of the system to capacitor switching. In general the controlled responses were somewhat more oscillatory than those obtained with the voltage magnitude control when the ESCR is 1.5. It has, however, given stable and smooth controlled response when the ESCR is higher.

5.2.3 Direct-axis current control

The response to a step down and up of the $I_{D,ref}$ (from 1% of rated Is to 0 and vice versa) is shown in Fig. 5.9. Doubling this step change has caused instability. The response to dropping the DC reference current by 50% rated then ramping it back (after the transients have settled) in 24 cycles is shown in Fig. 5.10. In general, this type of control shows a relatively good performance. It shows less oscillations as compared to the power factor control. Figure 5.11 shows the response of the system to a capacitor switching.

5.3 Load rejection

In this discussion, load rejection by the inverter means blocking the inverter. Blocking of the inverter is effected simply by using a bypass valve to divert the DC current from the inverter. On receiving the block command, all firing signals to the thyristors of the inverter are suppressed; at the same time a signal is sent to turn on the bypass valve.

These tests were performed on a system with ESCR=1.5, the purpose of which was to evaluate the effect of transformer saturation and effectiveness of the TCR in limiting the transient overvoltages (TOV) caused by a load rejection. For consistency, the load rejection has has been applied at the positive zero crossing of the phase A voltage.

Figure 5.12 shows the system response with no TCR and a linear transformer representation before and after the load rejection. In this case, the load rejection has been applied at a random point in time. The case of a linear transformer and no TCR was used to establish a base line. Transient overvoltages (TOV) lasting from 1 to 3 cycles show up right after the load rejection. The first overvoltage peak is the most critical, especially in phase B, where V_b has reached 2.22 pu or 122% of TOV, which is too high.

The corresponding system response with TCR and linear transformer is shown in Fig. 5.12 (b). The TOV has been reduced to approximately 67% with one TSC turned off. This is still too high.

The response with no TCR and a nonlinear transformer is given in Fig. 5.12 (c). A TOV of approximately 78% is reached (again in phase B).

Finally, with both nonlinear transformer and TCR, a 67% TOV in the first cycle is observed. The TCR was not able to react quickly and limit this first cycle TOV, but it was effective in the subsequent cycles (after 2 cycles). Figures 5.13 (a) and (b) show the voltages across the TSC for ESCR=3.97. Again, in this case, the load rejection has been applied at a random point in time. We can see that the residual voltage in the disconnected capacitor is higher than the nominal value, in effect acting like a track-hold capacitor, holding the peak transient voltage. Figure 5.13 (c) shows the same run on an expanded time scale.

Neither power factor nor direct-axis current controls of the TCR are applicable to the load rejection condition because of difficulty in establishing the reference values for these controls. The nominal power factor was 1 before the load rejection was applied ($I_D = 0$). After load rejection, and due to the absence of any other loads connected to the terminal bus voltage, the network current was capacitive and very small. Pure capacitive means the power factor is close to 0 ($\sin\phi = 0$) and I_D has maximum value. When the network current is very small, accurate measurement of the direct-axis current would be difficult, making its control less accurate.

As a brief scan of the variation of TOV with the point of wave at which the load rejection was initiated, the timing of the load rejection was changed from 0 to 120° and 240° with respect to the positive-going zero crossing of V_a. The

results obtained show that the highest OV present was at different phase voltages. For example, when point of wave at which load rejection was initiated was 0°, the highest OV appeared on V_a.

ESCR has been varied from 3.97, 3, 2, to 1.5 when the approximate values of the TOV recorded are plotted against the ESCR in Fig. 5.14; it is clear that as the ESCR is lowered, higher TOV were obtained. In this case, the timing of the load rejection was selected to correspond to the positive-going zero crossing of V_a, when the highest TOV appears on V_a.

5.4 Conclusion

The impact of a TSC-TCR compensator on the dynamic and transient responses of the sample AC/DC system was studied. The TCR controller gains have been selected through trial-and-error. The criteria used are the stability of operation and minimum oscillations before reaching steady-state.

From these tests, we can conclude that the terminal voltage control of the TCR is best suited for this purpose, perhaps because it is the most direct form of control for this application. Although the direct-axis current control showed good dynamic performances, setting the appropriate reference value for certain operating conditions can be a problem. The power factor control showed too much oscillation at low ESCR; this could be because of its complicated measurement as compared to the terminal voltage or the direct-axis current.

Fast ramping of the DC current could be a problem with weak AC support, but a very slow ramping would delay the restoration of the full capacity which might be very greatly needed. A compromise should be made.

Although transformer saturation moderates the TOV by absorbing excess reactive power from the system, it introduces excessive harmonics, which distort the AC voltage and might excite some natural frequencies.

Because of the time constants in its measurement and control loop, there will be some delay in TCR response. Supplementary devices, like the ZnO surge arrestors, may be needed to clamp the initial part of any TOV.

For a given system, the TOV increases in magnitude as the ESCR decreases.

The initial residual voltage on a switched-out capacitor of a TSC can be as high as the peak transient voltage.

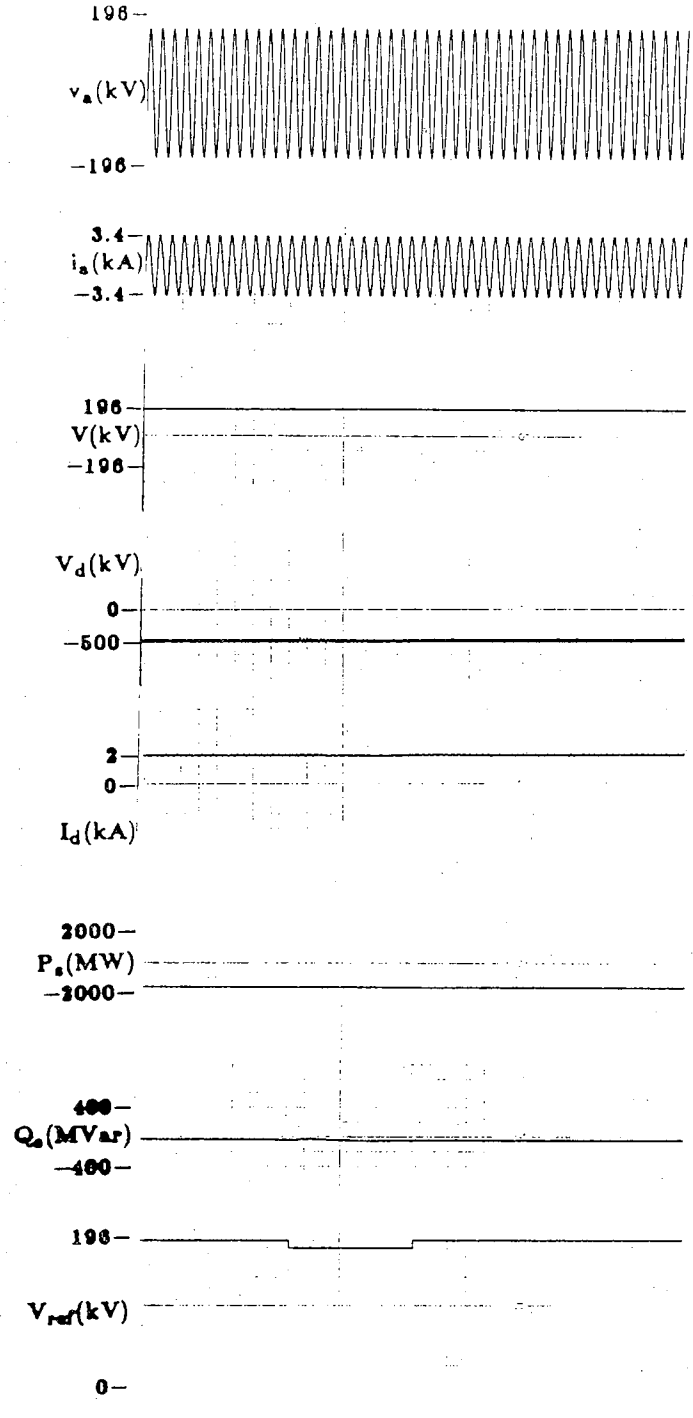

(a)

Figure 5.1 Dynamic response due to a step-change in V_{ref} (V-control, ESCR=1.5)

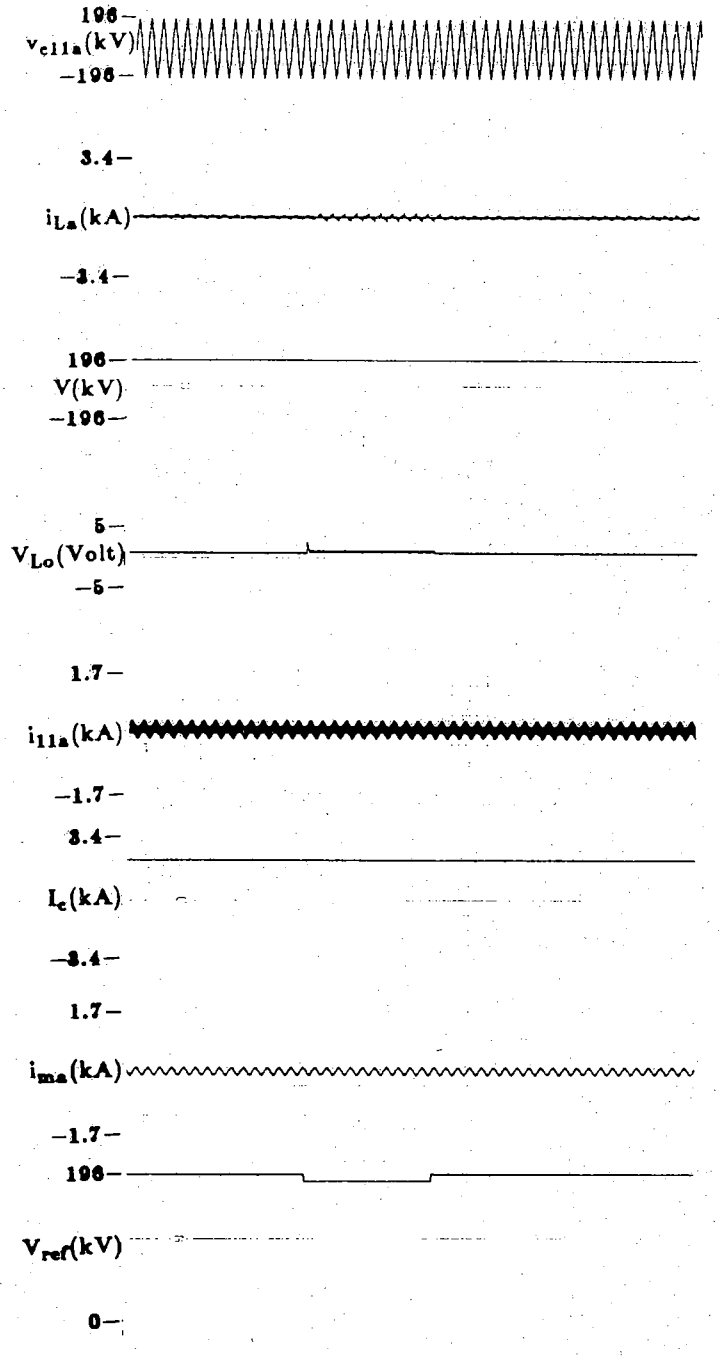

(b)

Figure 5.1 continued

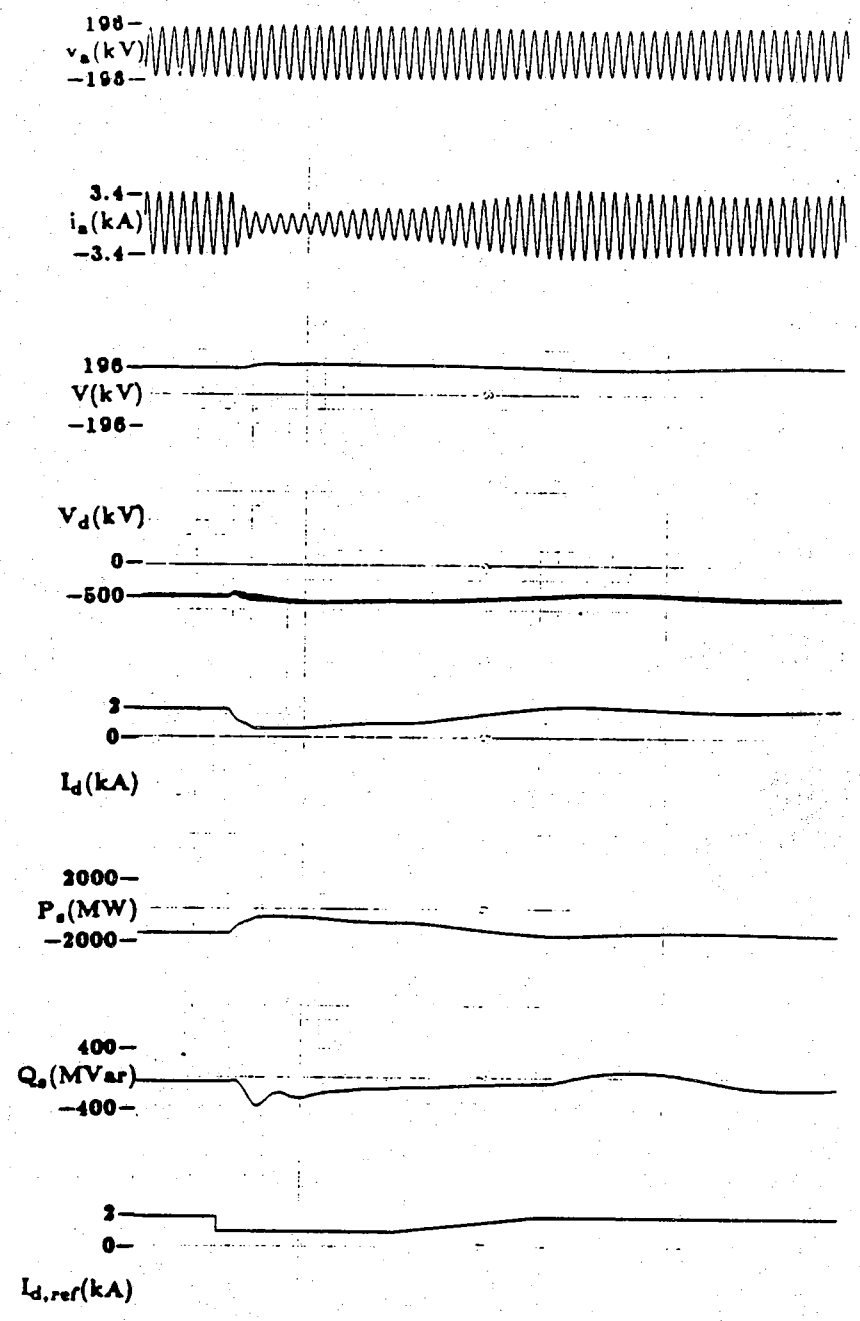

Figure 5.2 Dynamic response due to a drop and a ramp (12 cycles) in $I_{d,ref}$ (V-control, ESCR=1.5)

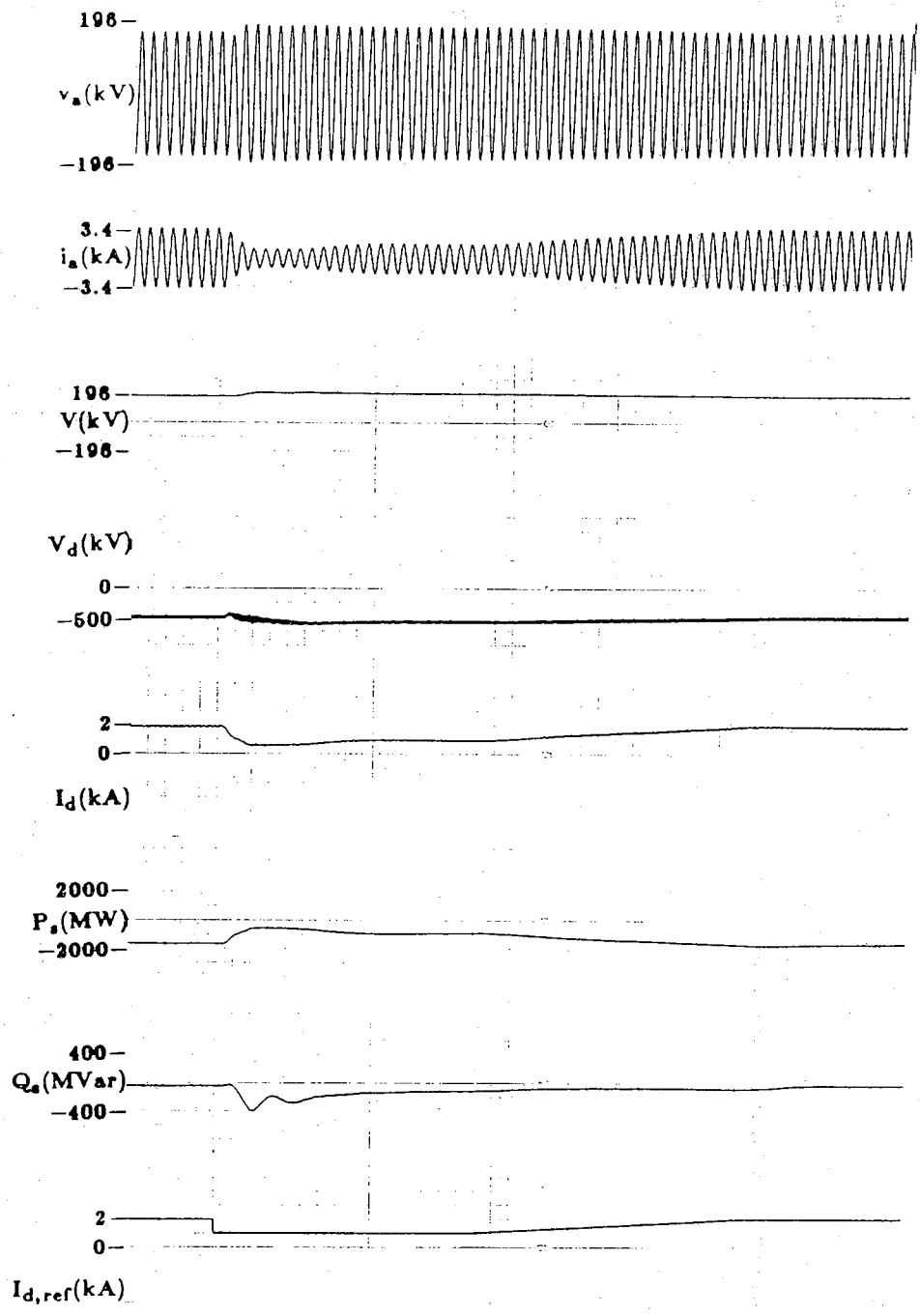

(a)

Figure 5.3 Dynamic response due to a drop and a ramp (24 cycles) in $I_{d,ref}$ (V-control, ESCR=1.5)

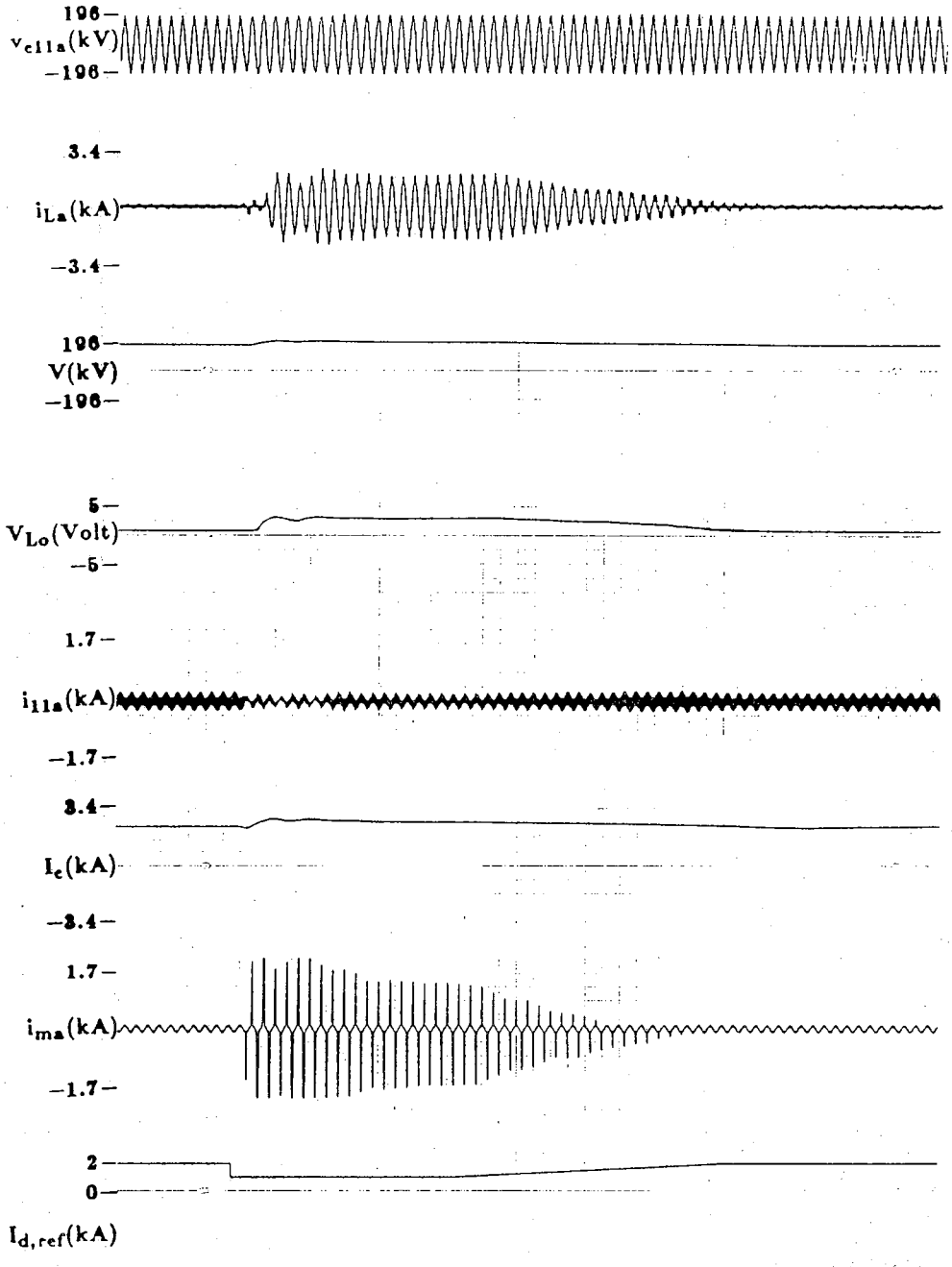

(b)

Figure 5.3 continued

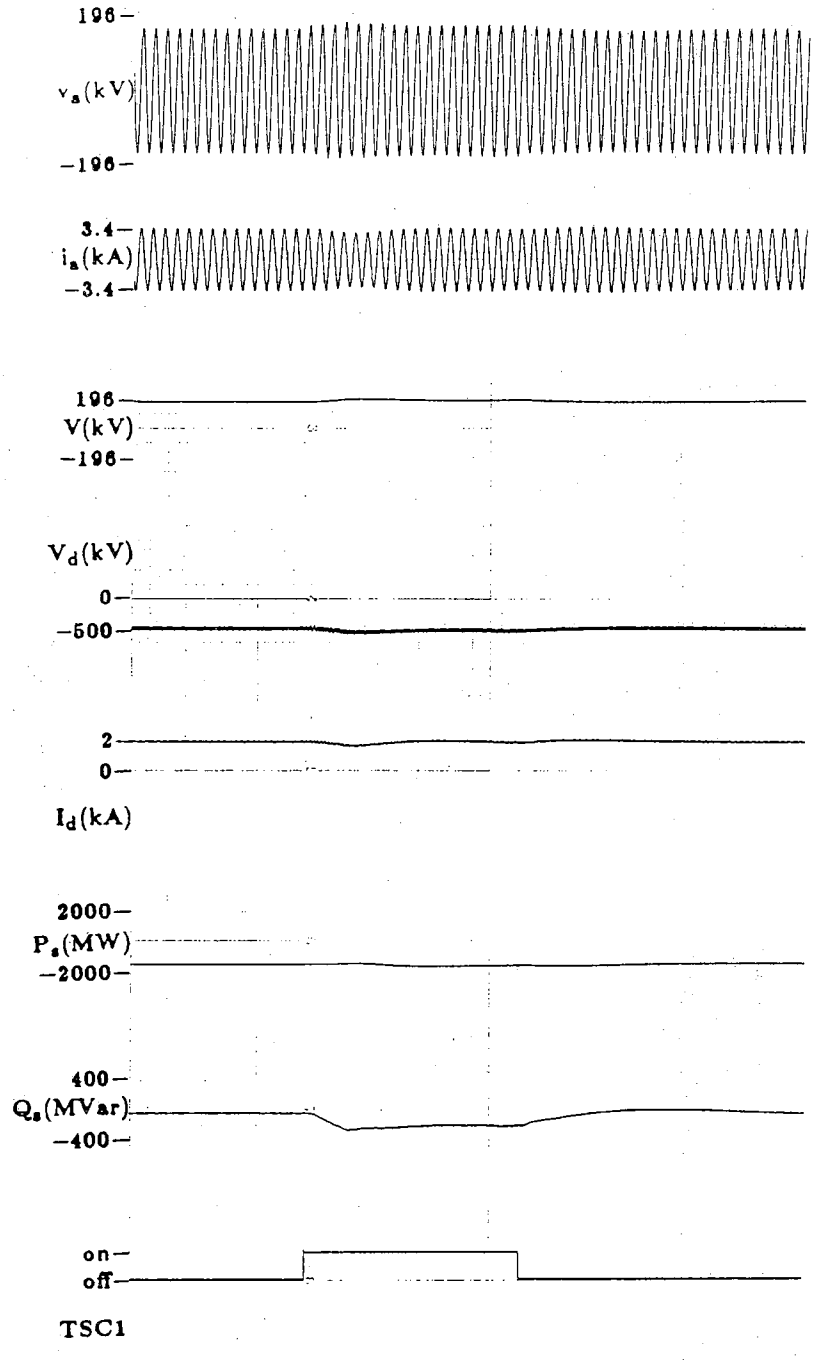

(a)

Figure 5.4 Dynamic response due to switching of a capacitor bank (V-control, ESCR=1.5)

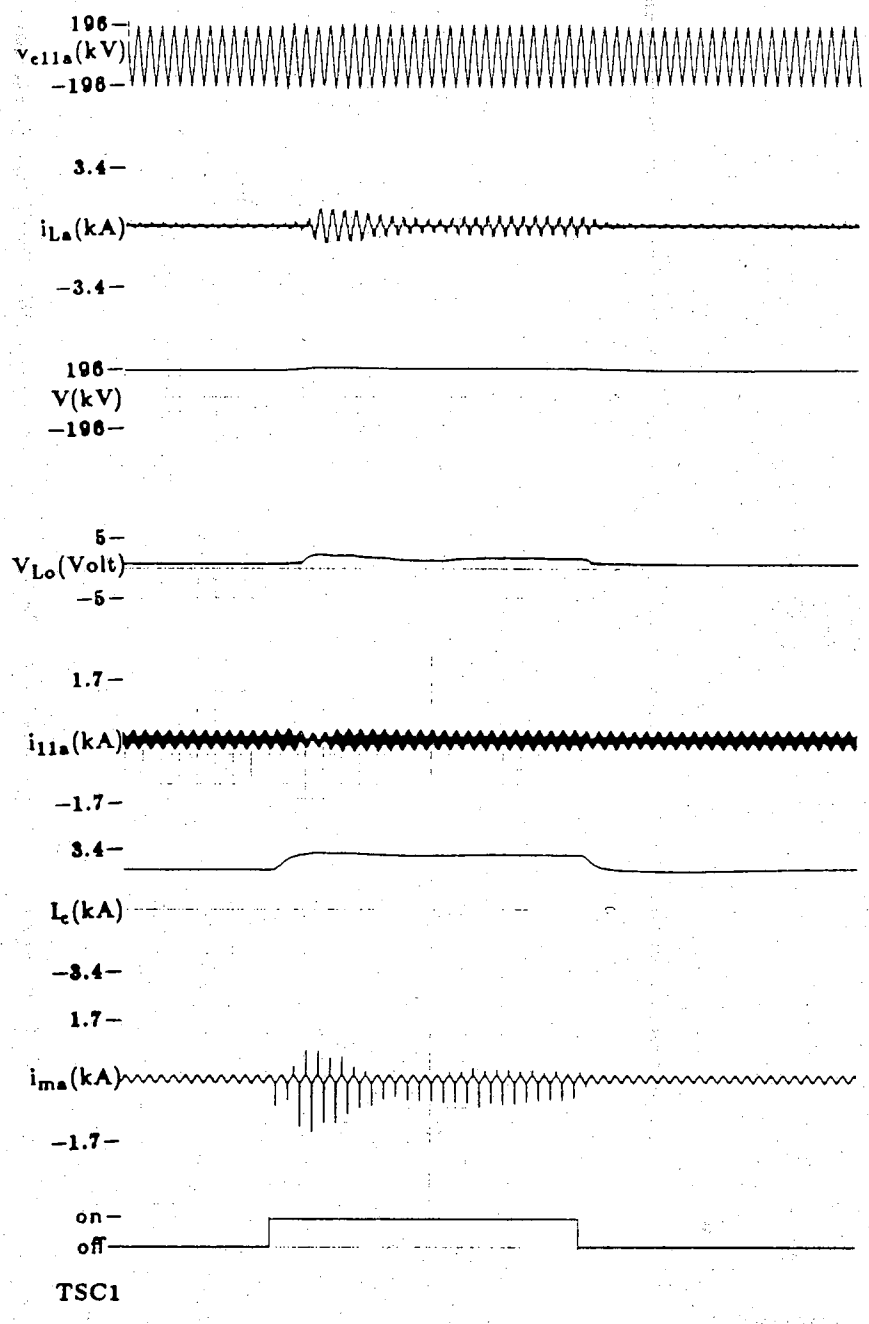

(b)

Figure 5.4 continued

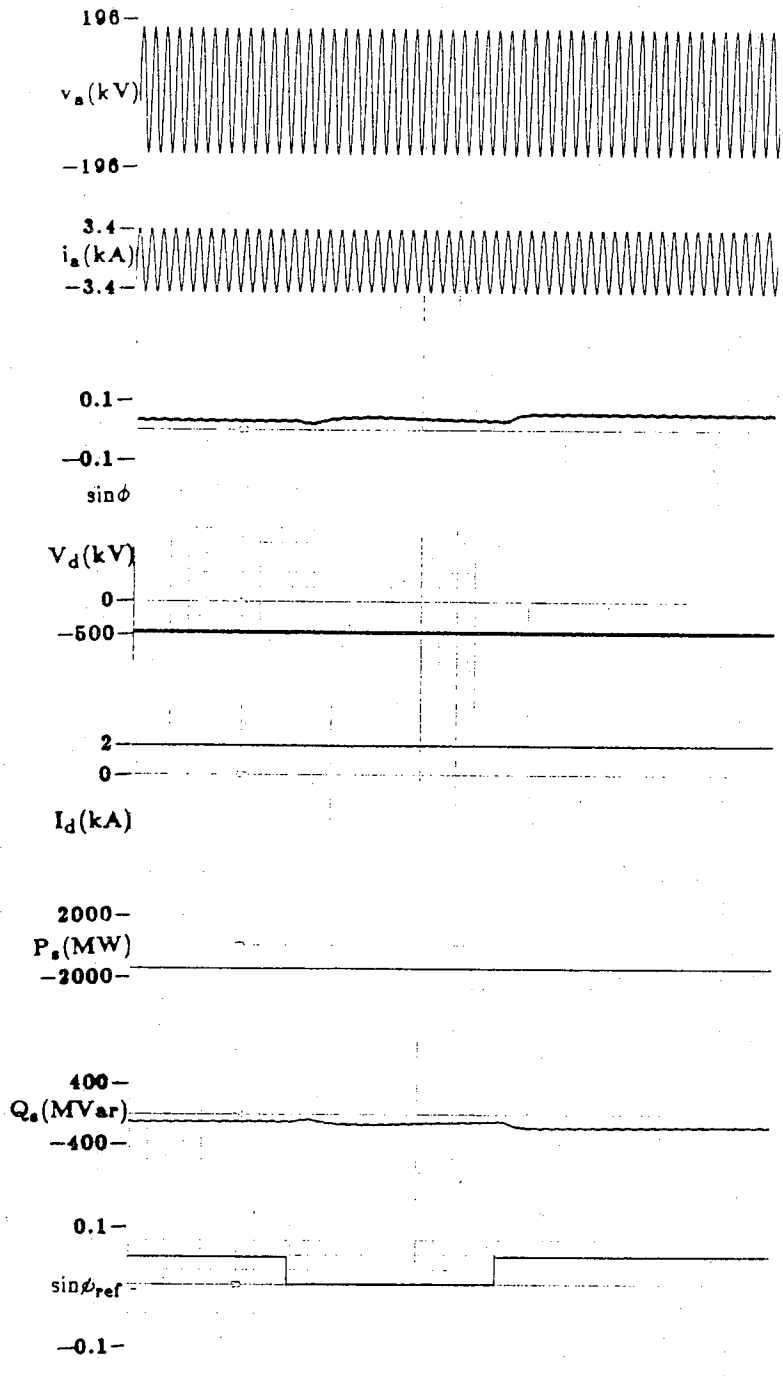

(a)

Figure 5.5 Dynamic response due to a step-change in $\sin\phi_{ref}$ ($\sin\phi$-control, ESCR=1.5)

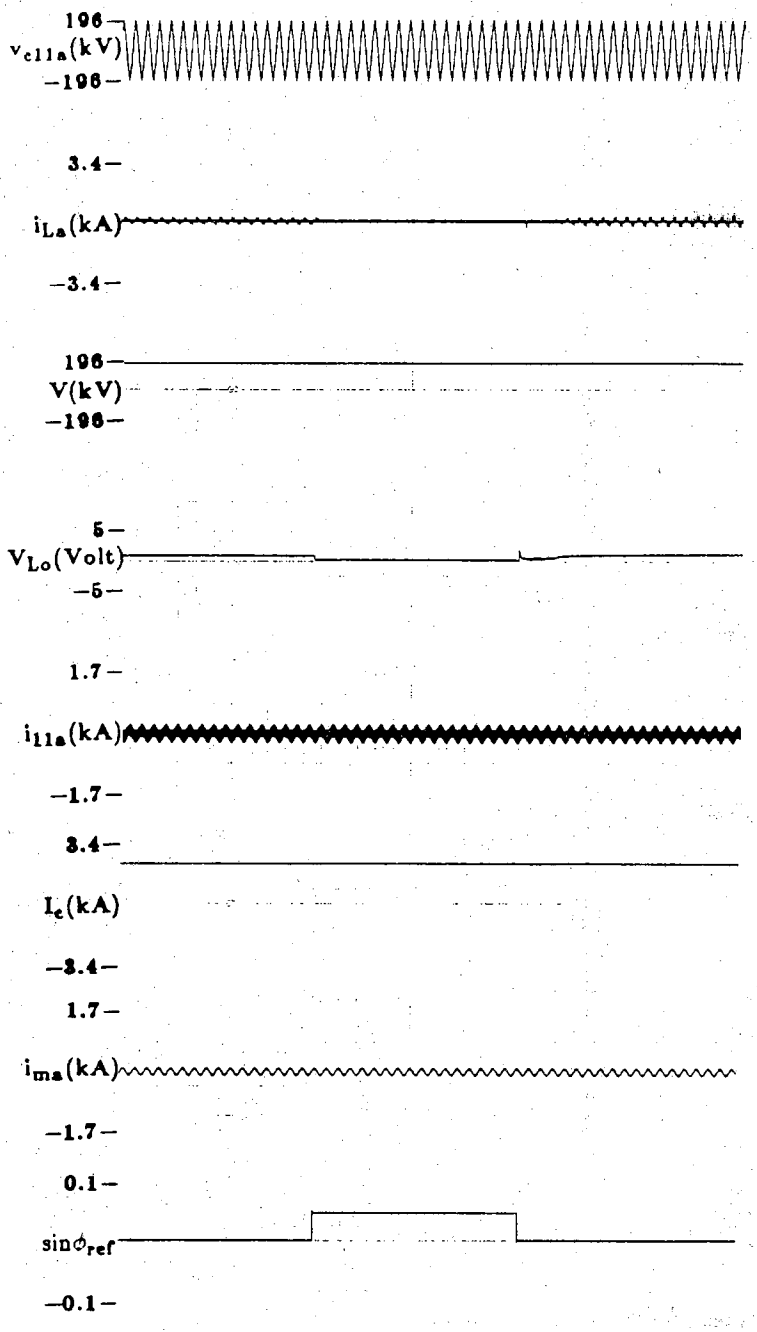

(b)

Figure 5.5 continued

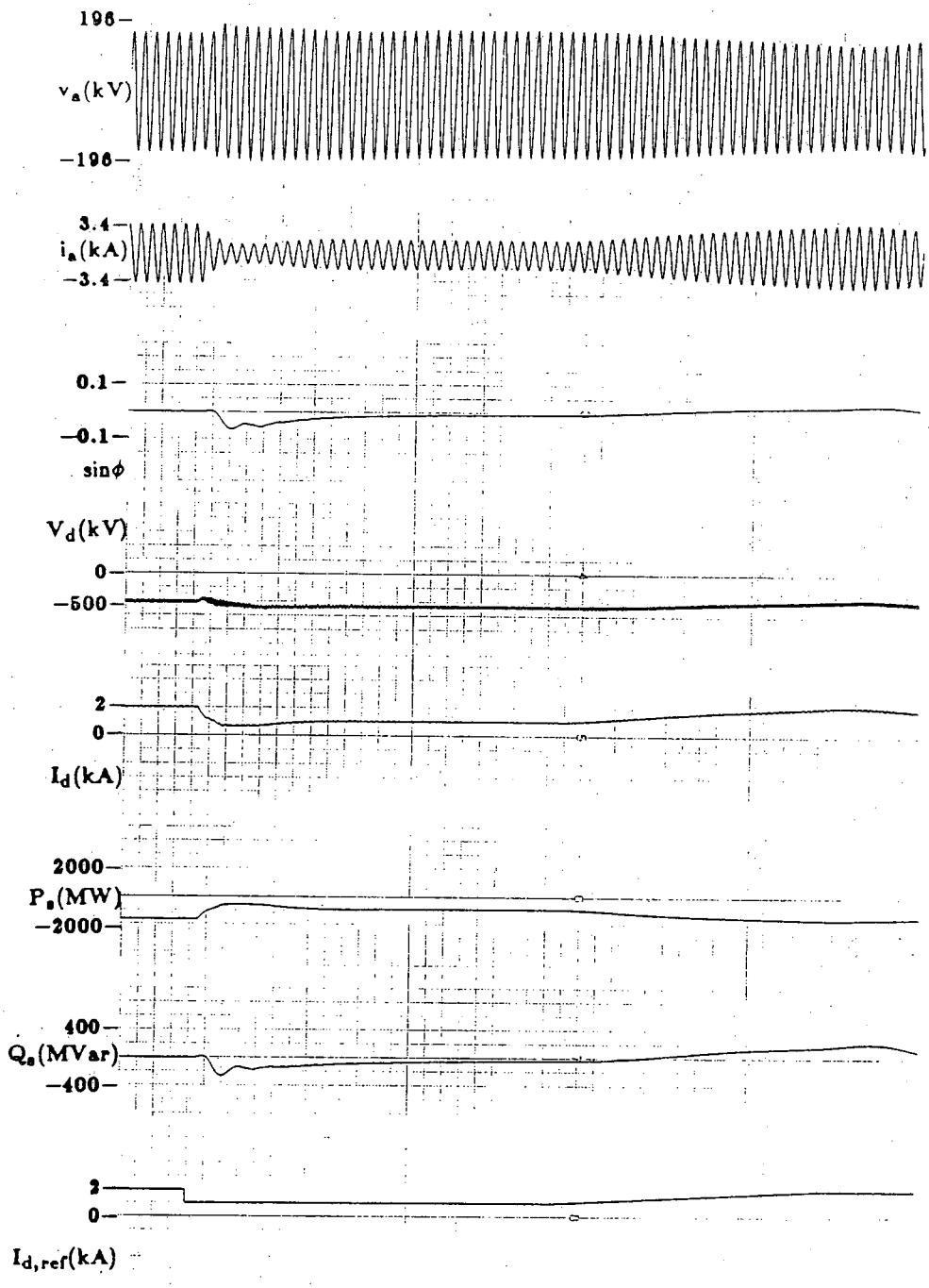

(a)

Figure 5.6 Dynamic response due to a drop and a ramp (24 cycles) in $I_{d,ref}$ (sinϕ-control, ESCR=1.5)

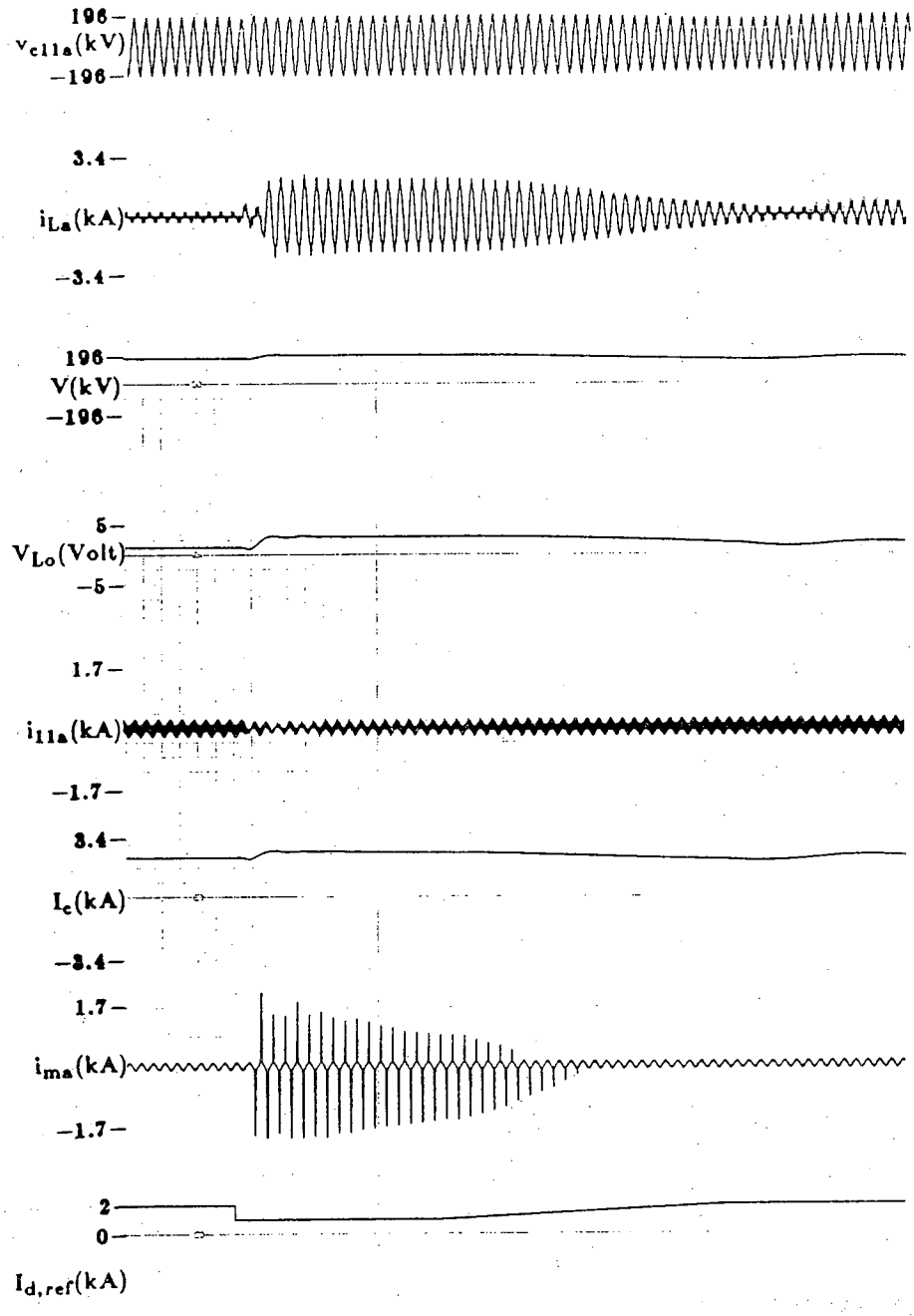

(b)

Figure 5.6 continued

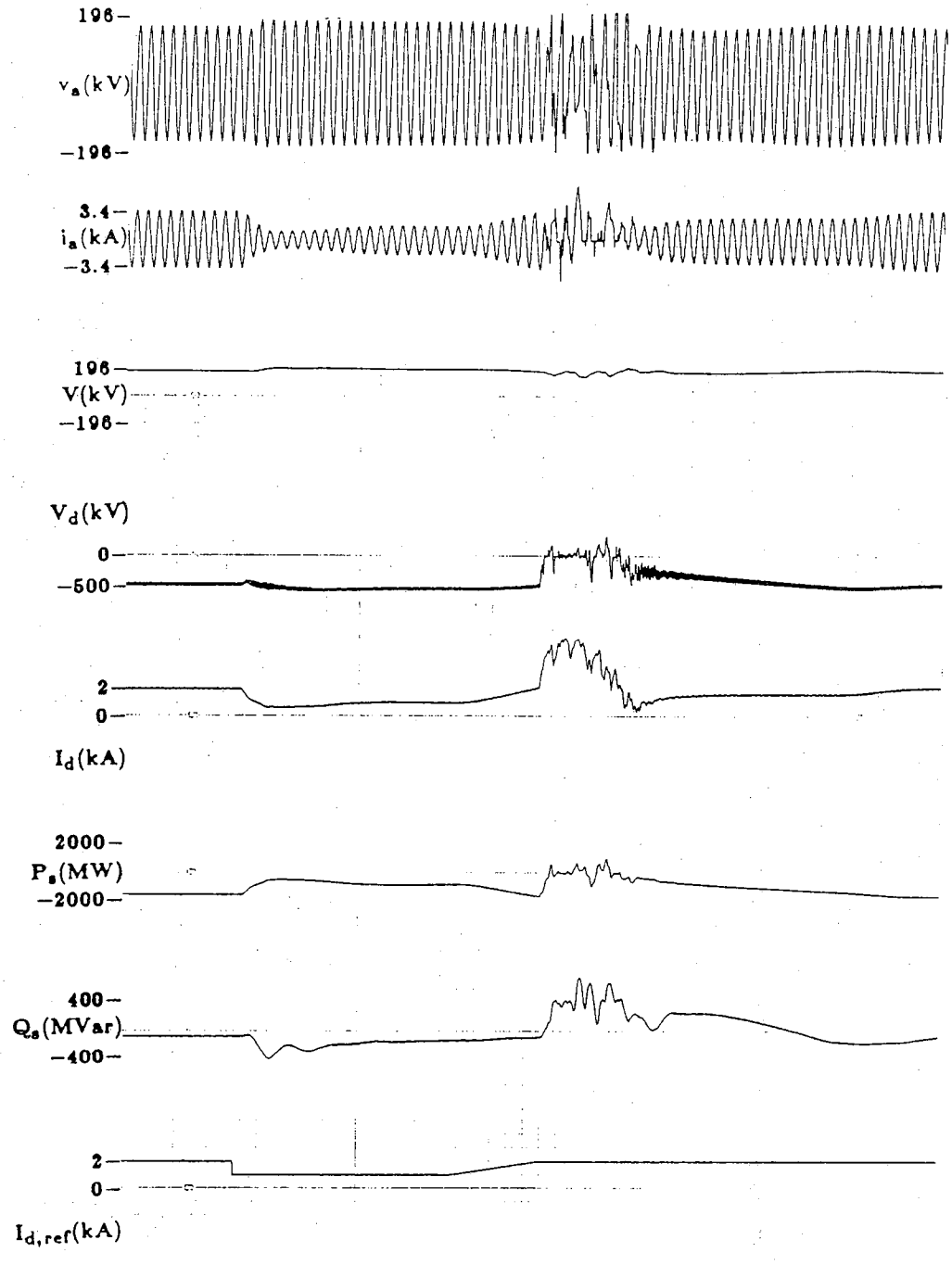

Figure 5.7 Unstability due to an increase in the rate of ramping to 9 cycles (sinϕ-control, ESCR=1.5)

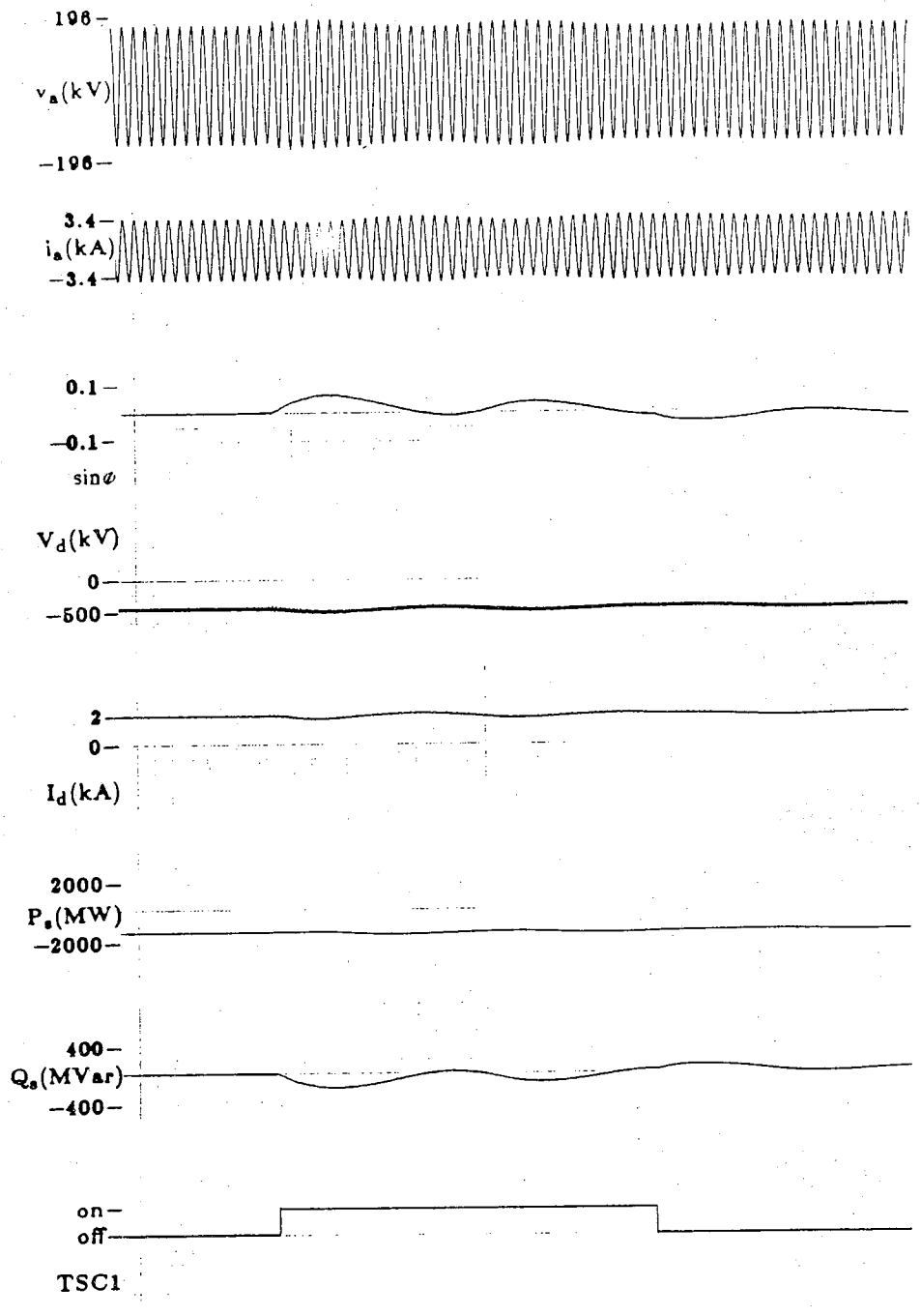

(a)

Figure 5.8 Dynamic response due to switching of a capacitor bank (sinϕ-control, ESCR=1.5)

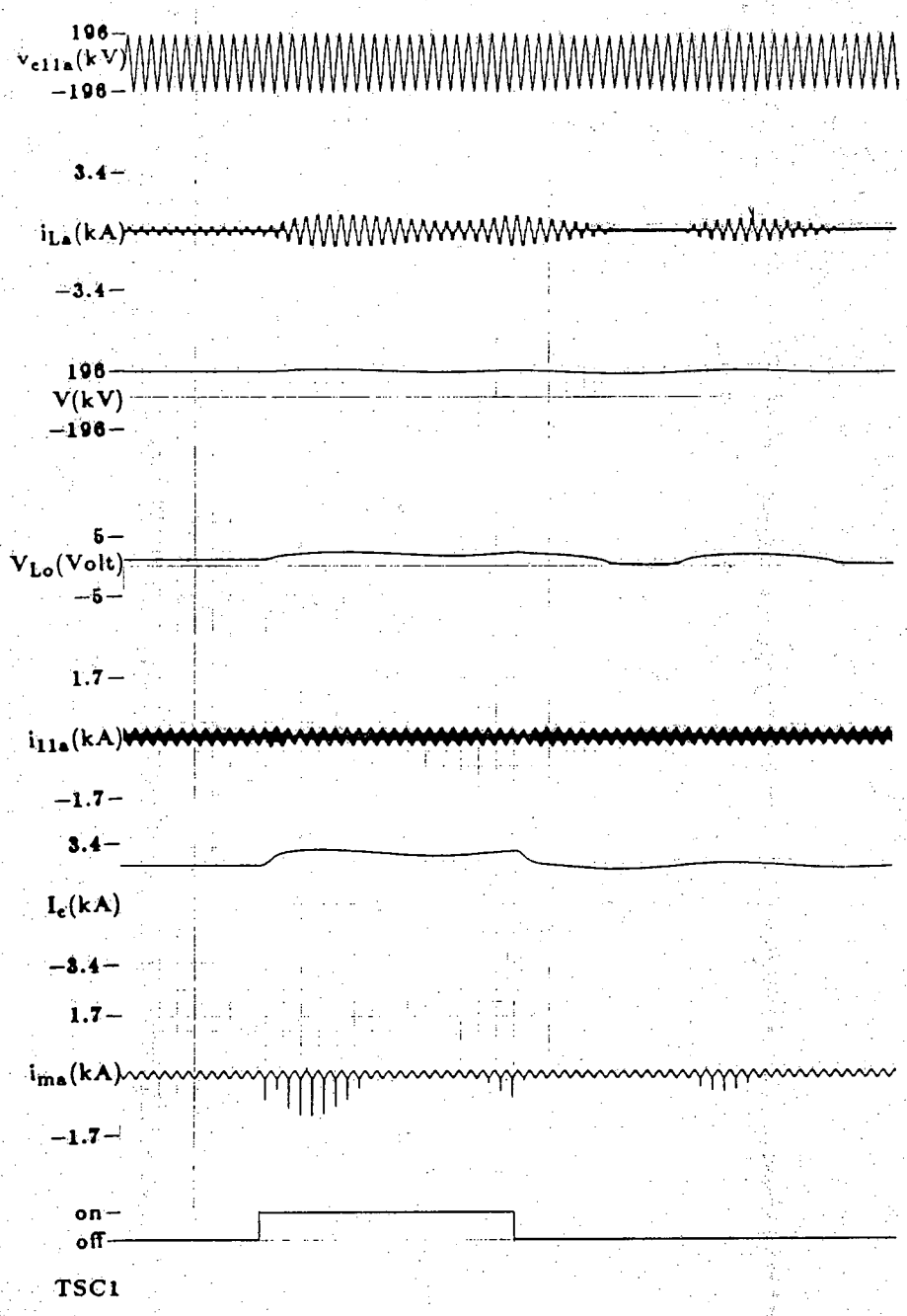

(b)

Figure 5.8 continued

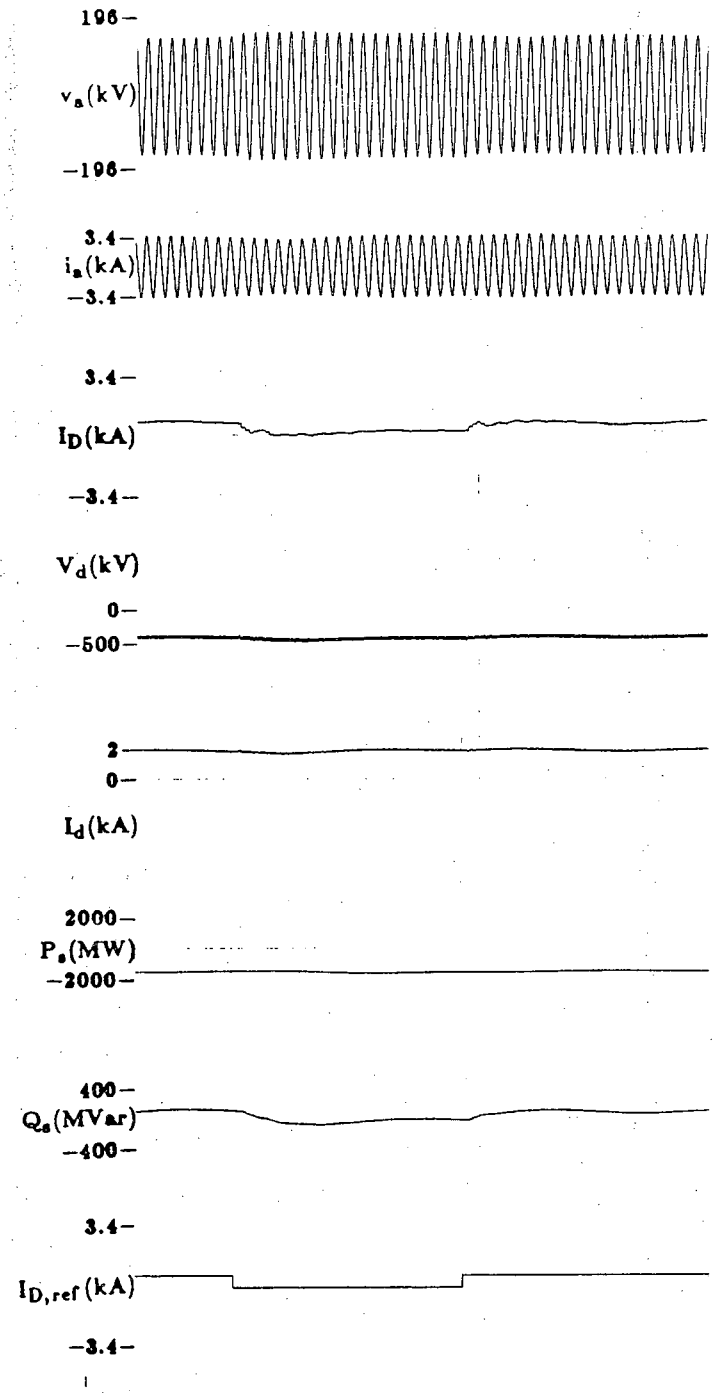

(a)

Figure 5.9 Dynamic response due to a step-change in $I_{D,ref}$ (I_D-control, ESCR=1.5)

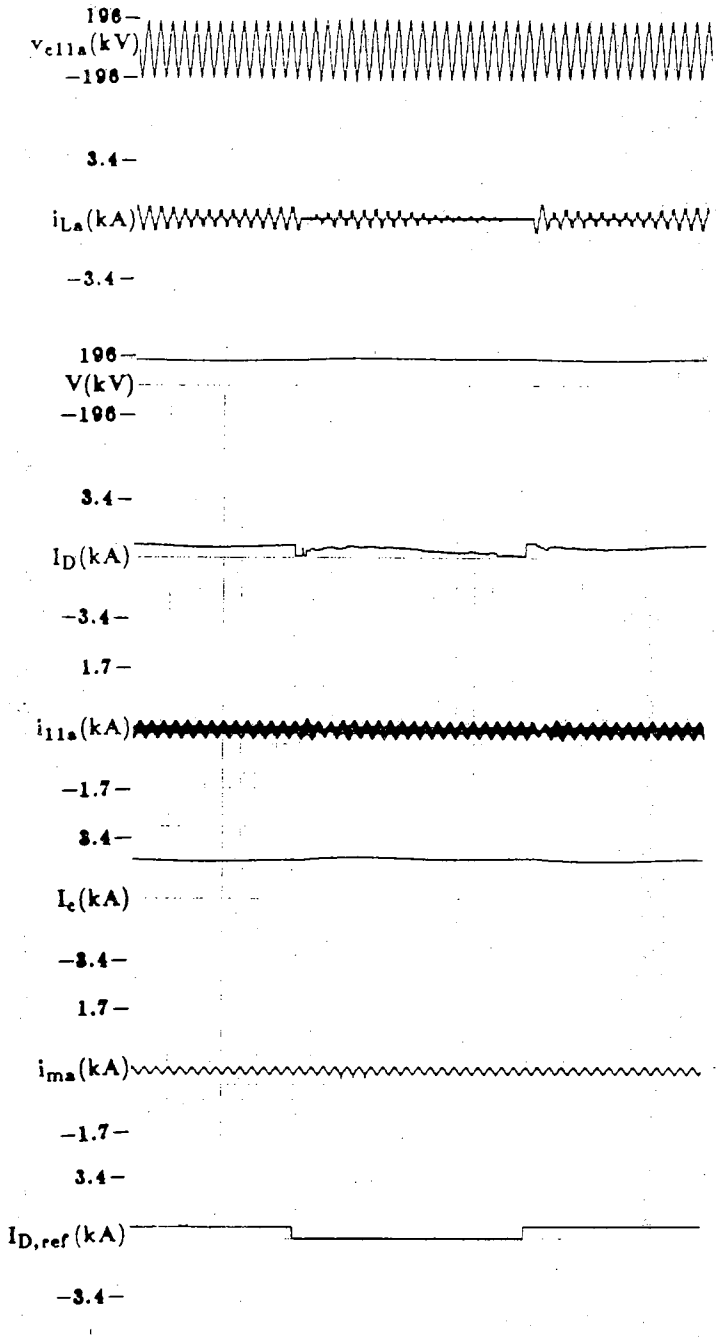

(b)

Figure 5.9 continued

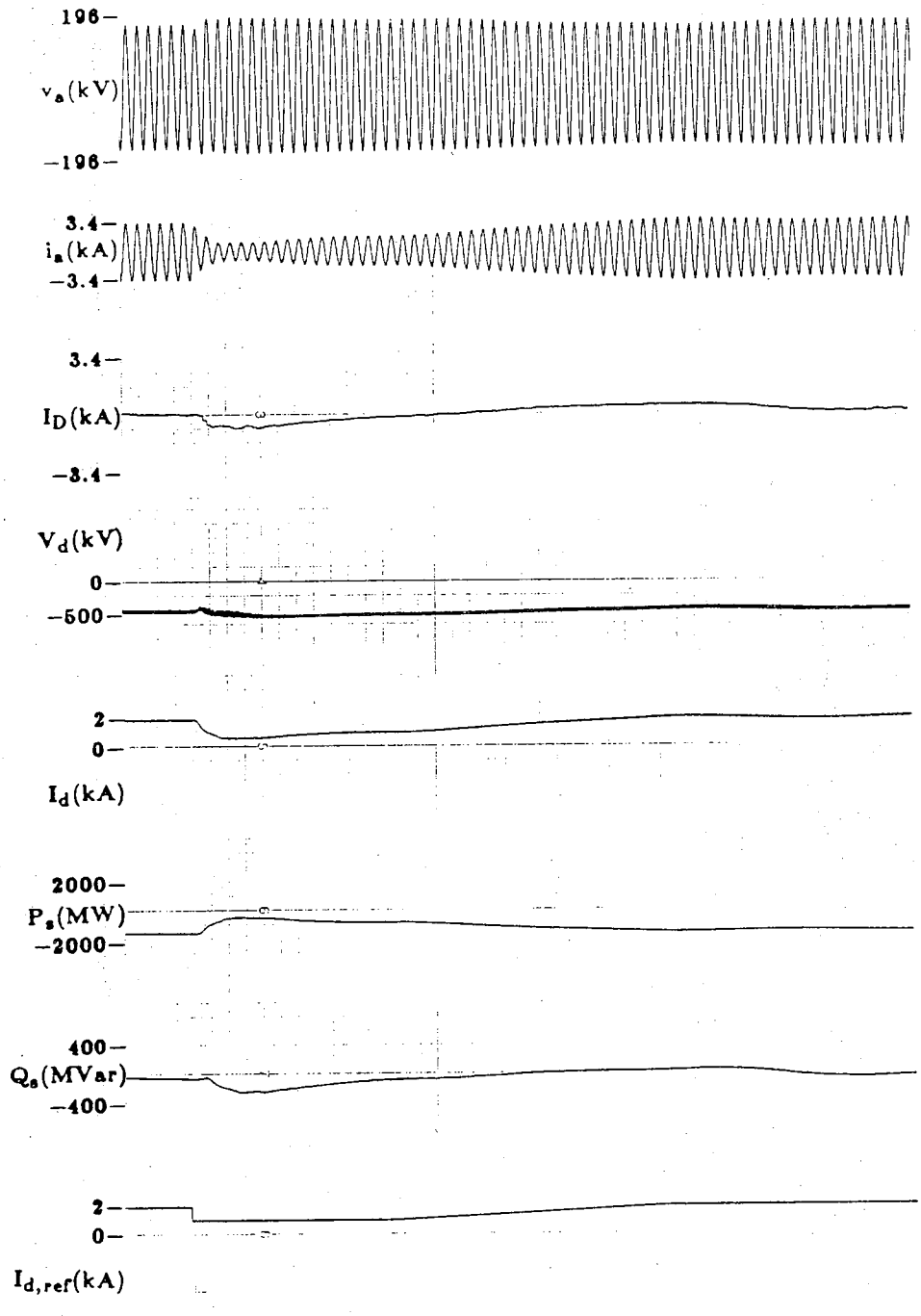

(a)

Figure 5.10 Dynamic response due to a drop and a ramp (24 cycles) in $I_{d,ref}$ (I_D-control, ESCR=1.5)

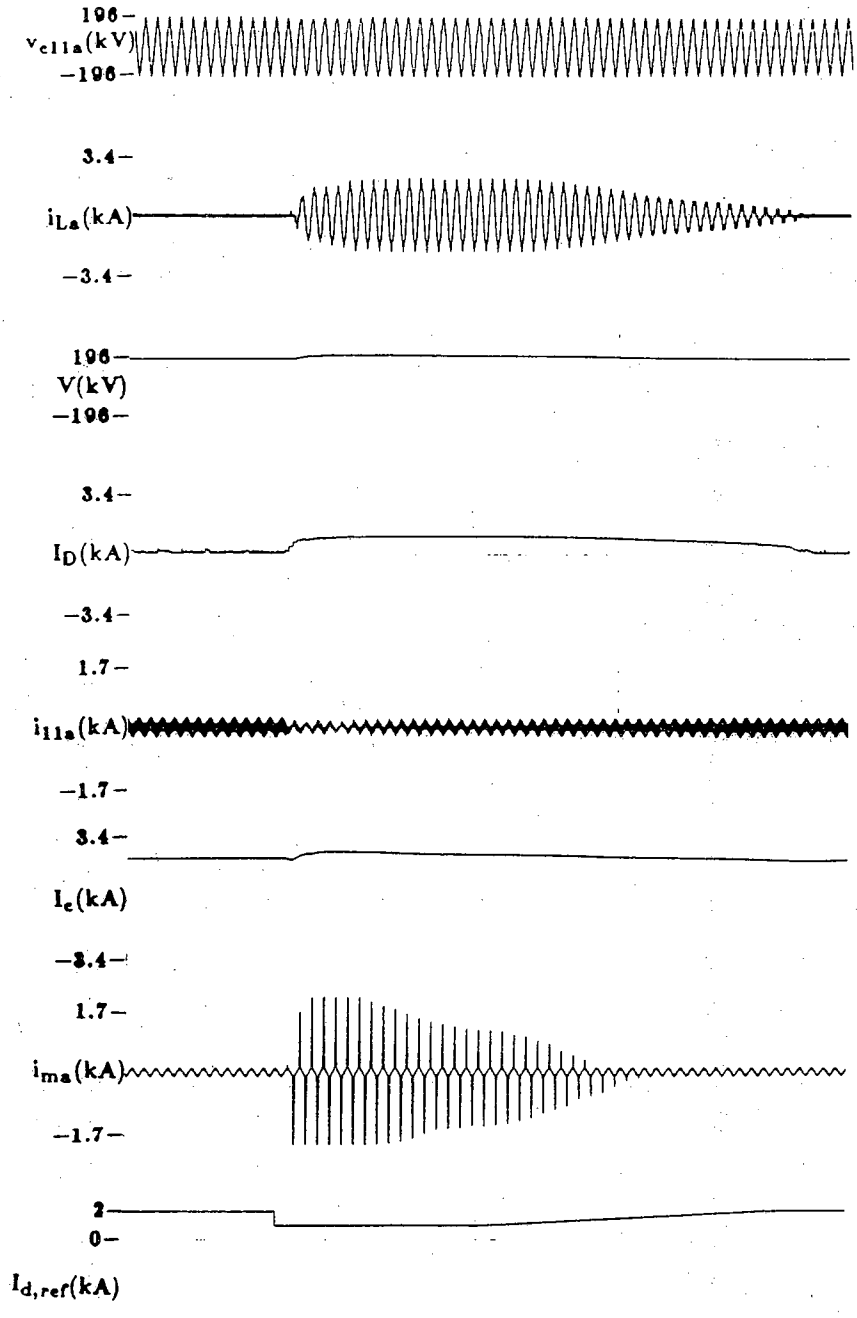

(b)

Figure 5.10 continued

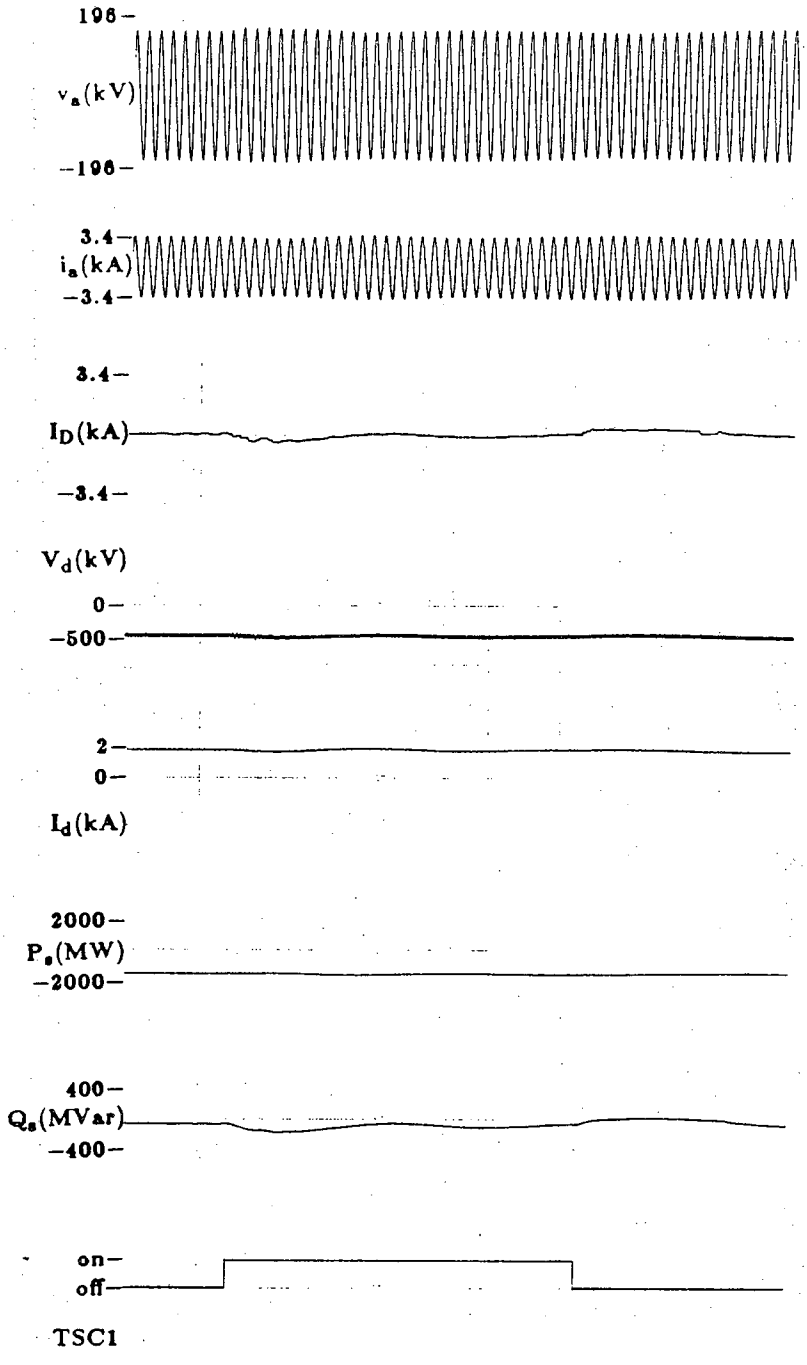

(a)

Figure 5.11 Dynamic response due to switching of a capacitor bank (I_D-control, ESCR=1.5)

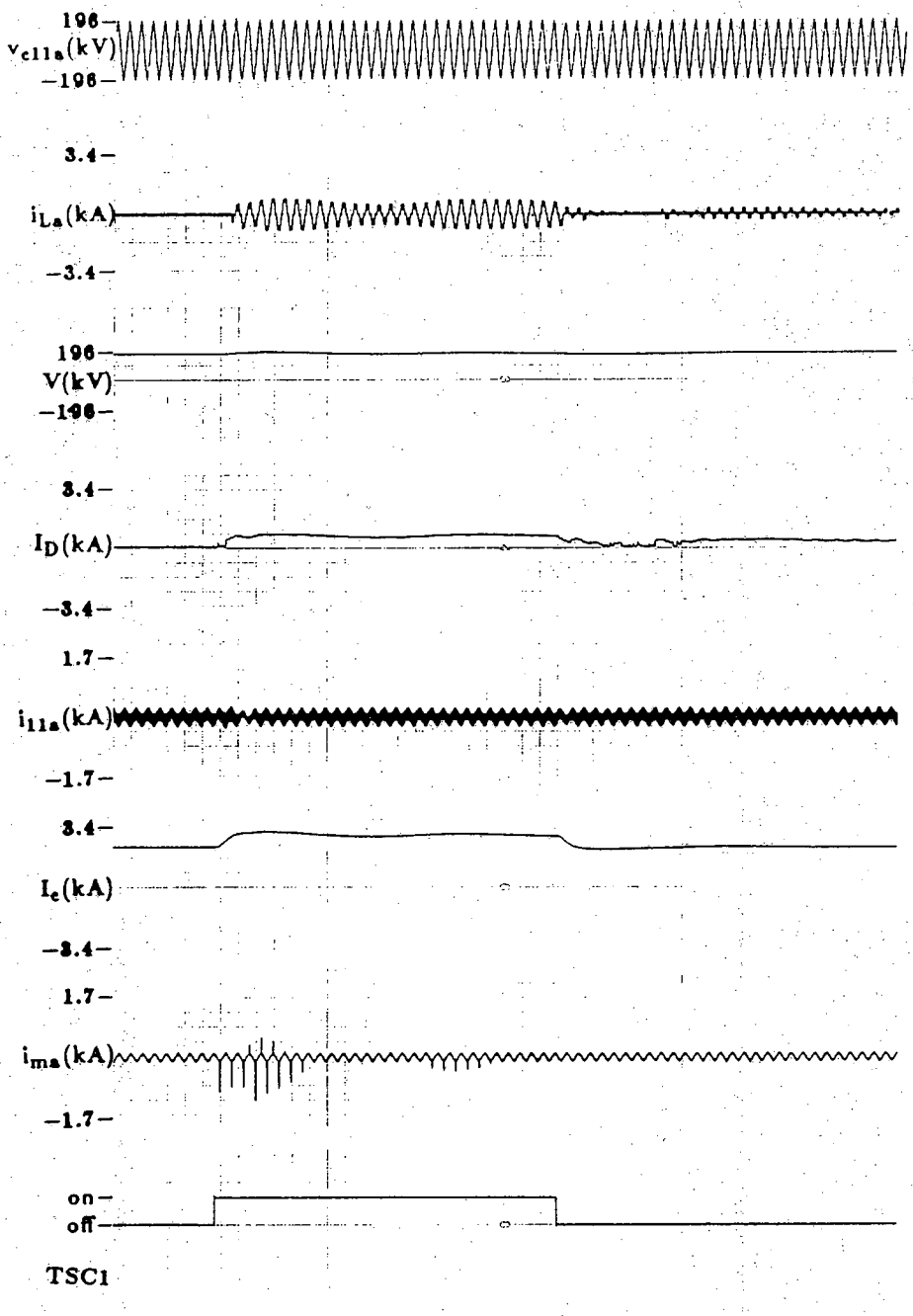

(b)

Figure 5.11 continued

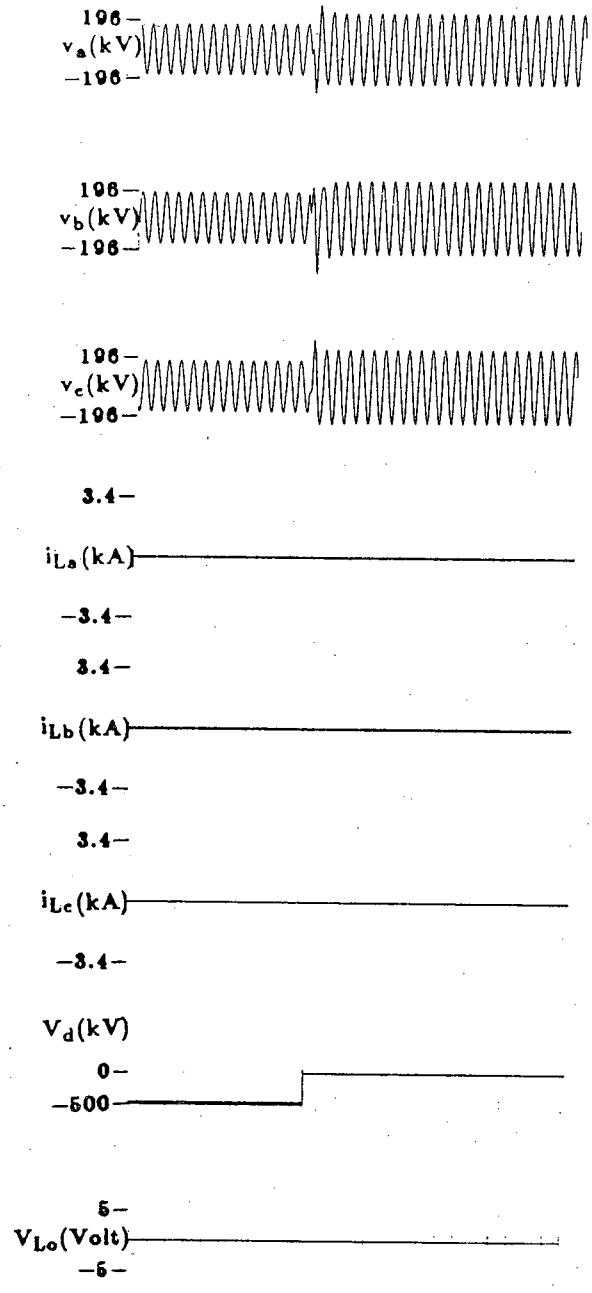

(a) Linear transformer and no TCR

Figure 5.12 Saturation and TCR effects on overvoltages due to a load rejection (ESCR=1.5)

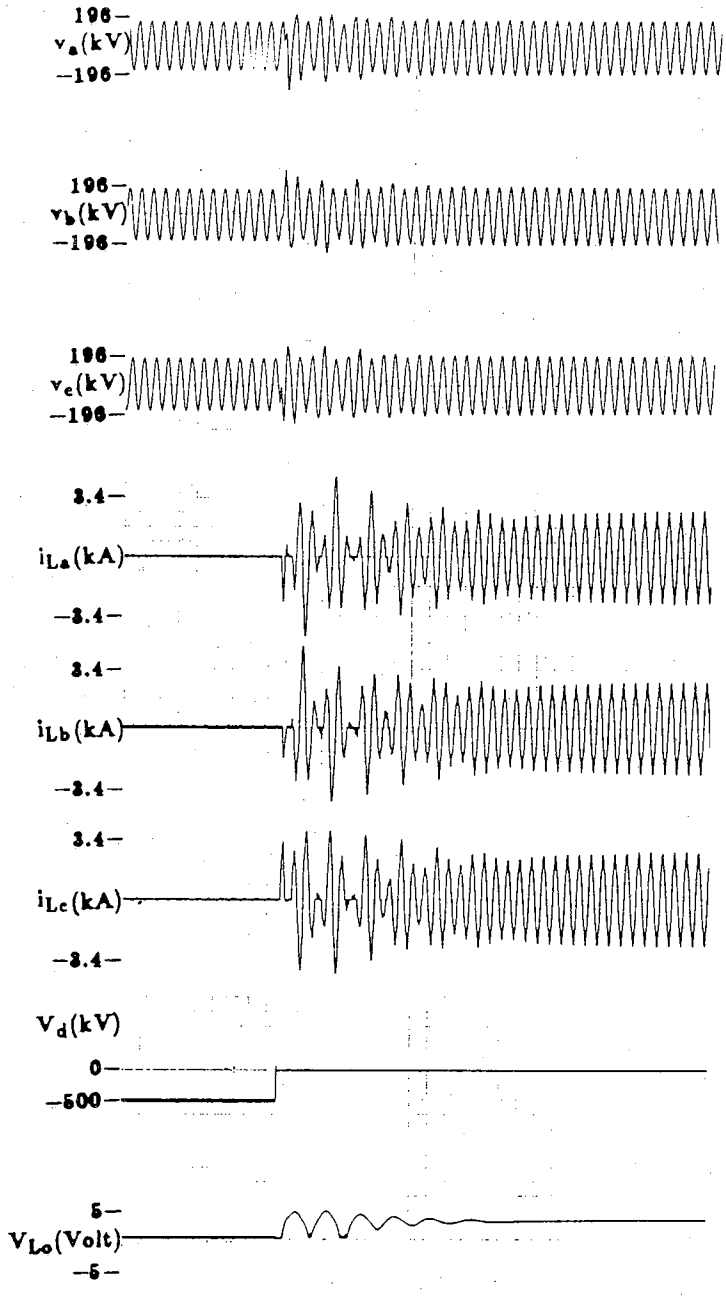

(b) Linear transformer and TCR

Figure 5.12 continued

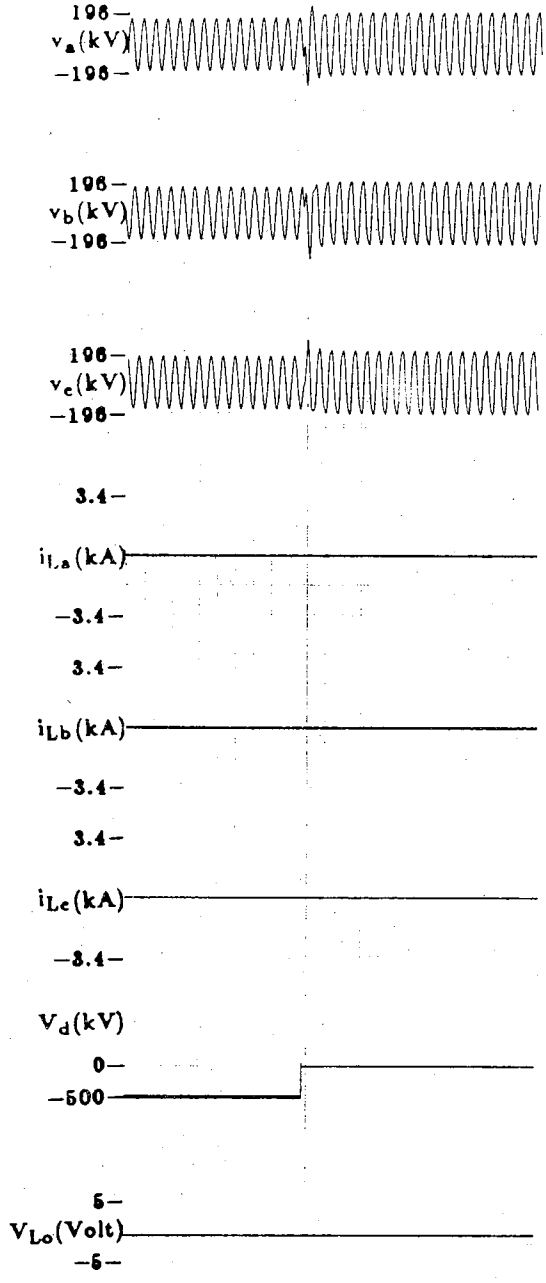

(c) Nonlinear transformer and no TCR

Figure 5.12 continued

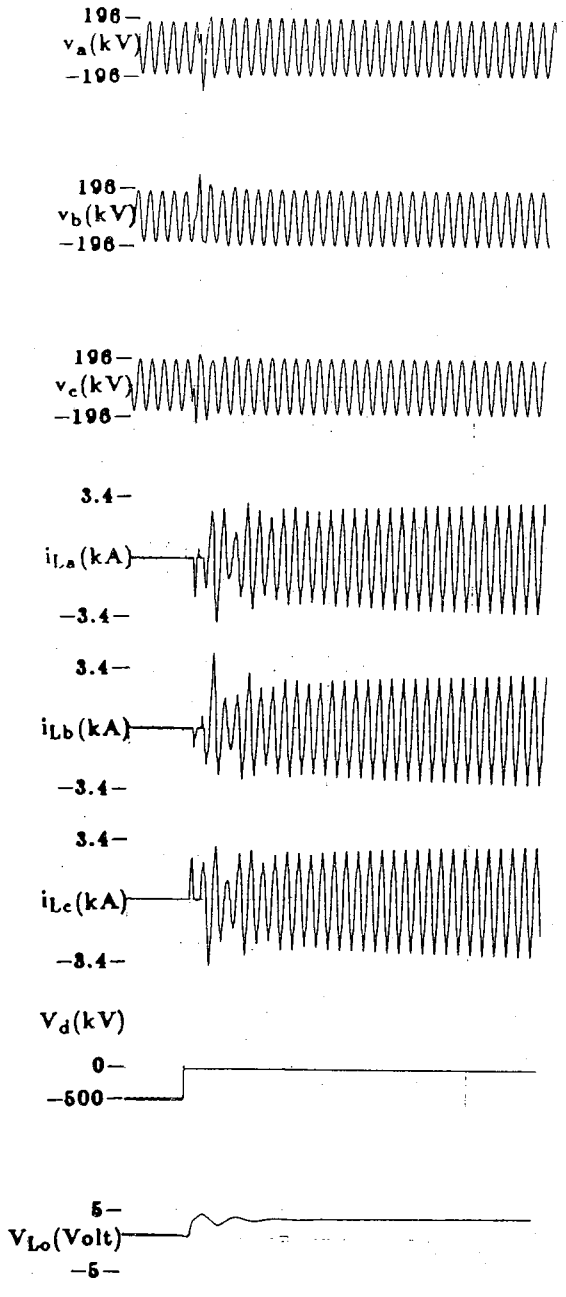

(d) Nonlinear transformer and ~~no~~ TCR

Figure 5.12 continued

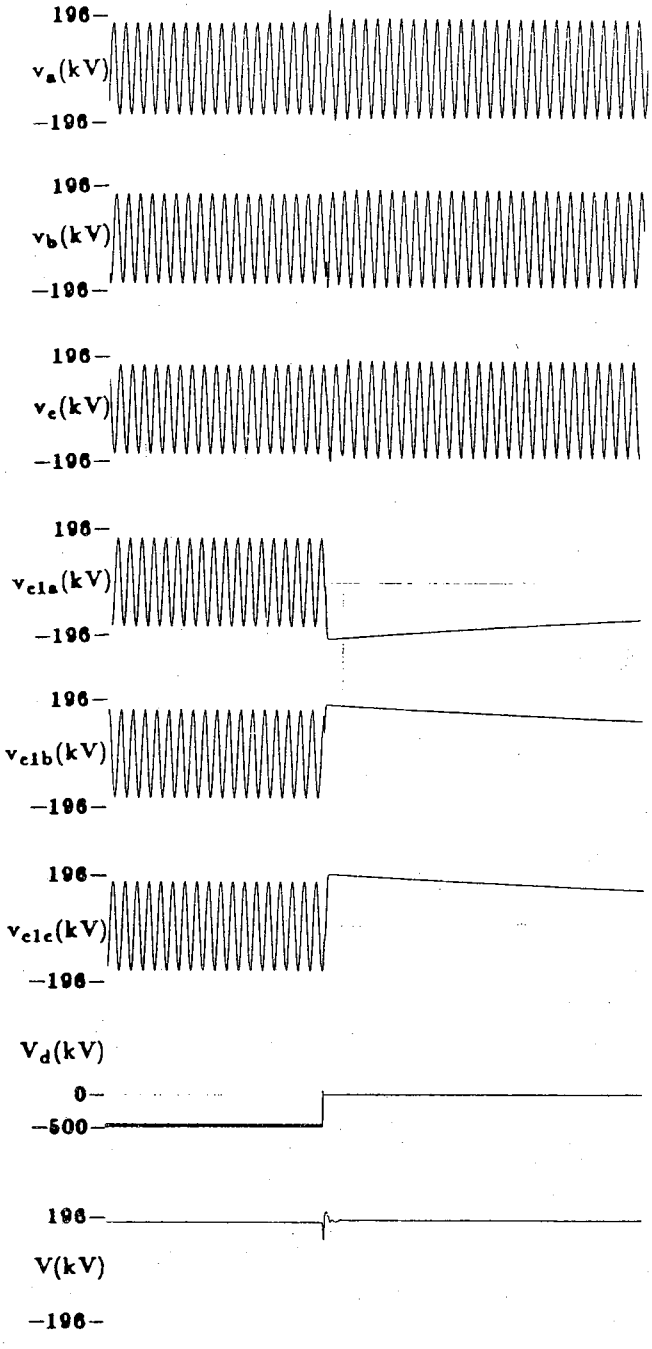

(a)

Figure 5.13 TCR and TSC operation during load rejection (ESCR= 3.97)

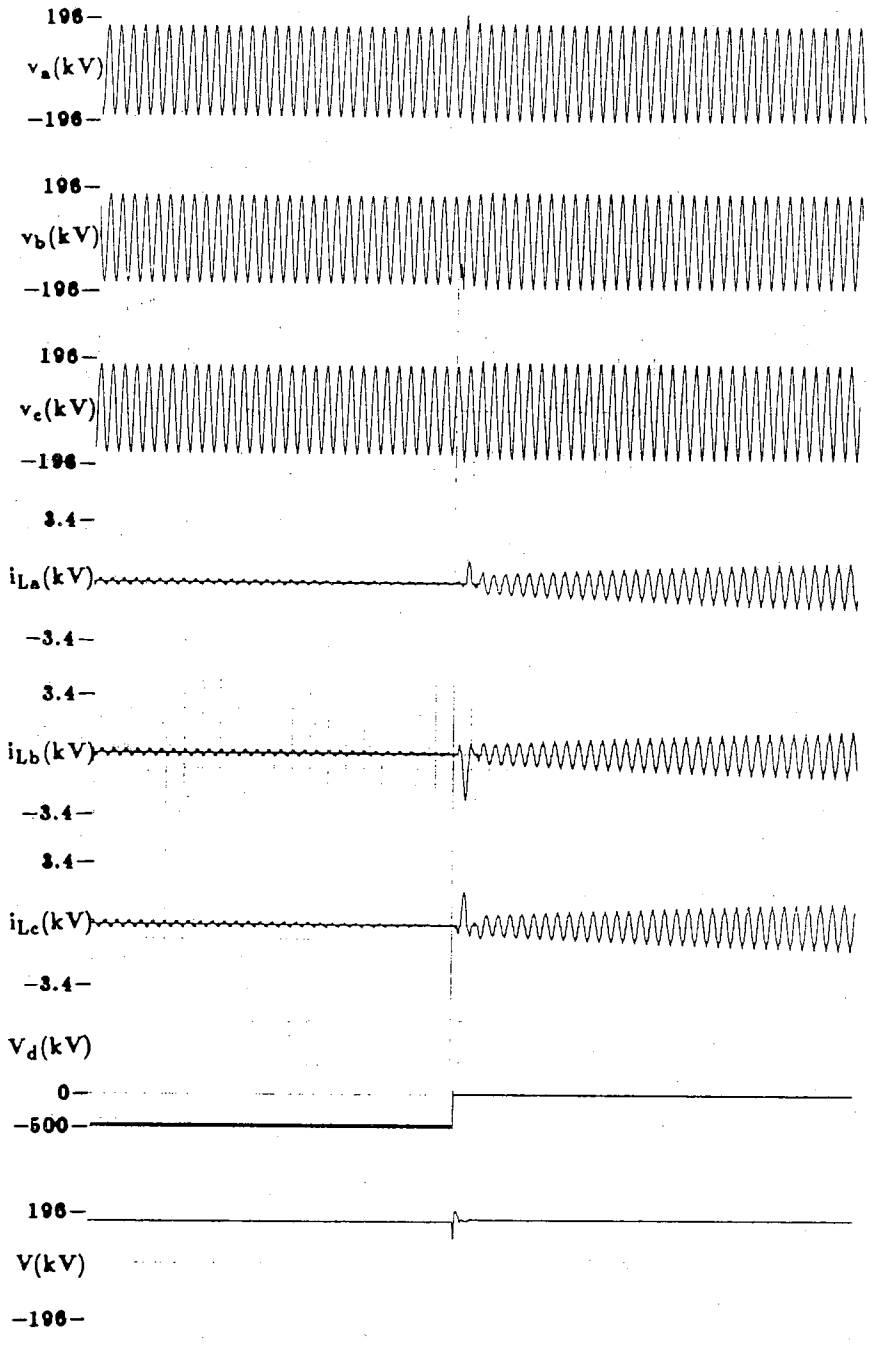

(b)

Figure 5.13 continued

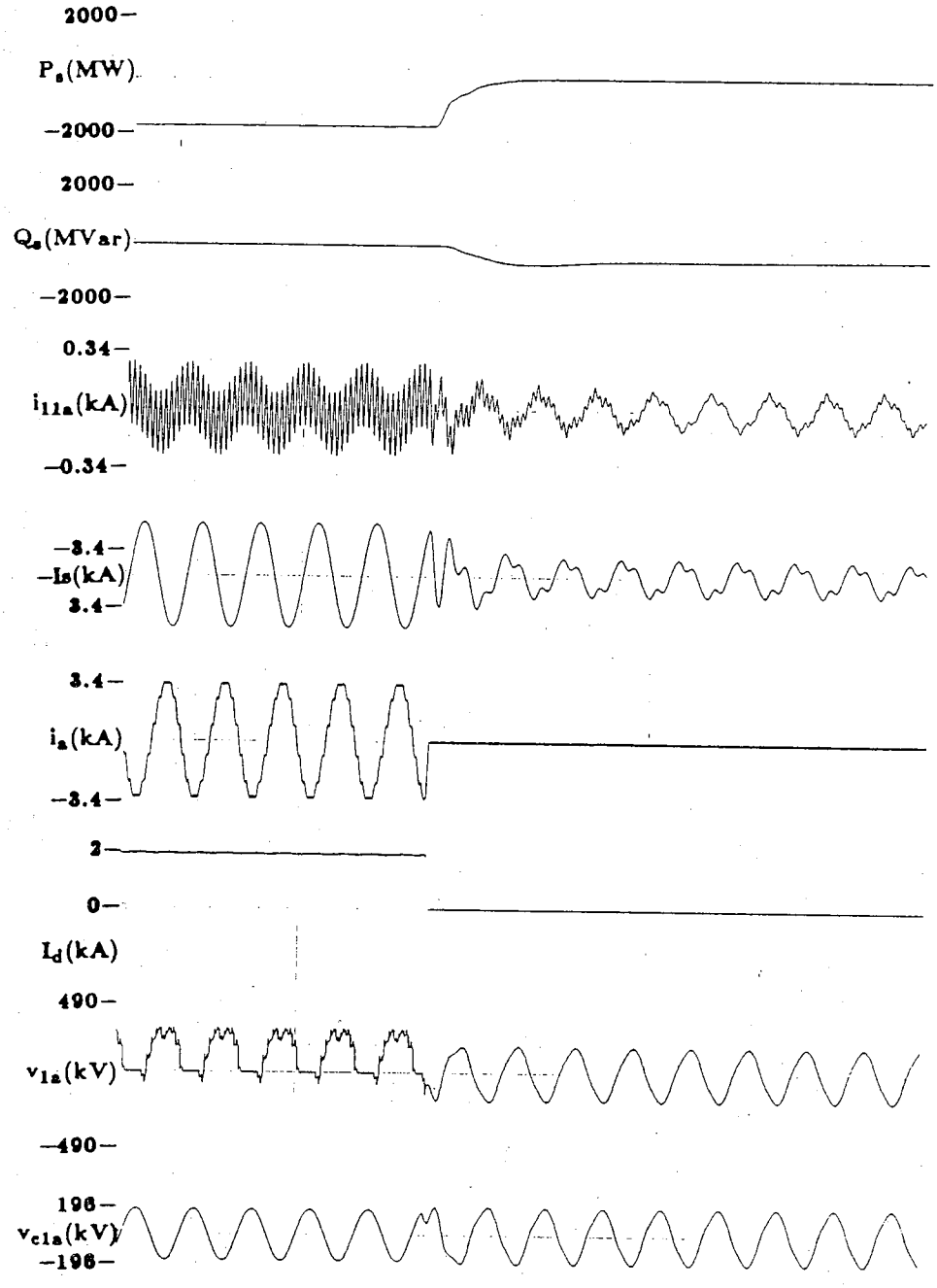

(c)

Figure 5.13 continued

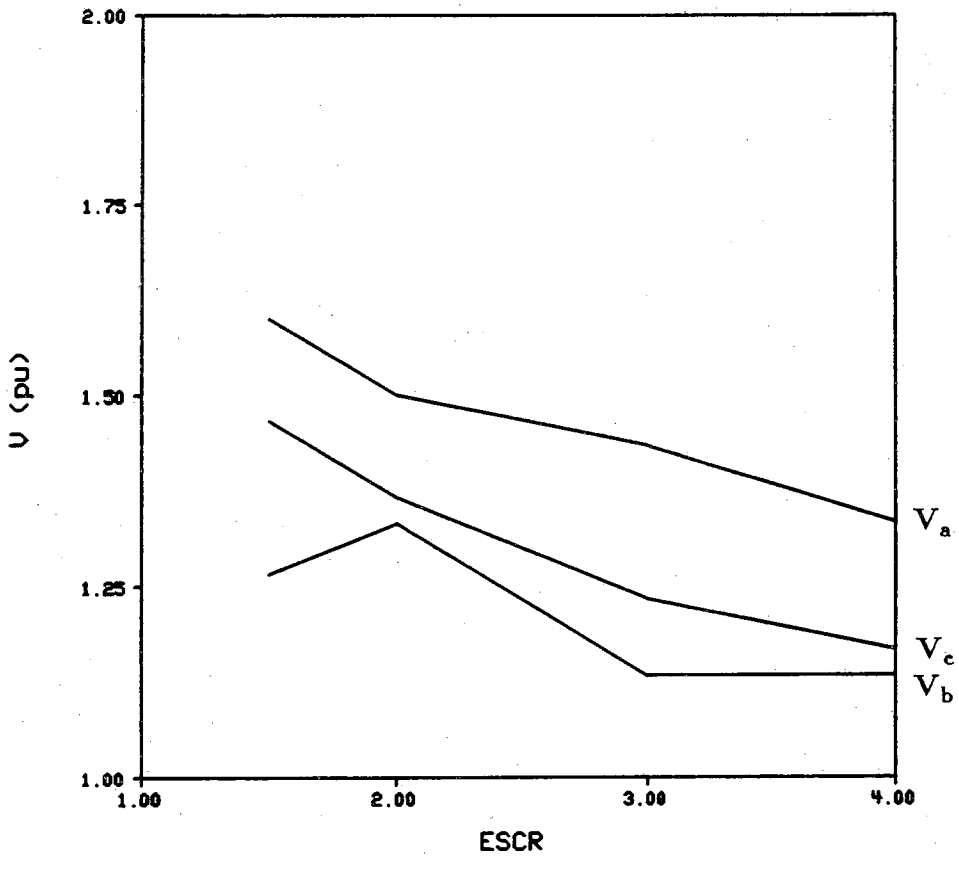

Figure 5.14 Overvoltages due to load rejection

CHAPTER 6

CONCLUSION AND RECOMMENDATIONS

6.1 Conclusion

The focus of this report has been on the harmonic generation and interaction between different nonlinear elements (HVDC converter, converter transformer saturation, and the thyristor-controlled reactor) present at the AC/DC junction bus.

The conclusions of this report could be summarized as follow:

- The detailed analog simulation of a sample AC/DC system was successfully realized where two common firing schemes for the inverter were implemented. The simulation was validated by steady-state load flow calculations based on the average-value model of the converters. Simulation techniques of the the nonlinear magnetization characteristics of the converter transformer, the thyristor-controlled reactor, the thyristor-switched capacitors, and the bypass valves were discussed and validated.
- A basic relation governing the extra harmonic orders in the AC and DC variables in the presence of harmonic voltages or fundamental frequency voltage unbalance was established. It was found that the individual pulse firing scheme is more sensitive to the AC voltage distortion, particularly when the distortion is large, than the equidistant pulse control firing scheme.
- It was also found that the effect a DC component in the transformer secondary side current tends to generate even harmonics on the AC side and odd harmonics on the DC side. These were found to satisfy the established relationship.
- It was shown that the effect of the TCR and saturation on the converter could worsen as the operating point is changed and that filters for the

fifth and seventh harmonics are necessary, especially for large rated TCRs.

- As a result of unbalance, triplen harmonics are generated on the AC side, and even harmonics on the DC side the order of which can be predicted using the relationship set forth. These triplen harmonics are not entirely of the conventional zero sequence (same magnitudes and same phases).
- The problem of voltage or power stability of an AC/DC system is very crucial. It was found that the system become unstable when the ESCR is lower than some minimum value, and that the steady-state voltage and power instabilities can be reasonably predicted by the appropriate sensitivity factors.
- It has also been shown that the TCR can play an effective role in stabilizing the AC voltage. Although adding shunt capacitors would also enhance the voltage support and the stability, it has the effect of lowering the ESCR, thus contributing to power voltage regulation.
- Three tests were performed on the three types of TCR controls. It was found that the power factor control presents more oscillatory response at lower ESCR, and that the terminal voltage control of the TCR is best suited for load rejection studies.
- Fast ramping of the DC current could be a problem with weak AC support. It was found that a 24 cycles ramp period shows a stable response while a faster response caused instability.
- The transformer saturation moderates the transient overvoltages by absorbing excess reactive power from the system. For load rejection studies, neither the transformer nor the TCR could limit (to an acceptable level) the first cycle of the transient overvoltages; hence, supplementary devices such as surge arrestors have to be used.
- It was found that as the ESCR decreases, the peaks of the transient overvoltages due to load rejection increase. The highest peak could appear in any phase of the terminal voltage and this depends on the timing of the load rejection.
- It was also found that the initial residual voltage on a switched-out capacitor of a TSC can be as high as the peak transient voltage.

6.2 Recommendations for future work

The formula which relates the AC and DC harmonics could be used to get a better understanding of how the bridge modulates the harmonics in the AC

and DC networks. Based on this formula, a valuable investigative attempt would be to compute the magnitude of the uncharacteristic harmonics from the bridge in a simpler manner.

Any unbalance in the AC terminal voltage is highly undesirable. The TCR could be used to balance these voltages. Extra harmonics would be generated. An investigation to determine the benefit of balanced AC terminal voltages versus the penalty of added harmonics may prove to be quite interesting.

The results presented from transient and dynamic studies show that the TCR cannot limit by itself the first transient overvoltage (TOV) peak. Moreover, it has been shown that the ramping rate of the DC current has to be large enough to avoid instability. These two points are worth further investigation.

LIST OF REFERENCES

LIST OF REFERENCES

[1] H. Frank, T. Peterson, "The use of thyristor-controlled static VAR compensators at HVDC converter stations", CIGRE Symposium, paper No. 400-06, Sept. 28-30, 1987, Boston.

[2] J.D. Ainsworth, A. Gavrilovic, H.L. Thanawala, "Overvoltage control by different types of reactive power compensation in AC/DC systems", Presented to IEEE conference on "Overvoltages and compensation on integrated AC/DC systems", Winnipeg, Canada, July 9-11, 1980, pp. 95-99.

[3] IEEE committee report, "Dynamic characteristics of North American HVDC systems for transient and dynamic stability evaluations", IEEE Trans., Vol. PAS-100, No. 7, July 1981, pp. 3356-3364.

[4] J. Arrillaga, *High voltage direct current transmission*, Peter Peregrinus Ltd, London, UK, 1983.

[5] Ake Ekstrom, Gote Liss, "A refined HVDC control system", IEEE Trans., Vol. PAS-89, No. 5/6, May/June 1970, pp. 723-732.

[6] J. D. Ainsworth, "The phase-locked oscillator - a new control system for controlled static converters", IEEE Trans., Vol. PAS-87, No. 3, March 1968, pp. 859-865.

[7] IEEE Working group, "Power system harmonics: an overview", IEEE Trans., Vol. PAS-102, No. 8, August 1983, pp. 2455-2460.

[8] A. Gavrilovic & al., "Interaction between AC and DC systems", CIGRE paper No. 14-09, Aug. 27 - Sept. 4, 1986.

[9] A. Gavrilovic and al., "Interaction between DC and AC systems", CIGRE Symposium, paper No. 200-20, Sept. 28-30, 1987, Boston.

[10] J.P. Bowles, "Alternative techniques and optimization of voltage and reactive power control at HVDC converter stations", presented to IEEE conference on "Overvoltages and compensation on integrated AC/DC systems", Winnipeg, Canada, July 9-11, 1980, pp. 5-5i.

[11] G.D. Breuer, R.L. Hauth, R.V. Pohl, H.S. Patel, "Voltage and VAR compensation studies for integrating DC links into AC systems", IEEE 1980, conference on "Overvoltage and compensation in an integrated AC/DC systems", Winnepeg, Canada, July 9-11, 1980, pp. 88-94.

[12] M. Erche, M. Schraudolph, M. Weibelzahz, "Reactive power control in AC/DC systems by HVDC converter station", CIGRE Symposium, paper No. 400-04, Sept. 28-30, 1987, Boston.

[13] E.V. Larsen, R.A. Walling, "Characterization and control of harmonic overvoltages at HVDC stations", CIGRE Symposium, paper No. 200-15, Sept. 28-30, 1987, Boston.

[14] H. Stemmler, "HVDC back-to-back interties on weak AC systems, second harmonic problems analyses and solutions", CIGRE Symposium, paper No. 300-08, Sept. 28-30, 1987, Boston.

[15] J. Reeve, T. Subba Rao, "Dynamic analysis of harmonic interaction between AC and DC power systems", IEEE PAS, Vol. PAS-93, No. 2, March/April 1974, pp. 640-646.

[16] J.D. Ainsworth, "Harmonic instability between controlled static converter and AC network", IEE Proc., Vol 114, July 1967, pp. 949-957.

[17] R. Yacamini, J.C. de Oliveira, "Instability in HVDC schemes at low order integer harmonics", IEE Proc., Vol. 127, Pt. C, No. 3, May 1980, pp. 179-188.

[18] CIGRE working group, "Static shunt devices for reactive power control", CIGRE, paper No. 31-08, 1974, pp. 1-19.

[19] R. Yacamini, N. Hatziargyriou, "Overvoltages caused by blocking twelve-pulse HVDC schemes", IEE Proc., Vol. 127, Pt. C, No. 3, May 1980, pp. 189-198.

[20] R. Yacamini, A.I. Taalab, "Effect of AC system impedance on the regulation and, hence, the stability margin of HVDC schemes", IEE Proc., Vol. 132, Pt. C, No. 4, Jul. 1985, pp. 202-207.

[21] S.M. Merry, E.R. Taylor, "Overvoltages and harmonics on ehv systems", IEEE Power Engineering Society, 1972 Winter Meeting, New-York, Jan. 30 - Feb. 4, 1972, pp. 2537-2544.

[22] Arun G. Phadke, James H. Harlow, "Generation of abnormal harmonics in high-voltage AC/DC power systems", IEEE Trans., Vol. PAS-87, No. 3 March 1968, pp. 873-882.

[23] T.J. Miller, *Reactive power control in electric systems*, John Wiley & Sons, New York, 1982.

[24] L. Gyugyi, R.A. Otto, T.H. Putman, "Principles and applications of static, thyristor-controlled shunt compensators", IEEE Trans., Vol. PAS-97, No. 5, Sept./Oct. 1978, pp. 1935-1945.

[25] J. Reeve, R. Adapa, "Evaluation of developments in DC models for AC/DC transient stability programs", CIGRE Symposium, paper No. 100-04, Sept. 28-30, 1987, Boston.

[26] C.M. Ong, C.T. Liu, C.N. Lu, "Generation of connection matrices for digital simulation of converter circuits using the tensor approach", IEEE Trans., Vol. PWRS-2, No. 4, Nov. 1987.

[27] EMTP rule book.

[28] K.R. Padiyar, A.G. Kothari, "Modelling and simulation of HVDC bridge converters", Electric machines and power systems, Vol. 13, No. 5, 1987, pp. 285-298.

[29] N. Vovos, G. Galanos, G. Giannakopoulos, "A mathematical model for dynamic simulation of HVDC systems", IEEE PES, 1983 Winter Meeting, March 7-9, pp. 1-9.

[30] J.P. Bowles, "AC system and transformer representation for HVDC transmission studies", IEEE Trans., Vol. PAS-80, No. 7, Sept./Oct. 1970, pp. 1605-1609.

[31] Esmat H. Badawy, Rida D. Youssef, "Representation of transformer saturation", Electric power research, No. 6, 1983, pp. 301-304.

[32] S. Prusty, M.V.S. Rao, "New method for predetermination of true saturation characteristics of transformers and nonlinear reactors", IEE Proc., Vol. 127, Pt. C, No. 2, Mar. 1980, pp. 106-110.

[33] C. Hatziantoniu, G.D. Galanos, J. Milias-Argitis, "An incremental transformer model for the study of harmonic overvoltages in weak AC/DC systems", IEEE Trans., Vol. PWRD-3, No. 3, July 1988, pp. 1111-1121.

[34] H.W. Dommel, A. Yan, R.J.O. Marcano, A.B. Miliani, "Case studies for electromagnetic transients", Dept. of EE, the University of British Columbia, Vancouver, B.C., Canada V6T 1W5.

[35] H.W. Dommel, "Transformer models in the simulation of electromagnetic transients", 5th power systems computation conference, Cambridge, England, Sept. 1-5, 1975, pp. 1-16.

[36] H.W. Dommel, "Transformer representation in the EMTP", draft version of section 6 of the "Electromagnetic transients program reference manual", Dept. of Electrical Engineering, the University of British Columbia 2356 Main Mall, Vancouver, B. C., Canada.

[37] E.P. Dick, W. Watson, "Transformer models for transient studies based on field measurements", IEEE Trans., Vol. PAS-100, No. 1, Jan. 1981, pp. 409-419.

[38] G.W. Swift, "Power transformer core behavior under transient conditions", IEEE Trans., Vol. PAS-90, No. 2, Sept./Oct. 1971, pp. 2206-2210.

[39] Discussion by R.A. Walling in [29].

[40] Kwa-sur Tam, Robert H. Lasseter, "Alternative twelve-pulse arrangement for static VAR control applications", IEEE Trans., Vol. PAS-102, No. 12, Dec. 1983,pp. 3728-3735.

[41] J. Avila-Rosales and F.L. Alvarado, "Nonlinear frequency dependent transformer model for electromagnetic transient studies in power systems", IEEE Trans., Vol. PAS-101, No. 11, Nov. 1982, pp. 4281-4288.

[42] H. G. Hingorani, M.F. Burbery, "Simulation of AC system impedance", IEEE paper 69TP 632 PWR.

[43] J.D. Ainsworth, A. Gavrilovic, H.L. Thanawala, "Static and synchronous compensators for HVDC transmission convertors connected to weak AC systems", CIGRE report, No. 31-01, 1980.

[44] E.L. Weeks, *Transmission and distribution of electrical energy*, Harper & Row, 1981.

[45] Manuals for power system simulator and EAI-680 scientific computing system, Purdue University, West Lafayette, Indiana, USA.

[46] E.W. Kimbark, *Direct current transmission*, Vol. 1, John Wiley & Sons, New York, 1971.

[47] D.P. Carroll, "HVDC transmission systems", course notes, Purdue University, West Lafayette, IN, USA.

[48] Eckhard Rumpf, S. Ranade, "Comparison of suitable control systems for HVDC stations connected to weak AC systems, Part I: new control systems, Part II: operational behavior of the HVDC transmission", IEEE/PES summer meeting and international symposium on high power testing, Portland, Ore., July 18-23, 1971, pp. 549-554(part 1) & 555-564(part II).

[49] Katsuhiko Ogata, *Modern control engineering*, Prentice-Hall, Inc., Englewood Cliffs, NJ, USA, 1970.

[50] Yuan-Yit Hsu, Chung-Yu Hsu, "Design of a proportional-integral power system stabilizer", IEEE Trans., Vol. PWRS-1, No. 2, May 1986, pp. 46-53.

[51] M.H.C. Barnes, "Modeling of static shunt VAR systems (SVS) for system analysis", CIGRE, ELECTRA, No. 51, March 1977, pp. 45-74.

[52] Laszlo Gyugyi, "Fundamentals of thyristor-controlled static VAR compensators in electric power system applications", IEEE, 87TH0187-5-PWR. 1987, pp. 8-27.

[53] R.H. Lasseter, S.Y. Lee, "Digital simulation of static VAR system transients", IEEE Trans., Vol. PAS-101, No. 10, Oct. 1982, pp. 4171-4177.

[54] Harry Frank, Tore Petersson, "Thyristor-switched shunt capacitors and their modeling for transmission applications", IEEE Power Engineering Society, 1978 Winter Meeting, New-York, Jan 29 - Feb 3, 1978, pp. 105-109.

[55] T.J.E. Miller, P. Chadwick, "An analysis of switching transients in thyristor switched capacitor compensated systems", IEE Proc., No. 205, 1981, pp. 104-107.

[56] P.C. Krause, *Analysis of electric machinery*, McGraw-Hill, New York, 1986.

[57] Uhlmann, *Power transmission by direct current*, Springer-Verlag Berlin, 1975.

[58] C. Adamson, N.G. Hingorani, *High voltage direct current power transmission*, Garraway Ltd., London, W. 8, England, 1960. New York, 1986.

[59] J. Arrillaga, A.E. Efthymiadis, "Simulation of converter performance under unbalanced conditions", IEE Proc., Vol. 115, No. 12, Dec. 1968, pp. 1868-1817.

[60] A.G. Phadke, J.H. Harlow, "Unbalanced converter operation", IEEE Trans., Vol. PAS-85, No. 3, March 1966, pp. 233-239.

[61] D.B. Giesner, J. Arrillaga, "Behavior of HVDC links under unbalanced - AC - fault conditions", IEE Proc., Vol 119, No. 2, February 1972, pp. 209-215.

[62] Yude Yao, A.M. Sharaf, "Uncharacteristic harmonics caused by AC system imbalances and the effect of smoothing reactor", presented at the third international symposium on harmonics in power systems (ICHPS), Nashville, Indiana, USA, Sept. 28 - Oct. 1, 1988, pp. 28-33.

[63] John Reeve, P.C.S. Krishnayya, "Unusual current harmonics arising from high-voltage DC transmission", IEEE Trans., Vol. PAS-87, No. 3, March 1968, pp. 883-893.

[64] Yacamini, "Harmonics produced by DC in converter transformer", IEE Proc., Vol. 125, No. 9, Sept. 1978, pp. 873-878.

[65] "IEEE recommended practice for measurement of electrical noise and harmonic filter performance of HVDC system", ANSI/IEEE Std 68-1977

[66] J. Arrillaga, D.A. Bradley, P.S. Bodger, *Power system harmonics*, John Wiley & Sons, New York, 1985.

[67] G. Gueth, P. Enstedt, A. Rey, and R.W. Menzier, "Individual Phase Control of a static Compensator for load compensation and voltage balancing and regulation", IEEE Trans., Vol. PWRS-2, No. 4, Nov. 1987, pp. 898-905.

[68] Ahmed Bensenouci, C.M. Ong, "AC current harmonics from HVDC converters", presented at the third international symposium on harmonics in power systems (ICHPS), Nashville, Indiana, USA, Sept. 28 - Oct. 1, 1988, pp. 203-208.

[69] A.E. Hammad, W. Kuhn, "A computation algorithm for assessing voltage stability at AC/DC interconnection", IEEE transaction, Vol. PWRS-1, No. 1, February 1986, pp. 209-216.

APPENDICES

Appendix A - System data

Table A1 System parameters

Parameters	*Converter 1 (Rectifier)*	*Converter 2 (Inverter)*
Peak Thevenin's voltage	137 kV	128 kV
Thevenin's impedance	0.6846 Ω, 6.8 mH	25.862Ω
Capacitor bank	18.051 μF	22.564 μF
11th harmonic filter (per pole)	0.82 Ω, 44 mH, 1.322 μF	same
13th harmonic filter (per pole)	0.92 Ω, 44 mH, 0.946 μF	same
High-pass filter 1 (per pole)	34.15 Ω, 4.8 mH, 4.5 μF	same
High-pass filter 2 (per pole)	none	56.7 Ω, 1.67 mH, 5.85 μF
Nominal DC voltage (per pole)	500 kV	4.69.16 kV
Nominal DC current	2 kA	same
Transformer reactance	8.264 Ω	same
Transformer turn's ratio	$\frac{N_s}{N_p} = 0.8859$	0.8475
Control angle	$\alpha_{nom} = 15°$	$\gamma_{min} = 18°$
6th harmonic filter (per pole)	0.28 H, 0.7 μF	same
DC High-pass filter 1 (per pole)	945 Ω, 14 mH, 3.5 μF	same
DC High-pass filter 2 (per pole)	100 Ω, 7.36 mH, 2.5 μF	same
DC line impedance (per mile, per pole)	18.25 mΩ, 137 mH 0.0433 μF	same

Table A2 Control system parameters

Parameters	*Converter 1 (Rectifier)*	*Converter 2 (Inverter with IP)*
K	249	same
T_b	0.01 sec	same
T_c	0.04 sec	same
T_d	4.60 sec	same
α-control (EP)		$K_p = 0.0035$, $K_i = 0.035$
I_{dc}-control (EP)		$K_p = 0.28$, $K_i = 0.35$
γ-control (EP)		$K_p = 0.418$, $K_i = 0.209$

Table A3 TSC and TCR parameters

Parameters	*Converter 1 (Rectifier)*	*Converter 2 (Inverter with IP)*
Thyristor-controlled reactor	none	1.05 Ω, 0.1392 H
Thyristor-swiched capacitor 1	none	0.296 Ω, 2.74 mH, 10 μF
Thyristor-swiched capacitor 2	none	0.296 Ω, 2.74 mH, 10 μF

Table A4 Converter transformer parameters

Parameters	*Converter 1 (Rectifier)*	*Converter 2 (Inverter with IP)*
ψ (Knee point)	none	122 $\frac{\text{kV.sec}}{\text{rad}}$
Linear slope	none	28.9 K Ω
Nonlinear slope	none	12 Ω

Table A5 TCR control parameters

Variable controlled	*parameters*
V	$K_p = 9.8$ pu $K_i = 5.0$ pu
$\sin\phi$	$K_p = 1.58$ pu $K_i = 12$ pu
I_D	$K_p = 0.96$ pu $K_i = 4.91$ pu

Note: The per unit (pu) values in Table A5 are on 2000 MVA and 240 KV base.

Appendix B - Voltage stability factor

It is assumed, in the following, that the inverter is controlling γ and the rectifier is controlling I_d.

To compute the voltage stability factor (VSF) for each value of the DC current I_d, we need to compute the corresponding steady-state variables such as V_d, V, and so on.

To do that, we use the following equations:

$$V_{do} = \frac{6\sqrt{3}\,t_1 V}{\pi} \tag{B.1}$$

$$V_d = V_{do}\cos\alpha - R_c I_d \tag{B.2}$$

$$\phi_d = \cos^{-1}\left(\frac{V_d}{V_{do}}\right) \tag{B.3}$$

$$P_d = n_p V_d I_d \tag{B.4}$$

$$Q_d = -P_d \tan\phi_d \tag{B.5}$$

$$V_{rms} = \frac{V}{\sqrt{2}} \tag{B.6}$$

$$\mathbf{I_s} = \left(\frac{\mathbf{E_{th}} - \mathbf{V}}{\mathbf{Z_{th}}}\right) \tag{B.7}$$

$$S_s = \frac{3I_s^* V}{2} \tag{B.8}$$

$$Q_c = \frac{3V_{rms}^2}{X_c} \tag{B.9}$$

$$Q_L = 3V_{rms}^2 B_L. \tag{B.10}$$

From Eq. B.7-8, we obtain the real and imaginary parts of S_s, P_s and Q_s, respectively. Next we solve,

$$P_s - P_d = 0 \tag{B.11}$$

$$Q_s + Q_c + Q_L - Q_d = 0 \tag{B.12}$$

with

$$B_{Lmin} < B_L < B_{Lmax} \tag{B.13}$$

where,

- t_1 - transformer tap
- V_{do} - open circuit DC voltage
- ϕ_d - converter power factor angle
- Q_c - reactive power generated by the effective capacitor (including the filters)
- R_c - commutating resistance ($R_c = \frac{6\sqrt{3}X_t}{\pi}$)
- θ_V - phase angle of V
- $\theta_{E_{th}}$ - phase angle of E_{th}
- n_p - number of poles
- * - conjugate
- bold - complex number (or value)

Referring to Fig. B1, the resultant outflow reactive power at the AC bus (q) is given by

$$q = Q_a + Q_d - Q_c - Q_L \tag{B.14}$$

where

$$Q_a = -Q_s \tag{B.15}$$

$$P_a = -P_s \tag{B.16}$$

and a small variation in q is given by

$$\Delta q = \Delta Q_a + \Delta Q_d - \Delta Q_c - \Delta Q_L. \tag{B.17}$$

The voltage stability factor is defined as the change in V when a change in the resultant outfow reactive power Δq occurs. In other words, the VSF is given by

$$VSF = (\Delta V/V)/\Delta q \tag{B.18}$$

with P_a and P_d are taken as constants. Equation B.18 can be written as

$$VSF = \frac{1}{\frac{\Delta Q_a}{\Delta V/V} + \frac{\Delta Q_d}{\Delta V/V} - \frac{\Delta Q_c}{\Delta V/V} - \frac{\Delta Q_L}{\Delta V/V}} \tag{B.19}$$

Now, we concentrate on the computation of each term in Eq. B.19.

The small variations in P_a and Q_a are respectively given by

$$\Delta P_a = \frac{\partial P_a}{\partial \delta}\Delta\delta + \frac{\partial P_a}{\partial V}\Delta V \tag{B.20}$$

$$\Delta Q_a = \frac{\partial Q_a}{\partial \delta}\Delta\delta + \frac{\partial Q_a}{\partial V}\Delta V \tag{B.21}$$

where δ is the angle between $\mathbf{V}$ and $\mathbf{E_{th}}$ ($\delta = \theta_{E_{th}} - \theta_V$). Since P_a is assumed constant, $\Delta P_a = 0$, and therefore an expression for $\frac{\Delta Q_a}{\Delta V/V}$ can be obtained.

Eq. B.1-5 with

$$\cos\gamma = \frac{2R_c I_d}{V_{do}} - \cos\alpha \tag{B.22}$$

where γ is taken as constant, have to be linearized to compute $\frac{\Delta Q_d}{\Delta V/V}$ (assuming P_d constant).

When only a capacitor (including filters) is used (no TCR), we have

$$\frac{\Delta Q_c}{\Delta V/V} = 2Q_c \tag{B.23}$$

$$\frac{\Delta Q_L}{(\Delta V/V)} = 0 \tag{B.24}$$

When a TCR and a capacitor are both used, we have

$$(\frac{\Delta Q_L + \Delta Q_c}{\Delta V/V}) = Q_c + Q_L - Q_{slp} \tag{B.25}$$

where,

$$Q_{slp} = \frac{3V_{rms}^2}{X_{slp}} \tag{B.26}$$

At this stage, the VSC could be computed for the specified DC current I_d. The whole process should be repeated if another value of I_d is selected.

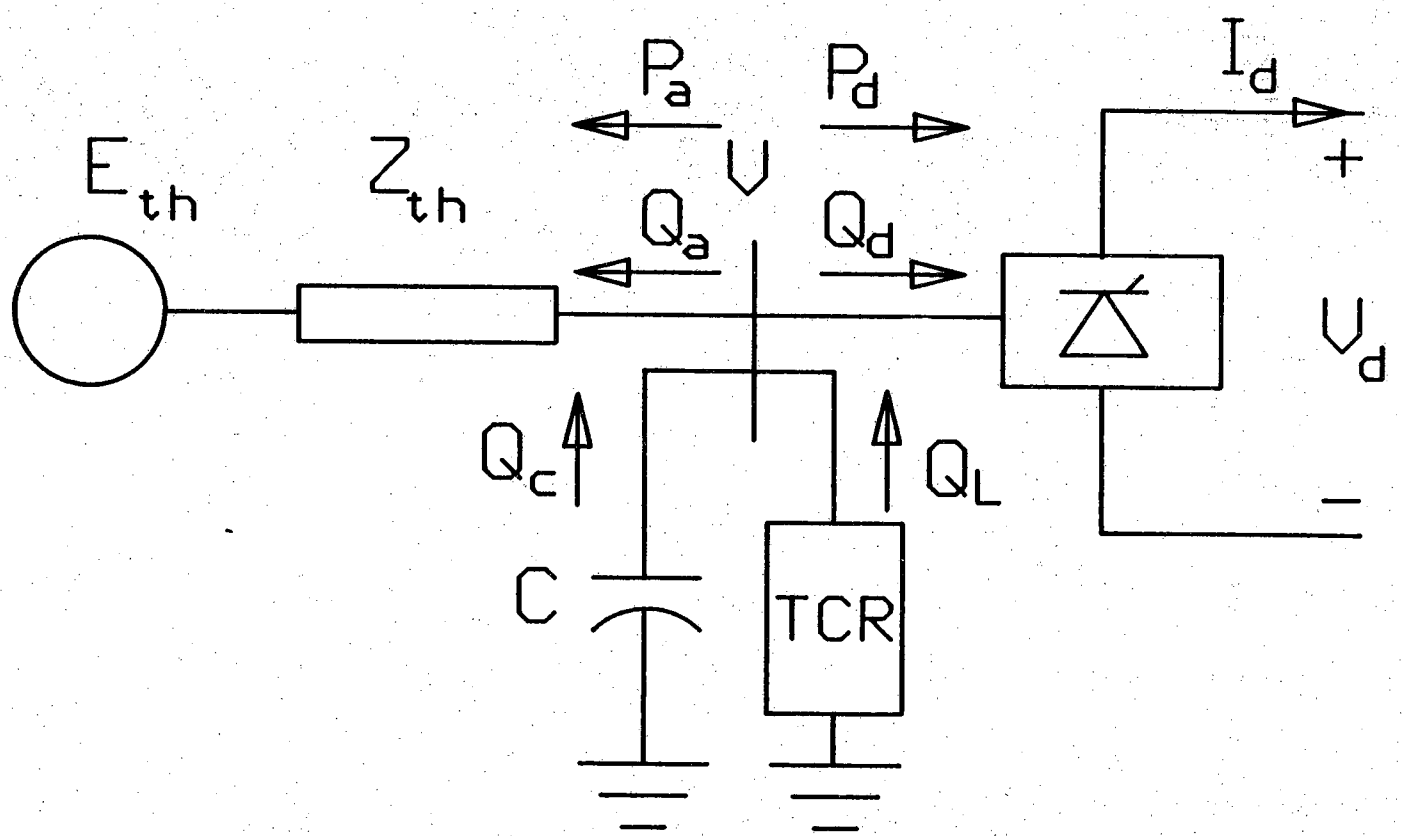

Figure B1 Simplified AC/DC system for VSF computation